EXHIBIT A

UNITED STATES DISTRICT COURT

DISTRICT OF MINNESOTA

In Re: Bair Hugger Forced Air Warming Devices Products Liability Litigation	)	File No. 15-MD-2666 (JNE/FLN)
	)	September 8, 2016
	)	Minneapolis, Minnesota
	)	Courtroom 12W
	)	2:37 p.m.

BEFORE THE HONORABLE JOAN N. ERICKSEN
UNITED STATES DISTRICT COURT JUDGE

And THE HONORABLE FRANKLIN D. NOEL
UNITED STATES MAGISTRATE JUDGE

(STATUS CONFERENCE)

APPEARANCES

FOR THE PLAINTIFFS:

LEVIN PAPANTONIO
Ben W. Gordon, Jr.
316 S. Baylen Street
Suite 600
Pensacola, FL 32502

MESHBESHER & SPENCE
Genevieve M. Zimmerman
1616 Park Avenue
Minneapolis, MN 55404

CIRESI CONLIN
Michael Ciresi
Michael Sacchet
225 South 6th Street
Suite 4600
Minneapolis, MN

(Appearances continued next page)

be -- the plaintiff should disclose their's. The defense should disclose their's, and then we should take the depositions of both. Those are the primary areas I wanted to comment on, Your Honor.

THE COURT: All right. Thank you, Mr. Gordon.

Mr. Blackwell?

MR. BLACKWELL: Good afternoon, Your Honors.

THE COURT: Good afternoon.

MR. BLACKWELL: Everyone. I agree with some of what Mr. Gordon said. We did agree on most of the dates, but we do have some fairly significant issues of difference.

This issue of the Defendant Fact Sheet is one that the Court has already addressed. This was raised before. It was discussed before. It was ruled on before. That there was no need for the plaintiffs to be requiring a Defendant Fact Sheet from the defendants when they can simply ask what they want to ask in discovery. And as Your Honors have seen already, they certainly have no problems asking for a lot in discovery. And they can ask that, could have asked that as well.

As to wanting to find out from the defendants about the particular machine that the plaintiff was using, that's part of the Plaintiff's Fact Sheet. It's their case. They're the ones who are claiming that there's a machine we made that's causing the plaintiff to have a surgical site

infection. There is no need to ask us that in Defendant's Fact Sheet, why would 3M know what particular machine or unit that the plaintiff was using at a particular hospital?

But the point is, and I think this particular issue previously was argued in fact to Your Honor, Judge Ericksen, and the response to the plaintiffs, well, you can ask what you want in discovery. There's not a need for a Defendant Fact Sheet for things such as information on the particular machine the plaintiff was using when that is the plaintiff's burden, since there's got to mean something that they start a lawsuit claiming that you made a machine that causes surgical site infection in my client for the plaintiffs. And that ought to presuppose a couple of things that in fact you've got some evidence as to the fact they were using a particular machine, and you can identify what it was. And you have some good faith basis based upon competent expert testimony for making that assertion in the first place just to satisfy requirements under Rule 11. And that factors into some of our other basic areas of disagreement.

With respect to the initial expert reports where the plaintiffs would be in favor of some scenario where we either are -- we're disclosing experts simultaneously. And I would submit, and I can't speak to Mr. Gordon's experience. I mean he does quite a lot as a source for what

the Court should do based on his experience in MDLs.

I've got my own, and I've been in many a case where in order for the defendant to know what is the case the defendant is to meet, the defendant is entitled to know who is going to opine as to the plaintiff's expert, what he or she is going to say in writing and both in a deposition, and then you can make an informed decision about what experts you want to then name as a defendant, and what opinions they need to espouse. And so all that this presupposes is a process where the plaintiffs first --

MAGISTRATE JUDGE NOEL: Can I ask you a question, Mr. Blackwell? Can you give me some examples where you've gone through, where you actually required depositions before the defendant depositions of the plaintiff's expert before the defendants even required to identify an expert?

MR. BLACKWELL: Yeah, I have, Judge Noel, and actually in federal courts in many parts of the country that's been the case where it is viewed the plaintiffs have the burden of proving their claim with respect to causation. And in some ways, it seems to save the Court time that before the defendant discloses, there is a fulsome understanding of what the plaintiff's assertion in fact is, and as opposed to having to put up an expert who is sort of shooting to some extent in the dark.

As to what is the basis for the plaintiff's claim

then, we couldn't be more in the dark at this point as to what their basis is for claiming that the Bair Hugger causes surgical site infections. We didn't get a good sense of it from science day other than looking at computational flow dynamics, those animations that the plaintiffs brought in here, and everything else we've asked them about sort of what was your basis in making this claim in the first place, what you should have had when you started the lawsuit. We've been told every time this is simply premature.

THE COURT: Could you just give me a second?

(Off the record Court discussion.)

(In open court.)

MAGISTRATE JUDGE NOEL: All right. Let me just ask one other question on that expert issue. So my understanding of the current pretrial order number 4 is initial expert reports and disclosures are due on December 1st of 2016. And that by "initial expert," I understand that to be any expert witness that a party is going to call to testify about an issue as to which that party has the burden of proof. So under these circumstances, nearly all of the initial experts presumably would be on the plaintiff's side. Although, I suppose if there's some affirmative defense you pled or something that you, the defendant, has the burden of proof on some issue and wants to call an initial expert, you would have to meet that. But

the rebuttal experts then would be experts who are going to be testifying in rebuttal to whatever initial experts have been disclosed; is that your understanding?

MR. BLACKWELL: That is my understanding, Your Honor. That is. And, again, everything I said was sort of premised on the idea that we would first be able to discover what opinions the plaintiff's experts are affirmatives espousing and to understand what they are and what the basis for those opinions are and have an opportunity to explore them.

THE COURT: You mean to take to their --

MR. BLACKWELL: Take the depositions.

MAGISTRATE JUDGE NOEL: I guess my only thought on that is ever since I was a lawyer and sort of followed the adage about the best defense being a good defense, so that defendants, even though they responding to things, they are working right away from the beginning and are preparing their case and, presumably, are retaining their experts and sort of getting geared up. And so I don't, I guess it surprises me, which was more of my question, I've never seen a case where a defendant has actually been given the opportunity to depose the plaintiff's experts before they even have to identify their own experts, because my sense is good defense lawyers probably already have their experts on retainer or at least identified for themselves so that

they're ready to go when the time comes. So --

MR. BLACKWELL: And we obviously have them, and I understand, Your Honor, that I'm swimming upstream on this one, based on Your Honor's own experience, I understand that. I have many cases where I have been allowed to do it, and we, obviously, you've seen from science day have in mind certain experts and what they may say.

MAGISTRATE JUDGE NOEL: And I understand that you're deposing a bunch of folks from around the world.

MR. BLACKWELL: Yes.

MAGISTRATE JUDGE NOEL: Who have written articles that plaintiffs have been relying on, so you'll have a better sense after that, I would assume, of what their case is based upon.

MR. BLACKWELL: Except they haven't said they necessarily are relying on those motions. Those are depositions that we have noticed, Your Honor.

MAGISTRATE JUDGE NOEL: Right, that you've identified those folks to depose because they've written articles, right, on this topic?

MR. BLACKWELL: Right, but still, again, there is an over-arching kind of issue and question in the case as to, you know, what the good reliable science says that this forced air warming device causes surgical site infections, and whether there's a reliable scientific methodology for

EXHIBIT B

UNITED STATES DISTRICT COURT

DISTRICT OF MINNESOTA

In Re: Bair Hugger Forced Air Warming Devices Products Liability Litigation	File No. 15-MD-2666 (JNE/FLN)
	June 15, 2017 Minneapolis, Minnesota Courtroom 15 9:45 a.m.

BEFORE THE HONORABLE JOAN N. ERICKSEN
UNITED STATES DISTRICT COURT JUDGE

THE HONORABLE FRANKLIN L. NOEL
UNITED STATES MAGISTRATE JUDGE

(STATUS CONFERENCE)

APPEARANCES

FOR THE PLAINTIFFS:

LEVIN PAPANTONIO
Ben W. Gordon, Jr.
316 S. Baylen Street
Suite 600
Pensacola, FL 32502

CIRESI CONLIN
Jan Conlin
Michael A. Sacchet
225 South 6th Street
Suite 4600
Minneapolis, MN

(Appearances continued next page)

maybe Your Honor contemplate now that we have the order of the bellwethers, perhaps it would be possible to have some case specific schedules put in, such that it's more of kind of a rolling discovery response on at least the handling of those cases, such that it can be more tailored to each case so we're not doing a hundred depositions in four months.

THE COURT: Okay. Let me think about that in a minute, and I want to talk to Judge Noel about that. Having reviewed the recent submissions having to do with the current schedule, I accept that some adjustment to the schedule makes sense.

At the moment, we've got depositions of experts to be completed on or before August 2nd. I'll move that to -- (crackling noise on speakers) -- $250,000 worth of improvements and that's what we get. I want you to be happy when you pay your taxes.

Okay, depositions, I'll move that to August 16th. Depositions of expert witnesses to be completed on or before August 16th.

Daubert and other dispositives general, to be filed rather than no later than August 15th, September 5th. So dispositives including Dauberts filed by September 5th. The opposition papers due September 26th, and the reply October 10th. I am free on October 25th, and also I think the day before and after that, so around that time we can

discuss how much time is needed, but that seems to be a good time. Works for everyone on our end.

MR. GORDON: Your Honor, from the plaintiff's standpoint, that's good for us. And with the Court's permission, I'm going to slip out.

THE COURT: Oh, bye.

MR. GORDON: Thank you, Your Honor.

MR. COFFIN: I'm going to go with him, Your Honor.

THE COURT: Bye.

MR. COFFIN: Thank you.

THE COURT: Mr. Gordon, look it, all your friends.

MR. GORDON: I'm sorry, Your Honor.

THE COURT: I feel like I wasn't invited to the party.

MR. HULSE: The entourage has left.

THE COURT: So first bellwether trial was scheduled to start on February 5th. Ms. Conlin, are you happy with your seat or did you want to move over?

MS. CONLIN: Oh, I'm okay here, Your Honor.

THE COURT: All right. And we'll move that to February 26th. Bellwether case specific discovery is now scheduled to be completed no later than October 2nd, and I understand that that has started because we're past the June 2nd date. So rather than October 2nd, I will make that October 16th. And then bellwether case specific dispositive

motions filed no later -- rather than November 1st, make that November 15th.

Setting aside for the moment, Mr. Blackwell, your point about some rolling discovery and so on with the bellwethers, is that agreeable with you that schedule?

MR. BLACKWELL: Well, it is. As Your Honor articulated it with this asterisk, and that relates to the November 15th date for dispositive motions for the bellwethers, the case specifics. And it's now that we know that plaintiffs are in fact going to also be naming case specific experts, it would be I think proper as with respect to the general causation disclose of experts that the plaintiffs -- we have a date for the plaintiffs to disclose their case specific experts, and then a date for rebuttal experts, so that we know first what it is they are going to put on with respect to case specific experts on the issue of specific causation before we respond to it, and the date of November 15th, Your Honor, could still nonetheless work just fine for filing any Daubert and/or the dispositive motions, but we're requesting whether it's possible to build in dates for the plaintiffs disclosures of case specific experts on specific cause, and a date for the rebuttal from the defendant.

THE COURT: Ms. Conlin, what kind of experts are we talking about for these case specifics?

MS. CONLIN: It's possible that in a specific case we may want, for example, an anesthesiologist or an orthopedic surgeon, but there is going to be considerable overlap between the experts that we've disclosed and perhaps our case specific experts. So perhaps to the extent we're going to name somebody new for a case specific putting in a deadline for that, that would be fine, but right now, we've also got our main experts who may be opining on case specific issues as well.

MAGISTRATE JUDGE NOEL: When you talk about an orthopedic surgeon or an anesthesiologist, would these be treating doctors or just some orthopedic surgeon who has expertise in infectious disease in connection with open wounds or something like that?

MS. CONLIN: Well, it could be a treating orthopedic surgeon or it could be an orthopedic surgeon that's opining on a case specific issue.

THE COURT: Do you know now whether you'll be having any such experts?

MS. CONLIN: The only experts that we're looking at right now is potential additional case specific maybe in the area of anesthesiology in light of some of their reports, which actually sort of gets into some of the rebuttal issues as well.

MR. BLACKWELL: And, Your Honor's, with all due

respect, I think it's going to remain so be seen, when we last addressed this issue before the Court, there were not going to be any case specific experts from plaintiffs.

MS. CONLIN: Well --

MR. BLACKWELL: May I finish, please?

MS. CONLIN: Sure.

MR. BLACKWELL: That has evolved as I expected it might because the second phase of the case is going to be supremely about how amongst a panoply of causes for surgical site infections do you determine it's the Bair Hugger. And there will have to be some testimony from the plaintiffs for how it is you have a reasonable scientific basis for excluding all of the other causes on a case specific basis, and that's what this phase will go to. That's why we are going to need case specific experts, and we presume there will be something from the plaintiffs that's also addressing this issue on a case specific basis because it won't be enough to simply rule the Bair Hugger in as a possible cause on a general causation.

THE COURT: You think that might be a different expert than the?

MR. BLACKWELL: They may be the same personalities, the same individuals, and but who the plaintiffs may put up in that regard not certain. We may have at least maybe a different expert, for example, on

damages on a case specific basis. But for the most part, it will be the other experts we've also named who just have case specific opinions also.

MS. CONLIN: And that actually was the point I was going to raise, and I didn't mean to interrupt you, but, obviously, with respect to damages on case specifics, there are going to be experts that testify in that. The fundamental disagreement between the parties, and you heard Mr. Blackwell articulate it again here today is we don't have to rule out every other cause. The law in Minnesota is whether the Bair Hugger was a substantial contributing cause to the infection. We believe that our experts will show that's the case.

THE COURT: So is there any reason case specific experts' depositions can't be on the same schedule or completed also by August 16th?

MR. BLACKWELL: The reason it may not work, Your Honor, is because we are just getting underway with the discovery itself, and we will not have been complete. We frankly will not have had all the information back from the various hospitals and facilities about their trend of causes by that August date, and I don't expect that when we serve discovery in the hospitals that they will be anxious to disclose to us what the history of surgical site infections have been at those facilities, and so I expect that's going

individuals. If required, defense will file a formal motion." So it's --

MR. HULSE: Something that's never happened, the plaintiffs did our work for us. They actually went ahead and filed.

THE COURT: You know, they probably do it a lot more than you give them credit for.

MR. HULSE: We welcome it.

THE COURT: Is there anything else, Ms. Conlin or Ms. Zimmerman or Mr. Hulse that we should talk about with respect to the St. Louis cases?

MR. HULSE: No, Your Honor. Like I said, I'm working on an almost daily basis with Brown & Crouppen to manage sorting those cases out, so severance will be helpful.

THE COURT: Okay. Ms. Zimmerman, are you okay with --

MS. ZIMMERMAN: Your Honor, if there's anything we can do to assist the Court, we dealt with this exact issue two months (inaudible), again, hundreds of clients that have been transferred in a similar way, if there's something we can do to help out.

THE COURT: All right. Thank you. The state proceedings, is there anything that needs to be said about the state proceedings. Ms. Ahmann?

MS. AHMANN: No, Your Honor, there's nothing to add.

THE COURT: Okay.

MS. CONLIN: No, Your Honor.

THE COURT: Okay. Is that true with respect to Canada as well? It looks like there's been no change there.

MR. BLACKWELL: No change, Your Honor.

THE COURT: And we've talked about the Super Bowl. The motion on the confidential designations is ready for hearing and will be heard, right? Okay. Is there anything else you have?

MAGISTRATE JUDGE NOEL: Okay, the only other thing I have to address is your respective letters regarding -- your respective letters of June 6th and 8th regarding initial and rebuttal expert reports.

I think we've covered this previously. It's the Court's position that whichever party has the burden of proof on an issue as to which you wish to call an expert witness, you need to disclose that report and the identity of the expert in accordance with the initial expert disclosure dates.

Any party who wants to call an expert witness to rebut what an initial expert's report has said needs to disclose a rebuttal expert report by the rebuttal disclosure date. There will be no replies to expert rebuttal reports.

The only thing left to do after an initial report and a rebuttal report have been disclosed is to depose each of those experts.

Are there any questions about that process? Ms. Conlin?

MS. CONLIN: I do, Your Honor, and the reason why we've raised it again was because we now have in the expert reports that were served by 3M on June 2nd. Let me give you a real life example of why we raised this issue.

We put in an initial report from Dr. Elghobashi, who was a CFD expert, who performed computational fluid dynamics work in this case. On June 2nd, we got in a rebuttal report from Mr. Abraham, whom I believe you recall was 3M's CFD witness at the science day hearing. He did, in fact, rebut Dr. Elghobashi's CFD work, but he also put in his own model that he did independently that he's affirmatively putting in evidence at trial.

My concern is we want to rebut that report. I mean and if it's through asking the questions at the deposition, that's fine, but they're going to put up affirmative evidence in their defense case, which our experts, if they listen to at trial or whatever, should have an opportunity to respond to and that's the issue.

I mean we've got, another example is we've got Dr. Lampotang for 3M who opined, which seemed curious in light

of the Court's rulings in the last couple of months, that the Bair Hugger is twice as effective in keeping the patient temperature increased as opposed to the HotDog. So are we to be able to rebut that when we hear that evidence at trial or are we hamstrung by what's happened in light of some of the prior rulings?

We just, you know, however the Court wants to handle it, but we have an absolute right to present a rebuttal case at trial, and we would like to be able to do that.

MR. BLACKWELL: Your Honor, if I may, I certainly disagree that it's an absolute right. And to the extent it's a right at all, they do have opportunity to explore whatever experts have said in the depositions of their experts and in the cross examination of our experts.

And I note for the Court that the plaintiffs have in response to our deposing experts been putting in upwards of an hour-plus of direct examination specifically for this purpose. So they're in fact doing it. And to point to some isolated instance of Elghobashi with respect to a CFD from Dr. Abraham, which has been in the public domain on 3M's website for a year. They have had it.

So this isn't some secret thing that just kind of came up kapoof. In fact, Your Honor's saw it on science day, same thing. So they've known about that, so they trot

that out to use it as a fulcrum for getting surrebuttal reports for everyone. And that just sets off exactly this cascade Your Honor's would like to avoid of having rebuttals, reaction with at least another rebuttal, another reaction, and it goes on and on in a process that will never respect any court schedule if that's allowed.

So to the extent that it seems to me that if the plaintiffs have further exploration, if our experts have said things that are irrelevant, the rules address that. If they feel that our expert reports are flawed, that's what cross-examination is for. If their experts have anything more to say, they've been exploring that in our deposition of their experts by taking directs on their experts. So it seems to me that the plaintiffs' needs are being addressed under the current rules, under the current schedule, and there's not a need for this sort of cascading process of surrebuttals and responses from us.

MS. CONLIN: Well, we didn't know whether they were calling Mr. Abraham as an expert. And in point of fact, we've had to serve when they've now identified them with report, we sent out subpoenas. We're still waiting for that information. We expect to start getting it on June 21st.

We're fine with not, we understand what the Court has ruled. We're simply saying I see this issue coming down

the pike. And if we get to trial, and Mr. Abraham gets up and talks about his CFD model, we want to be able to call Dr. Elghobashi in rebuttal and explain why that's wrong. That's all. And we have been doing directs because we feel like that's the one way to get out why our experts think what their experts are saying is wrong.

MAGISTRATE JUDGE NOEL: Okay. I think the Court has ruled that there will be no expert surrebuttal reports. The report is an initial report, there's a rebuttal report, and there are depositions, and it sounds to me like the depositions are serving their function.

Anything else on that issue, Ms. Conlin?

MS. CONLIN: No, Your Honor. As long as we're going to be able to present it in rebuttal at trial, we're fine with the order.

THE COURT: We're not making trial rulings at this point.

MAGISTRATE JUDGE NOEL: Anything else, Mr. Blackwell?

MR. BLACKWELL: In light of that, no, nothing else on that issue, Your Honor.

MAGISTRATE JUDGE NOEL: Okay.

THE COURT: Anything else, Ms. Conlin?

MS. CONLIN: No, Your Honor.

THE COURT: Not just on that, but on anything?

EXHIBIT C

Ciresi Conlin LLP

June 6, 2017

The Honorable Joan N. Ericksen
United States District Court
12W U.S. Courthouse
300 South Fourth Street
Minneapolis, MN 55415

The Honorable Franklin L. Noel
United States District Court
9W U.S. Courthouse
300 South Fourth Street
Minneapolis, MN 55415

Michael V. Ciresi
Founding Partner

E: MVC@CiresiConlin.com
P: 612-361-8201

225 South 6th St.
Suite 4600
Minneapolis, MN 55402
612-361-8200
CiresiConlin.com

Re: *In re Bair Hugger Forced Air Warming Devices Prod. Liab. Litig.*, MDL 15-2666

Dear Your Honors:

As you know, Pretrial Order 17 required initial expert reports to be exchanged on or before March 31, 2017 and rebuttal expert reports to be exchanged on or before June 3, 2017. Plaintiffs served seven expert reports on March 31, and Defendants served none. On June 3, Defendants served 13 expert reports, which incidentally contain opinions beyond matters contained in Plaintiffs' March 31 reports. Defendants' experts also reserved the right to offer additional opinions as new information arises during this litigation, including up to and during trial.

Pretrial Order 17 prohibits Plaintiffs from serving rebuttal reports. However, Plaintiffs assume their experts may offer rebuttal testimony at trial if deemed necessary in light of Defendants' expected expert trial testimony contained in their reports. See, e.g., UHS of Delaware, Inc. v. United Health Servs., Inc., 1:12-CV-485, 2017 WL 1945490, at *1 (M.D. Pa. May 10, 2017) (concluding that plaintiff "must have the opportunity to respond to evidence and opinions rendered in the first instance by defendants' experts"); see also Fed. R. Evid. 611(a) ("The court should exercise reasonable control over the mode and order of examining witnesses and presenting evidence so as to . . . make those procedures effective for determining the truth."); cf. Fed. R. Civ. P. 26(a)(2)(D)(ii) (stating that rebuttal experts may only "contradict or rebut evidence on the same subject matter identified by another party"). If the Court would prefer Plaintiffs to serve reports in response to Defendants' June 3 reports, an amendment to Pretrial Order 17 would be necessary.

Sincerely,

Michael V. Ciresi

cc: Jan M. Conlin
Ben W. Gordon
Genevieve M. Zimmerman
Jerry W. Blackwell
Bridget M. Ahmann

EXHIBIT D

UNITED STATES DISTRICT COURT
DISTRICT OF MINNESOTA

In re: Bair Hugger Forced Air Warming Products Liability Litigation

MDL No. 2666

VIDEOTAPED DEPOSITION OF
YADIN DAVID, Ed.D., P.E., C.C.E.
Houston, Texas
Tuesday, August 1, 2017

Reported by:
SUSAN PERRY MILLER, RDR, CRR, CRC
JOB NO. 124787

Y. DAVID

with warning to a non-air-use electric pads to a nonmoving blanket with much smaller air flow rate that does not disturb the unidirectional flow in the operating room, all provide for significant improvement in smaller amount of risk exposure and uninterrupting unidirectional flow in the OR. Those are two principles that I described in my report.

Q. Are you an expert in the relationship between particles and bacteria or infection risk?

A. Expert in the relationship between particle and bacteria. While I do not understand your question, I don't pretend to be expert in relationship between particle and bacteria.

Q. Okay. Did you look for any clinical data on any of the three devices identified in your report that might indicate their performance or infection risk?

A. The literature support my argument. Even 3M that bought Vital Health, in their disclosure to a press release saying that this is safe and effective device and would

Y. DAVID

supplement the product that they have. And when you do not have warm air circulating but it's a closed loop, I don't think that you need to be an expert to realize that you're removing a threat. You therefore are reducing exposure to the risk.

Q. Are you familiar with the concept that direct contact with a surface can pose an infection risk?

A. That makes sense.

Q. Is that something that you're familiar with in your work in the hospitals?

A. Well, hand hygiene is a typical example. Very, very known in hospitals.

Q. And reusable medical equipment that directly touches patients, that's also an example?

A. Well, it's not the same because most of the accessories that will touch patients will be disposable, single use, and probably sterile. So that's not the same as hands touching surfaces.

Q. Have you provided in your report all of the data that you reviewed with respect

Y. DAVID

to the alternative products that you've identified?

A. Yes, I did.

MS. EATON: Do I have any time left?

THE REPORTER: You're at 6:48.

MS. EATON: Okay. I'm going to reserve.

MR. BANKSTON: Yeah, I'm a little hot so we'll take a literally two- or three-minute break.

THE VIDEOGRAPHER: We're going off the record at 18:08.

(Recess, 6:08 p.m. to 6:17 p.m.)

THE VIDEOGRAPHER: We are back on the record at 18:17.

EXAMINATION

BY MR. BANKSTON:

Q. Dr. David, you were asked some questions about risk-benefit. Do you remember those questions?

A. I do.

Q. Okay. First of all, is it your opinion that the Bair Hugger should be taken

Y. DAVID

out of rooms and not replaced with any form of patient warming?

A. No.

Q. Okay. Are there other devices available, other design concepts which are feasible to be made without the same risk mechanism that you identified in your report?

MS. EATON: Object to the form of the question.

A. Right. I indicated in my report and so is my opinion that I identify specific product with different features that remove the risk introduced by the Bair Hugger 750 and yet serve the purpose of controlling patient temperature environment.

BY MR. BANKSTON:

Q. Does the literature you reviewed contain any studies or any opinions concerning whether any of these devices are similar in effectiveness to the Bair Hugger at maintaining patient temperature?

A. I was trying to scan in my memory where that might be in my report.

Q. Let me know.

Y. DAVID

A. And I think that --

Q. Well, can I direct you to a page maybe that I want to ask you about?

A. In the --

Q. Let me withdraw that -- let me withdraw that question, Dr. David. Can we take a look at your report? Can you flip to page 39 for me?

MS. EATON: And I'll just object to this as leading.

MR. BANKSTON: Okay.

BY MR. BANKSTON:

Q. Do you see a reference on 39 to Dr. Daniel Sessler?

A. Yeah, that's the one I was looking for, actually.

Q. Who is Dr. Daniel Sessler? What role does he play?

A. I understand that he was or is clinical consultant to 3M and might be working with other vendors.

Q. Did you rely on Dr. Sessler's opinions in any respect in this case?

A. Well, one thing that his study was

Y. DAVID

supportive is that resistant heating mattresses are of equal efficiency to the Bair Hugger forced-air blanket in maintaining temperature, and that's why I incorporate that study here.

Q. Okay. From your engineering background and experience, do you have any opinion on whether, apart from these four devices, just from an engineering concept standpoint, is it possible, more likely than not, to design a device that does not pose the risks you've identified but warms patients as effectively?

MS. EATON: Object to the form of the question.

A. These devices that I show as alternatives are demonstrating that. 3M engineers have several concepts that they came up with. One of them is the, I believe, recirculating, is basically what I have in my alternative design, so it is feasible.

BY MR. BANKSTON:

Q. Okay. You were asked some questions about speaking to hospitals about

Y. DAVID

Bair Hugger risk. Do you remember those questions?

A. Yes.

Q. Okay. When you began work on this case, did you sign a protective order?

A. I did.

Q. Okay. Did you review confidential materials in this case?

A. I did.

Q. Did you rely on any confidential materials in coming to your conclusions in this case?

A. Yes.

Q. Do you have any understanding of what will happen to you if you disclose 3M's confidential information in the things you've learned in this case?

A. I understand, and that's part why I didn't discuss that with hospitals.

Q. You take those obligations seriously in terms of protecting 3M's corporate property?

A. I do.

Q. When you, in your career, have been

Y. DAVID

evaluating medical devices for healthcare facilities, did you come to any understandings during those days regarding whether certain procedures had unique vulnerabilities to infection?

MS. EATON: Object to the form of the question.

A. There is no question that after so many years in the largest medical center in the country, as I worked in, you get exposed to condition of patients from A to Z and there are variation. There are patients that come in with sore throat and would go home. There are patients that come in with a brain tumor and it will be very difficult to deal with that.

So there are environments that are much more susceptible to condition that the patients are in than others, and specifically orthopedic surgery is one of those environments.

BY MR. BANKSTON:

Q. I would like to show you a document that's been previously marked in this

EXHIBIT E

UNITED STATES DISTRICT COURT

DISTRICT OF MINNESOTA

- -

In Re:

Bair Hugger Forced Air Warming

Products Liability Litigation

This Document Relates To:

All Actions MDL No. 15-2666 (JNE/FLM)

- -

DEPOSITION OF JOHN P. ABRAHAM, Ph.D.

VOLUME I, PAGES 1 - 396

JULY 20, 2017

(The following is the deposition of JOHN P. ABRAHAM, Ph.D., taken pursuant to Notice of Taking Deposition, via videotape, at the offices of Ciresi Conlin L.L.P., 225 South 6th Street, Suite 4600, in the City of Minneapolis, State of Minnesota, commencing at approximately 9:26 o'clock a.m., July 20, 2017.)

APPEARANCES:
On Behalf of the Plaintiffs:
Gabriel Assaad
KENNEDY HODGES
4409 Montrose Boulevard
Suite 200
Houston, Texas 77006
Genevieve M. Zimmerman
MESHBESHER & SPENCE, LTD.
1616 Park Avenue
Minneapolis, Minnesota 55404

On Behalf of the Defendants:

Peter J. Goss
Micah Hines
BLACKWELL BURKE P.A.
431 South Seventh Street
Suite 2500
Minneapolis, Minnesota 55415
ALSO PRESENT:
Ryan M. Stirewalt, Videographer
Nathan Bushnell

EXAMINATION INDEX

EXHIBIT INDEX

P R O C E E D I N G S
(Witness sworn.)
JOHN P. ABRAHAM, Ph.D.,
Called as a witness, being first duly sworn, was examined and testified as follows:
EXAMINATION
BY MR. ASSAAD:
Q. Please state your name for the record.
A. John, J-O-H-N, Patrick, P-A-T-R-I-C-K, Abraham, A-B-R-A-H-A-M.
Q. Have you ever had your deposition taken before?
A. Yes.
Q. Approximately how many times?
A. Six or seven.
Q. Were they all in the capacity of an expert witness?
A. Yes.
Q. And we'll get to those in a little bit. I'm sure -- You've been through the drill before, but I have to go over a few instructions --
(Interruption by the reporter.)
Q. You've been through the drill before, but I'm going to go over a few instructions. Fair?

First of all, I'm going to ask you numerous questions today. If you don't understand the question I'm asking, please let me know and I'll do my best to rephrase it. Fair?
A. Yes.
Q. If you answer the question that I've asked, I will assume that you understood the question. Fair?
A. Yes.
Q. At any time you want to take a break just please let me know. I just ask that you request a break after you answer a pending question. Fair?
A. Yes.
Q. Okay. We've met before; correct?
A. Yes.
Q. We've actually met at the deposition of Dr. Elghobashi; correct?
A. That is correct.
Q. And actually we had a -- two brief discussions at the hotel that we both stayed at in Irvine, California.
A. That is correct.
Q. And you agree with me that none of the conversations that we've had had any -- anything to do with the substantive issues in this case.
A. I agree.

A. Yes.
Q. Well there's air around the board; correct?
A. There is air in the blanket, and between the blanket and the skin.
Q. Okay. And some of the air goes around the board; correct?
A. I disagree.
Q. You disagree. Okay.
Is there any basis, scientific basis why you disagree except that based on your experience --
A. Yes.
Q. -- with forced-air warming blankets?
A. Yes.
Q. What's your basis?
A. I'll try to do a better job of explaining it, because I think it's -- multiple times. I'm going to use my arm and --
THE WITNESS: If you can't catch this on the screen, I apologize.
A. The way the person is sitting they're laying like this. [Demonstrating.]
Q. Is that how he's laying?
A. Well it's essentially this. They've got two arms out to the side and is --
Q. Is there anything between the arms?

A. As I recall, there's a pillow.
Q. Okay.
A. Okay. There are blank --
There is a hot warming blanket which wraps around the arm, and in fact I think a cartoon version of this was provided in Said Elghobashi's, maybe it was his supplemental report or something that I saw yesterday where he had these tubes around the arm. Okay? And that's -- that cartoon outlines this quite well, okay? So you have these tubes around the arm. The tubes have these little jets of air that are one millimeter in diameter, approximately. They hit the skin, they stop. We call that stagnation. So now you have a warm stagnant body of air.
Now the question is, where does it go? If I have warm air near my hands, is that warm air going to travel up my arms and then out the open space by my head? And mind you there is air jets all along the way. So there's some air being -- hitting the arm here, and stagnating. There's other air hitting the arm here. There's other air hitting the arm here. A tiny amount is at the hands, but there's air all the way along, and in fact in the center part of the -- the blanket. So you have air oozing out of this blanket very slowly, it hits the arms, it's stagnant.

Then what does it do? If you're hot air right here are you going to be able to go down to the bottom of the drapes and then emerge out into the room? That's possible. Or are you going to just migrate upwards along with buoyant forces? That is actually what happens. There is no physical mechanism that would force that stagnant warm air to go downwards to the floor and then come back up. It's the analogy that I used before; the match, or incense, or a cigarette. If you hold those things upside down, the smoke or the flame still rise.
Q. Are you done?
A. Yes.
Q. Okay. Let's talk about heat, though. Are you saying all the heat's going to go out the head and neck?
A. In my model all the hot air emerged by the head and neck. I did not allow heat to transfer by conduction, for example, through the arm-board.
Q. Okay. And we know through Settles' results that heat does travel by conduction and heats up the -- the -- underneath the operating room table.
A. We do --
MR. GOSS: Object to form.
A. -- not know that.

Q. Okay. So you disagree with Settles.
A. No.
Q. Okay.
A. I gave two explanations of how temperature measurements in the place he made them could be elevated, not -- one of them was not by conduction.
Q. Okay. But regardless of what method it was heated, it was done by the Bair Hugger.
A. I would agree.
MR. GOSS: Lack of foundation. You can answer if you know.
A. I would agree.
Q. I mean, conservation of energy, you need a heat source to increase temperature; correct?
A. I agree.
Q. Okay.
MR. GOSS: I'm sorry, Gabriel, can I take a bathroom break when you have a chance? Too much coffee.
MR. ASSAAD: If I said "no," would you be upset?
MR. GOSS: I'd be uncomfortable.
MR. ASSAAD: You can take a break.
MR. GOSS: Thanks.
MR. ASSAAD: Off the record.

THE REPORTER: Off the record, please.
(Recess taken from 5:09 to 5:16 p.m.)
BY MR. ASSAAD:
Q. So real quick a couple of things. Looking at that picture up there if you look on the left side it says -- it states, time, 1.2 seconds. Would you agree with me that the file that you provided to us was at a simulation time of 1.2 seconds?
A. No. I don't know if it was. That looks to be an expression that was made, and I can't recall if I made a time expression. Oh, I'm sorry. I thought you were looking at the bottom.
Q. No. The right -- left-hand side --
A. Yes.
Q. -- where it says "time."
A. I agree.
Q. Okay. So your model is basically a simulation of 1.2 seconds; correct?
MR. GOSS: Object to form.
A. The results shown here --
Q. Yes.
A. -- are the results after 1.2 seconds.
Q. Of simulation time.
A. Correct.
Q. Okay. Which is 1.2 seconds real time;

correct?
A. Correct.
Q. And as I understand it, the streamlines is a line based on the instantaneous velocity at a particular cell; correct?
A. Yes.
Q. Okay. It's not that you're following the air around the operating room and seeing where that particular air goes; correct?
A. It is an instant --
What the streamline is is an instantaneous --
Let me tell you how streamlines are made. The vectors which describe the flow direction and speed are all obtained at a time instant and then they are connected by their tangents, and that gives us streamlines. So it's an instantaneous trajectory of air.
Q. So one of the videos I believe lasted about three minutes, or three and a half minutes long that you provided in this case; correct?
A. I don't know that.
Q. Okay. Well the video is on YouTube. You've seen your videos on YouTube that 3M has put on with respect to your -- this CFD analysis.

A. I have seen the CFD analysis on YouTube.
Q. And you've created the YouTube videos which are about -- more than 1.2 seconds long; correct?
A. Correct.
Q. Okay. The fact that the video is -- say, for example, is three minutes long of streamlines, or two minutes, doesn't mean that you ran the model for two minutes; correct?
A. That is correct.
Q. Okay. And so it's your opinion today that you got quasi-steady state by running the model in 1.2 seconds.
A. Yes.
Q. Okay. Is it possible to run the model forward based on the TRN file?
A. Yes.
Q. Without the initial conditions?
A. Correct.
Q. Now the fact that this is the 264th time step, does that indicate to you what your time step was?
A. No. I don't -- Looking at this here, I don't see -- it doesn't tell me the time step and I don't recall, sitting here.
Q. Can you determine the time step by looking

at the ANSYS file?
A. Could you determine it? Yes, you could.
Q. How would you do that?
A. Well remember this file, the TRN file contains everything, in the sense that it contains the mesh, the geometry and the setup. So you could pull it into the setup.
Q. So if I told you you could take over this ANSYS program right now and determine the time step, that's something you could do?
A. I may be able to.
Q. How long would it take you?
A. Boy, I don't know how long it would take me.
Q. Well where would you look?
A. I would load this thing into the CFX, what's called the setup file, and I would look there.
Q. Okay. You used ANSYS Academic; correct?
A. Incorrect.
Q. "Incorrect"?
A. Incorrect.
Q. What did you use?
A. ANSYS Research.
Q. That's part of the Academics soft -- package; correct?
A. I recall them being separate. I mean, if

EXHIBIT F

UNITED STATES DISTRICT COURT

DISTRICT OF MINNESOTA

In re Bair Hugger Forced Air Warming Products Liability Litigation

MDL No. 15-2666 (JNE/FLN)

This Document Relates to All Actions

EXPERT REPORT OF

SAID ELGHOBASHI, M.SC., PH.D., D.SC.

Attached as exhibit 1 is my report, Effect of Heated-Air Blanket on the Dispersion of Squames in an Operating Room, Dated March 23, 2017

Attached as exhibit 2 is a Summary of Opinions.

Attached as exhibit 3 is my professional Resume.

I have not previously testified in trial or deposition.

My hourly charge for professional services is $800.00

Date: March 29, 2017

S Elghobashi

Said Elghobashi, M.Sc., Ph.D., D.Sc.

Exhibit 1

Effect of Heated-Air Blanket on the Dispersion of Squames in an Operating Room

Said Elghobashi

Mechanical and Aerospace Engineering
The Henri Samueli School of Engineering
4220 Engineering Gateway
University of California, Irvine
Irvine, CA 92697-3975
Phone: (949) 824-6131
Email: selghoba@uci.edu

March 23, 2017

Contents

Effect of Heated-Air Blanket on the Dispersion of Squames in an Operating Room

Abstract

A large-eddy simulation (LES) of the interaction between the ventilation air flow and forced hot air from a blower is performed to investigate the effect of hot air on dispersion of squames in a realistic operating room (OR) consisting of an operating table (OT), side tables, surgical lamps, medical staff, and a patient. Two cases with blower-off and blower-on are calculated together with Lagrangian trajectories of 3 million squames initially placed on the floor surrounding the OT. The squames particles are assumed as spheres of size 10 microns and the drag, lift and buoyancy forces are considered in calculating their instantaneous motion. It is shown that with the blower-off, squames are quickly transported by the ventilation air away from the table and towards the exit grilles. However, with the hot air blower turned on, the ventilation air flow above and below the OT is disrupted significantly. The rising thermal plumes from the hot blower air drag the squames above the OT and the side tables and then they are blown downwards toward the surgical site by the ventilation air from the ceiling. Temporal history of number of squames particles reaching four imaginary boxes surrounding the side tables, the OT, and the patient's knee shows that several particles reach these boxes with the blower turned on. The study shows that LES is necessary to accurately capture the mixing and transport in a turbulent flow and predict the dispersion of squames in an OR.

1 Introduction

Microbial skin colonizers, such as *Staphylococcus aureus*, have been known as a major cause of surgical site infections in operating rooms (Noble, 1975; Clark & de Calcina-Goff, 2009; Wood *et al.*, 2014). These bacteria typically colonize on human skin cells or squames which are routinely shed by humans, roughly about 10^7 particles per day (Noble, 1975). The squame particle size ranges over 4–20 μm of equivalent diameter (Noble *et al.*, 1963; Lees & Brighton, 1972).

Reduction of post-operative surgical site infections has been linked to two main factors: (i) ultra-clean ventilation (UCV) systems, and (ii) perioperative patient warming (Ng *et al.*, 2006; Legg *et al.*, 2012; Wood *et al.*, 2014). Ultra-clean ventilation aims to reduce the quantity of airborne bacteria in the operating room (OR) and most importantly near the surgical site. This is typically achieved by the constant delivery of highly filtered ultra-clean air with a downward uniform velocity of 0.3-0.5 m/s (McGovern *et al.*, 2011). The UCV performance depends critically on volumetric airflow, proper temperature gradients, use of uniform downward flowing ventilation air, potentially in the laminar regime (Memarzadeh & Manning, 2002; Pereira & Tribess, 2005). Surgeons and other medical equipment within the operating room (surgical lights, tables, patient, computers, etc.), motion of surgeon's arms and their bending motion (Chow & Wang, 2012) can disrupt this air flow

and create wakes, flow unsteadiness, and turbulence, thereby increasing the amount of cfu in the OR.

Perioperative patient warming is the other important clinical practice to prevent inadvertent surgical hypothermia, wherein the core temperature of the patient drops below 36°C. Preventing inadvertent perioperative hypothermia has several benefits that include reduced operative blood loss, reduced duration of surgery, improved wound healing, reduced wound infections, reduction in post-operative ulcers, reduced duration of hospital stay, and increased survival rates (Wood *et al.*, 2014; Ng *et al.*, 2006; Legg *et al.*, 2012). Monitoring and maintaining body temperature during surgery is therefore an accepted and required practice. Warttig *et al.* (2014) review different methods used to combat inadvertent perioperative hypothermia. These include use of warm cotton blankets, reflective blankets, warmed intravenous and irrigation solutions, circulating warm water mattresses, a reusable electric blanket, an electric heating pad, and forced-air warmers (Kellam *et al.*, 2013; Austin, 2015). Of these, active warming using forced air warming (FAW) devices, and passive warming based on the use of reflective blankets, are the two main techniques used to keep the patient's body warm and prevent hypothermia. Although passive heating techniques may show similar effectiveness as the FAW devices, the latter have been used for over two decades due to their efficacy in maintaining patient's core body temperature. These techniques use forced convection to increase the skin temperature and the total body heat content. These devices contain a blower (such as 3M™ Bair Hugger™) that extracts the room temperature air through an air-intake filter heats the air using a heating coil, and vents the air into the sterile field adjacent to the operative site (Albrecht *et al.*, 2011; Leaper *et al.*, 2009; Wood *et al.*, 2014). The filtered and warm air flows through a connecting hose into blankets made of plastic and exits the blankets through tiny holes over the patient's skin. However, this forced warm air has the potential to generate and mobilize airborne contamination in the operating room.

A number of studies have examined at the safety of forced-air warming, and whether FAWs can affect surgical site infections through mobilized airborne contamination. FAWs can potentially lead to surgical site contamination in two ways: (i) direct contamination of the air from the blowers that reaches the patient's body, and (ii) disruption of the ultra-clean ventilation air by the thermal plumes and turbulence. The former risk can potentially be reduced by using intake filers that are HEPA-rated and show high filtration efficiency. The latter has been studied extensively as reviewed

by Wood *et al.* (2014). It is hypothesized that the temperature gradients and resultant thermal plumes created by the FAW devices could disrupt the benefits of UCV flow, that is designed to be uniform and downwards. The interaction between the FAW and UCV flows may lead to increased surgical site infections (SSI).

McGovern *et al.* (2011); Legg *et al.* (2012) have shown that temperature gradients and excess heat created by FAW devices can transport air from the unsterilized floor level to the surgical site, thus increasing the potential risk of SSIs. Moretti *et al.* (2009) measured an increase in the bacterial load when FAWs were used. Lack of flow visualization is the main drawback of these studies as it does not provide information about whether the particles came from the floor or from the FAW blower. Legg *et al.* (2012); Sessler *et al.* (2011) used smoke particle visualization to understand the source of these particles near the surgical site comparing cases with no warming, FAW, and radiant warming. Although they found that FAW increased the particle count with blower turned on (almost 10-fold increase), they also showed that the uniform, laminar flow from the ultra-clean ventilation reduced the effect of particles by limiting their numbers near the surgical site.

It is clear from the available literature that the interaction between the UCV flow and the rising plumes from the forced-air warming devices plays a critical role in deciding whether FAWs indeed can lead to increased number of particles near the surgical site. However, there have not been detailed experimental measurements of flow patterns in the OR setting with the FAW blower turned on. Recently, McNeill *et al.* (2012, 2013) conducted particle-image velocimetry (PIV) measurements to understand the flow pattern in an OR with the ultra-clean ventilation system. This study, however, did not investigate the effect of FAW blower. McNeill *et al.* (2013) also made detailed measurements of temperature fields on surgeon's and patient's body to be used for computational modeling. Although the above PIV was able to visualize and measure the flow field, it was limited to planar data (2D PIV) and thus a full three-dimensional data are not available for the OR. Nevertheless, some useful information on the flow unsteadiness, turbulence within the room was obtained from the McNeill *et al.* (2013) study.

The only other way to characterize the flow field in an OR with and without FAW blowers, is to use computational fluid dynamics (CFD) modeling in three-dimensions. This, however, is a difficult task due to the size and complexity of the domain involving medical equipment, staff, computers, etc. There are only few CFD studies in the literature that used Reynolds-averaged Navier

Stokes (RANS) models (Memarzadeh & Manning, 2002; Memarzadeh, 2003; Chow & Wang, 2012), wherein only the time-averaged velocity field is computed. All information about the turbulence and velocity fluctuations is completely *modeled.* As is shown later (section 3), RANS approach is not predictive, since the instantaneous velocity field needed for calculating the trajectories of squames is not directly computed. Thus, RANS is incapable of accurately predicting the locations of squames at any time in the OR. Memarzadeh & Manning (2002); Memarzadeh (2003) investigated the effect of various UCV inlet flow conditions on the transport of squames particles in an OR. They considered a realistic OR with medical staff, equipment, surgical lamps, etc. and accounted for the thermal plumes created by heat radiated from various sources. However, they used a RANS model coupled with a Lagrangian particle-tracking of around 4000 representative particles. Their study did not include the FAW blower discharge. They showed that use of a uniform inlet flow with laminar conditions[1] is better for reducing the number of particles near the surgical site. In addition, they found that the thermal plume created by the hot surface of the surgical site prevented particles from reaching the site. They showed that roughly 2-5% of particles reach the surgical site, *provided they are originated very close, about* 1.3cm *above the site.* Particles originating from locations away from the surgery did not have a statistically significant probability of reaching the surgical site. As is discussed later in section 3, RANS model cannot compute the instantaneous velocity field needed to accurately calculate the forces on particles, and particle trajectories.

Chow & Wang (2012) investigated the ultra-clean ventilation flow and its effect on bacteria-carrying particles in an OR using a RANS model as well. They simulated the bacteria particles as a non-inertial pollutant, wherein an Eulerian transport equation for the concentration of the bacteria is calculated. In addition, they considered periodic bending movement of one of the surgeons performing the operation. They found that if the surgical staff stands upright (no bending), the UCV flow keeps the bacteria concentration very low (< 1 cfu/m^3) near the surgical site. However, with the surgeon's bending motion included, they showed that this concentration increased to larger than the recommended value (10 cfu/m^3).

All of the above computational studies are based on RANS modeling and did not include the

[1] It should be noted that the literature uses the terminology 'laminar flow' for the ultra-clean ventilation flow. Based on the standard values of air changes per hour (ACH) for an OR (25 per hour), the inlet grille sizes, and properties of air, the flow Reynolds numbers are much larger than 2000, a critical value beyond which turbulence occurs in a duct. The inlet grille flow, thus is not typically laminar. Although the level of turbulence in the inlet flow is not large ($< 10\%$), the flow contains velocity fluctuations and is unsteady.

FAW blower system together with a blanket cover above the patient. In order to assess the interaction between UCV and FAW blower, a systematic, predictive simulation is needed. Large-eddy simulation (LES) is a numerical technique that involves computing the properties of the large, energy-containing eddies of turbulence accurately, without any user adjustable tuning parameters, and models only the more homogeneous, small scales of turbulence (Pope, 2000; Piomelli, 2014). This technique provides the instantaneous three-dimensional velocity, temperature, and pressure fields and has been shown to be far more accurate than the RANS model. Section 3 outlines the differences between LES and RANS in detail. In addition, since the time dependent, three-dimensional velocity field is available in LES, then the forces on particles and their trajectories can be calculated accurately (Apte *et al.*, 2003*b*; Ham *et al.*, 2003; Apte *et al.*, 2009; Moin & Apte, 2006; Mahesh *et al.*, 2006). The only challenge with this technique is that it is computationally intensive and requires fine grid resolutions and small time-steps to capture the large-scales of turbulence. Recent advances made in algorithmic developments for LES on arbitrary shaped, unstructured grids (Mahesh *et al.*, 2004; Ham *et al.*, 2003; Moin & Apte, 2006; Mahesh *et al.*, 2006; Ham & Iaccarino, 2004) have facilitated application of LES to more realistic problems involving complex geometries and flow conditions. These advances have been successfully applied to turbulent, reacting flows in a gas-turbine combustion chamber and has led the gas-turbine industry to switch from RANS to the predictive LES technique in their design cycle (Moin & Apte, 2006; Mahesh *et al.*, 2006; Apte *et al.*, 2009).

LES applied to operating rooms with medical staff and other instruments is still challenging, owing to the size of the room and the complexity of the geometries involved. At the time of writing this report, only one LES study has been performed for an operating room by Saarinen *et al.* (2015). They studied the escape of air into an isolation room during opening and closing of a door and passage of a human figure. They used passive smoke visualizations to compute the volume flux of air when a door is opened. Although this study had some complex geometry (a human figure), it did not have the intricacies of the OR table, surgeons, patient and other medical equipment, nor it computer the dispersion of squames in the OR. Nevertheless, it showed that LES can accurately predict such flows through validation with experimental observations.

The main goal of the work reported here is to use large-eddy simulation to compute the interaction of the OR ultra-clean ventilation air flow and the flow created by forced air warming

system (such as 3M™ Bair Hugger™) and investigate their impact on the dispersion of squames. Specifically, computations are conducted for the cases with blower-off and blower-on, including the Lagrangian tracking of inertial squame particles, starting from the operating room floor, to prove whether the FAW system and the resultant thermal plumes play a role in transporting squame particles to the surgical site.

The rest of the report is arranged as follows. In section 2, details of the operating room geometry and CAD model are described. This includes the OR dimensions, the surgical lamps, four medical staff, an operating room table, two side tables, the blower, and the patient undergoing knee surgery. The numerical approach is described in section 3. This includes a detailed discussion of LES and RANS, the governing equations used for LES, the computational grid, and the boundary conditions. The numerical algorithm used is briefly summarized in section 3.5. This is followed by detailed description of the results in section 4 on flow field, particle trajectories and particle counts that reach the surgical site and other key regions of interest. Finally, the findings are summarized in section 5.

2 Operating Room Geometry and CAD Model

The operating room CAD (computer aided design) model was created using Ansys® SpaceClaim Direct Modeler™ (ANSYS, Inc., Canonsburg, PA, USA). The CAD model replicated a realistic operating room (OR) depicting a knee surgery being performed on a patient. An original baseline CAD model was obtained from M/E Engineering P.C. (Straub, 2016) and was further modified to incorporate the measured dimensions of the inlet air grilles and the surgical drape as shown below. Figure 1a shows the OR dimensions used to create the CAD model. The length, width and height of the room are 7.32m, 7.01m and 3.18m, respectively. These dimensions are from 3M video at: https://www.youtube.com/watch?v=QhzeInWIJ54. Figure 1b shows a close-up view of the surgeon's hands extended over the patient's knee mimicking a real world operating procedure.

The CAD model also includes several objects that are usually present in a real OR. Typically, there can be several combinations of such objects, but for this study the following objects were included in the model. These are shown in a top view in figure 2 and include: (i) OR Table; (ii) OR drape; (iii) patient's body under the drape with knee exposed; (iv) four surgeons (two of the surgeons have extended hands and two have hands down), (iv) two side tables, (v) two surgical lamps, (vi)

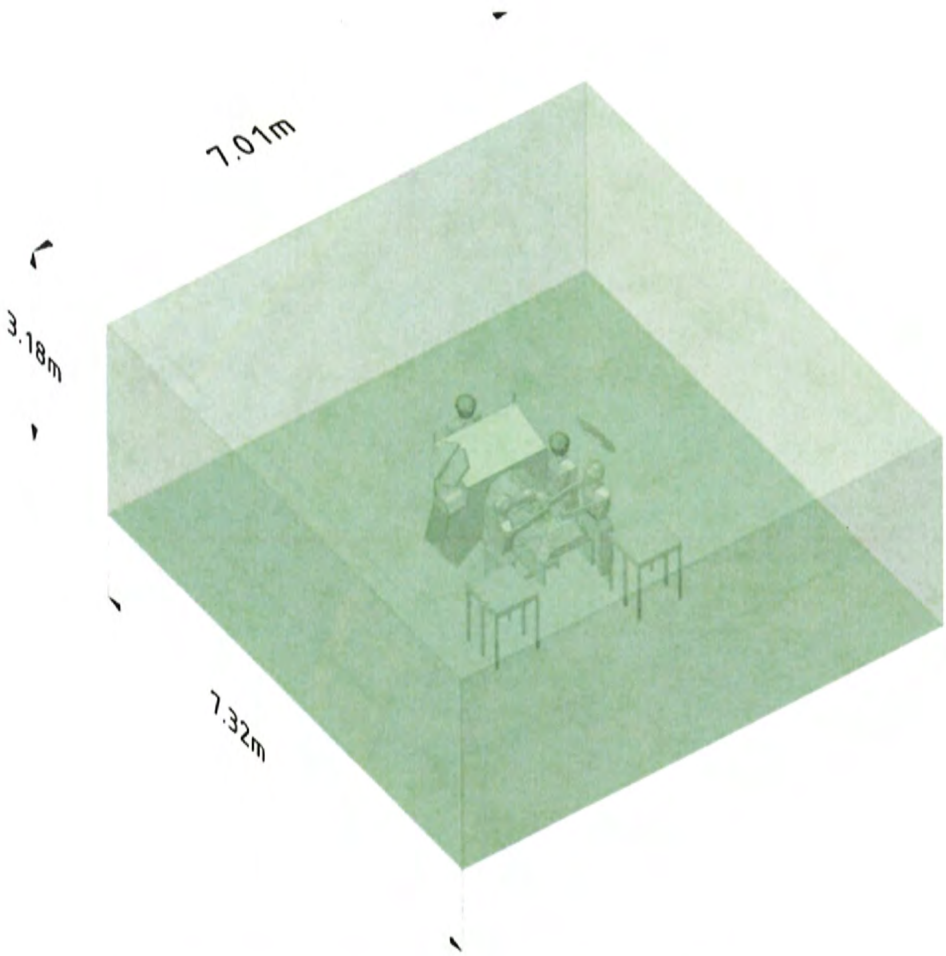

(a)

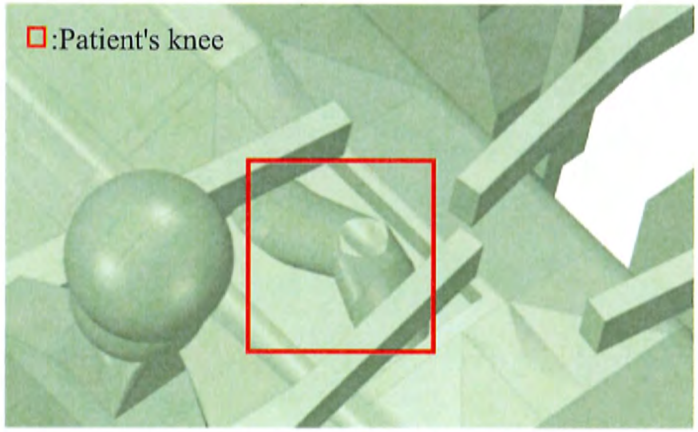

(b)

Figure 1: CAD model showing (a) operating room dimensions, and (b) closeup of the patient's knee.

3M™ Bair Hugger™ blower unit (partly visible near the top left corner under the drape).

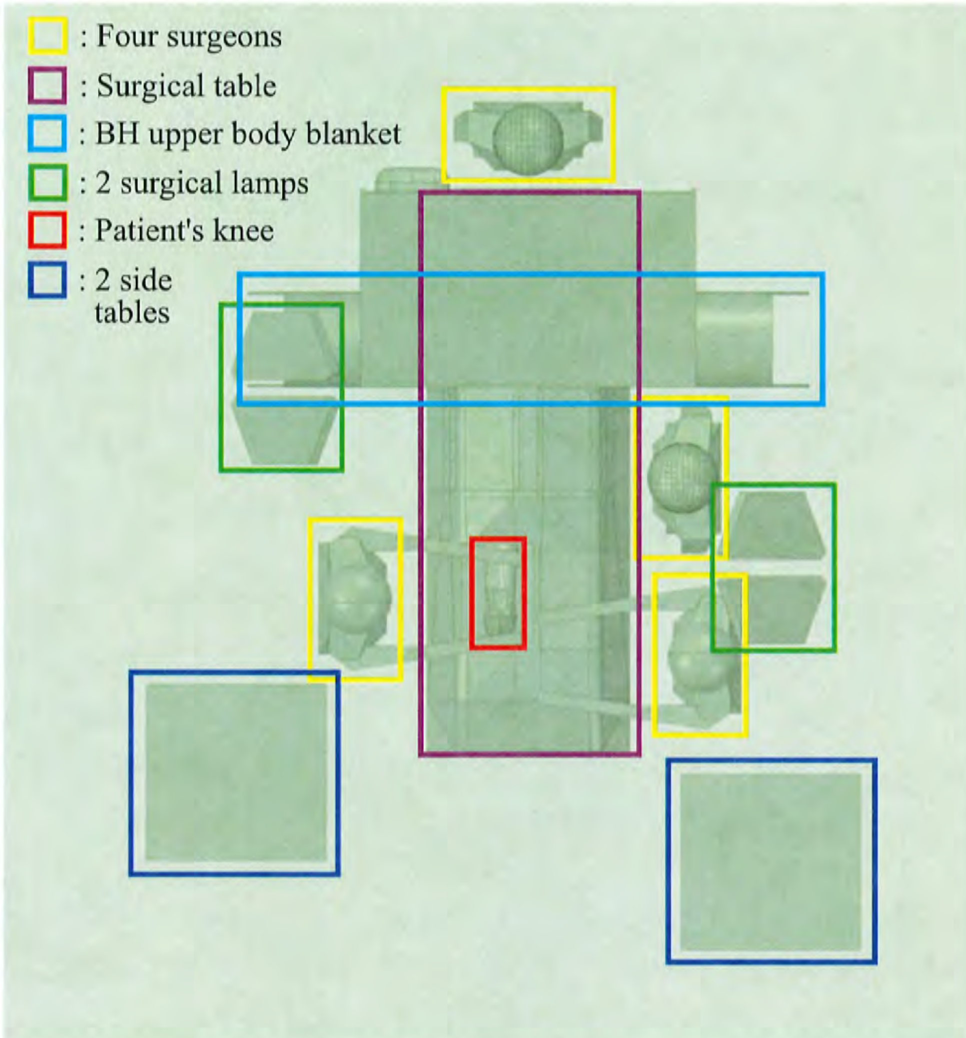

Figure 2: Close-up view of various objects included in the CAD model.

Figure 3 shows a side view of the OR table together with a few key dimensions. The bottom of the OR table is 0.94m above the floor of the room. The drape on the OR table covering the patient's torso is suspended 0.52m above the floor. The 3M™ Bair Hugger™ blower unit is also seen in the bottom right side of the figure.

The drape design from the base CAD model was modified to better represent the drape layout in a real OR room. The modifications mainly focused on using accurate dimensions and shape of the drape near the front end based on an actual picture taken in an OR room as shown in figure 4b. A corresponding CAD model used in the present study is shown in figure 4a. For the CAD model, the

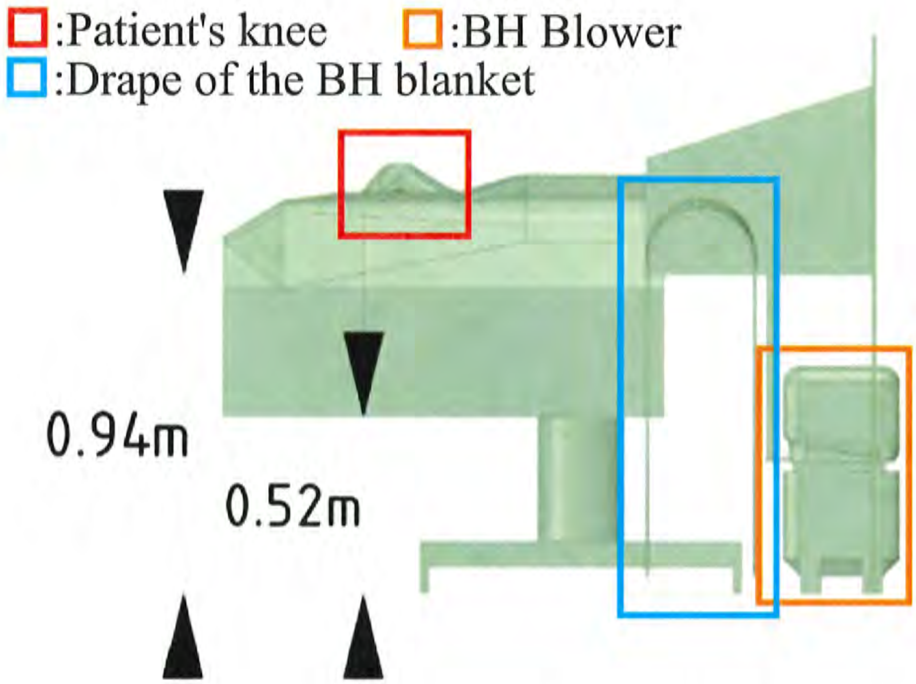

Figure 3: Side view of the OR table with some key dimensions. The 3M™ Bair Hugger™ blower unit is clearly visible on the bottom ride side.

front end of the drape was designed to mimic the shape obtained by dimensions A, D, C, E in figure 4a. The dimensions in the CAD model are given in both metric and imperial units (in brackets) in this figure to facilitate direct comparison with the real picture on the right. The distance between the vertical bars holding the drape, denoted by dimension F in Figure 4b, was also implemented in the CAD model.

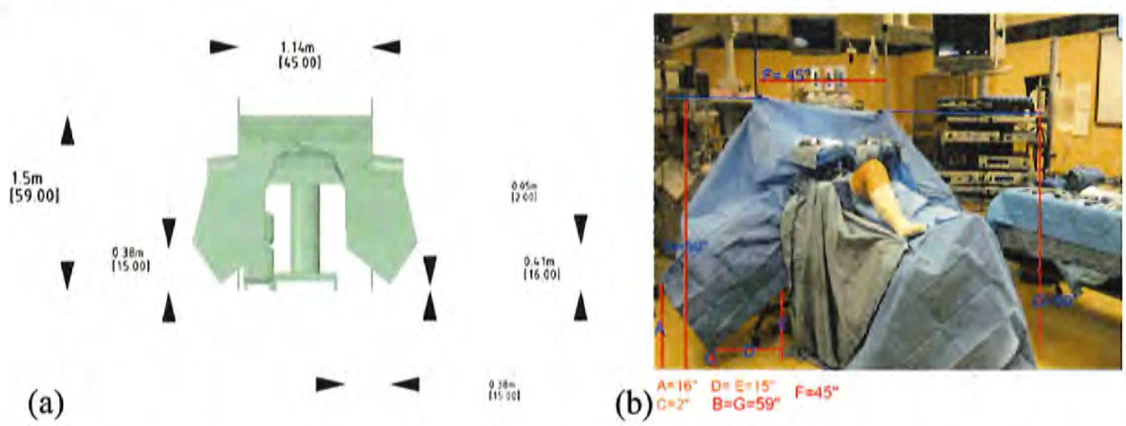

Figure 4: Drape dimensions and configuration: (a) model developed to match the drape dimensions, (b) actual drape picture in an OR room. The dimensions are shown in both metric and imperial units (in brackets).

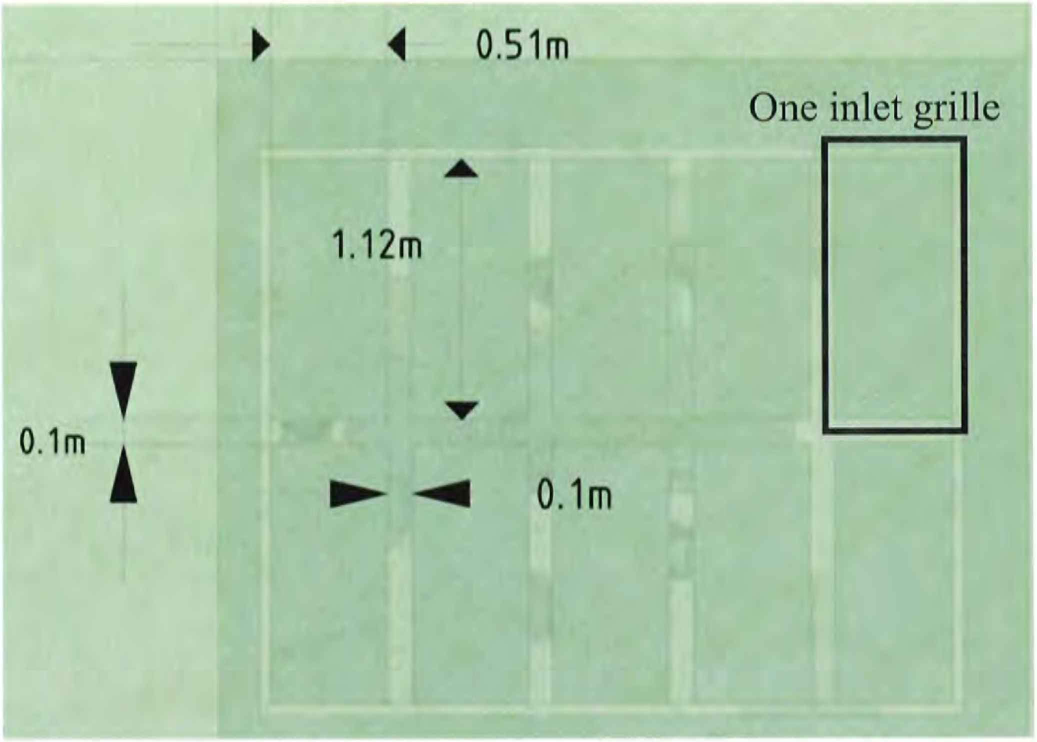

Figure 5: Ten inlet grills to supply clean filtered air into the OR.

The CAD model included ten inlet grilles (figure 5) for supplying clean filtered air to the OR. Each inlet grille is 0.51m in width and 1.12m in length. All ten grilles are of the same size. There is a gap of 0.1m between the neighboring grilles at all sides.

There are four exhaust (or outlet) vents, two on each side wall. Figure 6 shows two outlet grilles (with the other two outlets located on the opposite wall). Each outlet grille is 0.71m in width and 0.71m in length.

3 Numerical Simulation

A state-of-the art, fully parallel, unstructured, co-located grid flow solver based on principles of kinetic energy conservation for large-eddy simulation (Moin & Apte, 2006) of turbulent flow in the limit of zero-Mach numbers is used in this study. This solver is MPI-based, uses algebraic multigrid for the pressure Poisson equation, and third-order WENO-based scheme for transport of scalar fields such as temperature. It has been thoroughly validated for a number of different particle-laden turbulent flows (Apte *et al.*, 2003*b*,*a*, 2008*a*, 2009, 2008*b*) including swirling turbulent flow

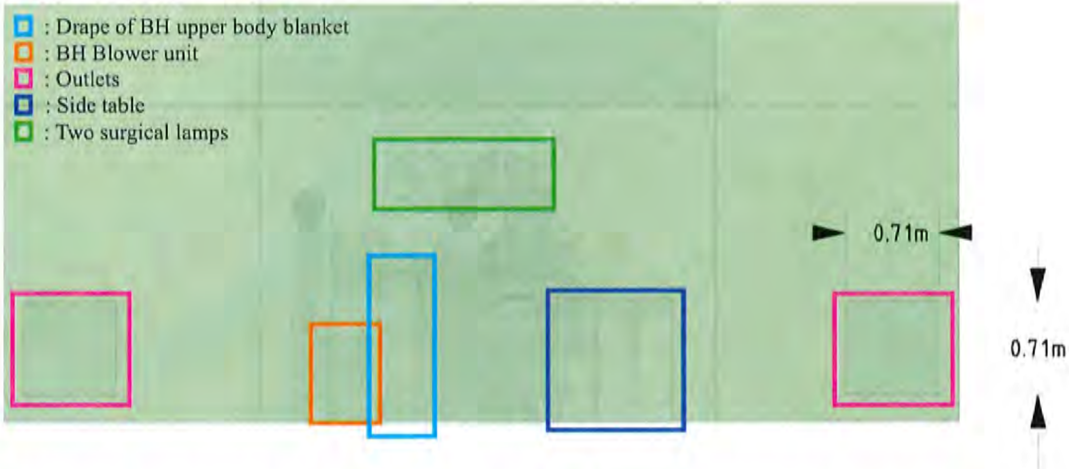

Figure 6: Outlet (exhaust) grilles for air exit from the room. Out of the four outlets in the CAD model, only two are visible in the picture. The other two outlets are on the the opposite wall.

in a co-axial combustor, turbulent reacting flow, as well as spray combustion in a realistic Pratt and Whitney gas-turbine combustion chamber (Moin & Apte, 2006; Mahesh *et al.*, 2006).

3.1 Large-eddy Simulation (LES): Introduction and Need

The physics of turbulent air flow containing heated buoyant plumes and laden with inertial particles in a real-life operating room is highly complex. Simulating such flows with predictive capability is difficult as turbulence, by nature, consists of a broad range of length- and time-scales and is inherently three-dimensional. In addition, the geometry of a realistic operating room consists of complex surfaces involving surgeons, operating table, surgical lights, patient, among other. If a probe measures the velocity at a certain location in such a flow, the velocity signal will show a broad range of frequencies and fluctuations around a mean. A typical kinetic energy spectrum obtained via Fourier transform of turbulent velocity field is shown in figure 7, especially for moderate to large Reynolds numbers. The spectrum is broad-band with large amount of kinetic energy per wavenumber present at large scales (small wavenumbers) and small amount of energy present at smaller scales (larger wavenumbers). There also exists an inertial range, scales in this regime simply transfer the energy from larger scales to smaller scales through a process commonly known as the energy cascade (Pope, 2000). As the Reynolds number increases, this spectrum is known to broaden. The largest scales ($\mathscr{L}$) of motion are typically confined by the size of the domain (for example, size of the inlet jet

or size of the room). However, as the Reynolds number increases, the smallest scales of motion (known as the Kolmogorov scales, η) are reduced until the kinetic energy is dissipated into internal energy by the viscous effects. Owing to this broad range of scales, prediction of turbulent flows at large Reynolds numbers becomes difficult and is only possible if the behavior of all scales of motion is captured properly.

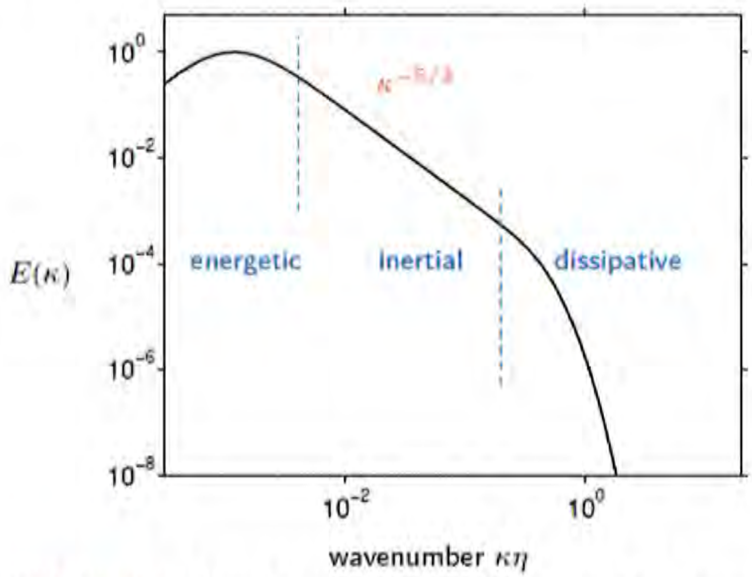

Figure 7: Schematic of a turbulence kinetic energy spectrum showing energy per wavenumber as a function of the wavenumber (Pope, 2000). The inertial range of scales is indicated by the -5/3 slope line that separates the energetic large scales and dissipative small scales of turbulence. In DNS, the grid resolution is fine enough to capture all scales, whereas in LES, the grid resolution is coarser (typically 10 times the Kolmogorov length scale), placing the grid cut-off somewhere in the inertial range.

Three basic approaches can be identified for prediction of turbulent flows: (i) direct numerical simulation (DNS), (ii) Reynolds averaged Navier-Stokes (RANS) modeling, and (iii) large-eddy simulation (LES), and are briefly described below.

DNS: In direct numerical simulation (DNS), the Navier-Stokes equations are solved on a computational grid that is fine enough, in space and time, to directly capture *all* the scales associated with the fluid flow motion without requiring any additional models. This means that the computational grid in three-dimensions is small enough to capture the smallest scales of turbulence and the time-step is small enough to capture the smallest time-scale associated with the flow. Using scaling arguments based on the Kolmogorov hypotheses (Tennekes & Lumley, 1972; Pope, 2000) used in the theory of turbulence, it can be shown that for a simple homogeneous, isotropic turbulence in a box, the grid resolution requirement ($\Delta \sim \mathscr{L}/\eta$; where $\mathscr{L}$ is the size of the large, energy-containing

eddies) for DNS varies as $Re_{\mathscr{L}}^{3/4}$, where $Re_{\mathscr{L}}$ is the Reynolds number based on $\mathscr{L}$ and the velocity fluctuations u, in one coordinate. Hence, the total number of mesh points needed in three-dimensions varies as $Re_{\mathscr{L}}^{9/4}$. A simple isotropic turbulence in a box at $Re_{\mathscr{L}} = 2000$, would require computational grid containing about 27M control volumes ($= 300^3$). In addition, based on numerical constraints of a computational solver, for a fluid flow of unit velocity, the grid spacings (Δ) and the time-steps (Δt) are roughly of the same order of magnitude ($\mathrm{CFL} = \mathrm{u}\Delta \mathrm{t}/\Delta \sim 1$) and thus the spatio-temporal resolution will require a computational power that increases as $Re_{\mathscr{L}}^{3}$. Owing to the grid requirements and associated computational costs, DNS is not practical for realistic engineering applications and is restricted to canonical geometries and flow problems to study the fundamentals of turbulence (Moin & Mahesh, 1998).

RANS: According to the above discussion, the computation of practical turbulent flows relies predominantly on the Reynolds-averaged Navier-Stokes (RANS) equations approach. In RANS, the governing equations are averaged in time to obtain equations for the *time-averaged* velocity field, $\overline{u}(\mathbf{x})$. Thus, in this approach, only the mean velocity field that varies in space is obtained, and all information about the time-dependent fluctuations of the velocity field around the mean flow is lost. Because the momentum equations are non-linear (owing to the inertial, advective terms), a time-average of the non-linear term creates additional quantities that are unknown, giving rise to the classical closure problem of turbulence (Tennekes & Lumley, 1972; Pope, 2000). In order to evaluate these terms, models are introduced wherein the effect of the entire spectrum of turbulence (involving the large, inertial, and small scales shown in Figure 7) is completely modeled. This is usually done by introducing two additional transport equations for the turbulence kinetic energy (k) and the kinetic energy dissipation rate (ε), giving rise to the $k - \varepsilon$ model. It should be noted that the transport equations for k and ε also contain a large number of unknown, unclosed terms which also need to be modeled. The model constants are obtained by fitting the RANS predictions to the experimental data on simple, canonical flows such as wall bounded channel flow, isotropic turbulence, or free-shear flows. Because these models and model constants *are not universal*, using them for a complex flow such as air circulation in an operating room, invariably provides inaccurate results. Experimental data is necessary to adjust the model constants and thus the RANS models are not *predictive*. However, since only the time-averaged velocity field is calculated, the RANS approach is computationally the least expensive because it does not require the spatio-temporal resolution

necessary for the DNS studies. There are modified approaches, wherein the large-time scale variations are captured by solving the RANS equations in an unsteady manner. These unsteady-RANS simulations also suffer from the same hypotheses and models used for the basic RANS and their predictive capability is also poor.

LES: The energy spectrum (figure 7) shows that a substantial portion of the turbulence kinetic energy (TKE) is contained in the large-scales, known as the energy containing scales. In LES, only the contribution of the large, energetic structures to momentum and energy transfer is computed exactly, and the effect of the small scales, also termed as unresolved or subgrid scales, of turbulence is modeled. Since the small scales tend to be more homogeneous, and less affected by the domain boundary conditions as compared to the large eddies, then the subgrid closure models used in LES are universal and can be applied to a range of flows as compared to the RANS closures. Owing to these differences between the LES and RANS approaches, LES has been shown to be far superior to RANS in accurately predicting turbulent mixing of momentum and scalar (Mahesh *et al.*, 2004), pollutant and heat transport, combustion (Pierce, 2001)), and particle dispersion (Apte *et al.*, 2003*b*; Ham *et al.*, 2003).

In LES, the Navier-Stokes (NS) equations are filtered in space (as opposed to time as done in RANS) using a local filter (Gaussian, box, spectral etc.) to obtain a filtered velocity field, $\overline{u}_i(\mathbf{x},t)$ (Pope, 2000). Using the local grid resolution as a spatial filter, the small, under-resolved scales of turbulence are filtered out. However, applying the filtering operation to the inertial, non-linear terms in the NS equations, gives rise to the closure problem. The resulting additional terms need to be modeled. Most often, the models used to close the unknown terms, known as Reynolds stresses, are based on the same types of assumptions, such as the gradient diffusion hypothesis, as employed in RANS. However, the fact that, in LES, modeling is only applied to capture the effect of unresolved, subgrid scales, which are homogeneous and universal, the closure models work very well in a wide range of problems. A dynamic procedure, typically employed in LES subgrid scale modeling, renders the modeling process completely free of any tuning parameters in contrast to RANS. All constants in the model are obtained directly in the calculations and are not set by the user. As long as the grid resolution is sufficient such that the motion of the energy-containing large eddies is captured correctly, unlike RANS, the LES approach can then be used in a truly predictive manner.

In addition, away from the boundaries, a typical LES grid can be 10 times coarser than a DNS grid in each direction (that is 10 times the Kolmogorov scale), resulting in significant savings in the computational cost. This makes LES an attractive tool compared to the DNS. However, there are still several challenges. Just like DNS, the LES computations are inherently three-dimensional and time-dependent, making the cost of the calculation large as the important large-scale spatio-temporal variations in the flow must still be resolved. In addition, the computational algorithm must not add large amounts of numerical dissipation as it has been shown that dissipative numerical approaches mask the physical dissipation present in turbulent flows and provide inaccurate predictions (Mittal & Moin, 1997; Kravchenko & Moin, 1997). These restrictions typically limits the use of LES to simple, canonical geometries and flows (as free-shear flows (jets, wakes, shear layers), wall bounded channel flows, or flow over backward facing step (Pierce, 2001; Piomelli, 2014)) for which the underlying algorithms are based on a non-dissipative schemes developed for structured Cartesian grids.

Applying LES to the complex and realistic geometries of engineering applications such as the the operating room; including the operating table, surgeons, patient and other equipment, or other applications such as gas-turbine combustors, propellers, among others, requires use of arbitrary shaped unstructured meshes. In recent years; however, considerable progress has been made in handling complex configurations and unstructured grids accurately (Piomelli, 2014). Mahesh *et al.* (2004); Ham *et al.* (2003); Mahesh *et al.* (2006) have developed a numerical algorithm for high-fidelity simulations of incompressible, variable density flows on unstructured grids. A novelty of their algorithm is that it is discretely energy-conserving which makes it robust at high Reynolds numbers *without numerical dissipation*. This makes LES applicable to complex configurations and it has been successfully used to simulate multiphase, spray combustion processes in a realistic Pratt and Whitney gas-turbine combustion chamber (Moin & Apte, 2006; Mahesh *et al.*, 2006; Apte *et al.*, 2009). These simulations are still computationally intensive, often requiring 3–4 weeks of simulation on parallel supercomputers, however, the detailed data obtained from the simulations are of significant importance to researchers and engineers since such information could not be obtained from laboratory experiments. This has led several gas-turbine industries, who generally use RANS in their design cycle, to switch from RANS-based approaches to LES.

Furthermore, turbulent flows laden with dispersed particles (either solid particles, or droplets or

bubbles) involve the complexity of capturing the dynamics of turbulence as well as that of the dispersed phase. The physics of particle-turbulence interactions is complex (Elghobashi, 1994, 2006), and depending upon the magnitudes of the particle relaxation times relative to the Kolmogorov time scales, heavier-than-fluid particles (solid particles, droplets, squames) can exhibit behavior such as preferential clustering on the edges of vortices (Eaton & Fessler, 1994; Rouson & Eaton, 2001; Kulick *et al.*, 2006; Reade & Collins, 2000; Eaton & Segura, 2006), whereas, lighter-than-fluid particles (bubbles) can break the vortical structures (Ferrante & Elghobashi, 2004; Druzhinin & Elghobashi, 1998; Ferrante & Elghobashi, 2007; Sridhar & Katz, 1999).

RANS is not capable of capturing this complex physics of particles interacting with turbulence because only the mean velocity field is computed by RANS, yet it is commonly used owing to its low cost. However, if the objective is to accurately simulate the dispersion of inertial particles in a turbulent flow, then a three-dimensional, instantaneous velocity field is necessary to calculate the forces on the particles. Inertial particle trajectories and dispersion are strongly influenced by the spatio-temporal variations in the velocity fields. Hence, using only the mean velocity field provides inaccurate dispersion characteristics. An improved RANS to capture the transient effects uses a model for particle motion that utilizes the local turbulence kinetic energy and introduces some randomness (typically a Gaussian distribution) in the particle equations (Sommerfeld *et al.*, 1992) is necessary. Recent work on the dispersion of squames in an operating room and the effect of different inlet air flow conditions used RANS together with such a stochastic, Lagrangian particle-tracking algorithm (Memarzadeh & Manning, 2002). Such a model must be tuned by the user to calculate different particle-laden flows and can behave differently in free-shear versus wall-bounded flows. As can be seen from the results presented by Sommerfeld *et al.* (1992); Chen & Pereira (1998), particle dispersion predicted using a RANS approach for turbulent flows in a wide range of applications involving swirling, separated flows do not agree with the experimental data. However, the same flowfields computed using LES (Apte *et al.*, 2003*b*; Moin & Apte, 2006; Apte *et al.*, 2008*b*, 2009) show considerably better predictive capability and agree with the experimental data very well. In LES, the resolved instantaneous velocity field, which varies in time and space, at the particle location is used to compute the forces on the particles as opposed to the time-averaged velocity in RANS. Accordingly, the effect of the energetic, turbulence scales (of the order of the grid resolution and larger) are completely captured in LES, thus predicting its impact on particle dispersion directly.

To summarize, it is essential to use LES instead of RANS to accurately predict the air circulation and dispersion of squames in an operating room for the following reasons:

- LES provides a three-dimensional, instantaneous flow field (velocity, pressure, temperature) of the resolved, energetic, large-scales, and only models the effect of the unresolved, subgrid (small) scales of turbulence. The subgrid scales tend to be more homogeneous, and less affected by the domain boundary conditions and thus allow the appropriate use of the eddy-viscosity models to calculate their stresses. RANS, on the other hand, only calculates the time-averaged velocity field and models the effect of all the scales of turbulence on the mean flow, resulting in unrealistic flow predictions.

- The subgrid model constants used in LES can be obtained dynamically, thus making LES truly predictive without any user-defined tuning parameters, whereas RANS model constants are not universal and often require manual tuning.

- LES is considerably more accurate in predicting passive as well as inertial particle dispersion since the instantaneous, three-dimensional resolved velocity field is available for computing the forces on the particles. In RANS, a random perturbation must be added to the mean velocity field to construct an artificial, time-dependent, three-dimensional velocity field needed to calculate the particle motion. This renders the calculation of particle dispersion highly inaccurate.

3.2 Governing Equations

The air flow in an operating room involves temperature variations within the room owing to various sources of heat; such as the operating room lamps, heat radiated from the medical personnel bodies, hot air discharged from a blower system, among others. The local temperature variations change the local air density. However, since the air flow in the room is low-speed (maximum velocity on the order of, $u \sim 0.5$ m/s compared to speed of sound of around, $c \sim 343$ m/s), the Mach number (u/c), that represents the ratio of acoustic to convective time-scales, is small ($<< 0.01$). Small Mach numbers mean that the convective time-scales are much larger than acoustic time-scales, and thus the compressibility effects are negligibly small. Under these conditions, the variable-density equations in the limit of zero-Mach number are valid and the pressure field at any point within the

domain and time can be split into a bulk thermodynamic pressure, P_0, and the dynamic pressure p that appears in the momentum equation,

$$P(x,t) = P_0(t) + p(x,t). \tag{1}$$

The background thermodynamic pressure (P_0) for the operating room is assumed constant and equal to the atmospheric pressure, $P_0 = 1$ atm.. Accordingly, the density of the air (assumed as ideal gas) varies only with the local temperature field according to the equation of state as,

$$\rho = \frac{P_0 R_{\text{universal}} T}{M_{\text{air}}}, \tag{2}$$

where $R_{\text{universal}}$ is the universal gas constant, M_{air} is the molecular mass of the air, and T is the absolute temperature. The governing equations for large-eddy simulation of turbulent flows with variable density in the limit of zero Mach number are given below.

3.2.1 Gas-phase equations

The spatially filtered, Favre averaged, governing equations used for large-eddy simulation of particle-laden, turbulent air flow with heat transfer and buoyancy effects are given as,

$$\frac{\partial \overline{\rho_g}}{\partial t} + \frac{\partial \overline{\rho_g} \tilde{u}_j}{\partial x_j} = 0. \tag{3}$$

$$\frac{\partial \overline{\rho_g} \tilde{u}_i}{\partial t} + \frac{\partial \overline{\rho_g} \tilde{u}_i \tilde{u}_j}{\partial x_j} = -\frac{\partial \overline{p}}{\partial x_i} + \frac{\partial}{\partial x_j}\left(2\overline{\mu}\tilde{S}_{ij}\right) - \frac{\partial q^r_{ij}}{\partial x_j} + (\overline{\rho_g} - \rho_0) g_i, \tag{4}$$

$$\frac{\partial \overline{\rho_g} \tilde{h}}{\partial t} + \frac{\partial \overline{\rho_g} \tilde{h} \tilde{u}_j}{\partial x_j} = \frac{\partial}{\partial x_j}\left(\overline{\rho_g} \tilde{\alpha}_h \frac{\partial \tilde{h}}{\partial x_j}\right) - \frac{\partial q^r_{hj}}{\partial x_j}, \tag{5}$$

where

$$\tilde{S}_{ij} = \frac{1}{2}\left(\frac{\partial \tilde{u}_i}{\partial x_j} + \frac{\partial \tilde{u}_j}{\partial x_i}\right) - \frac{1}{3}\delta_{ij}\frac{\partial \tilde{u}_k}{\partial x_k}. \tag{6}$$

Here, $\overline{\rho_g}$ is the filtered density, $\tilde{u}_i$ is the Favre averaged velocity field, $\overline{p}$ is the filtered pressure, μ is the dynamic viscosity, $\alpha_h = k/\overline{\rho}_g C_p$, is the thermal diffusivity (k is the conductivity and C_p the specific heat at constant pressure), g_i is the gravitational acceleration, and $\tilde{S}_{ij}$ is the filtered rate of

strain. In addition, the specific enthalpy, h, is given as,

$$h = \frac{T - T_0}{T_0}, \tag{7}$$

where T is the local temperature. Also, T_0 and ρ_0 are the temperature and density fields corresponding to the air inlet conditions and pressure of P_0.

The additional terms q^r_{ij} and q^r_{hj} in the momentum and the enthalpy equations, respectively, represent the subgrid-scale stress and energy flux and are modeled using the dynamic Smagorinsky model by Moin *et al.* (1991) as demonstrated by Pierce & Moin (1998*a*). The unclosed terms in Eqs. (4-5) are modeled using the gradient-diffusion hypothesis with eddy-viscosity/diffusivity,

$$q^r_{ij} = \overline{\rho_g}(\tilde{u}_i\tilde{u}_j - \widetilde{u_i u_j}) = 2\mu_t \tilde{S}_{ij} - \frac{1}{3}\overline{\rho_g} q^2 \delta_{ij}, \tag{8}$$

$$q^r_{hj} = \overline{\rho_g}(\tilde{h}\tilde{u}_j - \widetilde{hu_j}) = \overline{\rho_g}\alpha_t \frac{\partial \tilde{h}}{\partial x_j}, \tag{9}$$

where the eddy viscosity (μ_t) and eddy thermal diffusivity α_t are modeled as,

$$\mu_t = C_\mu \overline{\rho_g}\overline{\Delta}^2 \sqrt{\widetilde{S_{ij}}\widetilde{S_{ij}}}, \tag{10}$$

$$\overline{\rho_g}\alpha_t = C_\alpha \overline{\rho_g}\overline{\Delta}^2 \sqrt{\widetilde{S_{ij}}\widetilde{S_{ij}}}. \tag{11}$$

The coefficients C_μ, C_α are calculated dynamically at each time-step and for each grid point using the dynamic procedure as outlined by Germano *et al.* (1991). For the unstructured grids, the filter width $\overline{\Delta}$ is taken as $V_{cv}^{1/3}$ where V_{cv} is the volume of the grid element.

3.2.2 Equations for calculating the trajectories of individual squames

The human skin cells or squames typically are disc-shaped with a diameter ranging from 4–20μm and a thickness of 3–5μm with density close to that of liquid water (1000kg/m^3) (Noble *et al.*, 1963; Noble, 1975; Snyder, 2009). Although the squames shape is more disc-like, in the present work they are considered as non-deformable, spherical in shape. A spherical shape is assumed as the dynamics of the spherical particle is easier to calculate and also the lift and drag forces on small particles of disc or spherical shape are not significantly different. The diameter of the spherical

particle is assumed to be 10 microns and matches an average settling velocity of a disc-shaped particle considering the mean flow normal and parallel to the disc (see Appendix A). Recent work using RANS model by Memarzadeh & Manning (2002); Memarzadeh (2003) also approximates the squames particles as spherical with a size of 10 microns.

An Eulerian-Lagrangian approach is used wherein individual squames trajectories will be tracked in a Lagrangian frame. The different forces on the particles will be calculated using standard closure laws. The effect of the particles on the fluid flow will be negligible owing to their small concentration and thus a one-way coupling approach is adopted, wherein the squame motion uses the fluid flow parameters (velocity) to compute the forces, however, the effect of squames on the fluid momentum is neglected (Elghobashi, 1994, 2006). In addition, since the volume fraction of the squames in an operating room is not very large ($<< 10^{-3}$), collisions amongst the squames are neglected. The squame particle motion equation is that of Maxey & Riley (1983),

$$\frac{d}{dt}(\mathbf{x}_p) = \mathbf{u}_p \tag{12}$$

$$m_p\frac{d}{dt}(\mathbf{u}_p) = \mathbf{F}_g + \mathbf{F}_d + \mathbf{F}_\ell + \mathbf{F}_{am} + \mathbf{F}_p + \mathbf{F}_H, \tag{13}$$

where $\mathbf{x}_p$ is the particle (squames) centroid location, m_p is the mass of an individual particle, $\mathbf{u}_p$ is the particle velocity, $\mathbf{F}_g$ is the gravitational force, $\mathbf{F}_d$ is the drag force, $\mathbf{F}_\ell$ is the lift force, $\mathbf{F}_{am}$ is the added mass force, $\mathbf{F}_p$ is the pressure force, and $\mathbf{F}_H$ is the Basset history force.

The large ratio of particle density to air density, ρ_p/ρ_g, renders both the Basset history force and the added mass force negligible compared to the drag force. The ratio of the Saffman lift to the drag force is given by, $F_\ell/F_{drag} \sim \rho_g d_p^2 (du/dy)^{1/2}/\mu$, and is dependent on the shear rate and particle diameter. For particles with small diameter and low inertia this force can also be neglected in comparison to the drag force (Crowe *et al.*, 1996; Saffman, 1965). However, the lift force is incorporated in our calculations to account for the saltation of the squame particles from the operating room floor. The gravity, drag and lift forces are given as,

$$\mathbf{F}_g = (\rho_p - \overline{\rho}_g)\mathcal{V}_p \mathbf{g}; \quad \mathbf{g} = -9.81 m/s^2 \tag{14}$$

$$\mathbf{F}_d = -\frac{1}{8}C_d\overline{\rho}_g\pi d_p^2|\mathbf{u}_p - \tilde{\mathbf{u}}_{g,p}|(\mathbf{u}_p - \mathbf{u}_{g,b});\ \ C_d = \frac{24}{Re_p}(1+0.15Re_p^{0.687}), \tag{15}$$

$$\mathbf{F}_\ell = -C_\ell m_p\frac{\overline{\rho}_g}{\rho_p}(\mathbf{u}_p - \tilde{\mathbf{u}}_{g,p}) \times (\nabla \times \tilde{\mathbf{u}}_g)_p;\ \ C_\ell = \frac{1.61 \times 6}{\pi d_p}\sqrt{\frac{\mu}{\overline{\rho}_g}|(\nabla \times \tilde{\mathbf{u}}_g)_p|} \tag{16}$$

where the subscript p represents the squame particle, $\tilde{\mathbf{u}}_{g,p}$ represents the fluid velocity interpolated at the particle center location, $\mathcal{V}_p$ is the particle volume, d_p is the particle diameter, $Re_p = \overline{\rho}_g|\mathbf{u}_p - \tilde{\mathbf{u}}_{g,p}|d_p/\mu$ is the particle Reynolds number, C_d is the drag coefficient, C_ℓ is the lift coefficient.

The gas-phase velocity, $\tilde{\mathbf{u}}_g$, in the particle equations above, is computed at individual particle locations within a control volume using a generalized, tri-linear interpolation scheme for arbitrary shaped elements. Introducing higher order accurate interpolation is straight forward; however, it was found that tri-linear interpolation is sufficient to represent the gas-phase velocity field at particle locations. As mentioned earlier, in LES of particle-laden flows, the particles are presumed to be *subgrid*, and the particle-size is smaller than the filter-width used. The gas-phase velocity field required in equations (12) and (13) is the total (unfiltered) velocity, however, only the filtered velocity field is computed in equations (4). The direct effect of the unresolved (subgrid) velocity fluctuations on particle trajectories depends on the particle relaxation time-scale, and the subgrid kinetic energy. Pozorski & Apte (2009) performed a systematic study of the direct effect of subgrid scale velocity on particle motion for forced isotropic turbulence. It was shown that, in poorly resolved regions, where the subgrid kinetic energy is more than 30%, the effect on particle motion is more pronounced. A stochastic model reconstructing the subgrid-scale velocity in a statistical sense was developed (Pozorski & Apte, 2009). However, in well resolved regions, where the amount of energy in the subgrid scales is small, this direct effect was negligible. In the present work, the direct effect of subgrid scale velocity on the droplet motion is neglected. However, it should be noted that the particles *do feel* the subgrid scale stresses through the subgrid model that affects the resolved velocity field. For well-resolved LES of swirling, separated flows with the subgrid scale energy content much smaller than the resolved scales, the direct effect is shown to be small (Apte *et al.*, 2003*b*, 2009). This is the main advantage of LES as compared to RANS. In RANS, only the time-average mean velocity is available, and all scales of turbulence affecting the instantaneous fluctuations around the mean

must be modeled. Approximating the effect of turbulent fluctuations on the particle dispersion is thus necessary for RANS, whereas, it is implicitly accounted for in the LES.

Equations (12,13) are integrated using a fourth-order Runge-Kutta time-stepping algorithm. After obtaining the new particle positions, the particles are relocated, particles that cross interprocessor boundaries are duly transferred, boundary conditions on particles crossing boundaries are applied, source terms in the gas-phase equation are computed, and the computation is further advanced. Solving these Lagrangian equations thus requires addressing the following key issues: (i) efficient search and location of particles on an unstructured grid (ii) interpolation of gas-phase properties to the particle location for arbitrarily shaped control volumes (iii) inter-processor particle transfer. The details on efficiently locating the particles on unstructured grids, search algorithms for particles, and interpolation schemes can be found in the work by Apte *et al.* (2003*b*, 2009).

In addition, if the squames impact internal boundaries, a simple, perfectly elastic specular reflection is assumed wherein the squames reverse the wall-normal velocity and preserve the wall-tangential velocity. If the squames impact the patient's knee or the inlet (suction port) of the 3M^{TM} Bair Hugger^{TM} blower system, they are assumed to stick to the surface and are no longer advanced in the computations.

3.3 Computational grid

Use of high quality computational mesh is critical in LES for accurate prediction of the turbulent flow, but also having a stable numerical solution. However, to handle complex configurations, use of hybrid elements involving tetrahedrons, pyramids, hexagons and wedges, etc. is common in a typical computational grid. This helps with the grid generation surrounding complex features such as the operating table, the surgeons, the patient and the drape, for example. The transitions from one type of grid element to another; however, can lead to skewed elements. It is thus critical that the numerical algorithm be robust, stable and accurate at high Reynolds numbers on skewed or bad grid elements. A numerical algorithm developed for arbitrary shaped unstructured grids (Mahesh *et al.*, 2004; Ham *et al.*, 2003; Ham & Iaccarino, 2004; Mahesh *et al.*, 2006) that is based on kinetic energy conservation principles offers the much needed robustness and accuracy on such grids without resorting to explicit artificial dissipation. As discussed below, we use a research solver based on

such an algorithm.

For the present study, a computational mesh (figure 8) was generated using the CAD model described earlier to facilitate predictive large eddy simulations. The mesh was generated using both tetrahedral and hexahedral cells. The transition of mesh from tetrahedral cells to hexahedral cells was done using a combination of pyramid and wedge type cells. Care was taken to generate a computational grid that minimizes the grid skewness as much as possible. As shown below, in the regions away from the complex OR configuration involving the surgeons, the tables, the patient and the drape, a mostly hex-dominant mesh is used. As one approaches closer to the operating table, the computational grid is transitioned to a predominantly tetrahedra-based mesh (see figure 8b). The total mesh count for the computational domain is about 66 million.

Figure 9 shows the grid resolution near the air inlet cross-sections. The grid is appropriately refined to capture the shear layer generated by the inlet flow between the grilles. The mesh surrounding the OR table, patient, surgeons, side tables, the blower, and surgical lamps is predominantly tetrahedral. The tetrahedral mesh was carefully refined to capture surface curvature. Extra refinement was performed near surfaces which were in close proximity to other surfaces. This enhanced mesh refinement is to ensures that the effect of surface shapes on the flow and particles going around them will be captured by the simulation (figure 10a,b.)

As is shown in the above figures, a high quality mesh was generated for the present LES investigation. The minimum tetrahedral cell size (defined as cube root of the cell volume) used near all key regions such as drape, patient, operating bed, surgeons, etc. was around 1mm. Smallest grid spacing in proximity regions resolving the gaps between closely placed surfaces is 0.7mm. The coarsest tetrahedral cell size used away from the key regions is 2.5cm. As mentioned earlier in the report a fine mesh was used near the inlet regions to resolve the flow entering the operating room. A uniform hexahedral cell size of 2.5cm was used to resolve the air inlet grille faces with 20 cells along its width and 44 cells along its length. The gaps between the inlet grilles were resolved using a finer mesh with each cell size of 0.63cm. To capture the inlet air flow structures properly, a refined uniform mesh of 0.38cm was used along the flow direction. Finally, a uniform cell size of 2.5cm was used to resolve each outlet grille with 28 cells along its width and 28 cells along its length. Various mesh metrics were checked to ensure that the quality of the generated mesh was good. Figure 11a shows histogram plot of cell skewness in the mesh. The average skewness was

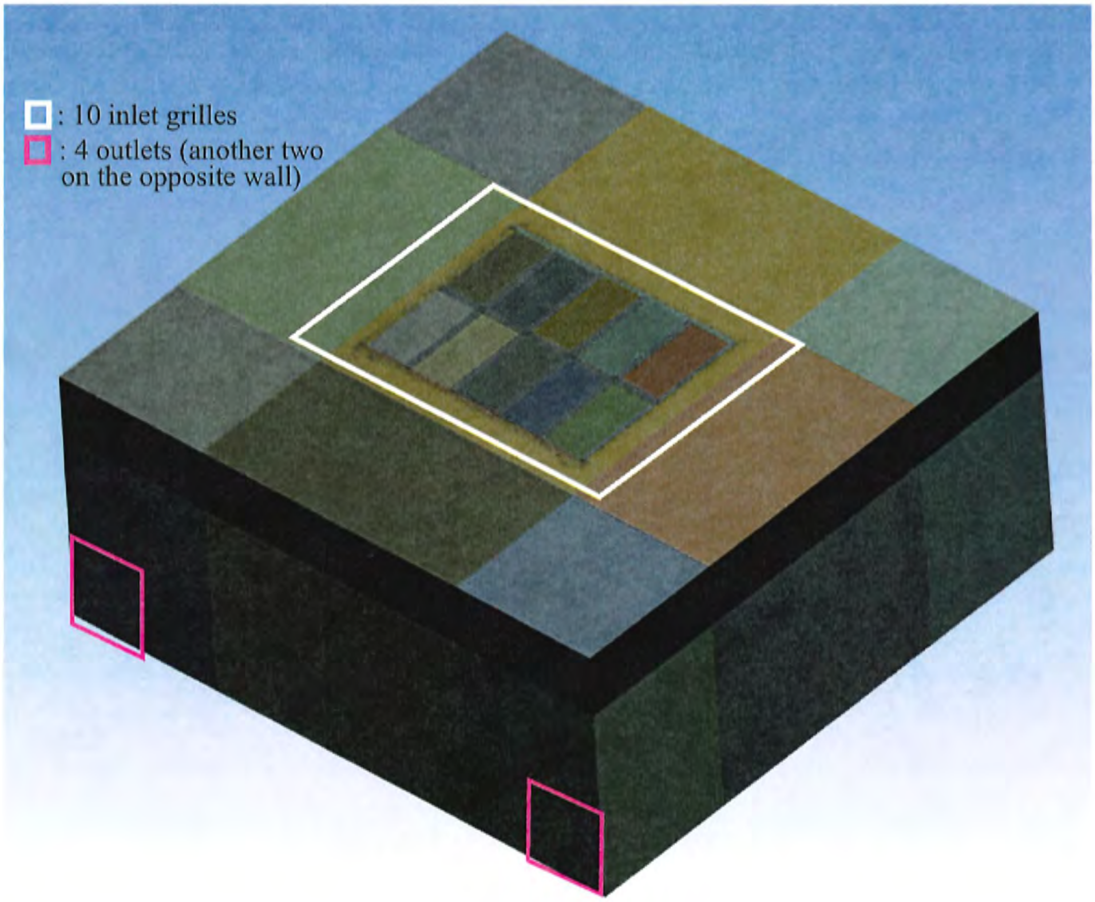

(a)

(b)

Figure 8: Computational mesh for the operating room model consisting of about 66M hybrid grid elements consisting of hexagons, tetrahedrons, pyramids and wedges: (a) the full 3D mesh, (b) cross-sectional slice showing hex-dominant mesh in the inlet and outlet regions and a tetahedral mesh near the operating table.

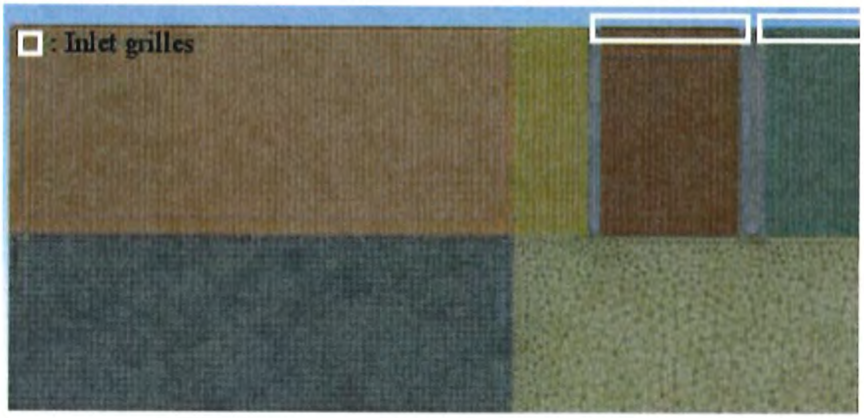

(a)

(b)

Figure 9: A cross section cut showing fine mesh near the ceiling of the room: (a) top view zoom-in, (b) top view showing all air inlet grilles.

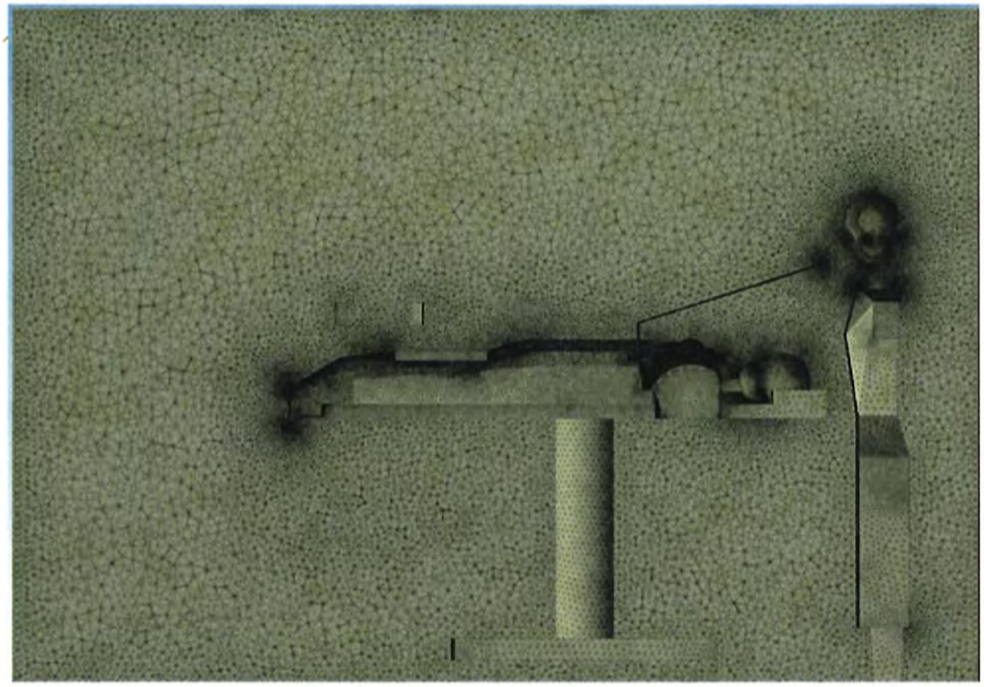

(a)

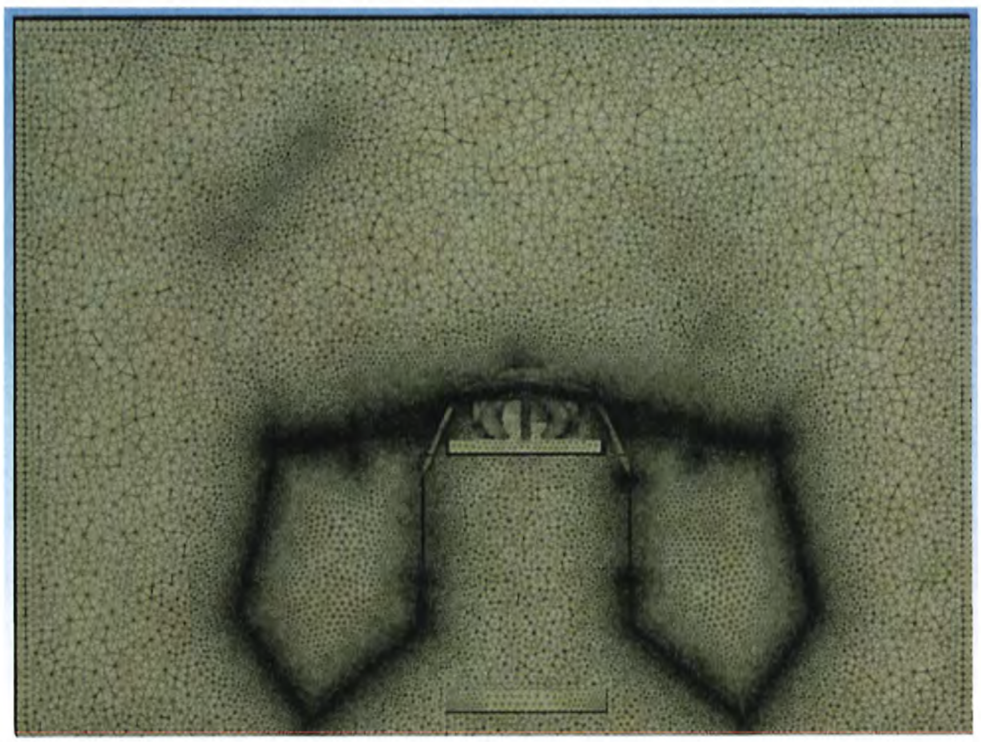

(b)

Figure 10: Mesh refinement near curved surfaces and surfaces that are in close proximity to others: (a) side view showing the entire operating table, (b) side view showing drapes.

0.14 and with maximum skewness was 0.91. Only 0.018% of cells had total skewness greater than 0.8 indicating the high quality of cells in the mesh. Another mesh metric that was checked was the aspect ratio of cells. The maximum aspect ratio was 16.2 and the average cell aspect ratio was 2.9, which indicate that a majority of cells in the mesh were mostly uniform (see figure 11b).

3.4 Boundary Conditions

This subsection provides details of all boundary conditions used in the calculation, starting with operating room (OR) air inlet conditions, heat sources, BH hot air blower inflow (suction) and outflow, and OR air outlet conditions.

3.4.1 Inlet boundary conditions

The dimensions of the operating room are shown in Table 1. As shown, there are 10 inlet grilles supplying air. The net supply air volumetric flow rate, $\dot{V}$, is 1.10436 $\mathrm{m^3/s}$ (0.39 $\mathrm{ft^3/s}$). Using the inlet flow rates, the air changes per hour (ACH) of the room is calculated as follows,

$$\mathrm{ACH} = \dot{V} \times 3600/(LWH) = 24.45 \text{ per hour,} \tag{17}$$

where L, W and H are the room length (in x), width (in y) and height (in z) directions. The ACH is according to the ASHRAE handbook Memarzadeh & Manning (2002), which suggests the ACH to be about 25 per hour for an operating room with recirculating air system.

The inlet boundary conditions are imposed at the 10 grilles on the ceiling of the operating room to model the inlet part of the forced ventilation system. The average inlet velocity, $\overline{U}_{in}$, is found to be 0.1933m/s based on,

$$\overline{U}_{in} = \dot{V}/(10 \times A_{grill}), \tag{18}$$

where A_{grill} is the area of the cross-section ($1.12 \times 0.51 = 0.5712\mathrm{m^2}$) and $\dot{V} = 1.1044\mathrm{m^3/s}$ ($39\mathrm{ft^3/s}$) is the net inlet volumetric flow rate. The air temperature of the inlet flow, T_{in}, is set to 59°F (15°C).

Based on Reynolds number for the inlet grilles, $Re_{in} = 9226.54$ (Table 1), the inlet flow is turbulent. In order to have completely predictive numerical simulation and to minimize the effect of boundary conditions, it is necessary to impose a proper, fully developed turbulent flow field at the in-

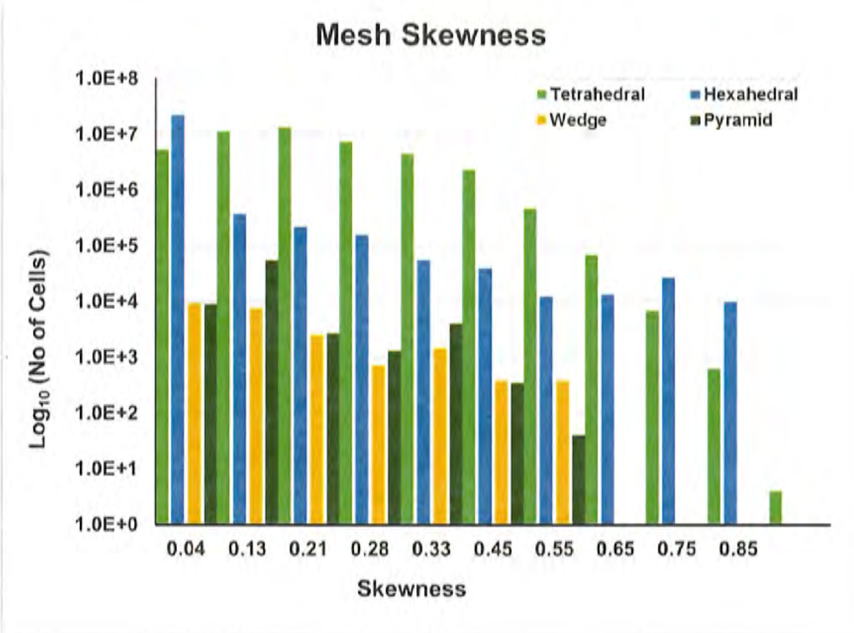

(a)

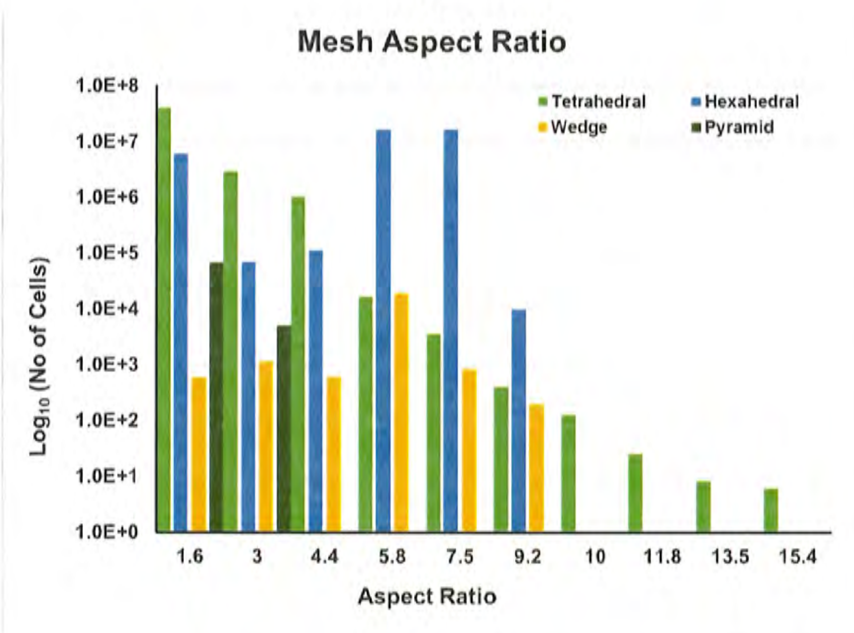

(b)

Figure 11: Statistics histograms of the quality of mesh used in the computation: (a) skewness, (b) aspect ratio.

Table 1: Operating room characteristics

Parameter	Value
Room dimensions [m], L, W, H	$7.315 \times 7.00 \times 3.175$
Supply air flow rate [m^3/s], $\dot{V}$	1.10436
ACH [1/hr]	24.45
Room air temperature [°C]	15
Inler air density [$\mathrm{kg/m}^3$], ρ_{in}	1.225
Supply air temperature [°C]	15
Room air pressure [Pa]	1.0131×10^5
Grille dimensions [m]	1.12×0.51
Grille Area [m^2]	0.5712
Grille hydraulic diameter [m], D_h	0.7
Mean inlet velocity [m/s], $\overline{U}_{in}$	0.1933
Inlet Reynolds number, $Re_{in} = \frac{\rho_{in}\overline{U}_{in}D_h}{\mu}$	9226.54

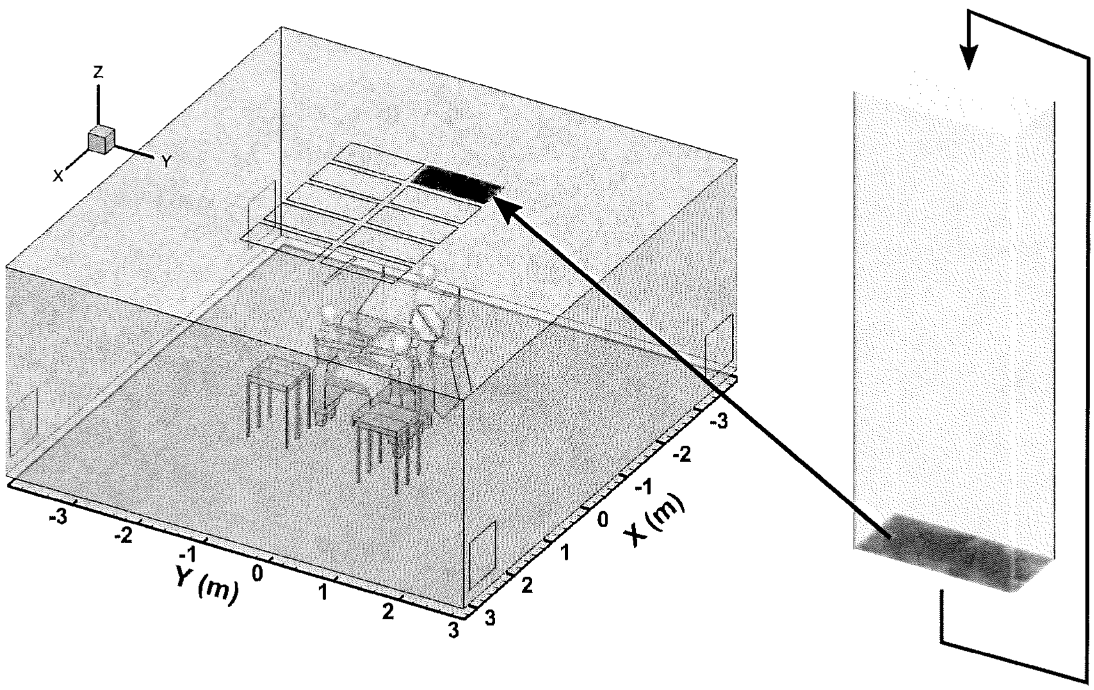

Figure 12: Schematic of the periodic duct used to generate inlet flow data.

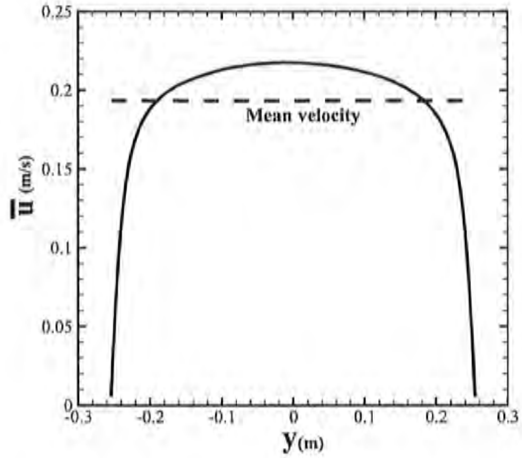

Figure 13: Mean velocity profile generated by a periodic duct flow for the inlet grilles.

let. Thus, a periodic turbulent duct flow was computed (figure 12) to produce a target mean flow rate equal to that prescribed ($\dot{V} = 1.10436\text{m}^3/\text{s}$) using a body force technique of Pierce & Moin (1998*b*). This also generates turbulence fluctuations at the inlet plane that satisfy the continuity equation. The cross-sectional area of the periodic duct used is the same as that of each grille ($1.12\text{m} \times 0.51\text{m}$), and the length is about 4.5 times the hydraulic diameter of the cross-section. The velocity field data at the inlet cross-section was recorded in time series for almost 400 seconds of physical time. Figure 13 shows the time-averaged velocity field in the center plane of the duct obtained from the periodic duct simulation. The turbulence intensity ($I = \sqrt{\frac{1}{3}(u_{rms}^2 + v_{rms}^2 + w_{rms}^2)}/\overline{U}_{in}$) at the inlet cross-section is 5-6% of the mean inlet velocity ($\overline{U}_{in}$), and is in agreement with the experimental measurements conducted by McNeill *et al.* (2012, 2013). Here, u_{rms}, v_{rms} and w_{rms} are the root-mean square velocity components in the x, y and z directions, respectively.

3.4.2 Hot air blower and other heat sources

A 3M™ Bair Hugger™ 750 blower draws air from the floor of the operating room, heats it and blows it into the blanket (3M™ Bair Hugger™ Model 522) that covers the torso region of the patient. The blanket is covered with a plastic drape. The maximum flow rate of the blower is $\dot{V}_{\text{blower}} = 0.021\text{m}^3/\text{s}$. The hot air moves along the surface of the drape that faces the patient and then it is discharged into the room along the drape edges. In the present calculation, the bottom surface (facing the floor) of the 3M™ Bair Hugger™ blower is considered as a suction surface with

surface area ($A_{extraction} = 0.03796\mathrm{m}^2$). A Dirichlet boundary condition is applied at this surface that prescribes the extraction velocity $\overline{U}_{extraction}$ as

$$\overline{U}_{extraction} = \frac{\dot{V}_{blower}}{A_{extraction}}, \tag{19}$$

giving an extraction velocity of $0.5532\mathrm{m/s}$. To model the hot air discharged along the edges of the drape. The total area of this edge of the drape is measured to be $A_{drape} = 0.07794\mathrm{m}^2$. A Dirichlet boundary condition is applied such that the air is injected into the room perpendicular to the edges of the drape with velocity, $\overline{U}_{drape}$, calculated as,

$$\overline{U}_{drape} = \frac{\dot{V}_{blower}}{A_{drape}}, \tag{20}$$

giving an average injection velocity along the drape edge as $0.2694\ \mathrm{m/s}$. The temperature of the hot air at the BH blower outlet is prescribed equal to 109°F (42.77°C) and the temperature of the air leaving the drape edge is set equal to 106°F (41.11°C) according to 3M video at: https://www.youtube.com/watch?v=QhzeInWlJ54. The flow rates at the inlet grilles and for the blower are summarized in Table 3.4.2.

Other heat sources in the surgical room are mainly the surgeons, patient, surgical lamps, and exposed surface of the patient's knee. These heat sources can cause warming of the air in contact with the surfaces and result in a rising thermal plume. For these surfaces, a Dirichlet condition was used for temperature based on the experimentally measured values. In their work, McNeill *et al.* (2012) conducted detailed measurements of detailed surface temperatures that may lead to buoyant plumes specifically to be used in CFD calculations. The values are summarized in Table 3.4.2, among which, the temperatures of surgeons and patient's heads as well as the surgical lamps are based on the work of McNeill *et al.* (2012) and the rest are from the *3M video*. For all other other solid surfaces, a no heat flux Neumann condition was specified, $\frac{\partial T}{\partial n} = 0$.

3.5 Numerical solution method

The computational approach is based on a co-located, finite-volume, energy-conserving numerical scheme on unstructured grids (Moin & Apte, 2006; Mahesh *et al*., 2006) and solves the variable

Table 2: Flow and temperature conditions

Parameter	Value
Inlet volume flow rate $\dot{V}$, [m^3/s]	1.1044
Temperature of inlet grille air, [°C]	15
Mean inlet velocity [m/s], $\overline{U}_{in}$	0.1933
BH blower volume flow rate $\dot{V}_{blower}$, [m^3/s]	0.021
Temperature of hot air leaving the drape edge, [°C]	41.11
Heads of the surgeons and patient, [°C]	31.44
The patient's knee , [°C]	37.78
Two surgical lamps, [°C]	93.92

density gas-phase flow equations in the limit of zero-Mach number. In this co-located scheme, the velocity and pressure fields are stored and solved at the centroids of the control volumes. Numerical solution of the governing equations of the continuum fluid phase and particle phase (squames) are staggered in time to maintain time-centered, second-order advection of the fluid equations. Denoting the time level by a superscript index, the velocities are located at time level t^n and t^{n+1}, and pressure, density, viscosity, and the scalar fields at time levels $t^{n+3/2}$ and $t^{n+1/2}$. Sqaumes position and velocity are advanced explicitly from $t^{n+1/2}$ to $t^{n+3/2}$ using fluid quantities at time-centered position of t^{n+1}.

3.5.1 Advancing the Lagrangian squames equations

The squames (particles) equations are advanced using a fourth-order Runge-Kutta scheme. Owing to the disparities in the flow field time-scale (τ_f) and the squames relaxation time (τ_p) sub-cycling of the squames equations may become necessary. Accordingly, the time-step for squames equation advancement (Δt_p) is chosen as the minimum of τ_p and the time-step for the flow solver (Δt). For the present simulations, the squames relaxation time, τ_p, based on the drag force, was found to be always larger than the time-step, Δt, used for solving the fluid flow equations in LES. Thus, the temporal evolution of the squames was well resolved by the flow time step, and subcycling of the particle equations was not necessary.

After obtaining their new positions, the squames are relocated, and the squames that cross inter-processor boundaries are duly transferred. Boundary conditions for squames crossing boundaries are applied and the computation is further advanced. Solving these Lagrangian equations thus requires

addressing the following key issues: (i) efficient search for locations of squames on an unstructured grid, (ii) interpolation of gas-phase properties to the squames location for arbitrarily shaped control volumes, (iii) inter-processor transfer of the squames.

Locating the squames particles in a generalized-coordinate structured code is straightforward since the physical coordinates can be transformed into a uniform computational space. This is not the case for unstructured grids used in the present simulations (Apte *et al.*, 2003*b*,*a*, 2009). The approach used here, projects the squames location onto the faces of the control volume and compares these vectors with outward face-normals for all faces. If the particle lies within the cell, the projected vectors point the same way as the outward face-normals. This technique is found to be very accurate even for highly skewed elements. A search algorithm is then required to efficiently select the control volume to which the criterion should be applied. An efficient technique termed as 'the known vicinity algorithm' was used to identify the control volume number in which the particle lies. Given the previous particle location, the known-vicinity algorithm identifies neighboring grid cells by traversing the direction the particle has moved. In LES, the time steps used are typically small in order to resolve the temporal scales of the fluid motion. Knowing the initial and final location of the particle, this algorithm searches in the direction of the particle motion until it is relocated. The neighbor-to-neighbor search is extremely efficient if the particle is located within 5-10 attempts, which is usually the case for 98% of the squames in the present simulation. Once this cell is identified, the fluid parameters are interpolated to the particle location using a generalized, tri-linear interpolation scheme for arbitrary shaped elements. Introducing higher order accurate interpolation is straight forward; however, it was found that tri-linear interpolation is sufficient to represent the gas-phase velocity field at particle locations. In the present case, particles are distributed over several processors used in the computation, and the load-imbalance was not significant. Details of the algorithm can be found in Apte *et al.* (2003*b*, 2009). The overall increase in computational cost due to addition of about 3 million particles was about 25% per time-step.

3.5.2 Advancing the Eulerian fluid flow equations

The scalar field (enthalpy or non-dimensional temperature; equation 5) is advanced using the old time-level velocity field. A second-order WENO scheme is used for scalar advective terms and centered differencing for the diffusive terms. All terms, except the source terms due to buoyancy

effect, are treated implicitly using Crank-Nicholson for temporal discretization. Once the scalar field is computed, the density and temperature fields are obtained from constitutive relations (equation 7) and the ideal gas law (equation 2). The cell-centered velocities are advanced in a predictor step such that the kinetic energy is conserved. The predicted velocities are interpolated to the faces and then projected. Projection yields the pressure at the cell-centers, and its gradient is used to correct the cell and face-normal velocities. The steps involved in solving the projection-correction approach for velocity field are briefly described below, Details of this algorithm may be found in Moin & Apte (2006); Mahesh *et al.* (2006); Apte *et al.* (2008*b*).

- Advance the fluid momentum equations using the fractional step algorithm. The density field is available at intermediate time level is obtained from arithmetic average at the two time steps $t^{n+3/2}$ and $t^{n+1/2}$.

$$\frac{\rho u_i^* - \rho u_i^n}{\Delta t} + \frac{1}{2V_{cv}} \sum_{\text{faces of cv}} \left[u_{i,f}^n + u_{i,f}^*\right] g_N^{n+1/2} A_f = \tag{21}$$

$$\frac{1}{2V_{cv}} \sum_{\text{faces of cv}} \mu_f \left(\frac{\partial u_{i,f}^*}{\partial x_j} + \frac{\partial u_{i,f}^n}{\partial x_j}\right) A_f + (\rho - \rho_0) g_i$$

  where f represents the face values, N the face-normal component, $g_N = \rho u_N$, and A_f is the face area. The superscript '$*$' represents the predicted velocity field, and $g_N^{n+1/2} = 0.5(g_N^n + g_N^{n+1})$.

- Interpolate the velocity fields to the faces of the control volumes and solve the Poisson equation for pressure:

$$\nabla^2 (p\Delta t) = \frac{1}{V_{cv}} \sum_{\text{faces of cv}} \rho_f u_{i,f}^* A_f + \frac{\rho^{n+3/2} - \rho^{n+1/2}}{\Delta t} \tag{22}$$

- Reconstruct the pressure gradient, compute new face-based velocities, and update the cv-velocities using the least-squares interpolation used by Mahesh *et al.* (2004); Ham *et al.* (2003); Mahesh *et al.* (2006),

$$\frac{\rho\left(u_i^{n+1} - u_i^*\right)}{\Delta t} = -\frac{\delta p}{\delta x_i}. \tag{23}$$

4 Results

The numerical simulation was initiated with stagnant air (zero velocity) in the operating room and proper boundary conditions. A simulation was carried out with the blower off and all surfaces at room temperature for about 67s of physical time, which corresponds to about 4 flow through times based on the average inlet air velocity and the height of the room. After the initial transients, the thermal boundary conditions were applied at the surgeons heads, the patient's knee, the surgical lights. A calculation was performed for another 54s to establish a stationary flow with the thermal plumes created by the surfaces with higher-than-ambient temperatures. At this time, calculation of statistics for time-averaged mean velocity field and turbulence intensity were initiated and also 3 million squame particles were placed at the floor in three different regions surrounding the operating table as described below. With the blower-off the time-step used in the calculation was $\Delta t = 6 \times 10^{-5}$s giving a CFL number of about 0.75. This time step was able to resolve the important time-scales of turbulence and particle motion accurately. The flow statistics were collected for a total of 80s after a stationary flow field was established and the squames trajectories were calculated for about 21s.

After the above calculation was completed, the remaining squames particles in the computational domain were removed, and the blower was turned on. With the blower discharging a hot air at higher speeds, the time-step was reduced by a factor of 2.5 to $\Delta t = 2.4 \times 10^{-5}$s maintaining the CFL number about 0.6. The reduction in time step is related to both the explicit treatment of the gravitational source term in the momentum equation as well as increased velocity at the blower discharge location. A calculation was performed for about 30s to obtain a developed plume from the hot air discharged by the blower. Flow statistics and the initial location of 3 million squames particles were initiated. With the blower-on, the flow statistics were collected for about 37s and particle trajectories were calculated for about 30s.

All calculations were performed on a parallel computer and used 1600 processors. The computational domain was decomposed such that each processor contains roughly the same number of control volumes. The overall calculation (including initial transient, the case with blower-off and the case with blower-on including particle trajectories for both cases) took about 2M CPU-hrs. For the case of blower-off, about 20s of physical time would cost roughly 100,000 CPU-hours, whereas

the same calculation with blower-on would cost roughly 220,000 CPU-hours. For each case, tracking 3 million trajectories of squames would add about 20-30% additional computing cost. This is because, initially the 3 million squames are clustered in a small region near the floor causing load imbalance as the particles were present on only a few processor domains. The flow statistics and particle trajectories are discussed below.

4.1 Flow characteristics

Figures 14a and 14b show the locations of two slices through the three-dimensional computational domain at $x = -0.88$m and $y = -0.162$m for which the mean velocity magnitude, turbulence intensity, and instantaneous temperature contours are plotted. The $x = -0.88$m slice shows a planar cut that includes the surgical lamp and the operating table (OT). The $y = -0.162$m slice shows a side view and contains 2 medical staff, a side table, the surgical lamp, and part of the inverted U-shaped drape. For these two slices, the flow characteristics with blower-off and blower-on are compared.

Figures 15, 16, and 17 show the contours of mean velocity magnitude, turbulence intensity, and instantaneous temperature, respectively, for the two cases of blower-off and blower-on. For the case of blower-off, figure 15a shows that the ventilation air from the ceiling inlet grilles moves downwards, gets deflected by the surgical lights and the table, impinges on the floor farther away from the table, and finally exits through the outlet grilles. Large recirculation regions are created on both sides of the table. The flow is not symmetric owing to asymmetries in the configuration itself. In comparison, with the blower turned on, the flow underneath and around the table is considerably modified as can be seen from the large velocity magnitudes under the table (figure 15b). The recirculation region is also disrupted by the rising air from the hot blower discharge. This difference is clearly visible from the turbulence intensity contours shown in figure 16a,b. With the blower-off, the maximum turbulence intensity level is about 30% in the high shear regions between the inlet air streams, as well as near the warm surgical lights due to the buoyant plume. With the blower-on, the turbulence intensity level is as high as 60% in regions affected by the rising thermal plumes from the blower hot air. The instantaneous temperature contours shown in figure 17a,b confirm that the increased turbulence level is mainly because of the thermal plumes from the hot blower air as can be seen by the high temperature regions under the OT.

Figures 18, 19, and 20 show the contours of mean velocity magnitude, turbulence intensity, and

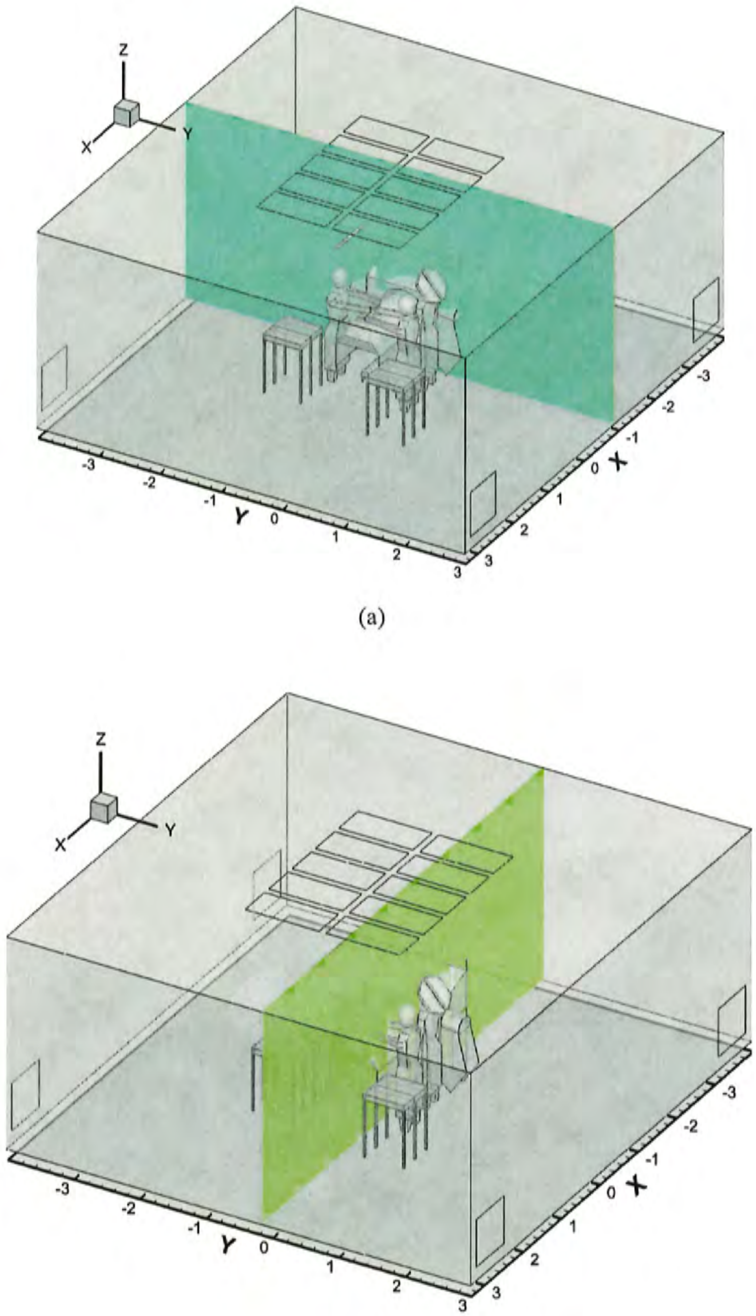

(a)

(b)

Figure 14: Locations of the planes for which contour plots of mean velocity magnitude, turbulence intensity and instantaneous temperature are presented to compare the effect of the blower discharge on the flowfield: (a) $x = -0.88$m (b) $y = -0.162$m.

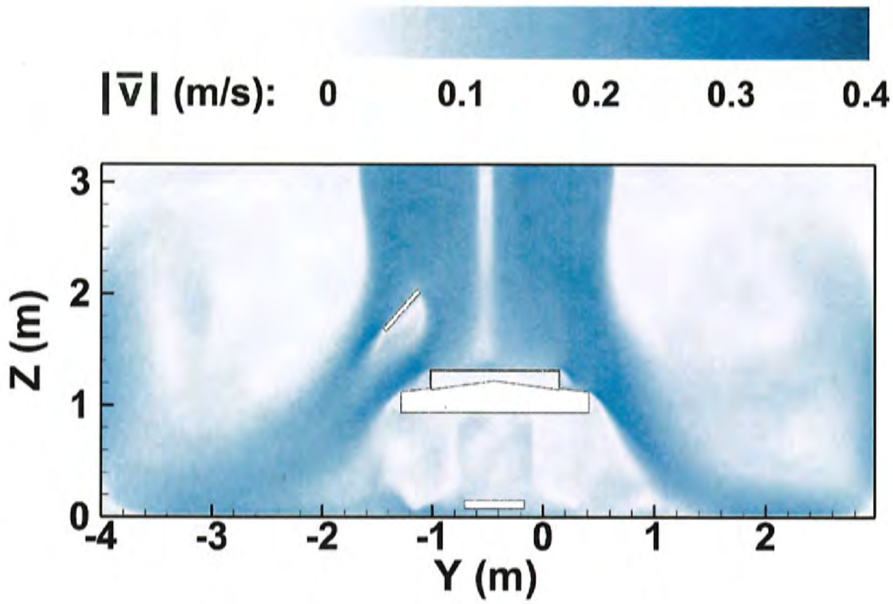

(a)

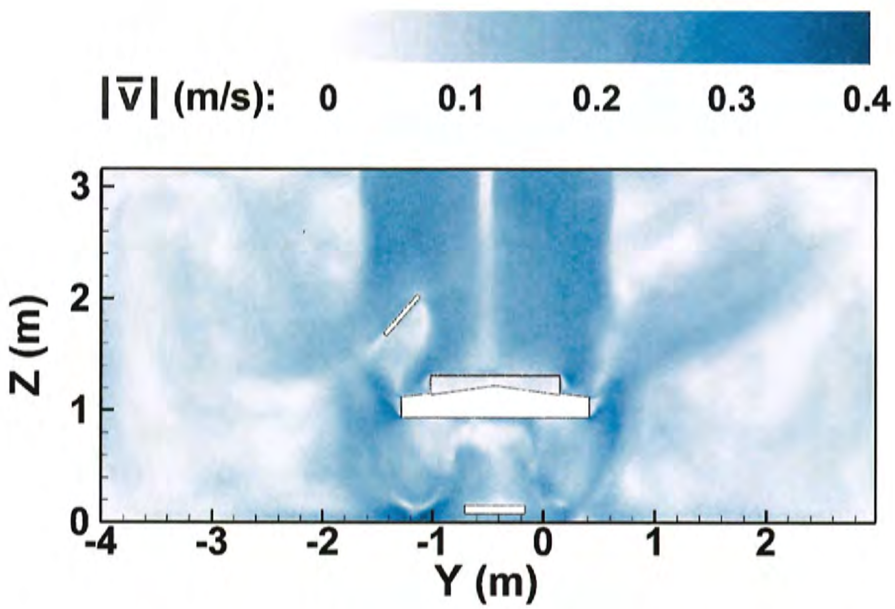

(b)

Figure 15: Contours of the mean velocity magnitude at $x = -0.88$m (a) with blower-off and (b) with blower-on. The time average is taken over a physical time of 80s (no blower) and 37s (with blower) after establishing a stationary state.

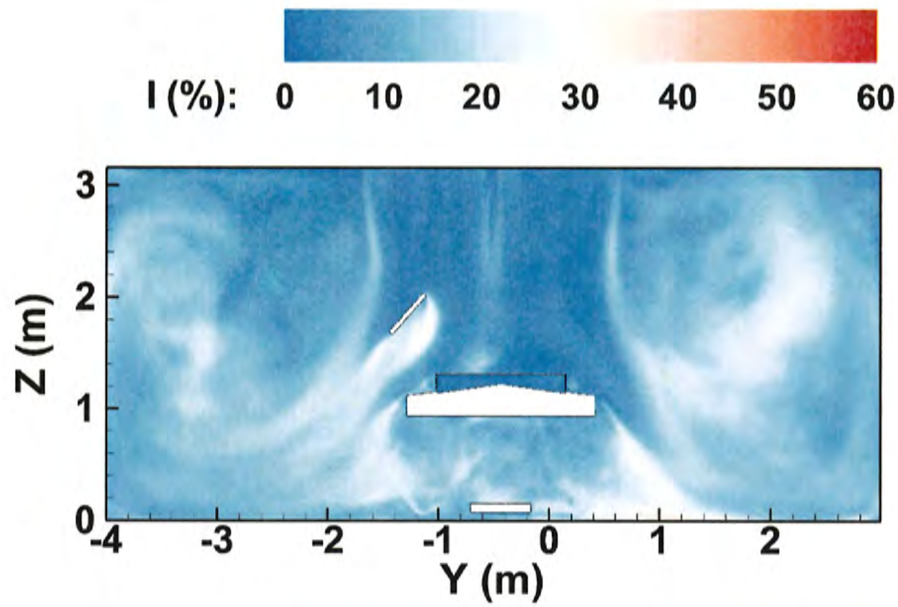

(a)

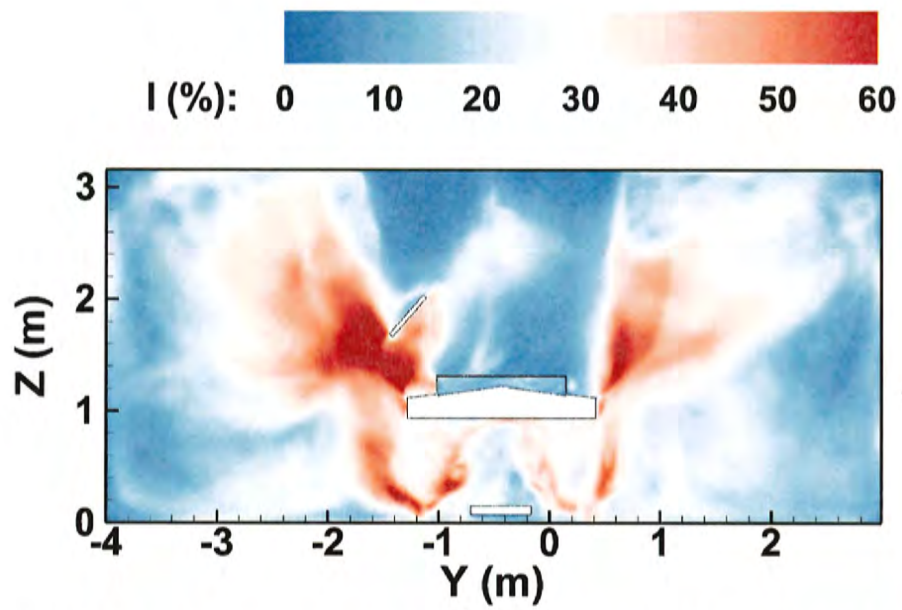

(b)

Figure 16: The turbulence intensity contours at $x = -0.88$m (a) with blower-off and (b) with blower-on. The time average is taken over a physical time of 80s (no blower) and 37s (with blower) after establishing a stationary state.

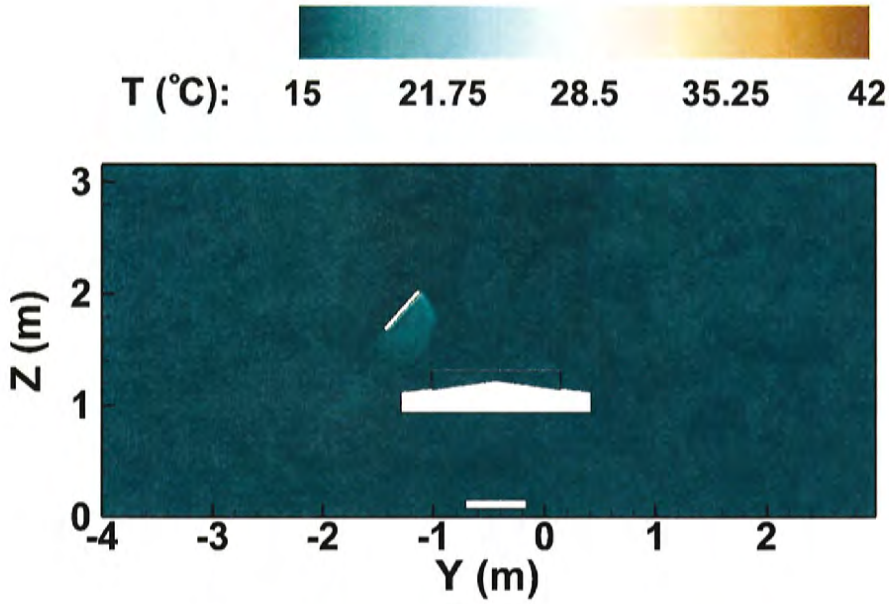

(a)

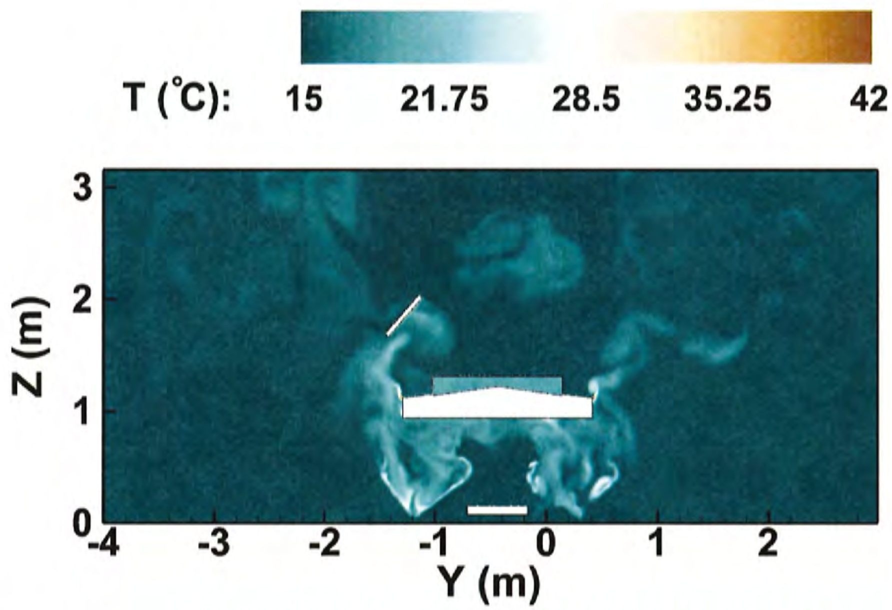

(b)

Figure 17: The instantaneous temperature contours at $x = -0.88$m (a) with blower-off and (b) with blower-on. These snapshots are at about 35s after a stationary flow field was obtained and calculation for flow statistics was initiated.

instantaneous temperature, respectively, for the cases of blower-off and blower-on at $y = -0.162$m. Similar trends as described before are observed. The hot blower air and the rising thermal plumes disrupt the downward ventilation air flow. The high temperatures and turbulence intensity under the inverted U-shaped drape are clearly visible. The flow is also highly asymmetric with the blower turned on owing to the orientation and location of the drape. It is also seen from figure 20b that the rising thermal plumes may reach the ceiling in some regions. With the blower off, however, the plumes from warm surfaces of surgical lights, surgeons heads, and patient's knee are weak and are not significant enough to disrupt the downward ventilation air flow.

4.2 Dispersion of squames

This section provides details of the initial locations of the squames, their trajectories, and statistics of sampling the particles in regions of interest with high potential of reaching the surgical site.

4.2.1 Initial locations of squames

In order to provide a worst-case (or least probable) scenario for the squames to be carried to the surgical site by the air convection, all 3 million squames were initially placed on the floor and randomly distributed in a small region surrounding the operating table within a height of about 1 cm above the floor of the OR. If these squames are lifted by the turbulent air and moved to the surgical site, other effects such as motion of medical equipment and staff, additional squames shed from the heads and faces of medical staff, surgical garments, etc. will have an even higher probability to reach the surgical site.

Table 3: Coordinates of color-coded regions for initial positions of squames as shown in figure 21.

Color-coded initial position	$(x,y,z)_{min}$ [m]	$(x,y,z)_{max}$ [m]
Red	(-1.40, -0.025, 0.0)	(0.70, 0.40, 0.01)
Green	(-1.80, -1.35, 0.0)	(-1.4, 0.4, 0.01)
Yellow	(-1.40, -1.35, 0.0)	(0.70, -0.855, 0.01)

Three million particles with a diameter of 10 micron are placed within a 1 cm thick layer above the floor of the OR. The region where the particles are located is around the OT, surrounding the feet of four surgeons present in the CAD model. To better visualize the trajectories the squames

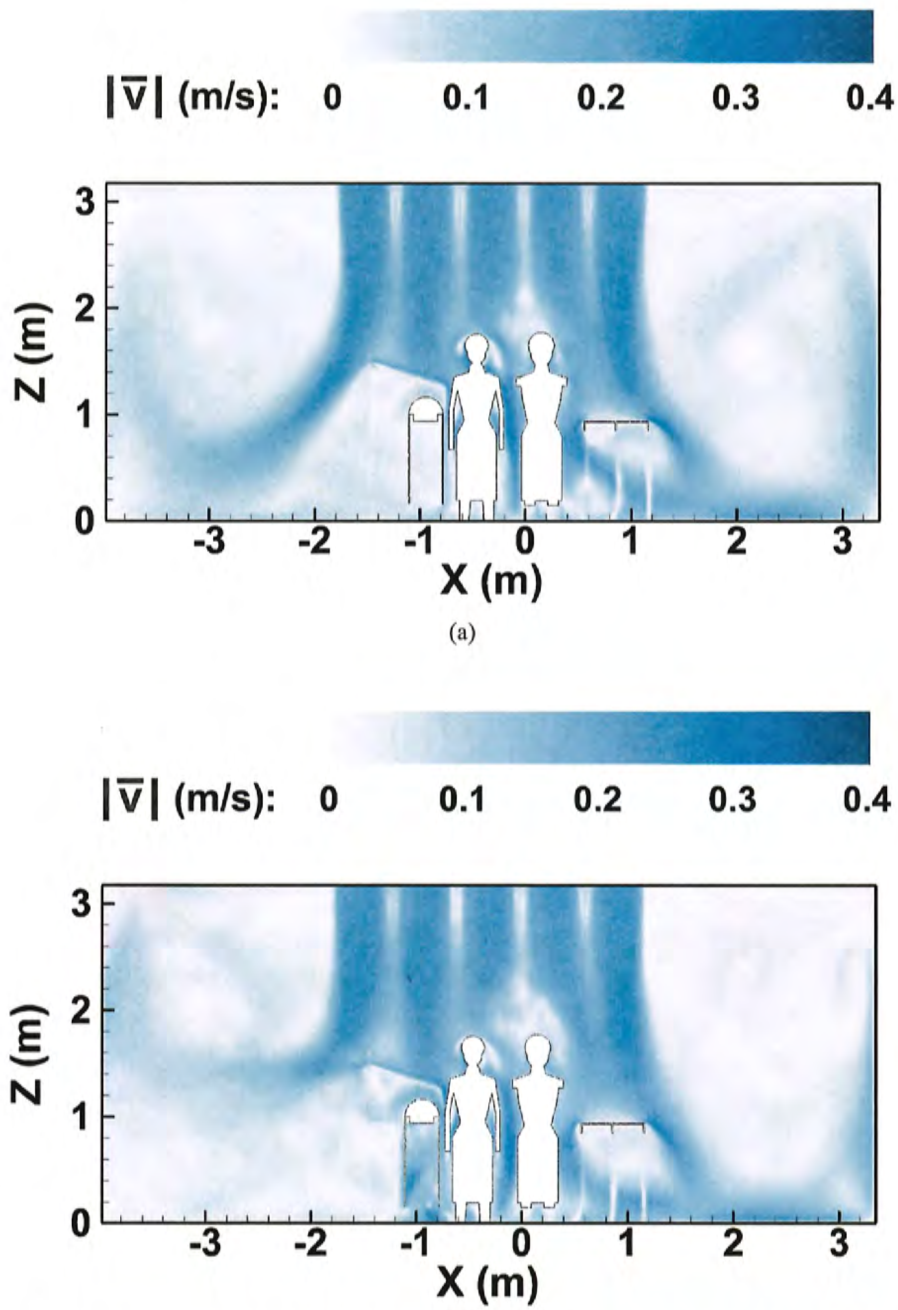

(b)

Figure 18: Contours of the mean velocity magnitude at $y = -0.162$m (a) with blower-off and (b) with blower-on. The time average is taken over a physical time of 80s (no blower) and 37s (with blower) after establishing a stationary state.

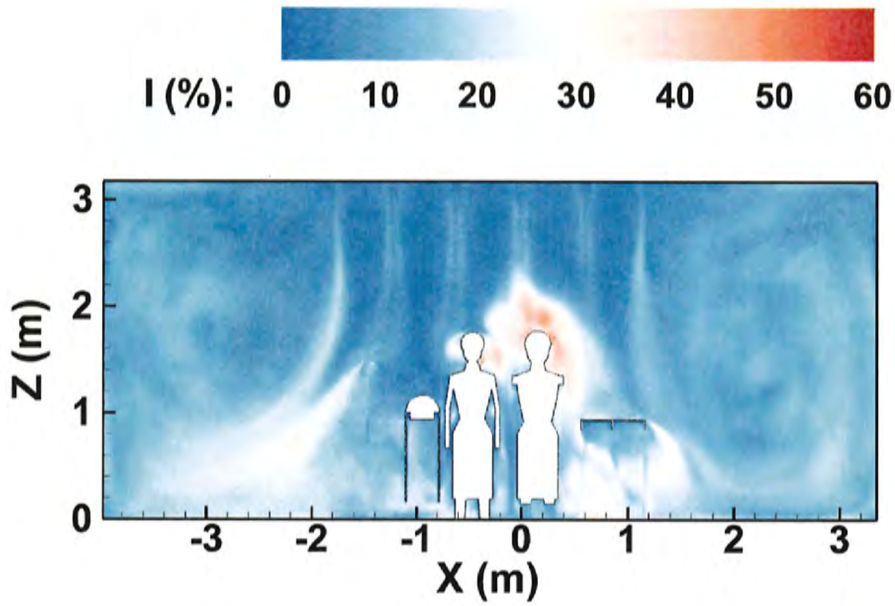

(a)

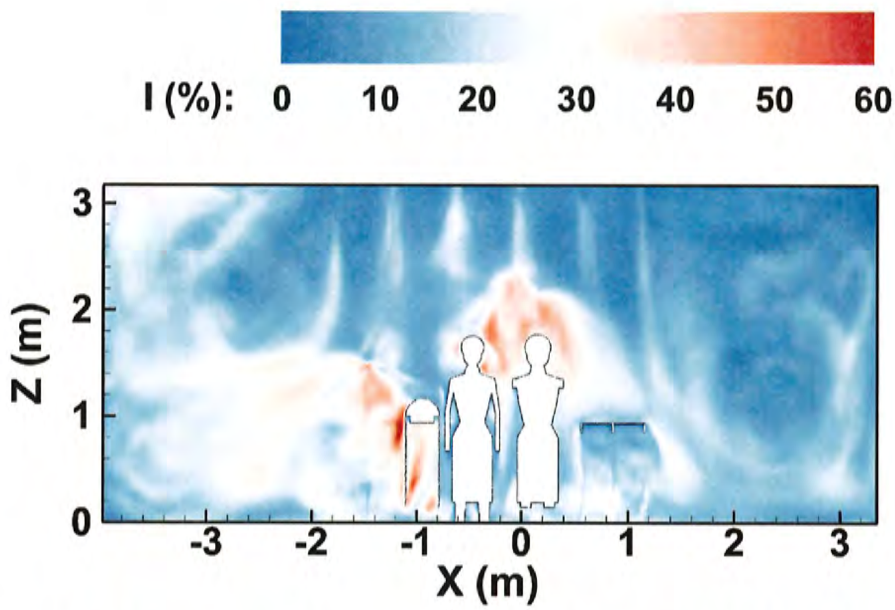

(b)

Figure 19: The turbulence intensity contours at $y = -0.162$m (a) with blower-off and (b) with blower-on. The time average is taken over a physical time of 80s (no blower) and 37s (with blower) after establishing a stationary state.

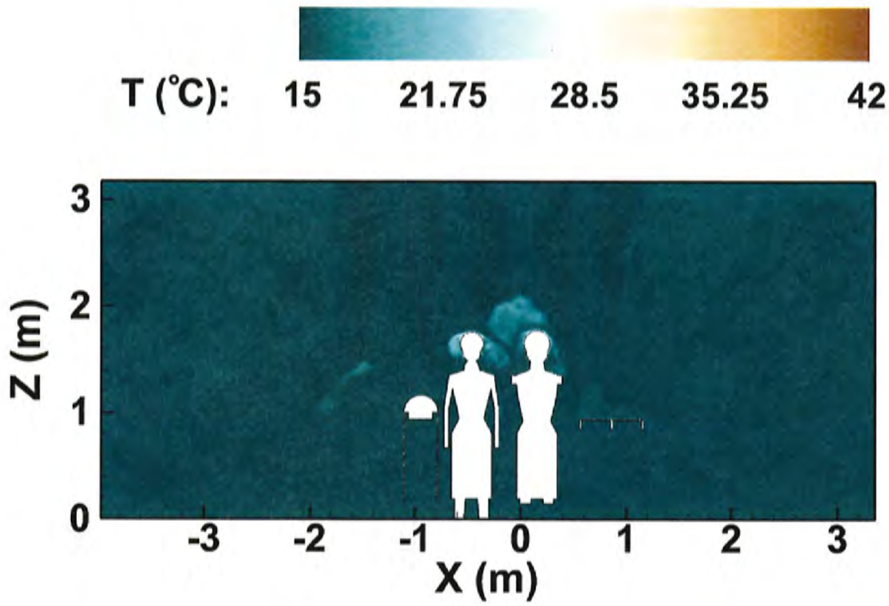

(a)

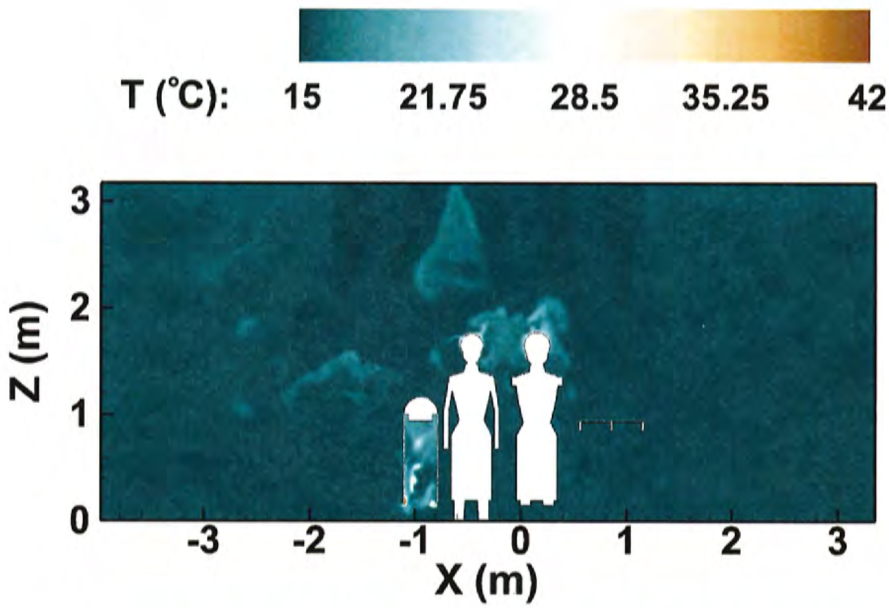

(b)

Figure 20: The instantaneous temperature contours at $y = -0.162$m (a) with blower-off and (b) with blower-on. These snapshots are at about 35s after a stationary flow field was obtained and calculation for flow statistics was initiated.

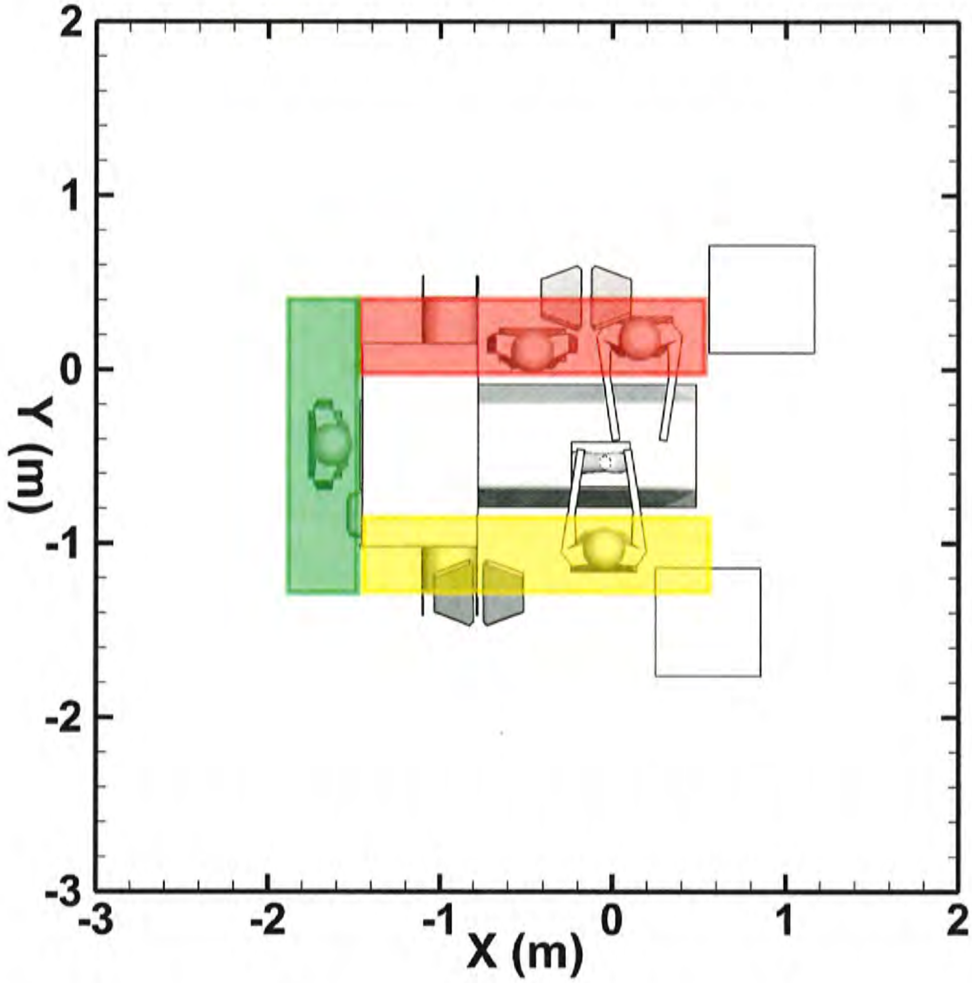

Figure 21: Three color-coded regions where the 3 million squames were initially distributed within a 1 cm height from the floor.

from different initial locations, the U-shaped region is divided into three rectangular sections color-coded as (i) red, (ii) green and (iii) yellow as shown in figure 21. One million squames are placed in each of the three sections at the same time, providing equal probability for the statistical analysis of motion of squames. The position of an individual squame particle in a section is chosen randomly using a uniform distribution. The squames of each section are tagged with distinct IDs. The actual coordinates of the three sections are given in Table 3.

4.2.2 Trajectories and snapshots of squames

In order to visualize the effect of the hot blower air on the trajectory of squames, instantaneous scatter plots of squames are displayed at 10s and 20s after their initiation with blower-off and blower-on in figures 22a,b and 23a,b, respectively. The squames are also color-coded based on their region of origin as highlighted in figure 21. Drastic differences between the blower-off and blower-on cases are observed. It is clear from figures 23a that the majority of the squames are dispersed by the ventilation air flow towards the outlet grilles when the blower is off. None of the squames actually rise to the level of the side tables or the OT. In contrast, in the case of blower-on, a large number of squames are lifted upwards by the rising thermal plumes. Some of the squames (mostly red-colored and some yellow-colored) are lifted above the surgeons heads and are blown towards the OT by the incoming ventilation air. Large number of squames are seen to be above the OT, several are surrounding the surgeons hands, above the side tables, and some are very close to the patient's knee and the surgical site. This is better visualized by the zoom-in view shown in figures 24a,b.

Figures 25, 26, and 27 show a different view angle for the squames at the same time instances as in the above discussion. It is again seen that with the blower-on several particles are lifted upwards by the thermal plumes and rise above the operating table and then are blown downwards by the incoming ventilation air.

Finally, figure 28 shows an instantaneous snapshot of squames very close to the patient's knee. It seen that several of the red-coded particles are near the bottom of the knee, whereas some yellow-coded particles are in the very close vicinity of the surgical site. Several particles are still suspended above the OT and are being transported downwards by the ventilation air and may potentially reach close to the surgical site.

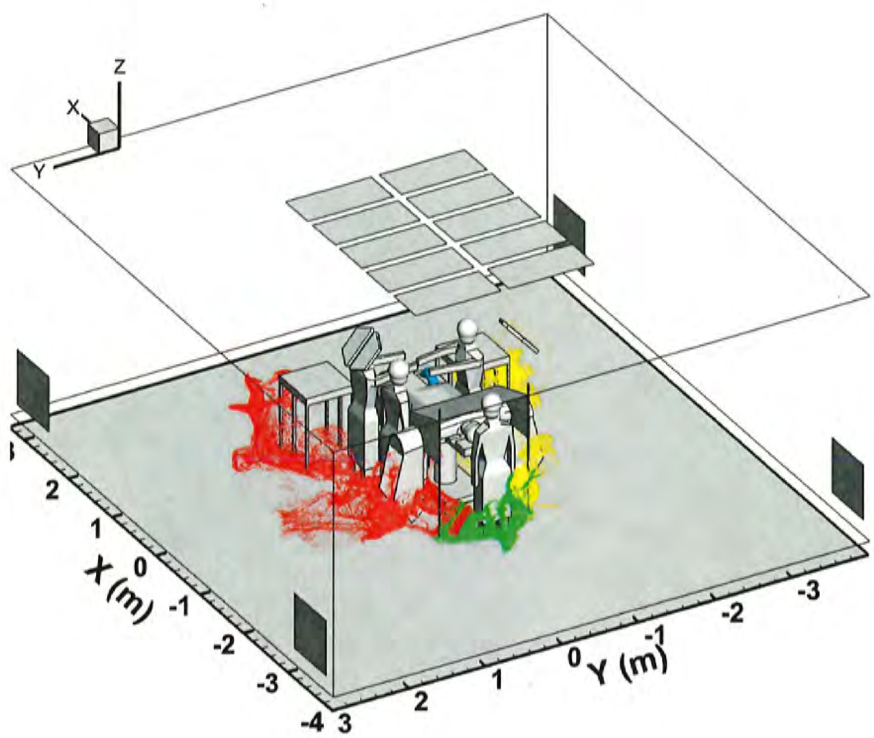

(a)

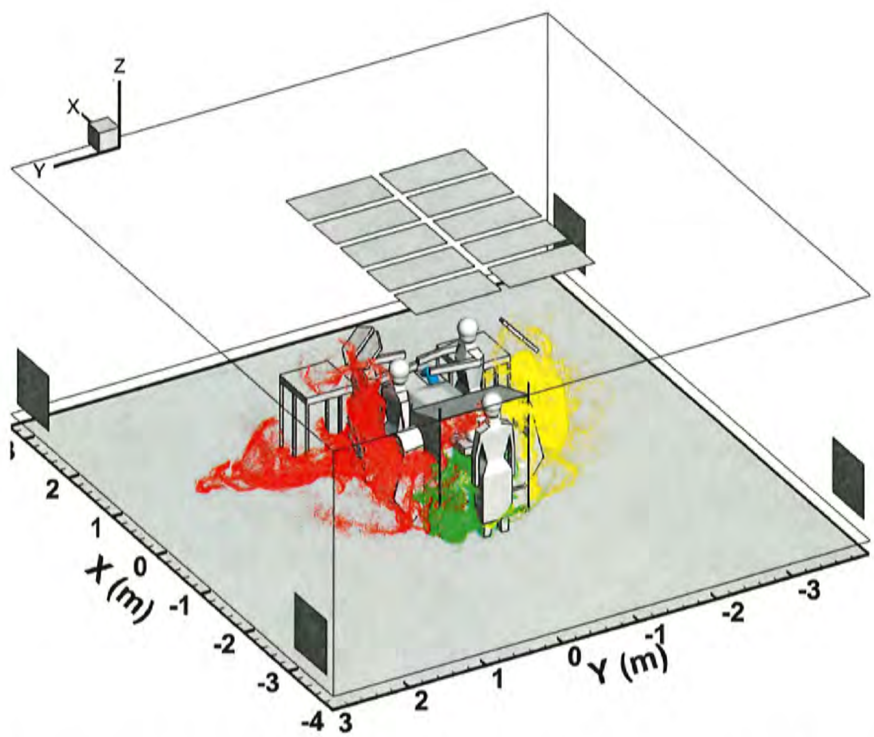

(b)

Figure 22: Instantaneous scatter plot of squames color-coded by their region of origin at 10s after initiation: (a) blower-off, (b) blower-on.

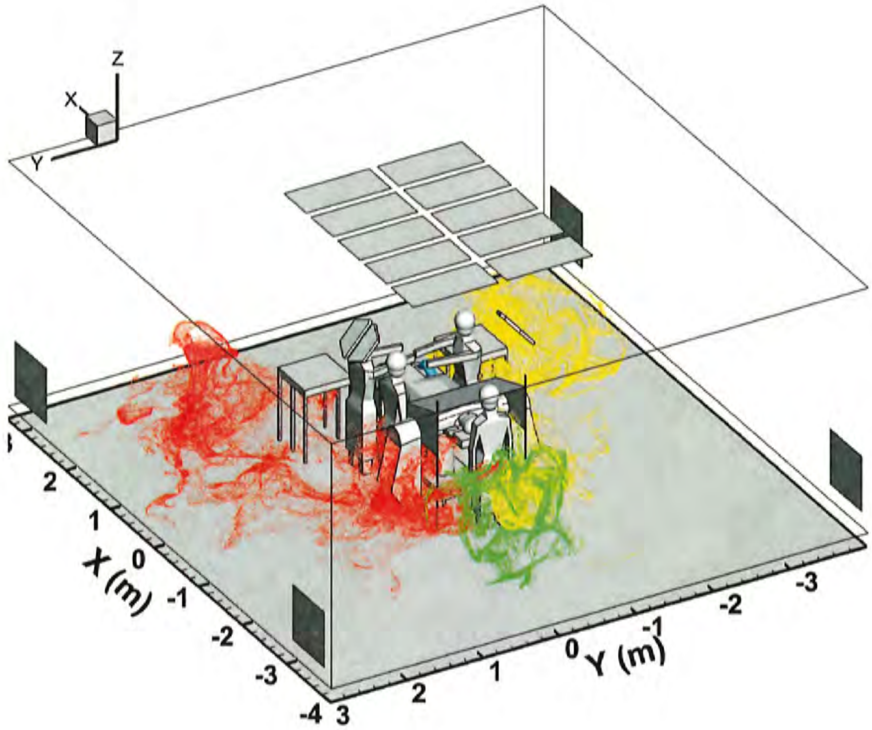

(a)

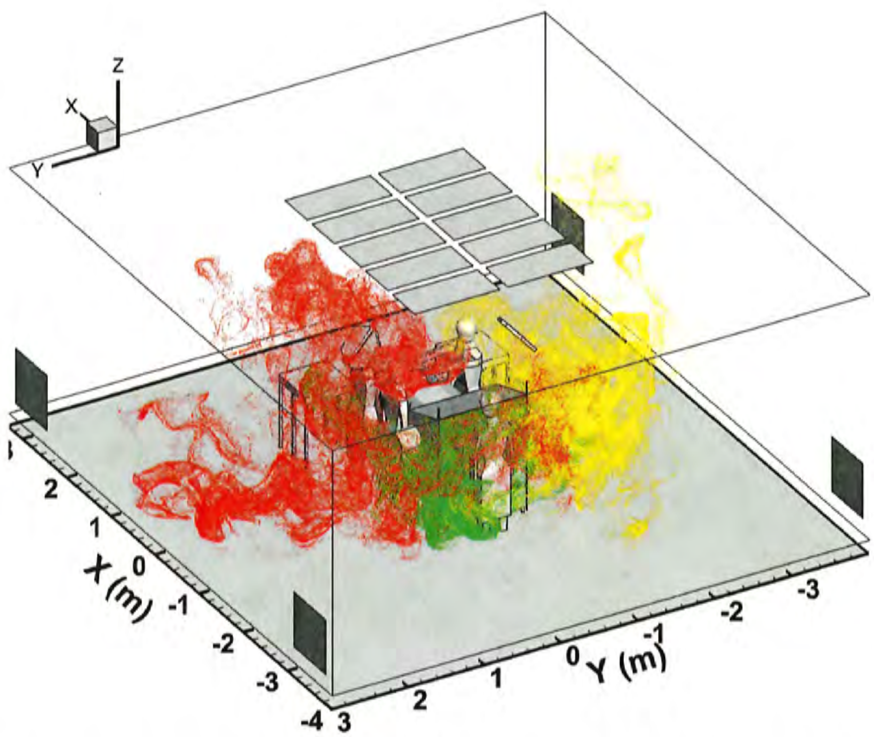

(b)

Figure 23: Instantaneous scatter plot of squames color-coded by their region of origin at 20s after initiation: (a) blower-off, (b) blower-on.

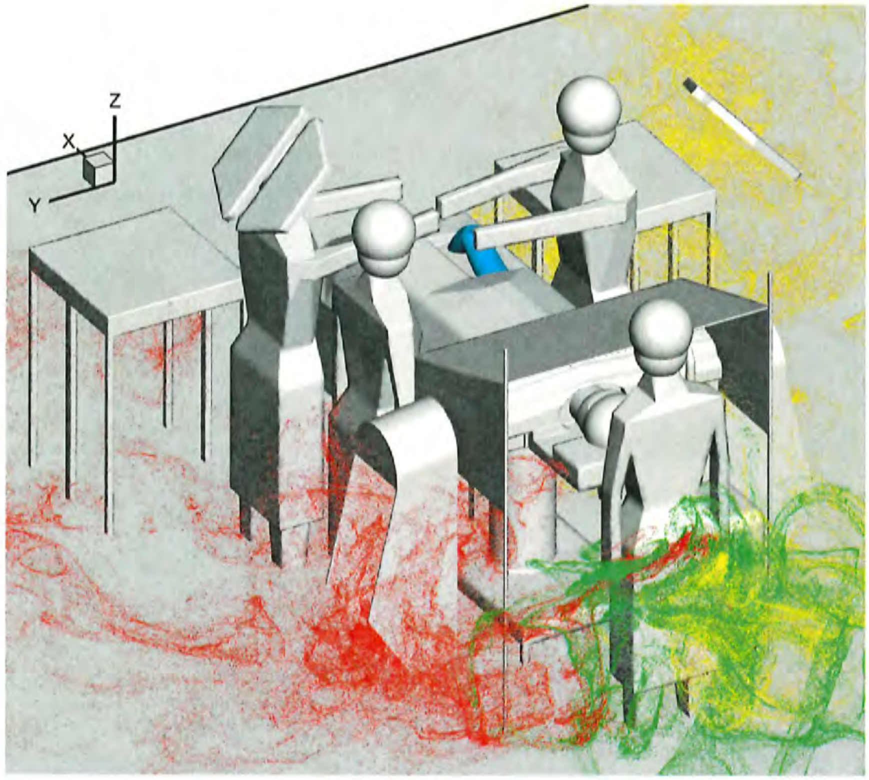

(a)

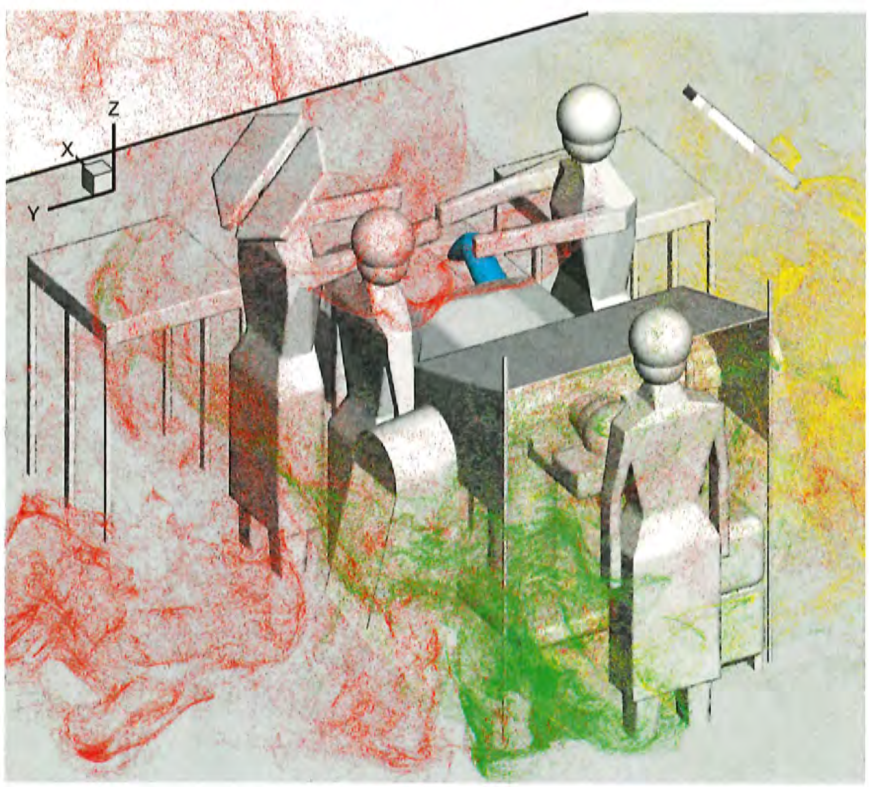

(b)

Figure 24: Zoom-in of the instantaneous scatter plot of squames color-coded by their region of origin at 20s after initiation: (a) blower-off, (b) blower-on.

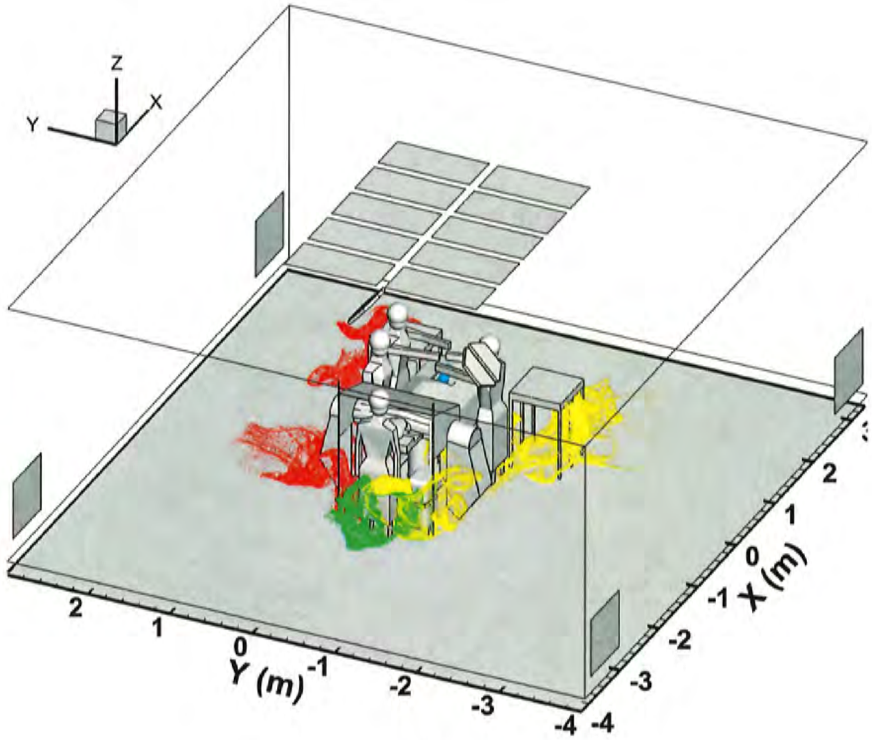

(a)

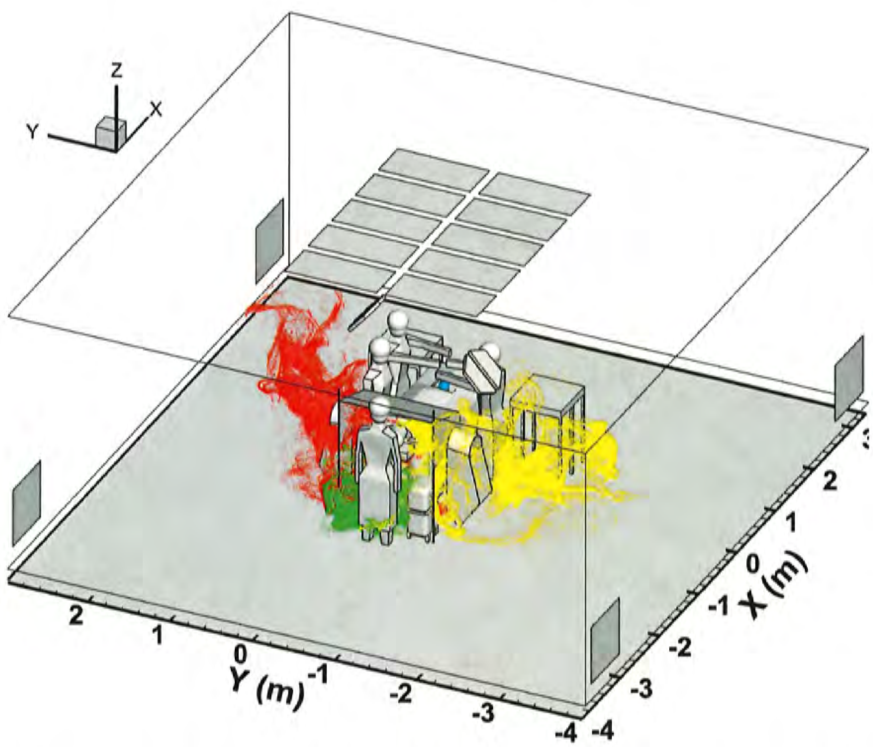

(b)

Figure 25: Instantaneous scatter plot of squames color-coded by their region of origin at 10s after initiation: (a) blower-off, (b) blower-on.

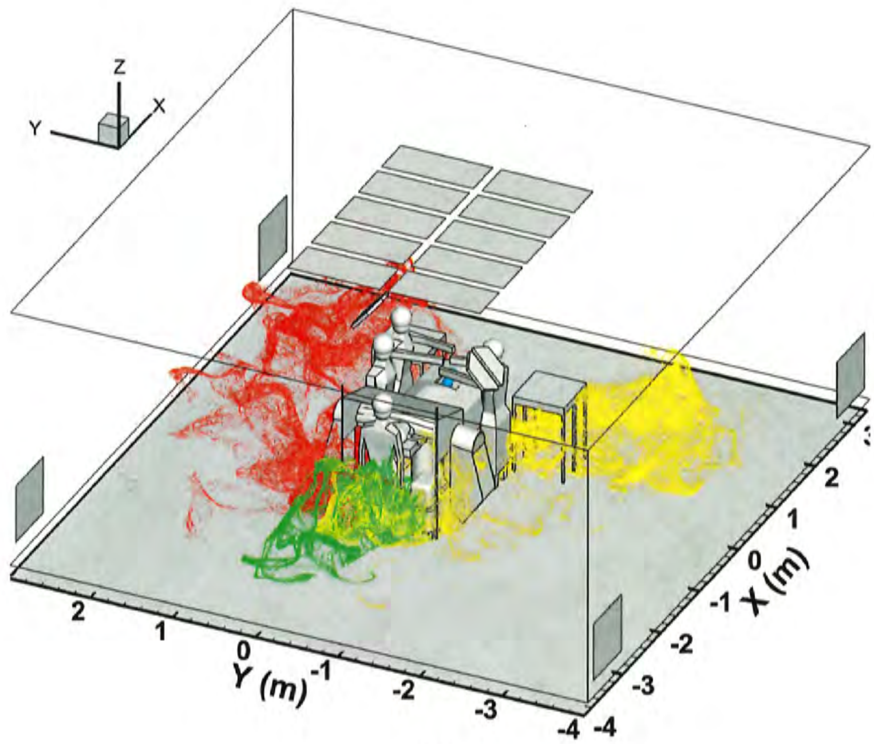

(a)

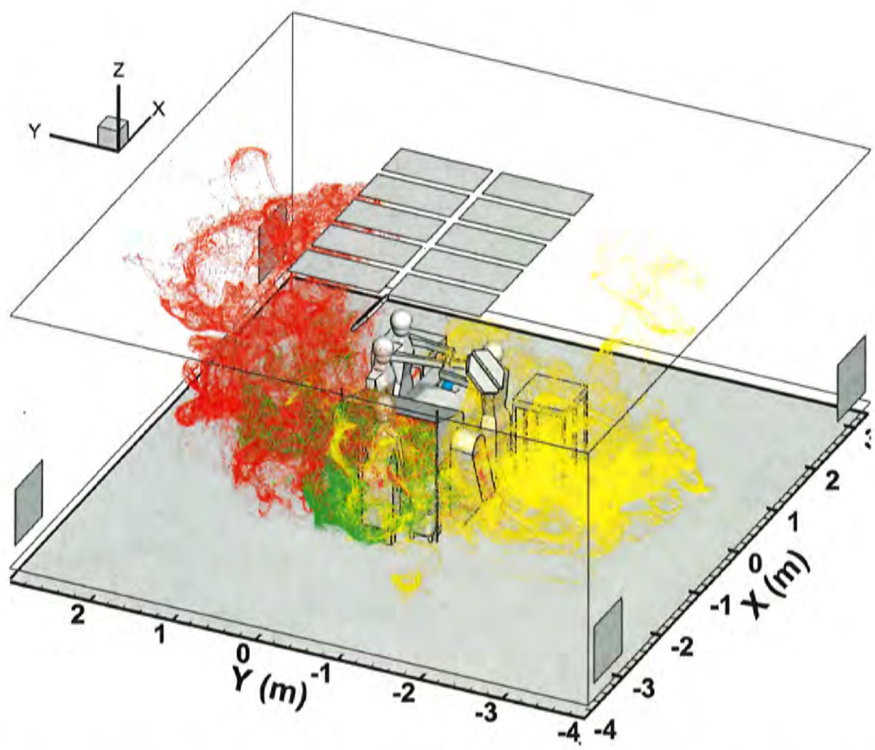

(b)

Figure 26: Instantaneous scatter plot of squames color-coded by their region of origin at 20s after initiation: (a) blower-off, (b) blower-on.

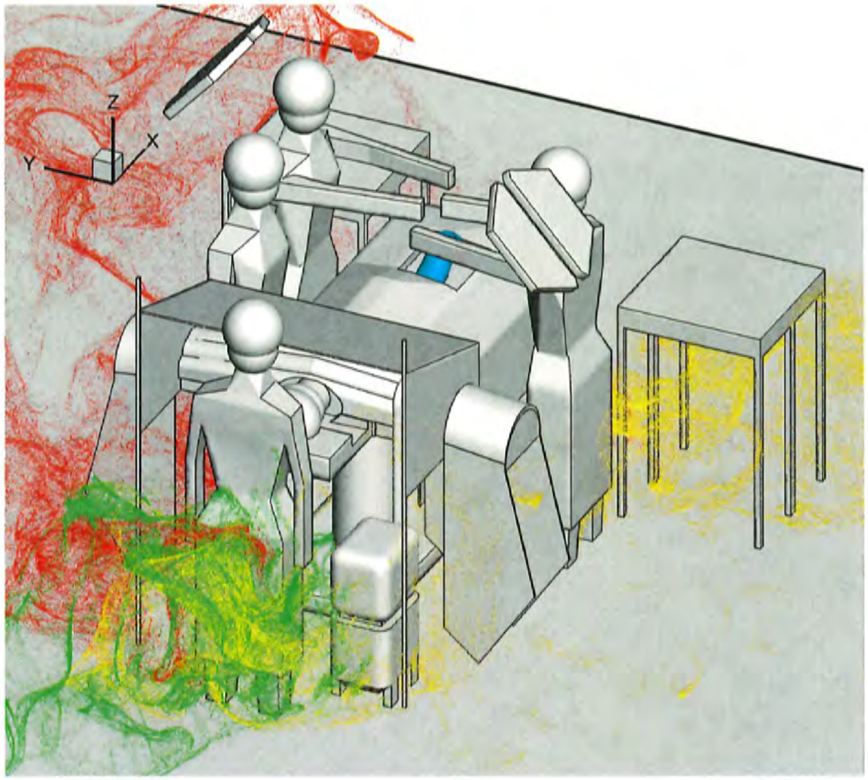

(a)

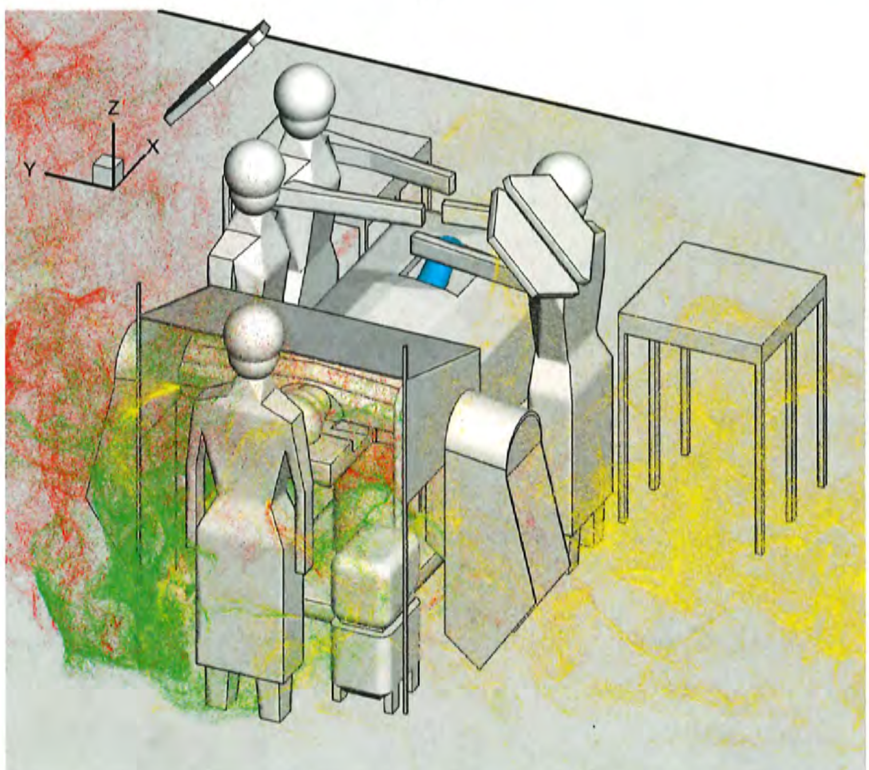

(b)

Figure 27: Zoom-in of the instantaneous scatter plot of squames color-coded by their region of origin at 20s after initiation: (a) blower-off, (b) blower-on.

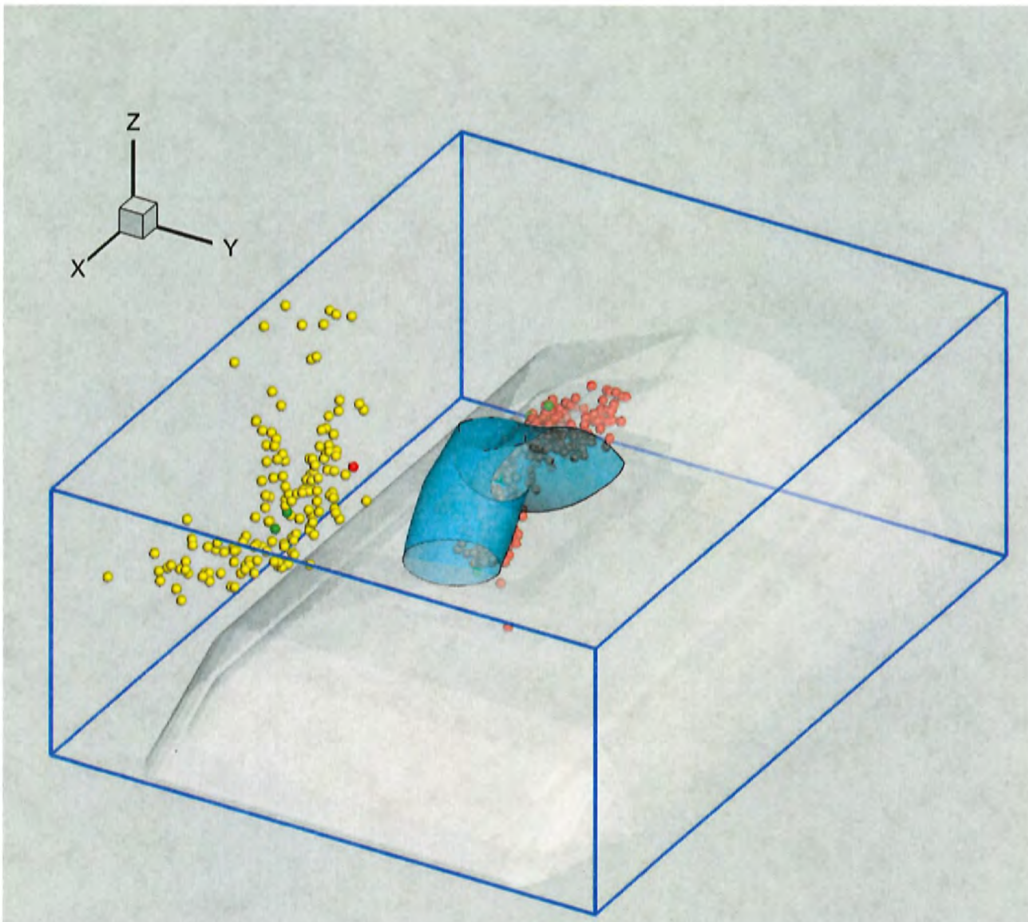

Figure 28: Zoom-in showing the instantaneous snapshot of squames near the surgical site at $t = 27$s.

4.2.3 Number density of squames in the regions of interest

To assess the probability of squames reaching the surgical site, four imaginary boxes were located as follows: two boxes covering the two side tables, a box around the OT, and a box around the patient's knee area. The surgeons and medical assistants are bound to use surgical instruments placed on the side tables. The possibility of squames reaching the surgical site is then dependent on the number density of squames within these four imaginary boxes (see figure 29). The number of squame particles inside the four boxes are recorded in time. A blue box (figure 29 (a) and (c)) is covering the whole OT. The top of this box is about 30 cm high, including the patient's whole body and the surgeons hands. An orange box (figure 29 (b) and (d)) is placed above the OT, just covering the patient's knee and part of the surgeon's hands; and the top of the box is only 2 cm above the surgeon's hands. One purple box (figure 29 (a) - (d)) is placed on each of the two side tables. The height of these boxes is about 1 cm, so that any surgical instrument placed on the side tables would be within the box.

Two computations of the trajectories of squames were performed after a statistically stationary flow field has been reached for the cases of blower-off and blower-on. Based on the average inlet air velocity and the height of the room, it takes 15 – 20s for a fluid particle to travel from the ceiling grille to the floor. First, the blower is turned off and only the ventilation air from the inlet grilles and thermal plumes created by the warm surfaces including surgical lights, surgeons' heads, patient's head, and patient's knee are responsible for the dispersion of squames. It was found that all the squames initiated in all three sections (red, green and yellow) are basically transported by the air flow reaching the floor and quickly dispersed to the for outlet grilles. After a calculation of about 25s of physical time, some squame particles do rise to the underside of the side tables, but none of the squames was found to enter the four imaginary boxes representing the regions of interest. It was concluded that without the hot air discharged from the blower, the ventilation air circulation alone cannot disperse the squames to the surgical site. The thermal plumes from various warm surfaces only slightly affect the air coming from the inlet grilles and do not affect the motion of the squames.

With the blower turned on, computations were carried out for about 30s of physical time to obtain a flow field with well established thermal plumes created by the hot air discharged from the blower. After reaching a stationary state, the squames were initiated in the same color-coded sections and the

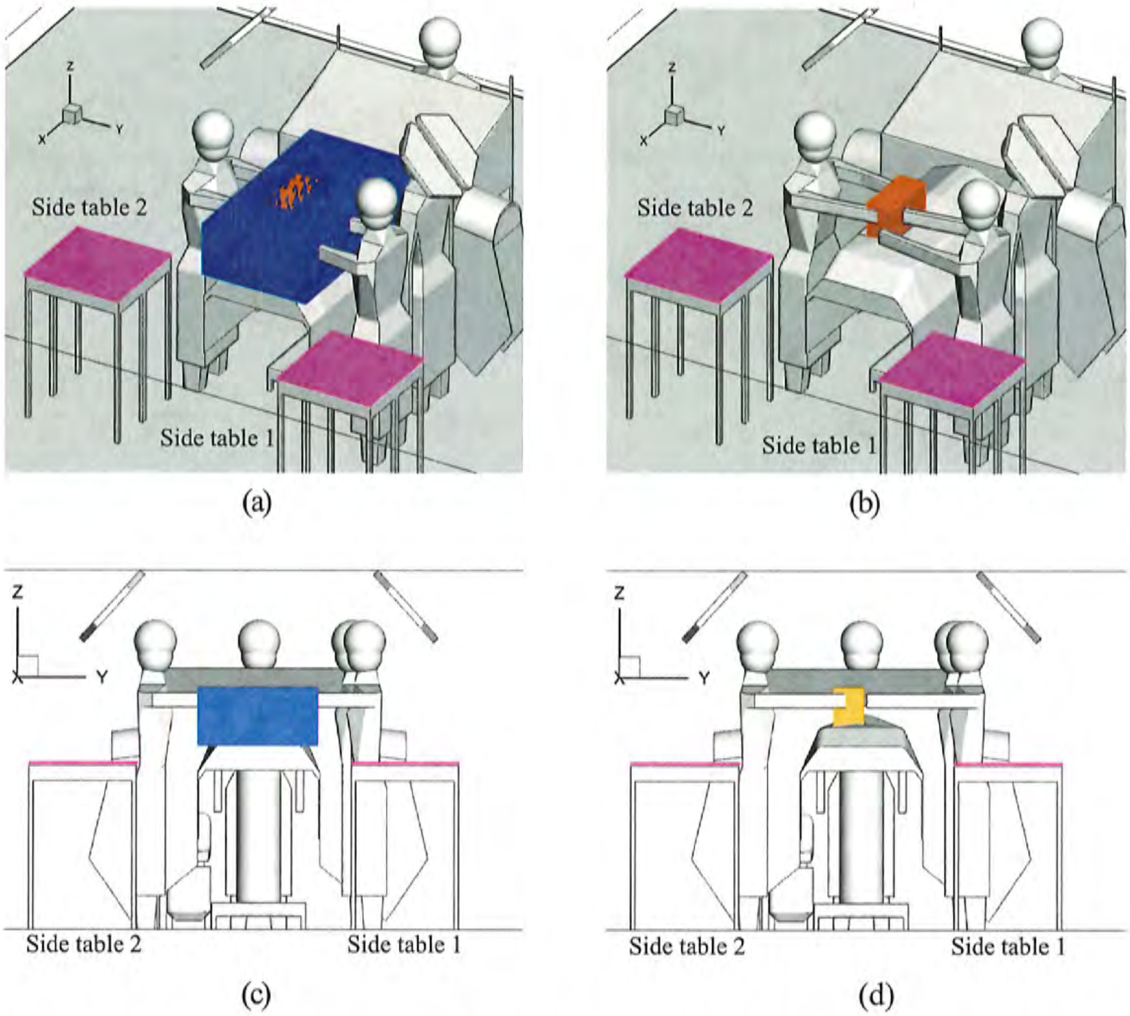

Figure 29: Four color-coded regions of interest, for recording the temporal history of the number of squames reaching them, shown in different views (a–d). The regions of interest include the zones above the two side tables, above the OT, and above the patient's knee.

computation continued for another 30s. With the blower on, hot air is discharged through the sides covering the patient's arms into the ambient air and strong thermal plumes rise under the operating table. Some of the edges of the drape are very close to the floor (see figure 4b) and the hot air plume drags squames with it making them rise upwards faster than in the case when the blower was off. A majority of the squame particles are transported away from the table towards the outlet grilles. However, a statistically significant number of particles are lifted above the operating table with some even reaching the height of the surgeons. The particles rise due to buoyancy and then get flushed down onto the operating table by the incoming ventilation air from the inlet grilles. The particles then do enter the imaginary boxes of interest, specifically above the operating table and the patient's knee.

Figures 30 and 31 show the number of squame particles as a function of time entering the four imaginary boxes of interest (above the side tables, above the operating table, and patient's knee). It can be seen from Figure 31b that no particles are found inside these boxes for the first 17s, which is about the time needed for the ventilation air to travel from the ceiling to the floor. After this time, the number of squame particles in the box above the OT increases almost in a linear fashion. Within 30s of physical time, the number of squame particles within the OT box are about 2500 and increasing. Figure 31a shows that at about 23s, some of the particles above the OT start to enter the box above the knee, which is a very narrow zone surrounding the patient's knee. The number of these particles increases linearly to about 600. Note that some of these particles do get trapped at the knee, some are carried away by the air flow and hence the number appears to be decreasing after about 25s . From the instantaneous snapshot of the squames shown in figures 24b and 27b, it can be seen that several particles are still above the OT and moving downward due to the air from the inlet grilles. It is thus expected that more particles will enter the box above the patient's knee, potentially raising the probability of infection. It is also interesting to note that the squame particles entering the box above the OT and above the knee are mainly the red-colored particles initiated from the side of the table with two surgeons. Owing to the asymmetry in the CAD model geometry, the flow pattern around each side of the table is different and the recirculation region created by the incoming air from the inlet grilles is also asymmetric. The rise and eventual trapping of the squames within the knee box is thus also related to which side of the table it originated from. The boxes above the side tables also entrain about 15 squame particles as can be seen from figures 30a,b. This suggests that

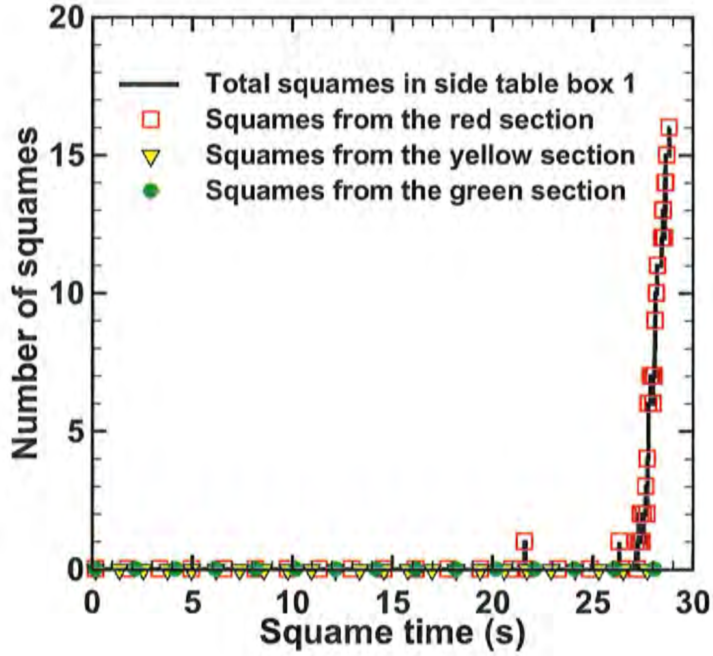

(a)

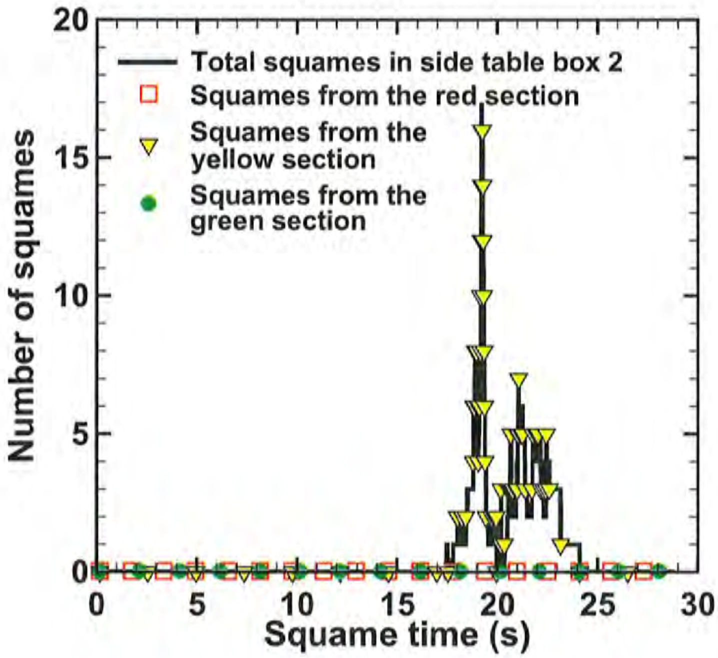

(b)

Figure 30: Temporal history of the total number of squames (shown by black color) entering four different regions of interest: (a) side table box 1, and (b) side table box 2Also shown in color is the number of color-coded squame particles entering from the red, green and yellow regions of the figure 21.

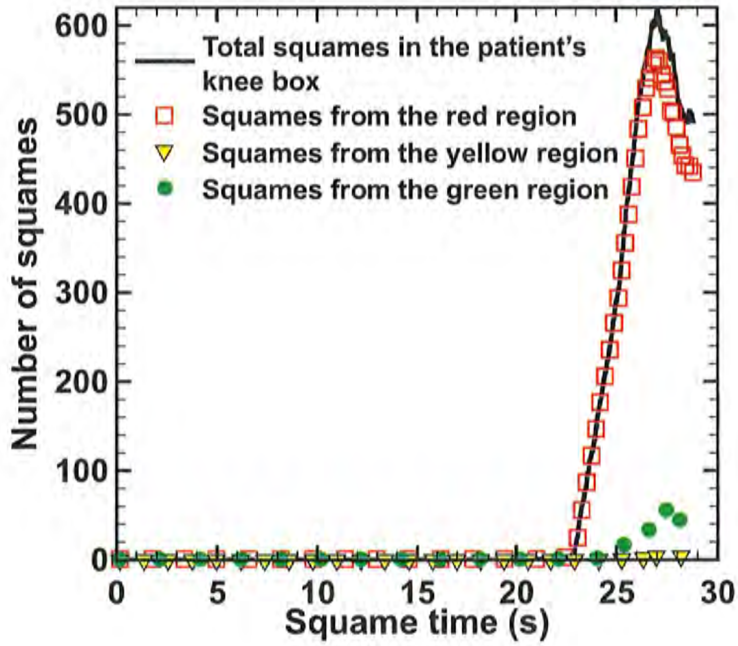

(a)

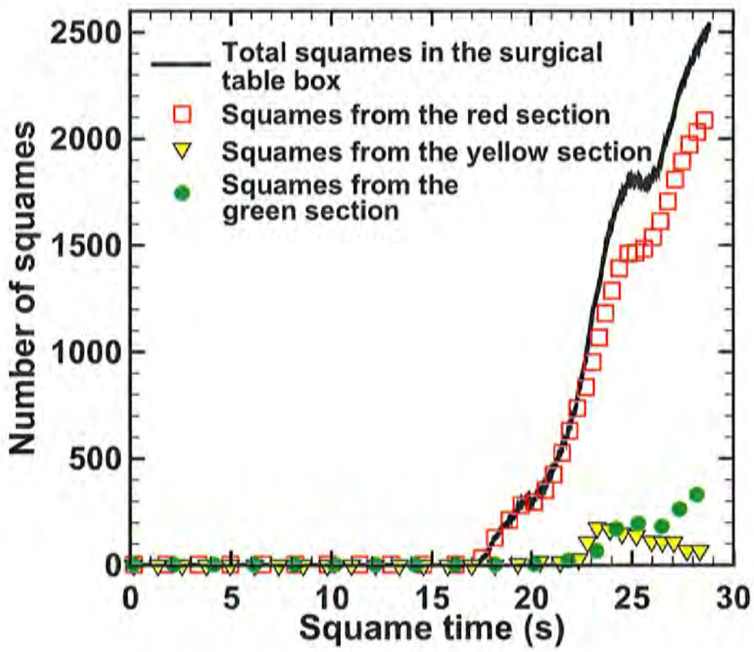

(b)

Figure 31: Temporal history of the total number of squames (shown by black color) entering four different regions of interest: (a) the patient's knee area, and (b) the OT box. Also shown in color is the number of color-coded squame particles entering from the red, green and yellow regions of the figure 21.

the surgical instruments on the side tables also have a small probability of carrying squames to the surgical site.

5 Summary and Concluding Remarks

A high-fidelity, large-eddy simulation (LES) was performed to study the interaction of the operating room (OR) ultra-clean ventilation air flow and the flow created by a forced air warming system (3M^{TM} Bair Hugger^{TM} blower) and its impact on the dispersion of squames particles. A full three-dimensional design of an OR with operating table (OT), surgical lamps, medical staff, side tables, a blower, and a patient undergoing knee surgery was constructed. Unstructured grid elements involving hexahedra, tetrahedra, pyramids and wedges were used to capture the complex geometry of the OR. An arbirary shaped, unstructured grid flow solver for LES based on governing equations for variable density in the limit of zero-Mach number was used. Ultraclean ventilation air enters the OR through 10 ceiling grilles with air changes per hour (ACH) of 24.45 and flow Reynolds number, based on the air inlet grille size and mean air inlet velocity, of 9226. The air inlet flow was developed from a periodic duct flow with the required target mass flow rate for each grille. No-slip conditions were applied for all solid surfaces and convective outflow condition was used at the four outlet grilles. Temperature values were specified at the surfaces of inlet grilles, the surgical lamps, heads of the medical staff, patient's head, and patient's knee and all other boundary surfaces were assumed adiabatic. Computations were performed on 1600 processors in parallel and flow statistics involving the time-averaged mean velocity field, turbulence intensity, and temperature distribution were computed.

Two computations were performed with the blower-off and blower-on to calculate a three-dimensional, time-dependent flow within the OR. Rising thermal plumes from the warm surfaces of surgeons heads, the patient's knee, patient's head, and the surgical lamp were calculated. With the blower on, air was drawn from the floor of the OR, heated, and blown into a blanket that covers the torso region of the patient. The blanket was covered with a plastic drape. The blower hot air generated forced convective currents and strong thermal plumes that interacted with the ultra-clean ventilation air. For both cases, trajectories of 3 million squames, placed initially on the floor in a small region surrounding the OT and surgeons, were calculated and contrasted to quantify the effect

of the hot air blower. The squames particles were assumed to be spherical in shape with 10 micron diameter and density of liquid water. The particle trajectories were tracked in a Lagrangian frame by computing the drag, lift, and buoyancy forces. The temporal variations of the number of squames particles within four imaginary boxes placed strategically above the two side tables, over the OT, and one surrounding the patient's knee were calculated and contrasted between the blower-off and blower-on cases. The following main conclusions can be drawn from these predictive computations:

1. For the case of blower-off, the ventilation air from the ceiling inlet grilles moves downwards, then is deflected by the surgical lights and the table, impinges on the floor farther away from the OT, and finally exits through the outlet grilles. Large recirculation regions are created on both sides of the table. The flow is not symmetric owing to asymmetries in the configuration of the OR contents. The maximum turbulence intensity level is about 30% in the high shear regions between the inlet air streams and the initial stagnant air in the OR, as well as near the warm surgical lights due to the buoyant plume. It is observed that the buoyant plumes from the patient's knee and other warm surfaces are relatively weak, and do not significantly alter the mean ventilation air flow.

2. For the case of blower-on, the mean flow underneath and around the OT is significantly modified and large levels of turbulence intensity are observed under the OT. The turbulence intensity levels are as high as 60% in regions affected by the rising thermal plumes from the blower. The instantaneous temperature contours confirm that the increased turbulence level is mainly because of the thermal plumes from the hot blower air causing higher temperature regions under the OT in comparison with the blower-off case. The flow is also highly asymmetric owing to the orientation and location of the drape. The rising thermal plumes are even observed to reach the ceiling in some regions and the downward ventilation flow from the inlet grilles was modified above the OT which also affected the recirculation region.

3. Drastic differences in the trajectories of the squames are observed between the blower-off and blower-on cases. With the blower-off, the majority of the squames are dispersed by the ventilation air flow towards the outlet grilles. None of the squames actually rise to the level of the side tables or the OT. In contrast, with the blower-on, a large number of squames are lifted upwards by the rising thermal plumes. Some of the squames are lifted above the surgeons

heads and are blown towards the OT by the downward moving ventilation air. Large number of squames are seen to be above the OT, several are surrounding the surgeons hands, above the side tables, and some are very close to the patient's knee and the surgical site. Majority of the squames that come close to the surgical site were found to have originated from the sides parallel to the length of the OT.

4. With the blower off, none of the squames particles were found to enter the four imaginary boxes placed above the side tables, OT, and a region surrounding the patient's knee. Some particles are lifted from the floor over time, but none rise close to the level of the imaginary boxes as the downward flow due to the ventilation air keeps the particles closer to the floor. With the blower turned on, hot air discharged from the edges of the drape and the resultant thermal plumes drag the squames, making them rise upwards. Some of the squames rise above the surgeons heads in the recirculation region on the sides of the OT. These particles are then flushed down onto the OT by the ventilation air from the inlet grilles. Statistically significant particles do enter the imaginary boxes of interest above the operating table and the patient's knee. Few particles are also observed above the side tables.

Starting with the worst-case scenario of having squames on the floor, it was shown that the hot air from the blower and the resultant thermal plumes are capable of lifting the particles and transporting them to the side tables, above the operating table, and the surgical site. It should be emphasized that if we also include the repetitive motion of the surgeons, the motion of medical assistants to fetch the surgical instruments placed on the side tables, and the resulting suspended squames shed by all staff in the OR, then the probability of dispersing the squames to the surgical site will be increased even further.

Although computationally intensive, large-eddy simulation of convective ventilation air flow and hot air from the blower in an OR is necessary to provide reliable predictions of the turbulent flow and dispersion of squames.

Appendix A

The aerodynamic behavior of squames suspended in a fluid is in general dependent upon the size and shape of the squames, their density, relative velocity with respect to the fluid motion, and density of the fluid. In the present study, the squames are suspended in air at room temperature (density ρ_g). The human skin cells or squames typically are disc-shaped with a diameter ranging from 4–20μm and a thickness of 3–5μm with density close to that of liquid water ($\rho_p = 1000\text{kg/m}^3$) (Noble *et al.*, 1963; Noble, 1975; Snyder, 2009).

Settling of a squame particle depends on its weight, the drag and buoyancy force on the particle, and its orientation relative to the flow direction. Owing to the changes in orientation and also resultant rotation and torque on disc particles, computing large number of trajectories in a Lagrangian frame is complicated. It is thus easier to assume these particles of spherical shape with an equivalent diameter such that their aerodynamic characteristics are matched. An equivalent diameter of the spherical particle should be calculated by matching the settling velocities for the two shapes.

Since $\rho_p/\rho_g = 1000$, the buoyancy force is much smaller compared to the weight of the particle. Then the settling velocity can be obtained from the balance of drag and gravitational forces,

$$F_d = F_g. \tag{24}$$

The drag and gravitational forces on a disc-shaped particle are given as,

$$F_d = C_{d,\text{disc}}\frac{1}{2}\rho_g U_{\text{disc}}^2 A_p, \tag{25}$$

$$F_g = (A_p h_{\text{disc}})\rho_p \text{g}; \;\; A_p = \frac{\pi}{4}D_{p,\text{disc}}^2 \tag{26}$$

where U_{disc} is the settling velocity of the disc, $C_{d,disc}$ is the drag coefficient, A_p is the frontal area of the circular disc, g is the gravitational acceleration, $D_{p,\text{disc}}$ is the diameter, and h_{disc} is the thickness of the disc. Equating the drag force to the weight of the disc to obtain the settling velocity as,

$$U_{\text{disc}} = \sqrt{2\text{g}\left(\frac{\rho_p}{\rho_g}\right)\left(\frac{h_{\text{disc}}}{C_{d,\text{disc}}}\right)}. \tag{27}$$

Following similar procedure, the settling velocity of a sphere of diameter $D_{p,\text{sphere}}$ can be ob-

tained as,

$$U_{\text{sphere}} = \sqrt{\frac{4}{3}g\left(\frac{\rho_p}{\rho_g}\right)\left(\frac{D_{p,\text{sphere}}}{C_{d,\text{sphere}}}\right)}, \tag{28}$$

where $C_{d,\text{sphere}}$ is the drag coefficient on a spherical particle.

In order to match the aerodynamic performance of the two shapes, the two settling velocities should be the same. Equating U_{disc} and U_{sphere} we get,

$$D_{p,\text{sphere}} = \frac{3}{2}h_{\text{disc}}\left(\frac{C_{d,\text{sphere}}}{C_{d,\text{disc}}}\right). \tag{29}$$

For Stokes flow ($Re \leq 1$), the drag coefficients are given as (Munson *et al.*, 1990),

$$C_{d,\text{sphere}} = \frac{24}{Re} \tag{30}$$

$$C_{d,\text{disc}} = \frac{20.4}{Re}, \quad \text{flow normal to circular disc} \tag{31}$$

$$= \frac{13.6}{Re}, \quad \text{flow parallel to circular disc.} \tag{32}$$

Using a disc thickness of $h_{\text{disc}} = 5\mu$m, and using the drag coefficients for the disc and the sphere, equation (29) gives an equivalent spherical diameter in the range of $D_{p,sphere} = 8.78$ and 13.2μm. Thus, an assumption of 10 micron spherical particle is reasonable to obtain similar dispersion behavior on an average as that of the disc-shaped squames particles.

References

ALBRECHT, MARK, GAUTHIER, ROBERT L, BELANI, KUMAR, LITCHY, MARK & LEAPER, DAVID 2011 Forced-air warming blowers: An evaluation of filtration adequacy and airborne contamination emissions in the operating room. *American journal of infection control* **39** (4), 321–328.

APTE, SV, GOROKHOVSKI, M. & MOIN, P. 2003*a* LES of atomizing spray with stochastic modeling of secondary breakup. *International Journal of Multiphase Flow* **29** (9), 1503–1522.

APTE, SV, MAHESH, K. & LUNDGREN, T. 2008*a* Accounting for finite-size effects in simulations of disperse particle-laden flows. *International Journal of Multiphase Flow* **34** (3), 260–271.

APTE, SV, MAHESH, K. & MOIN, P. 2008*b* Large–eddy simulation of evaporating spray in a coaxial combustor. *Proceedings of the Combustion Institute* **32**, accepted for publication.

APTE, SV, MAHESH, K., MOIN, P. & OEFELEIN, JC 2003*b* Large-eddy simulation of swirling particle-laden flows in a coaxial-jet combustor. *International Journal of Multiphase Flow* **29** (8), 1311–1331.

APTE, SOURABH V, MAHESH, KRISHNAN, GOROKHOVSKI, MICHAEL & MOIN, PARVIZ 2009 Stochastic modeling of atomizing spray in a complex swirl injector using large eddy simulation. *Proceedings of the Combustion Institute* **32** (2), 2257–2266.

AUSTIN, PAUL N 2015 Guest editorial. *AANA journal* **83** (4), 237.

CHEN, X-Q & PEREIRA, JCF 1998 Computation of particle dispersion in turbulent liquid flows using an efficient lagrangian trajectory model. *International journal for numerical methods in fluids* **26** (3), 345–364.

CHOW, TIN-TAI & WANG, JINLIANG 2012 Dynamic simulation on impact of surgeon bending movement on bacteria-carrying particles distribution in operating theatre. *Building and Environment* **57**, 68–80.

CLARK, RAYMOND P. & DE CALCINA-GOFF, MERVYN L. 2009 Some aspects of the airborne transmission of infection. *Journal of The Royal Society Interface* **6** (Suppl 6), S767–S782.

CROWE, CT, TROUTT, TR & CHUNG, JN 1996 Numerical models for two-phase turbulent flows. *Annual Review of Fluid Mechanics* **28** (1), 11–43.

DRUZHININ, OA & ELGHOBASHI, S. 1998 Direct numerical simulations of bubble-laden turbulent flows using the two-fluid formulation. *Physics of Fluids* **10**, 685.

EATON, JK & FESSLER, JR 1994 Preferential concentration of particles by turbulence. *International Journal of Multiphase Flow* **20**, 169–209.

EATON, J.K. & SEGURA, J.C. 2006 On momentum coupling methods for calculation of turbulence attenuation in dilute particle-laden gas flows. *Fluid Mechanics and its Applications* **81**, 39.

ELGHOBASHI, S. 1994 On predicting particle-laden turbulent flows. *Flow, Turbulence and Combustion* **52** (4), 309–329.

ELGHOBASHI, S. 2006 An updated classification map of particle-laden turbulent flows. *Fluid Mechanics and Its Applications* **81**, 3–10.

FERRANTE, A. & ELGHOBASHI, S. 2004 On the physical mechanisms of drag reduction in a spatially developing turbulent boundary layer laden with microbubbles. *Journal of Fluid Mechanics* **503**, 345–355.

FERRANTE, A. & ELGHOBASHI, S. 2007 On the accuracy of the two-fluid formulation in direct numerical simulation of bubble-laden turbulent boundary layers. *Physics of Fluids* **19**, 045105.

GERMANO, MASSIMO, PIOMELLI, UGO, MOIN, PARVIZ & CABOT, WILLIAM H 1991 A dynamic subgrid-scale eddy viscosity model. *Physics of Fluids A: Fluid Dynamics (1989-1993)* **3** (7), 1760–1765.

HAM, F., APTE, S., IACCARINO, G., WU, X., HERRMANN, M., CONSTANTINESCU, G., MAHESH, K. & MOIN, P. 2003 Unstructured LES of reacting multiphase flows in realistic gas turbine combustors. Annual Research Briefs 2003. *Center for Turbulence Research, NASA Ames/Stanford Univ* pp. 139–160.

HAM, FRANK & IACCARINO, GIANLUCA 2004 Energy conservation in collocated discretization schemes on unstructured meshes. *Annual Research Briefs* **2004**, 3–14.

KELLAM, MELISSA D, DIECKMANN, LORAINE S & AUSTIN, PAUL N 2013 Forced-air warming devices and the risk of surgical site infections. *AORN journal* **98** (4), 353–369.

KRAVCHENKO, AG & MOIN, PARVIZ 1997 On the effect of numerical errors in large eddy simulations of turbulent flows. *Journal of Computational Physics* **131** (2), 310–322.

KULICK, JD, FESSLER, JR & EATON, JK 2006 Particle response and turbulence modification in fully developed channel flow. *Journal of Fluid Mechanics Digital Archive* **277**, 109–134.

LEAPER, DAVID, ALBRECHT, MARK & GAUTHIER, ROBERT 2009 Forced-air warming: a source of airborne contamination in the operating room? *Orthopedic reviews* **1** (2), 28.

LEES, JULIENNE & BRIGHTON, WD 1972 Simulated human skin scales. *Journal of Hygiene* **70** (03), 557–565.

LEGG, AJ, CANNON, T & HAMER, AJ 2012 Do forced air patient-warming devices disrupt unidirectional downward airflow? *J Bone Joint Surg Br* **94** (2), 254–256.

MAHESH, K., CONSTANTINESCU, G., APTE, S., IACCARINO, G., HAM, F. & MOIN, P. 2006 Large-eddy simulation of reacting turbulent flows in complex geometries. *Journal of Applied Mechanics* **73**, 374.

MAHESH, K., CONSTANTINESCU, G. & MOIN, P. 2004 A numerical method for large-eddy simulation in complex geometries. *Journal of Computational Physics* **197** (1), 215–240.

MAXEY, MARTIN R & RILEY, JAMES J 1983 Equation of motion for a small rigid sphere in a nonuniform flow. *Physics of Fluids (1958-1988)* **26** (4), 883–889.

MCGOVERN, PD, ALBRECHT, M, BELANI, KG, NACHTSHEIM, C, PARTINGTON, PF, CARLUKE, I & REED, MR 2011 Forced-air warming and ultra-clean ventilation do not mix. *J Bone Joint Surg Br* **93** (11), 1537–1544.

MCNEILL, JAMES, HERTZBERG, JEAN & ZHAI, ZHIQIANG JOHN 2013 Experimental investigation of operating room air distribution in a full-scale laboratory chamber using particle image velocimetry and flow visualization .

MCNEILL, JAMES S *et al.* 2012 Field measurements of thermal conditions during surgical procedures for the development of cfd boundary conditions. *ASHRAE Transactions* **118**, 596.

MEMARZADEH, FARHAD 2003 Reducing risks of surgery. *ASHRAE journal* **45** (2), 28.

MEMARZADEH, FARHAD & MANNING, ANDREW P 2002 Comparison of operating room ventilation systems in the protection of the surgical site/discussion. *ASHRAE transactions* **108**, 3.

MITTAL, RAJAT & MOIN, PARVIZ 1997 Suitability of upwind-biased finite difference schemes for large-eddy simulation of turbulent flows. *AIAA journal* **35** (8), 1415–1417.

MOIN, P. & APTE, SV 2006 Large-eddy simulation of realistic gas turbine combustors. *AIAA Journal* **44** (4), 698–708.

MOIN, P. & MAHESH, K. 1998 Direct numerical simulation: A tool in turbulence research. *Annual Reviews in Fluid Mechanics* **30** (1), 539–578.

MOIN, P., SQUIRES, K., CABOT, W. & LEE, S. 1991 A dynamic subgrid model for compressible turbulence and scalar transport. *Physics of Fluids A.* **3**, 2746–2757.

MORETTI, B, LAROCCA, AMV, NAPOLI, C, MARTINELLI, D, PAOLILLO, L, CASSANO, M, NOTARNICOLA, A, MORETTI, L & PESCE, V 2009 Active warming systems to maintain perioperative normothermia in hip replacement surgery: a therapeutic aid or a vector of infection? *Journal of Hospital Infection* **73** (1), 58–63.

MUNSON, BRUCE ROY, YOUNG, DONALD F & OKIISHI, THEODORE H 1990 Fundamentals of fluid mechanics. *New York* **3** (4).

NG, V, LAI, A & HO, V 2006 Comparison of forced-air warming and electric heating pad for maintenance of body temperature during total knee replacement. *Anaesthesia* **61** (11), 1100–1104.

NOBLE, WC 1975 Dispersal of skin microorganisms. *British Journal of Dermatology* **93** (4), 477–485.

NOBLE, WC, LIDWELL, OM, KINGSTON, D *et al.* 1963 The size distribution of airborne particles carrying micro-organisms. *J Hyg (Lond)* **61** (385), e391.

PEREIRA, MARCELO LUIZ & TRIBESS, ARLINDO 2005 A review of air distribution patterns in surgery rooms under infection control focus. *Revista de Engenharia Térmica* **4** (2).

PIERCE, C.D. & MOIN, P. 1998*a* Turbulent flow over three-dimensional dunes: 2. Fluid and bed stresses. *Physics of Fluids* **10**, 3041–3044.

PIERCE, CHARLES DAVID 2001 Progress-variable approach for large-eddy simulation of turbulent combustion. PhD thesis, Citeseer.

PIERCE, CHARLES D & MOIN, PARVIZ 1998*b* Large eddy simulation of a confined coaxial jet with swirl and heat release. *AIAA paper* **2892**.

PIOMELLI, U 2014 Large eddy simulations in 2030 and beyond. *Philosophical Transactions of the Royal Society of London A: Mathematical, Physical and Engineering Sciences* **372** (2022), 20130320.

POPE, SB 2000 *Turbulent Flows*. Cambridge University Press.

POZORSKI, JACEK & APTE, SOURABH V 2009 Filtered particle tracking in isotropic turbulence and stochastic modeling of subgrid-scale dispersion. *International Journal of Multiphase Flow* **35** (2), 118–128.

READE, W.C. & COLLINS, L.R. 2000 Effect of preferential concentration on turbulent collision rates. *Physics of Fluids* **12**, 2530.

ROUSON, D.W.I. & EATON, J.K. 2001 On the preferential concentration of solid particles in turbulent channel flow. *Journal of Fluid Mechanics* **428**, 149–169.

SAARINEN, PEKKA E, KALLIOMÄKI, PETRI, TANG, JULIAN W & KOSKELA, HANNU 2015 Large eddy simulation of air escape through a hospital isolation room single hinged doorwayvalidation by using tracer gases and simulated smoke videos. *PloS one* **10** (7), e0130667.

SAFFMAN, PGT 1965 The lift on a small sphere in a slow shear flow. *Journal of fluid mechanics* **22** (02), 385–400.

SESSLER, DANIEL I, OLMSTED, RUSSELL N & KUELPMANN, RUEDIGER 2011 Forced-air warming does not worsen air quality in laminar flow operating rooms. *Anesthesia & Analgesia* **113** (6), 1416–1421.

SNYDER, OP 2009 A 'Safe Hands' hand wash program for retail food operations: a technical review. *Yeast* **55** (18.5), 14–8.

SOMMERFELD, M, ANDO, A & WENNERBERG, D 1992 Swirling, particle-laden flows through a pipe expansion. *Journal of fluids engineering* **114** (4), 648–656.

SRIDHAR, G. & KATZ, J. 1999 Effect of entrained bubbles on the structure of vortex rings. *J. Fluid Mech.* **397** (-1), 171–202.

STRAUB, A. 2016 *Bentley Microstation Design V8i, M/E Engineering, P.C.*. 150 North Chestnut Street, Rochester, NY 14604, www.meengineering.com.

TENNEKES, HENDRIK & LUMLEY, JOHN LEASK 1972 *A first course in turbulence*. MIT press.

WARTTIG, SHERYL, ALDERSON, PHIL, CAMPBELL, GILLIAN & SMITH, ANDREW F 2014 Interventions for treating inadvertent postoperative hypothermia. *The Cochrane Library* .

WOOD, AM, MOSS, C, KEENAN, A, REED, MR & LEAPER, DAVID J 2014 Infection control hazards associated with the use of forced-air warming in operating theatres. *Journal of Hospital Infection* **88** (3), 132–140.

Exhibit 2

Summary of Opinions

I have conducted a computation fluid dynamic simulation of a typical operating room and knee implant surgery procedure. In creating the three-dimensional model of the operating room and its setup, many assumptions were made to reduce the effects of the Bair Hugger patient warming system on disrupting the ventilation air flow. For example, the HVAC system modeled is superior to many, if not all, the HVAC systems used in operating rooms. Similarly, the assumptions made for draping, particle count, position of lights, etc. are all in favor of reducing the disruption caused by the Bair Hugger patient warming system.

Based upon my education, training, experience, and the computation fluid dynamics analysis discussed in Exhibit A, I will offer the following general causation opinions within a reasonable degree of engineering certainty:

1. The use of a Bair Hugger Model 750 Blower with the Bair Hugger Upper Body blanket disrupts the turbulent airflow around the operating table.

2. The use of a Bair Hugger Model 750 Blower with the Bair Hugger Upper Body blanket significantly increases the particle count over the surgical site, operating table, and side tables.

3. The use of a Bair Hugger Model 750 Blower with the Bair Hugger Upper Body blanket significantly reduces the effect of the operating room's HVAC system in protecting the surgical site from contaminants.

4. The use of a Bair Hugger Model 505 Blower with the Bair Hugger Upper Body blanket will have the same effects as stated in items 1 through 3 above, but at a reduced temporal rate, i.e. it would take longer time to observe the same effects of BH Model 750.

5. The Bair Hugger patient warming system significantly increases the number of contaminants reaching the operating table.

Name : S. E. Elghobashi June 2016
Nationality : U.S.A.

Education :

Degree	**Year**	**Institution**
M.Sc. (Mechanical Engineering)	1971	Univ. of Southern California, Los Angeles, USA.
Ph.D. (Mechanical Engineering)	1974	Imperial College, University of London, England.
D.Sc. (Mechanical Engineering)	1999	Imperial College, University of London, England.

Professional Activities (partial list)

Member of the National Academy of Engineering.
Fellow of the American Physical Society.
Fellow of the American Association for the Advancement of Science.
Fellow of the American Society of Mechanical Engineers.
Visiting Fellow of Cambridge University, Wolfson College, England, 1999.
Senior Award of International Conference on Multiphase Flow, Florence, Italy, May 25, 2016.
Chair of the Nominating Committee of American Physical Society, Div. Fluid Dynamics (2014-2015).
Member of Fellowship Committee of American Physical Society, Div. Fluid Dynamics (2009-11).
Member of Science and Engineering Advisory Committee (SETAC) of Blue Waters supercomputer project(2016-2017). https://bluewaters.ncsa.illinois.edu/setac
Senior member of the American Institute of Aeronautics and Astronautics(AIAA).
Member of the Combustion Institute.
Member of EuroMech.
Member of the Editorial Advisory Board of International J. of Multiphase Flow(2010-present).
Guest Editor of International J. of Multiphase Flow, Special Issue on Point-particle model for disperse turbulent flows, vol. 35, 2009.
DIC: Diploma of Membership of Imperial College in Mech. Engineering, 1974.
British Science Research Council (SRC) Scholarship (1971-1974).

Major Research Interests

Direct numerical simulation of turbulent flows, including multiphase and chemaically-reacting flows, and biomedical flows.

Research and Professional Experience

March 2015 -Present	**UC Distinguished Professor**, Mechanical and Aerospace Engineering Department, University of California, Irvine.
July 1985 - Feb. 2014	**Professor**, Mechanical and Aerospace Engineering Department, University of California, Irvine.

July 1997 -	June 2002	**Chairman**, Mechanical and Aerospace Engineering Department, University of California, Irvine.
Aug. 1984 -	July 1985	**Visiting Scientist**, DFVLR, German Aerospace Research Establishment, Institute of Atmospheric Physics, Oberpfaffenhofen, West Germany (Sabbatical Year).
July 1983 -	July 1984	**Vice Chairman** , Mechanical Engineering Department, University of California, Irvine.
July 1982 -	June 1985	**Associate Professor**, Mechanical Engineering Department, University of California, Irvine.
July 1978 -	June 1982	**Assistant Professor**, Mechanical Engineering Department, University of California, Irvine.
Jan. 1978 -	June 1978	**Staff Research Engineer**, Acurex Corporation, Aerotherm Division, Mountain View, California.
Oct. 1974 -	Dec. 1977	**Group Leader**, CHAM, (Concentration, Heat and Momentum), London, England and Huntsville, Alabama.

Reviewer for:

Journal of Fluid Mechanics
Physics of Fluids
Nature
Science
Physical review Letters
International Journal of Multiphase Flow
Journal of Combustion Science and Technology
Combustion and Flame
Journal of American Institute of Aeronautics and Astronautics
Journal of Fluids Engineering
Journal of Heat Transfer
International Journal of Numerical Heat Transfer
International Journal of Heat and Mass Transfer
International Journal of Heat and Fluid Flow
Progress in Energy and Combustion Science
Journal of Applied Mathematical Modeling
National Science Foundation
NASA
Department of Energy
University of California Energy Research Group
McGraw Hill Book Co.
John Wiley Book Co. and Wiley Interscience Europe.

Consulting

1974 - 1978

NASA- Lewis, NASA- Langley, NASA- Marshall, AFOSR, ARO, ONR

Westinghouse, General Electric, Airesearch
ALCAN, ALCOA, Corning, Phillip Morris
Ballistic Missile Advance Technology Center
Rolls-Royce, England
Rheinmetall, Germany
Societe National des Poudres et Explosifs, France
Spectron Development Labs.

1981 - 1996
Jet Propulsion Laboratory
Ballistic Missile Advance Technology Center
R&D Associates
Physical Research Inc.
P D A Engineering
1978 - 2000
Science Applications Inc.

Invited Keynote and Distinguished Lectures since 2000

L1. Elghobashi, S. " On the two-fluid and trajectory approaches for DNS of turbulent particle-laden flows", Part 1: DNS of bubble-laden flows via the two-fluid approach, [**Invited Lecture**] Von Karman Institute for Fluid Dynamics, Rhode-Saint-Genese, **Belgium**, April 3-7, 2000.

L2. Elghobashi, S. " On the two-fluid and trajectory approaches for DNS of turbulent particle-laden flows", Part 2: On the approximation of the two-way coupling terms in the trajectory approach, [**Invited Lecture**] Von Karman Institute for Fluid Dynamics, Rhode-Saint-Genese,
Belgium, April 3-7, 2000.

L3. Elghobashi, S. " On the point-force approximation in DNS of prticle-laden turbulent flows with two-way coupling", [**Invited lecture**] ERCOFTAC Conference on Dynamics of Particle-Laden Flows, Zurich, **Switzerland**, July 3-5, 2000.

L4. L4. Elghobashi, S. "Recent Advance in DNS of Particle-Laden Turbulent Flows" [**Invited Plenary lecture**], XI Congress on Numerical Methods and their Applications, ENIEF 2000 , San Carlos de Bariloche, **Argentina**, November 20-24, 2000.

L5. L5. Elghobashi, S. "The physical mechanisms of modifying the structure of turbulent homogeneous flows by dispersed particles ", [**Invited Plenary Lecture**], ERCOFTAC Conference on Small Particles in Turbulence , Seville, **Spain**, March 11-13, 2002.

L6. S. Elghobashi "On the physical mechanisms of drag reduction in a mirobubble-laden turbulent boundary layer" [**Keynote Lecture**] **at The 5th International Con-**

ference of Multiphase Flow (ICMF 2004), Yokohama, **Japan,** May 31 - June 3, 2004.

L7. S. Elghobashi "On the drag reduction in a mirobubble-laden spatially-developing turbulent boundary layer", **IUTAM Symposium** on Recent advances in disperse multiphase flow simulation- [**Invited Lecture**]- Chicago-October 2004.

L8. S. Elghobashi " Reynolds number effect on drag reduction in a microbubble-laden spatially-developing turb. boundary layer", **Euromech Conference on Hydrodynamics of bubbly flows-** [**Invited Lecture**]- Lorentz Center, Leiden, **the Netherlands,** June 6-8, 2005.

L9. S. Elghobashi "On drag reduction in a microbubble-laden spatially-developing turbulent boundary layer", **European Science Foundation- Challenging Turbulent Lagrangian Dynamics,** [**Invited Lecture**]- Castel Gandolfo, **Italy,** Sept. 1-4, 2005.

L10. S. Elghobashi "On drag reduction in a microbubble-laden spatially-developing turbulent boundary layer", **Thirteen IUTAM Advanced School & Workshop, Particle Dispersion in Turbulent Flows,** [**Invited Lecture I**] - CISM, Udine, **Italy,** September 12-16, 2005.

L11. S. Elghobashi " Reynolds number effect on drag reduction in a microbubble-laden spatially-developing turb. boundary layer", **Thirteen IUTAM Advanced School & Workshop, Particle Dispersion in Turbulent Flows,** [**Invited Lecture II**]- CISM, Udine, **Italy,** September 12-16, 2005.

L12. S. Elghobashi, " Direct simulation of turbulent flows laden with particles or bubbles", CIEMAT : Research Centre for Energy, Environment and Technology, [**Invited Lecture**], Madrid, **Spain,** June 21, 2006.

L13. S. Elghobashi, " DNS of the two-way interactions between dispersed solid particles and turbulent flows", **Workshop on multiphase turbulence: Dust storms, erosion, hurricanes and tornadoes,** [**Invited Lecture**], Xian, **China,** July 16-18, 2007.

L14. S. Elghobashi, " On the two-way interactions between dispersed solid particles and turbulent flows", **European Workshop on Direct and Large-Eddy Simulation,** [**Keynote Lecture**], Trieste, **Italy,** Sept. 8-10, 2008.

L15. S. Elghobashi " On the two-way interactions between dispersed particles and turbulent flows " , **March 2009 Meeting of American Physical Society** Pittsburgh, PA . Bulletin of APS, Vol. 54, 209, [**Invited Lecture**], March 18, 2009.

L16. S. Elghobashi " The physical mechanisms of two-way interactions between dispersed particles and turbulent flows", **Workshop on Clouds and Turbulence Institute for Mathematical Sciences,** Imperial College, [**Invited Lecture**], London, **England,** March 23-25, 2009.

L17. S. Elghobashi " How do inertial particles modify isotropic turbulence ?" **International Workshop- Solving the Riddle of Turbulence: What, Why, and How?** Max Planck Institute for Dynamics and Self-Organization, [**Invited Lecture**], Göttingen, **Germany,** May 6 - May 9, 2009.

L18. S. Elghobashi "How do inertial particles modify isotropic turbulence ?" **International Symposium on Turbulence"**, [**Invited Lecture**], Peking University, **Beijing, China,** Sept. 21-25, 2009.

L19. S. Elghobashi "How do inertial particles modify isotropic turbulence ?" **4th Latin-American Workshop on CFD "**, [**Keynote Lecture**], **Rio de Janiero, Brazil,** July 11-14, 2010.

L20. S. Elghobashi "On turbulence modulation by dispersed inertial particles"
13th European Turbulence Conference, ETC 13, [**Keynote Lecture**] **University of Warsaw, Poland,** September 12-15, 2011.

L21. F. Lucci, V.S. Lvov, A. Ferrante and S. Elghobashi, "Eulerian-Lagrangian bridge for the energy and dissipation spectra in homogeneous turbulence", [**Invited Lecture**], International Workshop on "Lagrange versus Euler for turbulent flows",
Wolfgang Pauli Institute, Vienna, Austria, May 7-12, 2012.

L22. S. Elghobashi "On the multi-way interactions between turbulent flows and suspended sediment"
International symposium on two-phase modeling for sediment dynamics in geophysical flows(THESIS-2013) [**Keynote Lecture**] **Chatou, Paris, France,** June 10-12, 2013.

L23. S. Elghobashi "On the multi-way interactions between turbulent flows and suspended particles"
Fluid-Mediated Particle Transport in Geophysical Flows (GEOFLOWS13), Kavli Institute for Theoretical Physics [**Invited Lecture**] **UCSB, Santa Barbara, California,** December 10, 2013.

L24. S. Elghobashi " Modulation of isotropic turbulence by dispersed particles," **Huazhong University of Science and Technology, Wuhan, China,** June 9, 2014. [**Plenary Lecture**].

L25. S. Elghobashi "Homogeneous shear turbulence modulation by dispersed small

particles," **Huazhong University of Science and Technology, Wuhan, China,** June 10, 2014. [**keynote Lecture**].

L26. S. Elghobashi "Modulation of isotropic turbulence by finite-size particles," **Huazhong University of Science and Technology, Wuhan, China,** June 11, 2014. [**keynote Lecture**].

L27. S. Elghobashi "How do dispersed inertial particles modify turbulent flows," Department of Mechanics and Engineering Science, **Peking University, China,** June 17, 2014 . [**Distinguished lecture**].

L28. S. Elghobashi "How do dispersed inertial particles modify turbulent flows," Center for Turbulence Research, **Stanford University,** July 25, 2014. [**Distinguished lecture**].

L29. S. Elghobashi "How do dispersed inertial particles modify turbulent flows," Computational and Applied Mathematics, **Pennsylvania State University,** October 10, 2014. [**Distinguished lecture**].

L30. S. Elghobashi "How do dispersed inertial particles modify turbulent flows," Aerospace Engineering department, **University of Minnesota,** April 21, 2015. [**Distinguished lecture**].

L31. S. Elghobashi "How do dispersed inertial particles modify turbulent flows," Mechanical Engineering department, **Northwestern University,** February 1, 2016. [**Distinguished lecture**].

L32. S. Elghobashi "How do dispersed inertial particles modify turbulent flows," Mechanical Engineering department, **MIT,** February 3, 2016. [**Distinguished lecture**].

Publications

Articles in Books

B1 Elghobashi, S.E., "Studies in the Prediction of Turbulent Diffusion Flames", **Studies in Convection**, Vol. 2, B.E. Launder, ed., Academic Press, London, (1977).

B2 Elghobashi, S. E.,and Nomura, K.N., "Direct Simulation of a Passive Diffusion Flame in Sheared and Unsheared Homogeneous Turbulence", **Turbulent Shear Flows 7** , pp. 313-329, W.C. Reynolds, ed., Springer-Verlag , (1991).

B3 Elghobashi, S. E. "Direct Simulation of turbulent flows laden with dispersed particles ", **Handbook on Multiphase Flow** , pp. 13-34:13-60, C. Crowe, ed., CRC , (2005).

B4 Elghobashi, S. E. "An updated classification map of particle-laden turbulent flows ", **Proceedings of IUTAM Symposium on Computational approaches to multiphase flow** , Springer pp. 3-10, , (2006).

B5 Loy, A.C., Jing, J., Zhang, J., Wang., Y., Elghobashi, S., Chen, Z. and Wong, B.J.F. "Anatomic optical coherence tomography of upper airways", **Optical Coherence Tomography: Technology and Applications,** Ed. W. Drexler and J. Fujimoto, Springer, Chapter 75, pp. 1145-2262, (2015).

Guest Editor

Elghobashi, S.E. " Point-Particle Models for Disperse Turbulent Flows", **International Journal of Multiphase Flow, Special Issue**, Volume 35, Issue 9, Pages 791-878, (September 2009).

Journal Papers

J1 Elghobashi, S.E., Pun, W.M. and Spalding, D.B., "Concentration Fluctuations in Isothermal Turbulent Confined Coaxial Jets",
Chem. Eng. Sci., Vol. 32, pp. 161-166 (1977).

J2 Elghobashi, S.E. and Wassel, A.T., "The Effect of Turbulent Heat Transfer on the Propagation of an Optical Beam Across Supersonic Boundary and Free Shear Layers",
Int. J. Heat and Mass Transfer, Vol. 23,pp.1229-1241 (1980).

J3 Elghobashi, S.E., Samuelsen, G.S., Wuerer, J.E., and LaRue, J.C., " Prediction and Measurement of Mass, Heat and Momentum Transport in a Nonreacting Turbulent Flow of a Jet in an Opposing Stream",
J. Fluids Engineering, Vol. 103, pp. 127-132 (1981).

J4 Megahed, I.E.A. and Elghobashi, S.E., "On the Numerical Solution of Indeterminate Steady Elliptic Flows",
Computer Methods in Applied Mechanics and Engineering, Vol. 26, pp. 225-240 (1981).

J5 Elghobashi, S.E. and Megahed, I.E.A., "Mass and Momentum Transport in a Laminar Isothermal Two-Phase Round Jet",
Int. J. Numerical Heat Transfer, Vol. 4 , pp. 317-329 (1981).

J6 Elghobashi, S.E. and Abou Arab, T.W., "A Two-Equation Turbulence Model for Two-Phase Flows",
Physics of Fluids, Vol. 26 , pp.931-938 (1983).

J7 Elghobashi, S.E. and Launder, B.E., "Turbulent Time Scales and the Dissipation Rate of Temperature Variance in the Thermal Mixing",
Physics of Fluids, Vol. 26 ,pp. 2415-2419 (1983).

J8 Modarress, D., Tan, H. and Elghobashi, S.E., "Two-Component LDA Measurement in a Two-Phase Turbulent Jet",
AIAA J. Vol. 22, pp. 624-630 (1984).

J9 Modarress, D., Wuerer, J. and Elghobashi, S.E., "An Experimental Study of a Turbulent Round Two-Phase Jet",
Chemical Engineering Communications, Vol. 28, pp. 341-354 (1984).

J10 Wassel, A.T. and Elghobashi, S.E., "Mathematical Simulation of Ocean Thermal Energy Conversion Sea Water Systems",
J. Solar Energy Engineering Vol. 106, pp. 198-205 (1984).

J11 Mostafa A.A. and Elghobashi, S.E., "A Study of the Motion of Vaporizing Droplets in a Turbulent Flow",
AIAA Progress in Astronautics and Aeronautics, Vol. 10,pp. 513-539 ,Oppenhiem and Soloukhin (editors) (1984).

J12 Elghobashi, S.E., Abou-Arab, T., Rizk, M. and Mostafa, A., "Prediction of the Particle-Laden Jet with a Two-Equation Turbulence Model",
Int. J. of Multiphase Flow, Vol. 10, pp. 697-710 (1984).

J13 Bellan J., and Elghobashi, S.E., "Fuel Composition Effects on High Temperature Corrosion in Boiler and Furnaces",
J. of Engineering for Power, Vol. 107, pp. 744-757 (1985).

J14 Rizk, M., and Elghobashi, S.E., "Wall Effects on the Motion of a Spherical Particle Suspended in a Turbulent Flow",
Physics of Fluids, Vol. 28, pp. 806-817 (1985).

J15 Mostafa, A.A. and Elghobashi, S.E., "A Two-Equation Turbulence Model for Jet Flows Laden with Vaporizing Droplets",
Int. J. of Multiphase Flow, Vol. 11, pp. 515-533 (1985).

J16 Schumann, U., Elghobashi, S.E., and Gerz, T., "Direct Simulation of Stably Stratified Turbulent Homogeneous Shear Flows",
Notes on Numerical Fluid Mechanics, Vol. 15, pp. 245-264 (1986).

J17 Prud'homme, M., and Elghobashi, S.E., "Turbulent Heat Transfer Near the Reattachment of Flow Downstream of a Sudden Pipe Expansion",
Int. J. Numerical Heat Transfer, Vol. 10, pp. 349-368 (1986).

J18 Conner, J. and Elghobashi, S.E., "Numerical Solution of Laminar Flow Past a Sphere with Surface Mass Transfer",
Int. J. Numerical Heat Transfer, Vol. 12, pp. 57-82 (1987).

J19 Rizk, M. and Elghobashi, S.E., "A Two-Equation Turbulence Model for Dispersed Dilute Two-Phase Confined Flows",
Int. J. of Multiphase Flow, Vol. 15, pp. 119-133 (1989).

J20 Gerz, T., Schumann, U. and Elghobashi, S., "Direct Simulation of Stably Stratified Homogeneous Turbulent Shear Flows",
J. Fluid Mechanics, Vol. 200, pp. 563-594 (1989).

J21 Tsau, F. , Elghobashi, S. E.,and Sirignano, W. " Effects of G- Jitter on a Thermally Buoyant Flow",
J. Thermophysics and Heat Transfer, vol. 6, pp. 246-254 (1992).

J22 Elghobashi, S. E., "Particle-Laden Turbulent Flows : Direct Simulation and Closure Models ",
J. Applied Scientific Research, vol.48, pp. 301-314 (1991).

J23 Elghobashi, S. E.,and Truesdell, G.C., "Direct Simulation of Particle Dispersion in a Decaying Isotropic Turbulence",
J. Fluid Mechanics, vol. 242, pp. 655-700 (1992).

J24 Nomura, K.N.,and Elghobashi, S. E. "Mixing characteristics of an inhomoge-

neous scalar in isotropic and homogeneous sheared turbulence",
Physics of Fluids, vol. 4, pp. 606-625 (1992).

J25 Kim, I. , Elghobashi, S. E., and Sirignano, W. " Three- dimensional flow over two spheres placed side by side",
J. Fluid Mechanics, vol. 246, pp. 465-488 (1993).

J26 Nomura, K.N.,and Elghobashi, S. E. " The structure of inhomogeneous turbulence in variable density nonpremixed flames",
Theoretical and Computational Fluid Dynamics, vol. 5, pp. 153-176 (1993).

J27 Elghobashi, S. E., and Truesdell, G.C., " On the two-way interaction between homogeneous turbulence and dispersed solid particles ; Part 1 : turbulence modification",
Physics of Fluids, vol. A5, pp. 1790-1801 (1993).

J28 Elghobashi, S. E., 'On Predicting Particle-Laden Turbulent Flows' ,
J. Applied Scientific Research, Vol. 52, 4, pp. 309-329 (1994).

J29 Truesdell, G.C., and Elghobashi, S. E." On the two-way interaction between homogeneous turbulence and dispersed solid particles ; Part 2 : particle dispersion",
Physics of Fluids, Vol. 6, pp. 1405-1407 (1994).

J30 Kim, I. , Elghobashi, S. E., and Sirignano, W. " Unsteady flow interactions between an advected cylindrical vortex tube and a spherical particle",
J. Fluid Mechanics, Vol. 288, pp. 123-155 (1995).

J31 Boratav, O. , Elghobashi, S. E., and Zhong, R. " On the alignment of the $\alpha-$strain and vorticity in turbulent nonpremixed flames",
Physics of Fluids, Vol. 8, pp. 2251-2253 (1996).

J32 Kim, I. , Elghobashi, S. E., and Sirignano, W. " Unsteady flow interactions between a pair of advected vortex tubes and a rigid sphere",
International J. Multiphase Flow, Vol. 23, pp. 1-23 (1997).

J33 Druzhinin, O. and Elghobashi, S., ' DNS of bubble-laden turbulent flows using the two-fluid formulation',
Physics of Fluids, Vol. 10, pp. 685-697 (1998).

J34 Kim, I. , Elghobashi, S. E., and Sirignano, W. ' On the equation for spherical particle motion : effects of Reynolds and acceleration numbers',
J. Fluid Mechanics, Vol. 367, pp. 221-253 (1998).

J35 Boratav, O. , Elghobashi, S. E., and Zhong, R.' On the alignment of strain,

vorticity and scalar gradient in turbulent, buoyant, nonpremixed flames',
Physics of Fluids, Vol. 10, pp. 2260-2267 (1998).

J36 Druzhinin, O. and Elghobashi, S., 'On the decay rate of isotropic turbulence laden with microparticles',
Physics of Fluids, Vol. 11, pp. 602-610 (1999).

J37 Druzhinin, O. and Elghobashi, S., ' A Lagrangian-Eulerian mapping solver for direct numerical simulation of a bubble-laden homogeneous turbulent shear flow using the two-fluid formulation ',
J. Computational Physics, Vol. 154, pp.174-196 (1999).

J38 Elghobashi, S. E., Zhong, R. and Boratav, O. ' Effects of gravity on turbulent nonpremixed flames',
Physics of Fluids, Vol. 11 , pp. 3123-3135 (1999).

J39 Zhong, R. , Elghobashi, S. E., Boratav, O. ' Surface topology of a buoyant turbulent nonpremixed flame',
Physics of Fluids, Vol. 12, pp. 2091-2100 (2000).

J40 Ahmed, A.M. and Elghobashi, S. E. On the mechanisms of modifying the structure of turbulent homogeneous shear flows by dispersed particles,
Physics of Fluids, Vol. 12, pp. 2906-2930 (2000).

J41 Druzhinin, O. and Elghobashi, S., ' Direct numerical simulation of a three-dimensional spatially-developing bubble-laden mixing layer with two-way coupling',
J. Fluid Mechanics, Vol. 429, pp. 23-61 (2001).

J42 Ahmed, A.M. and Elghobashi, S. E. Direct numerical simulation of particle dispersion in homogeneous turbulent shear flows ,
Physics of Fluids, Vol. 13, pp. 3346-3364 (2001).

J43 Ferrante, A. and Elghobashi, S. E. On the physical mechanisms of two-way coupling in particle-laden isotropic turbulence ,
Physics of Fluids, Vol. 15, pp. 315-329 (2003).

J44 Ferrante, A. and Elghobashi, S. E., ' A robust method for generating inflow conditions for direct simulations of spatially-developing turbulent boundary layers',
J. Computational Physics, Vol. 198, pp. 372-387 (2004).

J45 Latz, M. I., Juhl, A. R., Ahmed, A.M., Elghobashi, S. and Rohr, J. ' Hydrodynamic stimulation of dinoflagellate bioluminescence: A computational and experimental study',
J. Experimental Biology, Vol. 207, pp. 1941-1951(2004).

J46 Ferrante, A. and Elghobashi, S. E., ' On the physical mechanisms of drag reduction in a spatially-developing turbulent boundary layer laden with microbubbles', **J. Fluid Mechanics**, Vol. 503, pp. 345-355. (2004).

J47 Ferrante, A. and Elghobashi, S. E., Adams P., Valenciano M. and Longmire D. ' Evolution of quasi-streamwise vortex tubes and wall-streaks in a microbubble-laden turbulent boundary layer over a flat plate',
Physics of Fluids, Vol. 16(9), pp. S2 (2004).

J48 Ferrante, A. and Elghobashi, S. E., ' Reynolds number effect on drag reduction in a microbubble-laden spatially-developing turbulent boundary layer',
J. Fluid Mechanics, Vol. 543, pp. 93-106 (2005).

J49 Ferrante, A. and Elghobashi, S. E., ' On the effects of microbubbles on the Taylor-Green vortex flow',
J. Fluid Mechanics, Vol. 572 , pp. 145 - 177 (2007).

J50 Ferrante, A. and Elghobashi, S. E., ' On the accuracy of the two-fluid formulation in DNS of bubble-laden turbulent boundary layers',
Physics of Fluids, Vol. 19, 045105, pp.1-8 (2007).

J51 L'vov, V.S., Pomyalov, A., Ferrante, A. and Elghobashi, S. E., ' Analytical model of the time Developing turbulent boundary layer',
J. Exp. Theor. Phys., Vol. 86, issue 2, pp. 111-116 (2007).

J52 Lucci, F., Ferrante, A. and Elghobashi, S. E., ' Modulation of isotropic turbulence by particles of Taylor-lengthscale size',
J. Fluid Mechanics, Vol. 650, pp. 5-55 (2010).

J53 Lucci, F., Ferrante, A. and Elghobashi, S. ' Is Stokes number an appropriate indicator of turbulence modulation by large particles ?'
Physics of Fluids, Vol. 23, pp. 25101-1-7 (2011).

J54 Cleckler, J., Elghobashi, S. and Liu, F. 'On the motion of inertial particles by sound waves'
Physics of Fluids, Vol. 24, 033301 (2012).

J55 Lucci, F., L'Vov, V., Ferrante, A., Rosso, M. and Elghobashi, S. , ' Eulerian-Lagrangian bridge for the energy and dissipation spectra in isotropic turbulence ',
Theoretical and Computational Fluid Dynamics, DOI: 10.1007/s00162-013-0310-5(2013).

J56 Wang, Y. and Elghobashi, S. , ' On locating the obstruction in the upper

airway via numerical simulation ',
J. Respiratory Physiology & Neurobiology, Vol. 193, pp.1-10 (2014).

J57 Mylavarapu, G., Wang, Y., Elghobashi, S. and Gutmark, E. 'PIV measurements and numerical simulations of the flow in a human upper airway phantom',
Biomechanics and Modeling in Mechanobiology, submitted (2016).

Archival Conference Papers

C1 Elghobashi, S.E. and Pun, W.M., "A Theoretical and Experimental Study of Turbulent Diffusion Flames in Cylindrical Furnaces", **Proceedings of Fifteenth Symposium (International) on Combustion**, (1974).

C2 Elghobashi, S.E., Pratt, D.T., Spalding, D.B. and Srivatsa, S.K., "Unsteady Combustion of Fuel Spray in Jet Engine Afterburners", **Proceedings of Third International Symposium on Air Breathing Engines**, Munich (1976).

C3 Elghobashi, S.E. and Launder, B.E., "Modeling the Dissipation Rate of Scalar Fluctuations in a Thermal Mixing Layer", **Proceedings of Third Symposium on Turbulent Shear Flows**, (1981).

C4 Elghobashi, S.E. and Abou Arab, T.W., "A Second Order Turbulence Model for Two-Phase Flows", **Proceedings of Seventh International Heat Transfer Conference**, Munich (1982).

C5 Elghobashi, S.E. and Prud'homme, M., "On the Accuracy and Stability of Quadratic Upstream Differencing in Laminar Elliptic Flows", **Numerical Methods in Laminar and Turbulent Flow**, ed. Taylor, C., Johnson, J., and Smith, W., Pineridge Press, U.K., pp. 317-327 (1983).

C6 Mostafa A.A. and Elghobashi, S.E., "A Study of the Motion of Vaporizing Droplets in a Turbulent Flow", **Proceedings of Ninth International Colloquium and Dynamics of Explosions and Reactive Systems**, Poitiers, France, July (1983).

C7 Elghobashi, S.E., Abou Arab, T.W., Rizk, M. and Mostafa, A., "A Mathematical Model of the Turbulent Two-Phase Round Jet",**Proceedings of Fourth International Symposium on Turbulent Shear Flows**, Karlsruhe, Germany, Sept. (1983).

C8 Elghobashi, S.E., Rizk, M. and Mostafa, A., "A Mathematical Model of the Two- Phase Turbulent Axisymmetric Jet" , **Proceedings of the Third Multi-Phase Flow and Heat Transfer Symposium**, Miami, Florida, April (1983).

C9 Prud'homme, M. and Elghobashi, S.E., "Prediction of Wall-Bounded Turbulent Flows with an Improved Version of a Reynolds-Stress Model", **Proceedings of Fourth International Symposium on Turbulent Shear Flows**, Karlsruhe, Germany, Sept. (1983).

C10 Elghobashi, S.E. and J.C. LaRue, "The Effect of Mechanical Strain on the Dissipation Rate of a Scalar Variance", **Proceedings of Fourth International Sym-**

posium on Turbulent Shear Flows, Karlsruhe, Germany, Sept. (1983).

C11 Rizk, M. and Elghobashi, S.E., "A Mathematical Model for a Turbulent Gas-Solid Suspension Flow in a Vertical Pipe", **Proceedings of Fifth International Symposium on Turbulent Shear Flows**, Cornell Univ., August (1985).

C12 Elghobashi, S.E., Gerz, T. and Schumann, U., "Direct Simulation of Turbulent Homogeneous Shear Flow with Buoyancy", **Proceedings of Fifth International Symposium on Turbulent Shear Flows**, Cornell Univ., August (1985).

C13 Elghobashi, S.E., Gerz, T. and Schumann, U., "Direct Simulation of the Initial Development and the Homogeneous Limit of the Thermal Mixing Layer", **Proceedings of Sixth International Symposium on Turbulent Shear Flows**, Toulouse, France, (1987).

C14 Elghobashi, S. E.,and Nomura, K.N., "Direct Simulation of a Fast Chemical Reaction in a Homogeneous Turbulent Shear Flow", **Proceedings of Seventh Symposium on Turbulent Shear Flows**, Stanford, pp. 711-716 (1989).

C15 Elghobashi, S. E., and Truesdell, G.C., "Direct Simulation of Particle Dispersion in a Decaying Grid Turbulence", **Proceedings of Seventh Symposium on Turbulent Shear Flows**, Poster Session, Stanford (1989).

C16 Tsau, F. , Elghobashi, S. E., and Sirignano, W. " Effects of G- Jitter on a Thermal Buoyant Flow", Paper no 90-653, **AIAA 28th Aerospace Science Meeting**, Reno, Nevada, January (1990).

C17 Tsau, F. , Elghobashi, S. E.,and Sirignano, W. " Prediction of a Liquid Jet in a Gaseous Crossflow", Paper no 90-2067, **AIAA 26th Joint Propulsion Conference**, Orlando, Florida, July (1990).

C18 Nomura, K.N., and Elghobashi, S. E. "Direct Simulation of an Isothermal Nonpremixed Flame in a Homogeneous Turbulent Shear Flow", Paper no 90-148, **AIAA 28th Aerospace Science Meeting**, Reno, Nevada, January (1990).

C19 Kim, I. , Elghobashi, S. E., and Sirignano, W. " Three- dimensional droplet interactions in dense sprays", Paper no 91-0073, **AIAA 30th Aerospace Science Meeting**, Reno, Nevada, January (1991).

C20 Truesdell, G.C., and Elghobashi, S. E. "Direct numerical simulation of a particle-laden homogeneous turbulent flow ", **Proceedings of First ASME-JSME Fluids Engineering Conference**, Portland, Oregon, ASME-FED, Vol. 121, pp. 11-17, June

(1991).

C21 Elghobashi, S. E., and Truesdell, G.C., "On the interaction between solid particles and decaying turbulence ", **Proceedings of Eighth Symposium on Turbulent Shear Flows**, Munich, Germany , September (1991).

C22 Sirignano, W.A., Chiang, C.H., Kim, I. and Elghobashi, S. E. " Aerodynamic interactions amongst neighboring droplets", **4th International Symposium on Computational Fluid Dynamics**, Davis, Calif., September (1991).

C23 Kim, I. , Elghobashi, S. E., and Sirignano, W. " Three- dimensional flow computation for two interacting, moving droplets", Paper no 92-0343, **AIAA 30th Aerospace Science Meeting**, Reno, Nevada, January (1992).

C24 Nomura, K.N., and Elghobashi, S. E. " The structure of inhomogeneous turbulence in variable density nonpremixed flames", **Proceedings of IUTAM Symposium on Eddy Structure and Identification in Free Turbulent Shear Flows**, Poitiers, France, October (1992).

C25 Elghobashi, S. E. and Truesdell, G.C., " On the two-way interaction between homogeneous turbulence and dispersed solid particles", Papaer AIAA 93-1875, **AIAA /ASME 29th Joint Propulsion Conference**, Monterey, CA (1993).

C26 Elghobashi, S. E." On Predicting particle-laden turbulent flows ", **Proceedings of Seventh Workshop on Two-Phase Flows, Erlangen**, Germany, pp 211-219, April 11 (1994). [**Invited Lecture**]

C27 Elghobashi, S. E." Effects of the two-way coupling on particle dispersion ", **Proceedings of Seventh Workshop on Two-Phase Flows, Erlangen, Germany**, pp 224-230, April 13 (1994). [**Invited Lecture**]

C28 Kim, I. , Elghobashi, S. E., and Sirignano, W. " Unsteady flow interactions between a pair of advected cylindrical vortex tube and a rigid sphere", Paper no 95-0105, **AIAA 33th Aerospace Science Meeting**, Reno, Nevada, January (1995).

C29 Elghobashi, S. E., Lee, Y.Y. and Zhong, R. " Effects of gravity on sheared and nonsheared turbulent nonpremixed flame", **Third International Microgravity Combustion Workshop, NASA Lewis"**, Cleveland, Ohio, April 11-13 (1995).

C30 Kim, I. , Elghobashi, S. E., and Sirignano, W. " " The motion of a spherical particle in unsteady flows at moderate Reynolds numbers", **AIAA, 34th Aerospace Sciences Meeting**, Reno, NV, January (1996).

C31 Elghobashi, S. "Direct simulation of dispersed dilute two-phase turbulent flows",

Part 1: Decaying Turbulence, **Proceedings of the 1996 Lecture series programme, Von Karman Institute for Fluid Dynamics**, Rhode-Saint-Genese, Belgium, January 29-February 2, 1996. [**Invited Lecture**]

C32 Elghobashi, S. "Direct simulation of dispersed dilute two-phase turbulent flows", Part 2 : Homogeneous shear, **Proceedings of the 1996 Lecture series programme, Von Karman Institute for Fluid Dynamics**, Rhode-Saint-Genese, Belgium, January 29-February 2, 1996. [**Invited Lecture**]

C33 Elghobashi, S. and Lasheras, J. " Effects of gravity on sheared turbulence laden with bubbles or droplets", **Third Microgravity Fluid Physics Conference, NASA Lewis**, Cleveland, OH, June 13-15, 1996.

C34 Elghobashi, S., Boratav, O. and Zhong, R. " Effects of gravity on sheared and nonsheared turbulent nonpremixed flames", **Fourth International Microgravity Combustion Conference, NASA Lewis**, Cleveland, OH, May 19-21, 1997.

C35 Elghobashi, S. and Ahmed, A.M. ' DNS of turbulent homogeneous shear flow laden with particles: Two-way coupling', **Japan Society of Mechanical Engineers, Centennial Grand Congress,** Tokyo, Japan, July 18-19, 1997. [**Invited Lecture**]

C36 Druzhinin, O. and Elghobashi, S. 'DNS of bubble-laden turbulent flows using a two-fluid formulation', **Third International Conference on Multiphase Flow,** Lyon, France, June 8-12, 1998.

C37 Elghobashi, S. and Lasheras, J. 'Effects of gravity on sheared turbulence laden with bubbles or droplets' **Fourth Microgravity Fluid Physics and Transport Phenomena Conference,** NASA-Lewis, Cleveland, Ohio, August 12-14, 1998.

C38 Elghobashi, S. and Zhong, R. 'Effects of gravity on sheared turbulent nonpremixed flames' **Fifth International Microgravity Combustion Conference,** NASA-Lewis, Cleveland, Ohio, May 18-20, 1999.

C39 Elghobashi, S. " On the two-fluid and trajectory approaches for DNS of turbulent particle-laden flows", Part 1: DNS of bubble-laden flows via the two-fluid approach, **Proceedings of the 2000 Lecture series programme, Von Karman Institute for Fluid Dynamics**, Rhode-Saint-Genese, Belgium, April 3-7, 2000. [**Invited Lecture**]

C40 Elghobashi, S. " On the two-fluid and trajectory approaches for DNS of turbulent particle-laden flows", Part 2: On the approximation of the two-way coupling terms in the trajectory approach, **Proceedings of the 2000 Lecture series programme, Von Karman Institute for Fluid Dynamics**, Rhode-Saint-Genese, Belgium, April 3-7, 2000. [**Invited Lecture**]

C41 Ferrante, A. and Elghobashi, S. 'Effects of Reynolds number on drag reduction in a microbubble-laden spatially-developing turbulent boundary layer' **Second International Symposium on Seawater Drag Reduction,** Busan, Korea, May 23-26, 2005.

C42 Ferrante, A. and Elghobashi, S. ' On the accuracy of the two-fluid formulation in DNS of a microbubble-laden turbulent boundary layer 26^{th} **Symposium on Naval Hydrodynamics,** Rome, Italy, 17-22 September 2006.

C43 Ferrante, A. and Elghobashi, S. ' On the effects of finite-size particles on decaying isotropic turbulence' **International Conference on Multiphase Flow, ICMF 2007,** Leipzig, Germany, July 9 – 13, 2007.

C44 Lucci, F., Ferrante, A. and Elghobashi, S. ' Turbulence modulation by particles of the Taylor-lengthscale size: is Stokes number an appropriate indicator ?' **International Conference on Multiphase Flow, ICMF 2010,** Tampa, Florida, May 30- June 4, 2010.

Abstracts of Papers Presented at Conferences

A1 Mostafa A.A. and Elghobashi, S.E., "Prediction of a Turbulent Round Gaseous Jet Laden with Vaporizing Droplets", Western States/The Combustion Institute, UCLA, October (1983).

A2 Bellan J. and Elghobashi, S.E., "Impact of Fuel Composition on Deposits and on High-Temperature Corrosion in Industrial Furnaces", Western States Meeting, The Combustion Institute, UCLA, October (1983).

A3 Rizk, M. and Elghobashi, S.E., "Turbulent Fluid and Particle Interaction Near a Plane Wall", **Bull. Am. Phys. Soc.**, Vol. 28, pp. 1378 (1983).

A4 Rizk, M. and Elghobashi, S.E., "The Motion of a Spherical Particle Suspended in a Turbulent Flow Near a Plane Wall", **Proceedings of International Symposium on Two-Phase Annular and Dispersed Flows**, Pisa, Italy, June (1984).

A5 Elghobashi, S. E., and Truesdell, G.C., "Direct Simulation of Particle Dispersion in a Homogeneous Turbulent Shear Flow", Paper no. 73 f ,**AIChE Annual Meeting**, San Francisco, November (1989).

A6 Elghobashi, S. E. "Direct numerical simulation and modelling of particle-laden turbulent flows", **Shell Conference on Computational Fluid Dynamics** , Apeldoorn, The Netherlands, December 11,1989.

A7 Elghobashi, S. E., and Truesdell, G.C., "Direct Simulation of Particle Dispersion in Grid Turbulence and Homogeneous Shear Flows", **Bull. Am. Phys. Soc.**, Vol. 34, pp. 2311 (1989).

A8 Elghobashi, S. E., and Truesdell, G.C., "Direct Numerical Simulation of Particle-Laden Decaying Isotropic Turbulence", **21st Annual Meeting of The Fine Particle Society**, San Diego, Calif., August (1990).

A9 Kim, I. , Elghobashi, S. E., and Sirignano, W. " Three- dimensional flow interactions between two neighboring spheres", **Bull. Am. Phys. Soc.**, Vol. 36, pp. 2622 (1991).

A10 Elghobashi, S. E., and Truesdell, G.C., " On the modification of the energy spectrum of homogeneous turbulence by dispersed solid particles ", **Proceedings of Sixth Workshop on Two-Phase Flows**, Erlangen, Germany, pp 211-219, March 30 (1992). [**Invited Lecture**]

A11 Elghobashi, S. E., " On predicting particle-laden turbulent flows", **Workshop**

on turbulence in particulate multiphase flow, Fluid Dynamics Laboratory, Battelle Pacific Northwest Laboratory, Richland, WA, March 22, 1993.[**Invited Lecture**]

A12 Elghobashi, S. E., " Direct numerical simulation of particle dispersion and turbulence modulation in homogeneous turbulence", **NATO Advanced Research Workshop on Chaotic Advection, Tracer Dynamics, and Turbulent Dispersion**, Alessandria, Italy, May 24-28, 1993. [**Invited Lecture**]

A13

Elghobashi, S. E." One of the unresolved questions in predicting particle-laden turbulent flows ", **International Symposium on Numerical Methods for Multiphase Flows**, Lake Tahoe, NV, June 19-24 (1994). [**Invited Lecture**]

A14 Elghobashi, S. E." Mathematical models of particle-laden turbulent flows ", **Proceedings of 2nd International Workshop on Mathematical Modeling of Turbulent Flows, Tokyo**, Japan, July 29 (1994). [**Invited Lecture**]

A15 Elghobashi, S. E." Direct numerical simulation of particle-laden homogeneous turbulence ", **Proceedings of of 2nd International Workshop on Mathematical Modeling of Turbulent Flows, Tokyo**, Japan, July 30 (1994). [**Invited Lecture**]

A16 Nomura, K.N., and Elghobashi, S. E. "Interaction of chemical energy release and small-scale turbulence in a nonpremixed reacting flow", **47th Annual Meating of the American Physical Society**, Div. of Fluid Dynamics, Atlanta, GA, (1994).

A17 Elghobashi, S. E." DNS of bubble dispersion in homogeneous turbulent shear flows ", **ONR bubbly flow workshop**, UC San Diego, February 23-24 (1995).

A18 Elghobashi, S. E. "Direct simulation of particle dispersion in a homogeneous turbulent shear flow", Presented at the **Annual ASME/JSME Fluids Engineering Conference**, Hilton Head, S.C., August 13-18, (1995). [**Invited lecture**]

A19 Elghobashi, S., Boratav, O. and Zhong, R. 'Buoyancy effects on the structure of turbulence in nonpremixed flames', **48th Annual Meeting of American Physical Society,** Div. Fluid Dynamics, Irvine, CA, November 1995.

A20 Elghobashi, S. and Ahmed, A. " Bubble dispersion and turbulence modification in a homogeneous shear flow", **ONR workshop on Bubbly Flows,** UCSD, La Jolla, February 22-23, 1996.

A21 Elghobashi, S., Boratav, O. and Zhong, R. "Effects of buoyancy on turbulent nonpremixed flames', Presented at the **'International Conference on Turbulent Heat Transfer'**, San Diego, CA, March 10-15, 1996. [**Invited lecture**]

A22 Boratav, O. Elghobashi, S. and Zhong, R. 'Buoyancy effects on the struc-

ture of turbulence in nonpremixed flames', **SIAM - 6th International Conference on Numerical Combustion,** New Orleans, March 4-6, 1996.

A23 Elghobashi, S. and Ahmed, A. "On the two-way interactions between a turbulent homogeneous shear flow and dispersed particles", **Eighth Workshop on Turbulent Two-Phase Flows**, Merseburg, Germany, March 25-29, 1996.[**Invited lecture**]

A24 Elghobashi, S. " How do particles modify the turbulence energy of homogeneous shear flows ?", **ASME Fluids Engineering Conference**, San Diego, CA, July 8-11, 1996. [**Invited Lecture**]

A25 Elghobashi, S. and Ahmed, A. " How do particles modify the turbulence energy of homogeneous shear flows ?", **49th Annual Meeting of American Physical Society,** Div. Fluid Dynamics, Syracuse, NY, November 1996.

A26 Elghobashi, S., Zhong, R. and Boratav, O. " Evolution of flame surface in buoyant and nonbuoyant turbulent nonpremixed reactions", **49th Annual Meeting of American Physical Society,** Div. Fluid Dynamics, Syracuse, NY, November 1996.

A27 Latz, M., Juhl, A., Elghobashi, S., Ahmed, A. and Rohr, J. "Response of dinoflagellates in well-characterized laminar and turbulent flows: differentiating the effect of shear and acceleration", **Annual meeting of the American Society of Limnology and Oceanography (ASLO)**, Santa Fe, New Mexico, February 1997.

A28 Druzhinin, O. and Elghobashi, S. " A closure model for bubble-laden turbulent flows" **ONR workshop on Dynamics of Bubbly Flows, UCSD, February 19-21, 1997.**

A29 Elghobashi, S. " Modification of a homogeneous turbulent shear flow by dispersed particles" **Workshop on Turbulence Transport and Numerical Modeling, Center for Nonlinear Studies,** Los Alamos National Laboratory, June 3-7, 1997.[**Invited Lecture**]

A30 Elghobashi, S. and Druzhinin, O. " DNS of bubble-laden turbulent flows using the two-fluid formulation" **50th Annual Meeting of American Physical Society,** Div. Fluid Dynamics, San Francisco, CA, November 1997.

A31 Boratav, O., Elghobashi, S. and Zhong, R. " Persistence of strain in buoyant and nonbuoyant turbulent nonpremixed flames" **50th Annual Meeting of American Physical Society,** Div. Fluid Dynamics, San Francisco, CA, November 1997.

A32 Elghobashi, S. and Druzhinin, O. " DNS of bubble-laden turbulent flows using the two-fluid formulation" **ONR workshop on Dynamics of Bubbly Flows,** Caltech, February 25-27, 1998.

A33 Druzhinin, O. and Elghobashi, S. " A Lagrangian-Eulerian mapping solver for DNS of a bubble-laden homogeneous turbulent shear flow using the two-fluid formulation" **51st Annual Meeting of American Physical Society, Div. Fluid Dynamics,Philadelphia, PA,** November 22-24, 1998. Published in **Bulletin of APS, Vo. 43, 1965-2144, 1998**.

A34 Druzhinin, O. and Elghobashi, S. " A bubble-laden turbulent mixing layer: DNS and Closure model" **ONR workshop on Dynamics of Bubbly Flows,** UCSD, February 24-26, 1999.

A35 Druzhinin, O. and Elghobashi, S. " On the point-force approximation in DNS of particle-laden flows with two-way coupling " **51st Annual Meeting of American Physical Society, Div. Fluid Dynamics,New Orleans,LA** November 21-23, 1999. Published in **Bulletin of APS, Vol. 44, 15-194, 1999**

A36 Druzhinin, O. and Elghobashi, S. " DNS and Closure model for a bubble-laden turbulent mixing layer:" **ONR workshop on Dynamics of Bubbly Flows,** CALTECH, March 1-3, 2000. *

A37 Druzhinin, O. and Elghobashi, S. " On the point-force approximation in DNS of prticle-laden turbulent flows with two-way coupling", ERCOFTAC Conference on Dynamics of Particle-Laden Flows, Zurich, Switzerland, July 3-5, 2000.

A38 Elghobashi, S. " Recent Advance in DNS of Particle-Laden Turbulent Flows" **[Invited Plenary lecture], XI Congres on Numerical Methods and their Applications, ENIEF 2000** ,San Carlos de Bariloche, Argentina, November 2000.

A39 Druzhinin, O. and Elghobashi, S. " The properties of a spatially-developing bubble-laden mixing layer with two-way coupling" **53rd Annual Meeting of American Physical Society,** Div. Fluid Dynamics, Washington D.C., November 2000.

A40 Ahmed, A. and Elghobashi, S. " On the physical mechanisms of modifying the structure of turbulent homogeneous shear flows by dispersed particles " **53rd Annual Meeting of American Physical Society,** Div. Fluid Dynamics, Washington D.C., November 2000.

A41 Elghobashi, S. E." DNS of bubble-laden turbulent shear flows ", **ONR bubbly flow workshop,** CALTECH, Pasadena, April 17-19, 2001.

A42 Druzhinin, O. and Elghobashi, S. 'Direct numerical simulation of a three-dimensional spatially-developing bubble-laden mixing layer with two-way coupling', **4th International Conference on Multiphase Flow-ICMF 2001,** New Orleans, May 26-31, 2001.

A43 Elghobashi, S." The physical mechanisms of modifying the structure of turbulent homogeneous shear flows by dispersed particles ", **Euromech Colloqium 421: Strongly-Coupled Dispersed Two-Phase Flows** , LEGI, Grenoble, France, September 10-12, 2001.

A44 Elghobashi, S." The physical mechanisms of modifying the structure of turbulent homogeneous flows by dispersed particles ", **[Invited Plenary Lecture], ERCOFTAC Conference on Small Particles in Turbulence** , Seville, Spain, March 11-13, 2002.

A45 Elghobashi, S. and Ferrante, A. " DNS of bubble-laden spatially-developing turbulent boundary layer with one-way coupling" **ONR workshop on Dynamics of Bubbly Flows,** UCSD, La Jolla, Calif., April 3-4, 2002.

A46 Ferrante, A. and Elghobashi, S. " Dispersion of bubbles in a spatially-developing turbulent boundary layer" **55th Annual Meeting of American Physical Society,** Div. Fluid Dynamics, Dallas, Texas, November 2002.

A47 Elghobashi, S. and Ferrante, A. " DNS of bubble-laden spatially-developing turbulent boundary layer with two-way coupling" **ONR workshop on Waves and Dynamics of Bubbly Flows,** Caltech, Pasadena, Calif.,February 19-20, 2003.

A48 Elghobashi, S. and Ferrante, A. " DNS of bubble-laden spatially-developing turbulent boundary layer" **5th Euromech Fluid Mechanics Conference,** Toulouse, France, August 24-28, 2003.

A49 Ferrante, A. and Elghobashi, S. "Drag reduction in a spatially-developing turbulent boundary layer laden with microbubbles," **ERCOFTAC Multiphase Flow Conference, ETH, Zurich, Switzerland,** November, 2003.

A50 Elghobashi, S. and Ferrante, A. " Drag reduction in a bubble-laden spatially-developing turbulent boundary layer over a flat plate", **56th Annual Meeting of American Physical Society,** Div. Fluid Dynamics, East Rutherford, New Jersey, November 2003. Published in **Bulletin of APS, Vol. 48, p.116, 2003**.

A51 Ferrante, A. and Elghobashi, S. " A method for generating inflow conditions for direct simulations of spatially-developing turbulent boundary layers" **56th Annual Meeting of American Physical Society,** Div. Fluid Dynamics, East Rutherford, New Jersey, November 2003. Published in **Bulletin of APS, Vol. 48, p.119, 2003**.

A52 Elghobashi, S. and Ferrante, A. " The physical mechanisms of drag reduction in a microbubble-laden turbulent boundary layer with one-way coupling" **ONR workshop on Dynamics of Bubbly Flows,** UCSD, La Jolla, Calif., March 24-25, 2004.

A53 Elghobashi, S. "On the physical mechanisms of drag reduction in a mirobubble-laden turbulent boundary layer" **Keynote Lecture at The 5th International Conference of Multiphase Flow (ICMF 2004)**, Yokohama, Japan, May 31 - June 3, 2004.

A54 Elghobashi, S. " On the drag reduction in a mirobubble-laden spatially-developing turbulent boundary layer", IUTAM Symposium on Recent advances in disperse multiphase flow simulation- [**Invited Lecture**]- Chicago-October 2004.

A55 Ferrante, A. and Elghobashi, S. " Effects of bubble diameter on drag reduction in a spatially developing turbulent boundary layer over a flat plate", **57th Annual Meeting of American Physical Society,** Div. Fluid Dynamics, Seattle, Washington, November 2004. Published in **Bulletin of APS, Vol. 49, p.129, 2004.**

A56 Elghobashi, S. " On the drag reduction in a mirobubble-laden spatially-developing turbulent boundary layer", **ONR workshop on Dynamics of Bubbly Flows,** Reston, VA, April 4-5, 2005.

A57 Elghobashi, S. " Reynolds number effect on drag reduction in a microbubble-laden spatially-developing turb. boundary layer", **Euromech Conference on Hydrodynamics of bubbly flows- [Invited Lecture]**- Lorentz Center, Leiden, the Netherlands, June 6-8, 2005.

A58 Elghobashi, S. "On drag reduction in a microbubble-laden spatially-developing turbulent boundary layer", **European Science Foundation- Challenging Turbulent Lagrangian Dynamics, [Invited Lecture]**- Castel Gandolfo, Italy, Sept. 1-4, 2005.

A59 Elghobashi, S. "On drag reduction in a microbubble-laden spatially-developing turbulent boundary layer", **Thirteen IUTAM Advanced School & Workshop, Particle Dispersion in Turbulent Flows, [Invited Lecture I]**- CISM, Udine, Italy, September 12-16, 2005.

A60 Elghobashi, S. " Reynolds number effect on drag reduction in a microbubble-laden spatially-developing turb. boundary layer", **Thirteen IUTAM Advanced School & Workshop, Particle Dispersion in Turbulent Flows, [Invited Lecture II]**- CISM, Udine, Italy, September 12-16, 2005.

A61 Ferrante, A. and Elghobashi, S. " Effects of microbubbles on the Taylor-Green vortex flow" , **58th Annual Meeting of American Physical Society,** Div. Fluid Dynamics,Chicago, IL, November 2005. Published in **Bulletin of APS, Vol. 50, p.130, 2005.**

A62 Elghobashi, S. and Ferrante, A. " Reynolds number effect on drag reduction

in a microbubble-laden spatially-developing turbulent boundary layer " , **58th Annual Meeting of American Physical Society,** Div. Fluid Dynamics,Chicago, IL, November 2005. Published in **Bulletin of APS, Vol. 50, p.132, 2005.**

A63 Elghobashi, S. " On the accuracy of the two- fluid formulation in DNS of a microbubble-laden turbulent boundary layer", **ONR 2006 Ship Wave-breaking and Bubble Wake Review**, Caltech, Pasadena, CA, March 29-30, 2006.

A64 Ferrante, A. and Elghobashi, S. " On the accuracy of the two-fluid formulation in DNS of bubble-laden turbulent boundary layers" , **59th Annual Meeting of American Physical Society, Div. Fluid Dynamics,** Tampa, FL, November 2006. Published in Bulletin of APS, Vol. 51, 2006.

A65 Elghobashi, S. " DNS of the two-way interactions between dispersed solid particles and turbulent flows", **Workshop on multiphase turbulence: Dust storms, erosion, hurricanes and tornadoes, [Invited Lecture],** Xian, **China,** July 16-18, 2007.

A66 Ferrante, A. and Elghobashi, S. " Fully resolved DNS of freely moving finite-size particles in decaying isotropic turbulence" , **60th Annual Meeting of American Physical Society, Div. Fluid Dynamics,** Salt Lake City, UT, November 2007. Published in Bulletin of APS, Vol. 52, 2007.

A67 Cleckler,J., Liu, F. and Elghobashi, S. " Aerosol particle motion induced by non-linear sound waves" , **61th Annual Meeting of American Physical Society, Div. Fluid Dynamics,** San Antonio, Texas, November 2008. Published in Bulletin of APS, Vol. 53, 2008.

A68 Elghobashi, S. "On the two-way interactions between dispersed solid particles and turbulent flows", **European Workshop on Direct and Large-Eddy Simulation, Keynote Lecture,** Trieste, **Italy,** Sept. 8-10, 2008.

A69 Lucci, F., Ferrante, A. and Elghobashi, S. " DNS of fully resolved spherical particles dispersed in isotropic turbulence " , **61th Annual Meeting of American Physical Society, Div. Fluid Dynamics,** San Antonio, Texas, November 2008. Published in Bulletin of APS, Vol. 53, 2008.

A70 Elghobashi, S. " On the two-way interactions between dispersed particles and turbulent flows ",**[Invited Lecture], March 2009 Meeting of American Physical Society** Pittsburgh, PA . Published in Bulletin of APS, Vol. 54, 209, March 18, 2009.

A71 Elghobashi, S. " The physical mechanisms of two-way interactions between dispersed particles and turbulent flows", **Workshop on Clouds and Turbulence Institute for Mathematical Sciences,** Imperial College, **[Invited Lecture]**, London, **England,**

March 23-25, 2009.

A72 Elghobashi, S. " How do inertial particles modify isotropic turbulence ?" **International Workshop- Solving the Riddle of Turbulence: What, Why, and How?** Max Planck Institute for Dynamics and Self-Organization, [**Invited Lecture**], Göttingen, **Germany,** May 6-9, 2009.

A73 Elghobashi, S. "How do inertial particles modify isotropic turbulence ?" **International Symposium on Turbulence"**, [**Invited Lecture**], Peking University, **Beijing, China,** Sept. 21-25, 2009.

A74 Lucci, F., Ferrante, A. and Elghobashi, S. " On the effects of Taylor-lengthscale size particles on isotropic turbulence ", **62nd Annual Meeting of American Physical Society, Div. Fluid Dynamics,** Minneapolis, Minnesota. Published in Bulletin of APS, Vol. 54, No. 19, p. 159, November 20-23, 2009.

A75 Lucci, F., Ferrante, A. and Elghobashi, S. " Is Stokes number an appropriate indicator for turbulence modulation by particles of Taylor-length-scale size? ", **63nd Annual Meeting of American Physical Society, Div. Fluid Dynamics,** Long Beach, California. Published in Bulletin of APS, Vol. 55, No. 16, p. 150, November 20-23, 2010.

A76 Cleckler, J., Liu, F. and Elghobashi, S. " Numerical simulation of particle dispersion in an acoustic field ", **63nd Annual Meeting of American Physical Society, Div. Fluid Dynamics,** Long Beach, California. Published in Bulletin of APS, Vol. 55, No. 16, p. 319, November 23, 2010.

A77 Lucci, F., L'Vov, V., Ferrante, A. and Elghobashi, S. " On the Lagrangian Power Spectrum of Turbulence Energy in Isotropic Turbulence ", **64th Annual Meeting of American Physical Society, Div. Fluid Dynamics,** Baltimore, MD , Published in Bulletin of APS, Vol. 56, No. 18, p. 80, November 20-22, 2011.

A78 Wang, Y. and Elghobashi, S. " Direct numerical simulation of the flow in the pediatric upper airway ", **34th Annual Int. Conf. of the IEEE Engineering in Medicine & Biology (EMB) Society,** San Diego, CA, August 28-September 1, 2012.

A79 Wang, Y. and Elghobashi, S. " Direct numerical simulation of the flow in the human upper airway ", **65th Annual Meeting of American Physical Society, Div. Fluid Dynamics,** San Diego, CA , Published in Bulletin of APS, Vol. 57, No. 17, p. 333, November 18-20, 2012.

A80 Wang, Y. and Elghobashi, S. " On locating the obstruction in the human upper airway,Direct numerical simulation ", **66th Annual Meeting of American Physical Society, Div. Fluid Dynamics,** Pittsburgh, PA, November 24-26, 2013.

A81 Y. Wang, L. Oren, E. Gutmark a and S. Elghobashi, " DNS and PIV measurements of the flow in a model of the human upper airway", **67th Annual Meeting of American Physical Society, Div. Fluid Dynamics,** San Francisco, CA, November 23-25, 2014.

Technical Reports

Yeh, G.C.K. and Elghobashi, S.E., "A Two-Equation Turbulence Model for a Dispersed Two-Phase Flow with Variable Density Fluid and Constant Density Particles", Defense Nuclear Agency Report DNA-TR-86-42, 1986.

Elghobashi, S.E. and Rizk, M.A., "The Effect of Solid Particles on the Turbulent Flow of a Round Gaseous Jet: A Mathematical and Experimental Study", DOE/PC,30303-5, December (1983).

Wassel, A.T., Elghobashi, S.E., and Wenger, R.S., "Analysis of the Sea Water Systems of Ocean Thermal Energy Conversion Pilot Plants", SAI Report No. 82R-018-LA, October (1982).

Bellan, J. and Elghobashi, S.E., "Present and Projected Status of Computer Modeling in Furnace and Boiler Technology', US DOE, Jet Propulsion Lab. Report, Nov. (1982).

Elghobashi, S.E., Lockwood, F.C. and Naguib, A.S., "The Calculation of Combustion Processes", Imperial College Mech. Engr. Dept., HTS/74/8, (1974).

Elghobashi, S.E., Pun, W.M., "A Theoretical and Experimental Study of Turbulent Diffusion Flames in Cylindrical Chambers", Imperial College, Mech. Engr. Dept., HTS/74/3, (1974).

Elghobashi, S.E., "Concentration Fluctuations in Isothermal Turbulent Confined Jets", Imperial College, Mech. Engr., HTS/75/23, (1975).

Elghobashi, S.E., "Prediction of the Three Dimensional Flow and Radiation Heat Transfer Inside a Cylindrical Glass Furnace", for Corning, (1977).

Elghobashi, S.E., "Prediction of the Three Dimensional Flow Inside a Liquid- Metal Fast-Breeder Reactor Steam Generator", for Westinghouse, (1978).

Elghobashi, S.E., "Prediction of the Flow and the Concentration of CO and NO_x inside a Burning Cigarette", for Philip Morris, (1977).

Elghobashi, S.E., "Prediction of the Flow Around the Earth and the Influence of Temperature Gradients on Both Hemispheres", for NASA Marshall, (1977).

Elghobashi, S.E., "Prediction of the Flow Inside a Crystal-Growth Device at Near-Zero Gravity", for NASA Marshall, (1978).

Elghobashi, S.E., "Prediction of the Effects of Low Gravity and Heat Transfer on the Trajectories of Blood Cells in an Electrophoresis Chamber", for NASA Marshall, (1978).

Elghobashi, S.E., "Prediction of the Flow and Electrical Properties of a Rocket Exhaust Plume", for US Air Force, (1978).

Elghobashi, S.E., Spalding, D.B. and Thyagraja, A., "Prediction of Three Dimensional Supersonic Flow of a Conical Body Interacting with a Plane Blast Wave", prepared for Ballistic Missile Defense Advance Technology Center, Huntsville, (1976).

Elghobashi, S.E., "Prediction of Transient Flow and Heat Transfer in 155 MM Gun Barrel and its Exhauster", prepared for Rheinmetall, West Germany (1976).

Elghobashi, S.E., "Prediction of Three Dimensional flow and Chemical Reaction in a Can Combustor with Fuel Spray", prepared for Airesearch Co. of Arizona (1976).

Elghobashi, S.E., Spalding, D.B. and Srivatsa, S.K. "Prediction of Three Dimensional Flow in a Hall-Cell Aluminum Smelter", prepared for ALCOA (1975).

Elghobashi, S.E., Moult, A. and Spalding, D.B., "Prediction of Compressible Flow in the Combustion Chamber of a Solid-Propellant Rocket" prepared for Societe National des Poudres et Explosifs, France (1975).

Elghobashi, S., Rosten, H. and Spalding, D.B.," Effects of gravity on Methane-air combustion", **NASA-CR 2671**, (1974).

Elghobashi, S., Pratt, D.T., Runchal, A.K., Spalding, D.B. and Srivatsa, S.K. " Unsteady combustion of fuel spray in jet engine afterburners, The CID4 computer program," CHAM 551/1, (1975).

Elghobashi, S., Spalding, D.B. and Srivatsa, S.K., " Prediction of hydrodynamics and chemistry of confined turbulent methane-air flames with attention to formation of oxides of nitrogen,"**NASA CR-135179**, (1977).

Elghobashi, S. and Spalding, D.B., " Equilibrium chemical reaction of supersonic hydrogen-air jets (The ALMA computer program)", **NASA CR-2725**, (1977).

Invited Research Presentations (1983- Present)

"How do dispersed inertial particles modify turbulent flows ?" **École Polytechnique,** The Hydrodynamics Laboratory (LadHyX), **Palaiseau, France,** June 14, 2013.

"How do dispersed inertial particles modify turbulent flows ?" **University of California, San Diego,** Mechanical and Aerospace Engineering Dept., June 3, 2013.

"Direct numerical simulation of the flow in the upper airway via lattice Boltzmann method" **National Institute of Health,** Bethesda, MD, April 29, 2013.

"On the physical mechanisms of drag reduction in a spatially-developing turbulent boundary layer laden with microbubbles " **École Normal Supérieur, Paris, France,** March 17, 2011.

"Direct numerical simulation of the flow in the upper airway via lattice Boltzmann method" **National Institute of Health,** Bethesda, MD, Feb. 24, 2011.

"Turbulence modulation by dispersed inertial particles" Mech. Eng. Dept., **Univ. of California, Berkeley,** February 11, 2011.

" On the two-way interactions between dispersed particles and turbulent flows" **School of Engineering and Mathematical Sciences, City University, London, England,** March 26, 2009.

"On the effects of finite-size solid particles on decaying isotropic turbulence", **Institut de Mècanique des Fluides de Toulouse, IMFT, Toulouse, France,** June 28, 2007.

"On the physical mechanisms of drag reduction in a spatially-developing turbulent boundary layer laden with microbubbles " **Ecole Polytechnique,** The Hydrodynamics Laboratory (LadHyX), **Palaiseau, France,** June 26, 2007.

"Turbulence modification in flows laden with particles or bubbles" **The Johns Hopkins University,** Mechanical Engineering Department, February 15, 2007.

" Direct simulation of turbulent flows laden with particles or bubbles", **Invited Lecture,** CIEMAT **: Research Centre for Energy, Environment and Technology, Madrid, Spain, June 21, 2006.**

"On drag reduction in a spatially-developing turbulent boundary layer laden with microbubbles", **Department of Mechanics and Aeronautics, University of Rome "La Sapienza", Rome,, Italy,** September 5, 2005.

"On the drag reduction in a mirobubble-laden spatially-developing turbulent boundary

layer," **School of Mechanical and Aerospace Engineering, Center for Turbulence and Flow Control Research, Seoul National University, Seoul, South Korea**, May 27, 2005.

"On the physical mechanisms of drag reduction in a mirobubble-laden turbulent boundary layer", **Department of Mechanical Engineering, University of Tokyo, Japan, June 7, 2004.**

"On the physical mechanisms of drag reduction in a spatially-developing turbulent boundary layer laden with microbubbles", **Mech. Eng. Dept., Univ. California, Santa Barbara, California**, February 14, 2004.

"Recent advances in DNS of particle-laden turbulent flows ", **Institute for Scientific Computing Research, Lawrence Livermore Research Laboratory, Livermore, California** , August 7, 2003.

"DNS of turbulent flows laden with particles ", **Institute for Scientific Computing Research, Lawrence Livermore Research Laboratory, Livermore, California** , March 27, 2003.

" On the physical mechanisms of modifying the structure of turbulent homogeneous shear flows by dispersed particles", **Mechanical Engineering Dept., Stanford University, Stanford, California,** October 30, 2001.

"Recent Advances in DNS of Turbulent Flows Laden with Particles, Droplets or Bubbles", **Universite Pierre et Marie Curie, Paris, France**, September 19, 2001.

"Recent advances in direct numerical simulations (DNS) of turbulent shear flows laden with particles ", **Institute for Scientific Computing Research, Lawrence Livermore Research Laboratory, Livermore, California** , May 4, 2001.

"Recent Advances in DNS of Turbulent Flows Laden with Particles, Droplets or Bubbles", **The Aerospace Corporation, Los Angeles, California**, April 17, 2001.

"Recent advances in direct numerical simulations (DNS) of turbulent shear flows laden with particles ", **Institute for Scientific Computing Research, Lawrence Livermore Research Laboratory, Livermore, California** , May 4, 2001.

" On the physical mechanisms of modifying the structure of turbulent homogeneous shear flows by dispersed particles ", **ETH, Zürich, Switzerland**, October 4, 2000.

" Recent advances in direct numerical simulations (DNS) of turbulent shear flows laden with particles ", **Paul Scherer Institute, Villigen, Switzerland**, October 3, 2000.

" Recent advances in direct numerical simulations (DNS) of turbulent shear flows laden with particles and bubbles", **Mechanical Engineering Department, Imperial College, London**, April 6, 2000.

" Recent advances in direct numerical simulations (DNS) of turbulent shear flows laden with particles and bubbles", **Mechanical and Aerospace Engineering Department, Univ. California, San Diego**, March 15, 2000.

" Direct numerical simulation of particle-laden flows: the trajectory and two-fluid approaches", **Dept. of Mechanical Engineering, Univ. of Illinois, Urbana-Champaign**, November 9, 1999.

" Evolution of flame surface in buoyant and nonbuoyant turbulent nonpremixed reactions", **Graduate Aeronautical Laboratories, California Institute of Technology**, January 16, 1998.

" How do particles modify the turbulence energy in a homogeneous shear flow ?", **Department of Chemical Engineering, Univ. of California, Santa Barbara,** April 16, 1997.

" Direct numerical simulation of particle-laden homogeneous turbulent shear flows", **CEA : Atomic Energy Commision - Military Applications Division,** Bordeaux, France, April 2, 1997.

" Mathematical models of particle-laden flows", **CEA : Atomic Energy Commision - Military Applications Division,** Bordeaux, France, April 2, 1997.

" DNS of surface topology of turbulent nonpremixed flames ", **CEA : Atomic Energy Commision - Military Applications Division,** Bordeaux, France, April 2, 1997.

"Effects of buoyancy on turbulent diffusion flames", Dept. of Mechanical Engineering, **Yale University**, June 10, 1996.

"Particle dispersion and turbulence modification in a homogeneous shear flow", Dept. of Mechanical Engineering, **California Institute of Technology**, April 23, 1996.

" Particle dispersion and turbulence modulation in a homogeneous shear flow", Aerospace Engineering Dept., **University of Southern California,** October 4, (1995).

" DNS of particle dispersion in homogeneous shear turbulence" **Institut de Mecanique des Fluides de Toulouse, Toulouse, France**, September 12, (1995).

" DNS of a turbulent diffusion flame under different gravity conditions" **Institut de Mecanique des Fluides de Toulouse, Toulouse, France,** September 12, (1995).

" DNS of particle dispersion in homogeneous shear turbulence" **Technical University of Delft, Delft, Netherlands**, September 7, (1995).

" DNS of a turbulent diffusion flame under different gravity conditions" **Technical University of Delft, Delft, Netherlands**, September 7, (1995).

" On the two-way interaction between homogeneous turbulence and dispersed solid particles",**Naval Command, Control and Ocean Surveillance Center, San Diego, CA,** Oct. 19, 1993.

" On the two-way interaction between homogeneous turbulence and dispersed solid particles", **Arizona State University, Tempe, Arizona**, Oct. 8, 1993.

" Direct numerical simulation of particle dispersion and turbulence modulation in homogeneous turbulence",**NATO Advanced Research Workshop on Chaotic Advection, Tracer Dynamics, and Turbulent Dispersion, Alessandria, Italy,** May 24-28, 1993.

" On predicting particle-laden turbulent flows", Workshop on turbulence in particulate multiphase flow,**Fluid Dynamics Laboratory, Battelle Pacific Northwest Laboratory, Richland, WA,** March 22, 1993.

" On the two-way interaction between homogeneous turbulence and dispersed solid particles", **AMES Dept. Univ. of California, San Diego,** February 5, 1993.

" On the two-way interaction between homogeneous turbulence and dispersed solid particles",**NASA Langley Research Center,** December 14, 1992.

" On the modification of energy spectrum of homogeneous turbulence by dispersed solid particles",**Department of Mathematics, UCI,** May 21, 1992.

" The two-way coupling between solid particles and homogeneous decaying turbulence", **Mechanical and Aerospace Engineering Department, Princeton University,** August 23, 1991.

" Direct simulation of particle-laden homogeneous turbulence",**Los Alamos National Laboratory,** May 25, 1991.

"The effect of turbulence on the propagation of an electromagnetic wave in a compressible turbulent boundary layer", Workshop on Aerothermal Technology Development,**U.S. Strategic Defense Command , Huntsville, Alabama,** June 13, 1991.

"Direct numerical simulation and closure modelling of particle-laden turbulent flows", Workshop on Turbulence Simulation and Modelling , **NASA-Marshall, Huntsville,**

Alabama, April 14-15, 1991.

"Direct numerical simulation of particle dispersion in sheared and unsheared homogeneous turbulence", **Mechanical Engineeing Department, University of Southern California,** March 1, 1990.

"Direct numerical simulation and modelling of particle-laden turbulent flows", **German Aerospace Organization (DLR), Munich, Germany,** December 4,1989.

"Direct numerical simulation of particle dispersion in homogeneous turbulent flows", **University of Kaiserslautern , West Germany,** December 5,1989.

"Direct numerical simulation of particle dispersion in isotropic and sheared turbulent flows", **Institut de Mecanique des Fluides, Toulouse, France,** December 6,1989.

"Direct numerical simulation of particle dispersion in homogeneous turbulent flows", **University of Rouen, France,** December 7,1989.

"Direct numerical simulation and modelling of particle-laden turbulent flows",**Shell Conference on Computational Fluid Dynamics, Apeldoorn, The Netherlands,** December 11,1989.

"Direct numerical simulation of particle dispersion in homogeneous turbulent flows", **Norway Institute of Technology, Trondheim, Norway,** December 15,1989.

"Direct numerical simulation of particle dispersion in grid-generated turbulence", Workshop on droplets and sprays,**AFOSR and ONR Contractors Meeting, Ann Arbor, Michigan,** June 21,1989.

"Direct numerical simulation of particle dispersion and chemical reaction in turbulent flows",**G.M. Research Laboratory, Thermal Science Department, Warren, Michigan,** June 22,1989.

"Direct numerical simulation of stratified turbulent homogeneous shear flow", **Idaho National Engineering Laboratory, Idaho Falls,** September 8,1988.

"Direct numerical simulation of stratified turbulent homogeneous shear flow",**Center for Microgravity and Materials Research, University of Alabama, Huntsville** , August 5, 1988.

"Direct simulation of stable stratified turbulent homogeneous shear flows", Third International Symposium on Stratified Flows, **California Institute of Technology,** February 3-5, 1987.

"Direct simulation of the passive-scalar mixing layer",**Institut de Mecanique des Fluides, Toulouse, France,** September 11, 1987.

"Direct simulation of stratified homogeneous turbulent shear flow",**Department of Aerospace Engineering, University of Southern California,** October 8, 1986.

"Direct simulation of stratified homogeneous turbulent shear flow", **Institut de Mecanique Statistique de la Turbulence, Marseille, France,** October 22, 1986.

"Direct simulation of homogeneous turbulent shear flow", **Mechanical Engineering Department, University of California, Irvine,** July 22, 1986.

"Direct simulation of stratified homogeneous turbulent shear flow",**AMES Department, University of California, San Diego,** February 3, 1986.

"Direct simulation of turbulent shear flow with buoyancy",**Jet Propulsion Laboratory, California Institute of Technology,** May 30, 1986.

"Direct numerical simulation of a turbulent homogeneous shear flow with buoyancy", **Mechanical Engineering Dept., University of California, Irvine,** October 18, 1985.

"Direct simulation of turbulent homogeneous shear flow", **DFVLR, Institute of Atmospheric Physics, Oberpfaffenhofen, West Germany** , June 21, 1985.

"Prediction of the turbulent jet laden with vaporizing droplets" **Dept. of Fluid Mechanics, University of Erlangen, West Germany,** May 22,1985.

"Experimental study of the turbulent jet laden with particles", **University of the German Armed Forces, Aerospace Department, Munich, West Germany,** February 7,1985.

"Measurement and prediction of the turbulent two-phase jet", **University of Karlsruhe, Mechanical Engineering Dept.,** December 13,1984.

"Prediction of the turbulent jet laden with solid spherical particles",**DFVLR, Institute of Atmospheric Physics, Oberpfaffenhofen, West Germany** , December 5, 1984.

"Recent developments in mathematical modeling of dispersed two- phase flows", presented at the Mechanical Engineering Dept., Technical University of Munich, West Germany, November 27,1984.

"Recent developments in mathematical modeling of dispersed two- phase flows", presented at the **Mechanical Engineering Dept., University of California, Berkeley,** March 20, 1984.

"Effects of dispersed two-phase flows on turbulence structure", **Office National d'Etudes et de Recherches Aerospatiales (ONERA), Paris, France,** September 19, 1983.

"Turbulence modulation in a turbulent two-phase jet : theory and experiment", Mechanical Engineering Department, **University of Kaiserslautern, West Germany,** September 16, 1983.

"Passive-scalar time-scales in turbulent flows", **DFVLR, Institute of Atmospheric Physics, Oberpfaffenhofen, West Germany** , September 15, 1983.

"Mathematical models of temperature variance and time-scales for the thermal mixing layer ", **Institut de Mecanique Statistique de la Turbulence, Marseille, France,** July 8, 1983.

"Experimental and theoretical study of dispersed two-phase turbulent jets", **Institut de Mecanique des Fluides, Toulouse, France,** July 6, 1983.

EXHIBIT G

BIOMEDICAL ENGINEERING CONSULTANTS

Supplemental Report

Yadin David, Ed.D., P.E., C.C.E.

This report sets forth additional information relating to several specific products which are consistent with the alternative design concepts I discussed in my initial report. My initial report outlined several design concepts and provides an example of each. This supplemental report outlines further examples of commercially available patient warming alternatives. The below list is not meant to be exhaustive but examples of active and passive warming devices that are a reasonable and safer alternative design used for patient warming.

1. Kanmed WarmCloud

The Kanmed WarmCloud, "a pressure relieving warm air mattress, is designed to be used pre, per and post operatively."[1] Much like the Berchtold TableGard discussed in my initial report, the Kanmed WarmCloud uses forced-air to achieve underbody heating without exhausting air around the operating site.

The one major difference between the TableGard and WarmCloud is that the WarmCloud features a "a single use Warm Air mattress."[2] Like in the Bair Hugger, this lowers the initial cost but adds the cost of a disposable. As such, the overall economic feasibility of the device is similar to the Bair Hugger. In May 2008, a randomized trial was published comparing the Kanmed WarmCloud with the Bair Hugger.[3] The study found that the devices maintained similar temperatures, with the WarmCloud being more effective. The authors concluded that the "WarmCloud device is optimally suited to maintain core normothermia for longlasting procedures."[4]

2. Inditherm Warming Blanket

I have reviewed guidance documentation created in August 2011 from the National Institute for Health and Clinical Excellence (NICE) endorsing the use of the Inditherm patient warming device, a design incorporating the use of resistive heating blanket. According to NICE, "the Inditherm patient warming mattress uses flexible, carbon-based conductive polymer technology that aims to generate a uniform, direct heating surface. It is a low voltage, reusable device that does not require disposable products. The temperature of the mattress is maintained by

[1] TAB 1 - Kanmed WarmCloud User Manual.
[2] TAB 2 - Kanmed WarmCloud Brochure, p. 2.
[3] TAB 3 - Peroperative temperature management. Comparison of a forced air warming device and a dynamic air mattress device in plastic surgery. European Journal of Anaesthesiology, May 2008.
[4] *Id.*

a control unit and is user-selectable."[5] The mattress is designed using "a viscoelastic foam pad which is designed to mould itself to the shape of the patient."[6] Numerous published studies show that the Inditherm mattress achieves comparable temperature results as forced-air warming.[7] In addition, the NICE researchers considered the risk of infection:

> Mindful of possible transmission of infection, the Committee asked the expert advisers and the manufacturer about cleaning the Inditherm mattress between patients. It was told that the mattress is cleaned in the same way as the normal operating table mattress.[8]

According to NICE, "the annual cost of the Inditherm patient warming system in the cost model was approximately £1300 per operating theatre."[9] Because it does not use disposables, "the average annual cost saving associated with use of the Inditherm patient warming system is estimated to be £9800 per theatre."[10]

3. LMA PerfecTemp

The LMA PerfecTemp "is an underbody resistive warming system that combines servocontrolled underbody warming with viscoelastic foam pressure relief."[11] In 2011, a clinical trial was published comparing the PerfecTemp to the Bair Hugger. Researchers found that "core temperatures were no different, and significantly noninferior, with underbody resistive heating in comparison with upper-body forced-air warming."[12] I have also reviewed a PowerPoint presentation created by the Department of Outcomes Research at the Cleveland Clinic. According to the Cleveland Clinic, "the blanket uses an antimicrobial / antifungal fabric cover,"[13] and they also noted that it presents "no chance of potential increase risk of contamination."[14] The researchers noted that the device "pays for itself, by significant reduction of disposables," and that it "can generate hundreds of thousands of dollars in savings."[15] Finally, the Cleveland Clinic's testing showed that "PerfecTemp warms more surface area than forced air."[16]

---

[5] TAB 4 - National Institute for Health and Clinical Excellence Guidance Document on Inditherm, p. 5.
[6] *Id.*
[7] *Id.* at p. 6-9.
[8] *Id.* at p. 11.
[9] *Id.* at p. 12.
[10] *Id.*
[11] TAB 5 - A Randomized Comparison of Intraoperative PerfecTemp and Forced-Air Warming During Open Abdominal Surgery. Anesthesia & Analgesia, June 2011.
[12] *Id.*
[13] TAB 6 - Cleveland Clinic PowerPoint on PerfecTemp, p. 6.
[14] *Id.* at p. 10.
[15] *Id.* at p. 11.
[16] *Id.* at p. 13.

4. Barrier Easy Warm

The Barrier Easy Warm is "a disposable, active self-warming blanket."[17] In 2014, the Easy Warm blanket was subject to a multicenter study on its effectiveness. The authors described the blanket as follows:

> The blanket has pouches with warmers containing iron, which is activated when exposed to ambient air. The blanket remains active at an average temperature of 44°C for a minimum of ten hours. The blanket is easy to use, requires no electricity and can be used through the entire perioperative period.[18]

The researchers found "a significantly lower incidence of hypothermia intraoperatively and postoperatively" when using the Easy Warm blanket.[19] Although the product was launched in 2014,[20] the technology for air-activated warmers using iron has existed for nearly 100 years, and consumer products using this technology, such as hand warmers commonly used in the cold outdoors such as camping, have been widely available for decades.

5. Reflective Blankets

Comparable patient warming goal can also be achieved by the operative use of common reflective blankets following pre-warming. In July 2016, researchers conducted a randomized, controlled trial comparing the Bair Hugger and reflective blankets. The study "showed that after active prewarming, intraoperative passive warming with reflective thermal blankets was as effective as active warming with Bair Hugger blankets in hip and knee arthroplasty surgeries."[21] The authors noted that "reflective blankets do not disrupt airflow and therefore have no potential for this increase in surgical site infection."[22] The use of common reflective blankets "eliminates any laminar airflow disruption" and "eliminates the transfer of potential pathogenic organisms by the device."[23] These blankets have long been available, as the first reflective blankets were developed by NASA in the 1964.[24]

6. Cotton Blankets

Cotton blankets (passive warming) have been used by the medical community prior to the development of active warming products such as the Bair Hugger. Studies have shown that cotton

---

[17] TAB 7 - Reduced hypothermia and improved patient thermal comfort by perioperative use of a disposable active self-warming blanket: A randomized multicenter trial. Presented at: 67th Annual Postgraduate Assembly in Anesthesiology; 2013 Dec 13-17.
[18] *Id.*
[19] *Id.*
[20] TAB 8 - Barrier Easy Warm Press Release.
[21] TAB 9 - Reflective Blankets Are as Effective as Forced Air Warmers in Maintaining Patient Normothermia During Hip and Knee Arthroplasty Surgery, The Journal of Arthroplasty, July 2016.
[22] *Id.*
[23] *Id.*
[24] *See* https://www.nasa.gov/offices/oct/40-years-of-nasa-spinoff/emergency-blankets

blankets are just as effective as active warming products for surgeries that last less than 2 hours similar to the type of surgeries that are the subject of this litigation. Furthermore, since cotton blankets do not use convective warming but are conductive warming devises, there are no risks such as disruption of the airflow or the increase in pathogens over the surgical site that are present during the use of the Bair Hugger.

7. Pre-warming

Prewarming patients for 30 to 60 minutes prior to induction of anesthesia is an effective and safer alternative design to prevent hypothermia in patients undergoing surgeries of less than 2 hours.[25] Since 2001, studies have shown that pre-warming was just as effective as intraoperative warming for surgeries lasting less than two hours.[26] Since pre-warming is performed outside the operating room, there are no risks associated with pre-warming that are evident in the Bair Hugger system.[27] Pre-warming does not disrupt the airflow in the operating room and does not increase pathogens over the sterile field.

CONCLUSION

It is my opinion to a reasonable degree of biomedical engineering certainty that each of these devices are economically feasible, and that each qualifies as a reasonable safer alternative design to the Bair Hugger in achieving patient warming during orthopedic surgery. Each of these alternative designs eliminates the risk of airborne infection and achieves comparable core temperatures.

Yadin David, Ed.D., P.E., C.C.E.

[25] J. Andrzejowski, J. Hoyle, G. Eapen, D. Turnbull; Effect of prewarming on post-induction core temperature and the incidence of inadvertent perioperative hypothermia in patients undergoing general anaesthesia, *BJA: British Journal of Anaesthesia*, Volume 101, Issue 5, 1 November 2008, Pages 627–631, https://doi.org/10.1093/bja/aen272

[26] Melling, A.C., Ali, B., Scott, E.M. and Leaper, D.J., 2001. Effects of preoperative warming on the incidence of wound infection after clean surgery: a randomised controlled trial. *The Lancet*, *358*(9285), pp.876-880.

[27] A.V. Duren; Prewarming, Arizant Healthcare, January 2005, p. 3MBH00297660.

EXHIBIT H

Professional Background

I am the Mid-west and Texas Engineering Lead Engineer for SimuTech Group. SimuTech Group is the largest reseller of ANSYS product in North America. SimuTech Group is an elite ANSYS Channel partner.

In my roles at SimuTech including as a Lead Engineer, I have performed more than 50 external consulting projects using a variety of advanced Computation Fluid Dynamic (CFD) techniques for many different industries. Computation Fluid Dynamics uses computers to calculate fluid motion by solving a set of equations based on the fundamental laws of physics. My engineering expertise includes CFD Modeling of many different situations including Multiphase and Turbulent Fluid Flows. Also, I teach both public/project specific CFD training and provide technical CFD support to various professional engineers on a multitude of fluid dynamics topics. I am an ANSYS Certified Professional, Fluid Technical.

I gained my Ph.D. in Chemical and Process Engineering from the University of Canterbury in New Zealand.

Refer to Appendix I for my complete Resume.

Summary

John Abraham, Ph.D.'s CFD modeling does not support his conclusions because there are numerous errors in his CFD models. The errors are as follows:

- Dr. Abraham erred by using a steady state streamline on a single transient result. Streamlines require a steady state solution to be accurate, and the transient model Dr. Abraham used is not steady. It can clearly be shown the results will change depending on which result he chooses to use.
- Dr. Abraham erred by not running his transient model long enough. Dr. Abraham's model ran for 1.2 seconds (Bair Hugger 750 model) and 5.07 seconds (Bair Hugger 505 model) of simulation time. The model did not run long enough to predict the fluid motion in the operating room as he has defined it. The results can be shown to be dependent on the definition of his unknown initial condition.
- Dr. Abraham uses results from a model that will diverge. This is outside standard industry practices and highly likely to give inaccurate results.
- Dr. Abraham uses a mesh that is under resolved and has unacceptable quality elements, thus resulting in incorrect results. If he refined his mesh he would get different results.
- Dr. Abraham used a high-resolution scheme with his LES which is known to cause errors in the solution.
- Dr. Abraham used streamlines, he should have used particle tracking. Particle tracking is significantly more accurate and the industry standard approach to particle distribution problems. Further, the question that is at issue is particle location, not streamlines.
- Dr. Abraham does not support any of his assumptions with any sensitivity analysis.

- Dr. Abraham's validation is not document enough to be confirmed by his results, also his choice of validation does not prove the accuracy of his methodology of a steady sate streamline on a single transient timestep to accurately particle motion.
- Dr. Abraham has numerous changes (and assumptions) to his model that are undocumented and have no justification greatly reducing any confidence in modeling process undertaken by him.

Overview of CFD

Computational fluid dynamics (CFD) is an advanced engineering method for calculating flow. CFD is a branch of fluid mechanics that uses numerical methods and algorithms to solve problems that involve fluid flows. These problems can be either flow within a confined space, external flow around a solid body, or a combination of both.

The governing equations for CFD are derived from basic principles of physics, including the conservation of mass, energy and Newton's second Law of motion. Almost all CFD models use a set of governing equations for mass and momentum, with additional equations as needed, such as turbulent flow, multi-phase flow, reactions, combustion, equations of state, etc. The flow region that is to be analyzed is subdivided into many small elements. The CFD solution process is an iterative procedure where the governing equations are simultaneously solved for the numerous individual elements. Computers perform these numerous calculations.

The governing equations that describe the momentum transfer in Newtonian fluid are called the Navier-Stokes equations. A Newtonian fluid is one where the shear stress is linearly proportional to the velocity gradient. Many common fluids such as air, water, oil, and gasses meet the criteria for a Newtonian fluid. The principal equations solved in almost all CFD models are the Navier-Stokes equations combined with the conservation of mass equation. The Navier-Stokes equations were first derived in the first half of the nineteenth century. Numerical techniques are required to solve them, except for some special cases, due to the complexity of the mathematical equations.

CFD Methodology

- The basic process for a CFD analysis is as follows. First, a geometric model is developed that defines the fluid flow passage. The geometric model includes the smallest details which influence the flow.
- The model is then subdivided into smaller discrete cells (mesh). The mesh may be uniform or non-uniform.
- The Navier-Stokes equations, conservation of mass, and the appropriate modeling equations necessary for a specific application (such as: conservation of energy, turbulence, etc.) are defined throughout the model.
- The material properties of the fluid(s) modeled are defined.
- Boundary conditions are defined. This involves specifying the fluid behavior and properties at the boundaries of the flow volume.

- The equations are then solved using an iterative procedure. The iterative method is based upon numerical techniques and involves changing the values at each mesh cell until the values correctly give agreement based on the equations defined by the model. The solution is then considered "converged."
- Finally, a postprocessor is used for the analysis and visualization of the resulting solution.
- Additionally, the model is then resolved to gain an understanding of the impact of modeling inputs by undertaking sensitivity studies.

Fee Schedule

SimuTech Group, Inc. for whom I work is being compensated by Kennedy Hodges L.L.C. My company's compensation rate is $250 per hour for work outside of Deposition and Trail appearances. For Deposition and Trail appearances my company's compensation rate is $500 per hour. Plus, reimbursements for direct expenses.

Review

My comments and opinions are based on my review of the CFX transient files Abraham00000001.trn and 2540_full.trn as they relate to the Abraham Expert Report.pdf provided by Dr. Abraham. In addition, I also reviewed the Abraham00000003 (2).agdb file CAD file.

No sensitivity testing

Due to the highly nonlinear nature of fluid problem, sensitivity testing if typically preformed to check the impact of modeling assumptions. Dr. Abraham also gives a comparative statement, (*"that forced-air patient warming does not meaningfully impact air flow currents in operating room"*), however he does not have any baseline models to compare against, so he can only guess at what the air flow patterns would be like with the Bair Hugger turn off. He also doesn't look at any effect of people being in the operating room.

Dr. Abraham assumptions in his modeling approach are also not supported with any sensitivity analysis, to test the validity of his assumptions.

Transient modeling

Transient models change with time. Transient modeling is not unique to CFD, it is a common technique across engineering.

The underlying equations that define fluid motion are transient. Steady state modeling is a simplification that can only be accurately when the flow is not changing with time.

A transient CFD model is defined by a set of initial condition that define the original state of the fluid system and then the model is solved for a specific duration defined by the user.

During a transient solution the solver will produce information at each node of the mesh at each timestep that can be post processed. For practicable reasons (like hard drive space), the user might choose to write the information to hard drive only periodically. The *.trn files provided by Dr. Abraham are the transient result files generated a specific time.

Initial Conditions are not defined

Dr. Abraham does not state what his initial conditions the model definition is incomplete without it and it is unclear what he modeled.

Transient Duration

Dr. Abraham makes an error by not running his transient models long enough. Dr. Abraham models were only run for 1.2s and 5.07s for Abraham00000001.trn and 2540_full.trn respectively (Figures 1 and 2).

Transient model results are dependent on the initial conditions particularly given the short duration of his transient solution, the solution is highly dependent on the unknown initial conditions and not by the stated model definition. Figures 3 through 7 show the temperature contour. Although streamlines were added to give an approximate understanding relative distance the air could have traveled given the time solved and the speed of the air movement in the room, a more accurate method would be to use the industry standard approach to look at the solution with some combination of contour plots and/or monitor plots, however since on the single transient result files was only available, this is not possible. Figures 8 and 9 show the velocity contour and streamlines from the inlet.

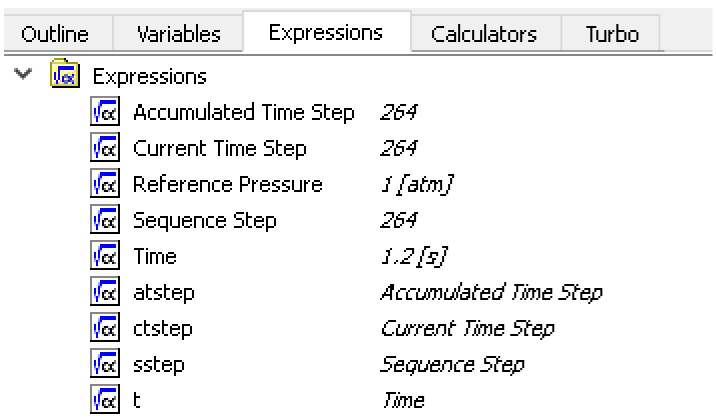

Figure 1 Timestep and time information from Abraham000001.trn

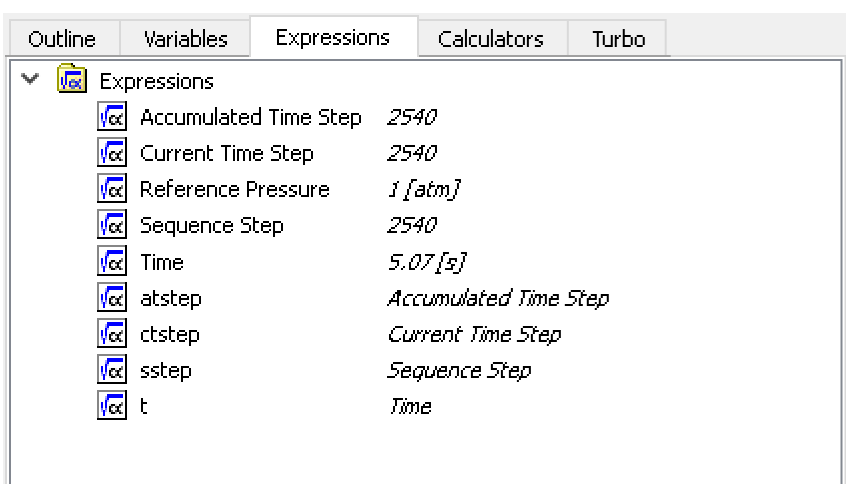

Figure 2 Timestep and time information from 2540_full.trn

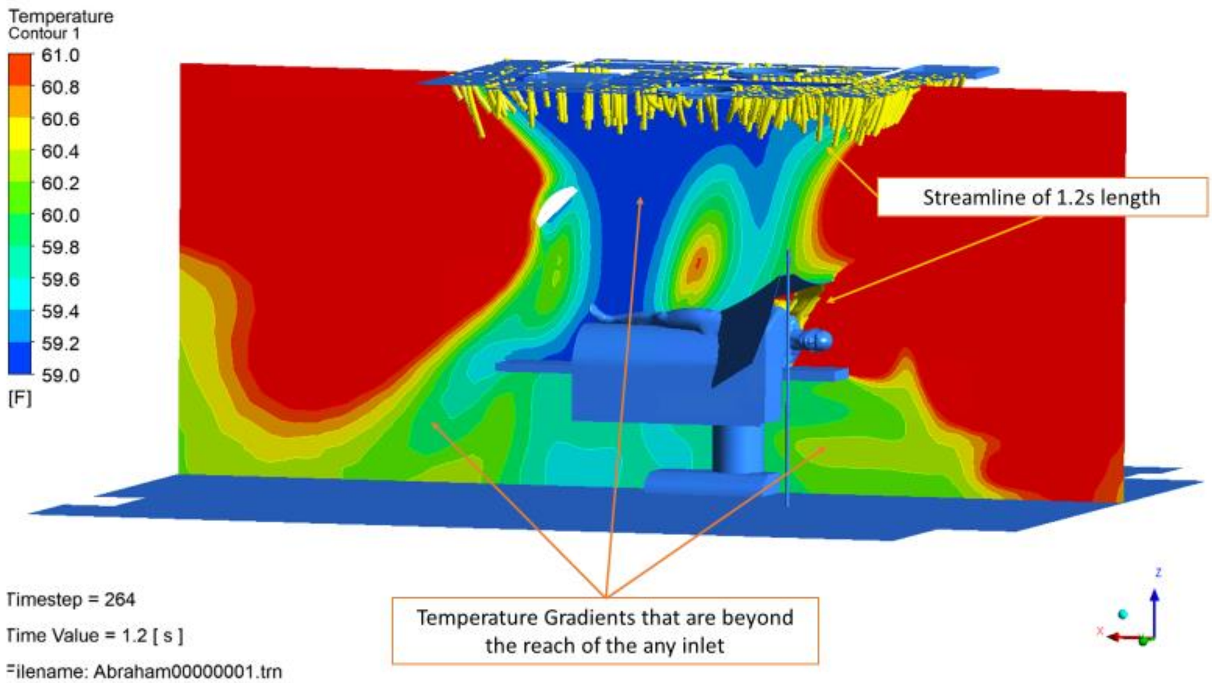

Figure 3 The temperature is contour plotted on a plane at y = -3.85986 (m), with the scale trimmed to 59.0 (°F) and 61 (°F) for the Abraham00000001.trn results. Yellow streamlines are added to show approximately the distance the inlet flows traveled in 1.2 (s).

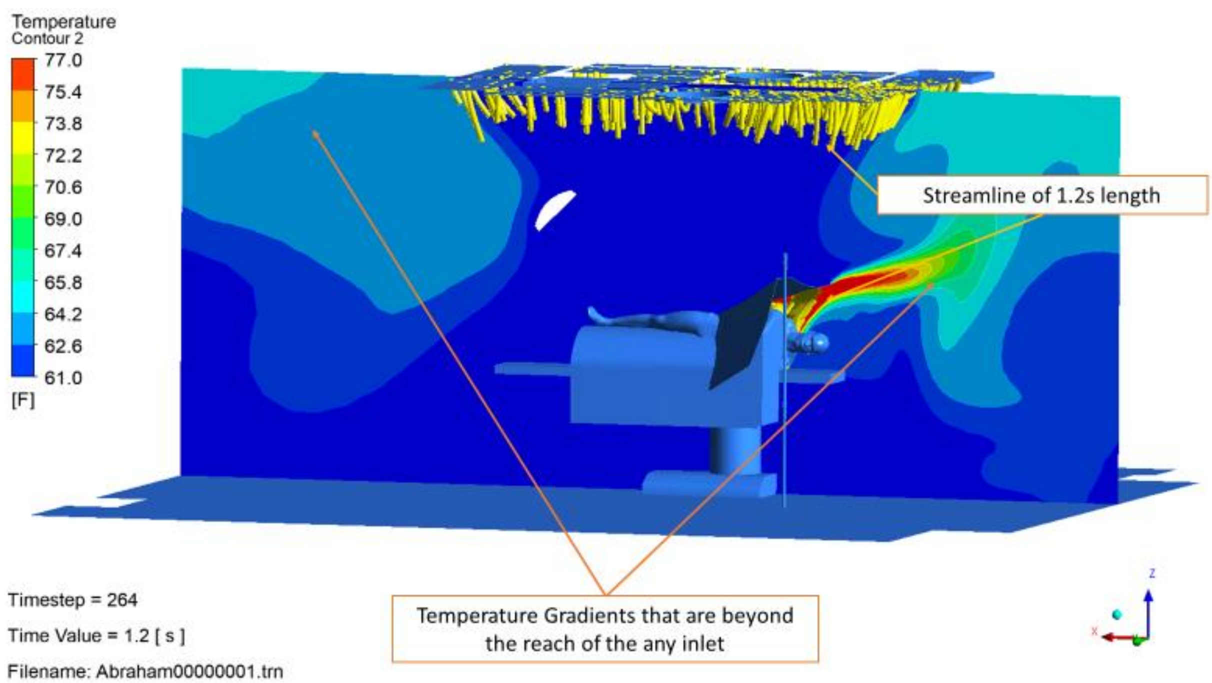

Figure 4 The temperature is contour plotted on a plane at y = -3.85986 (m), with the scale trimmed to 61 (°F) and 77 (°F) for the Abraham00000001.trn results. Yellow streamlines are added to show approximately the distance the inlet flows traveled in 1.2 (s).

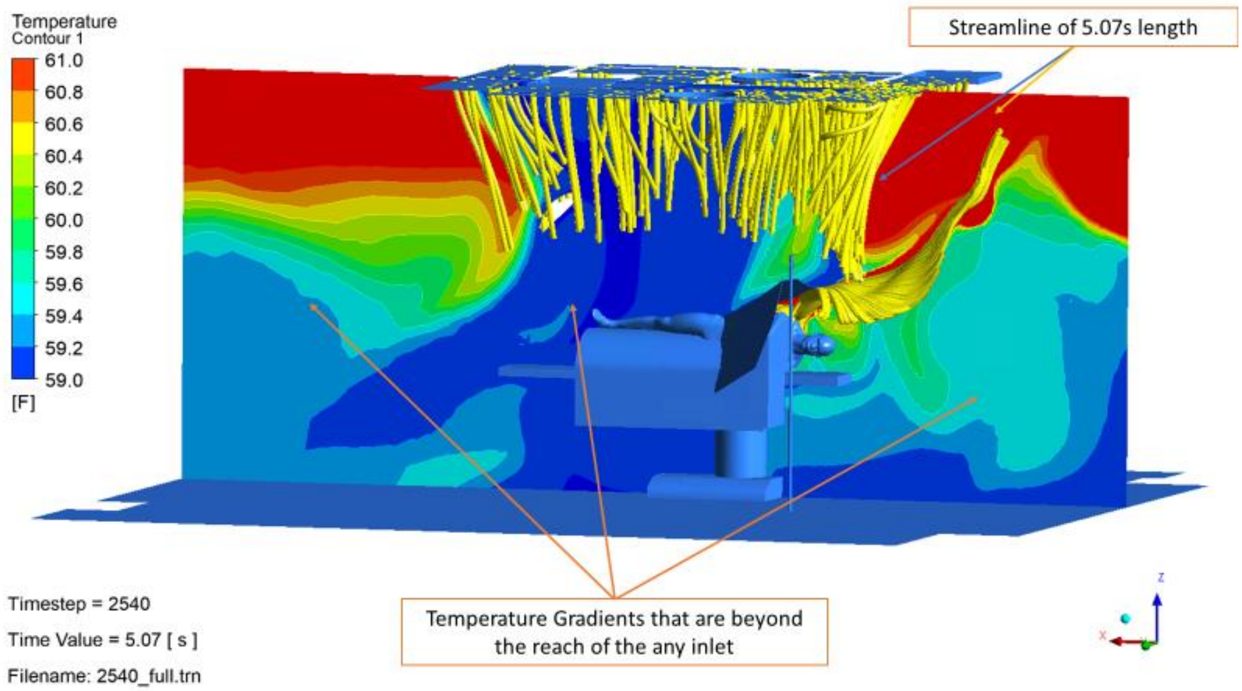

Figure 5 The temperature is contour plotted on a plane at y = -3.85986 (m), with the scale trimmed to 59.0 (°F) and 61 (°F) for the 2540_full.trn results. Yellow streamlines are added to show approximately the distance the inlet flows traveled in 5.07 (s).

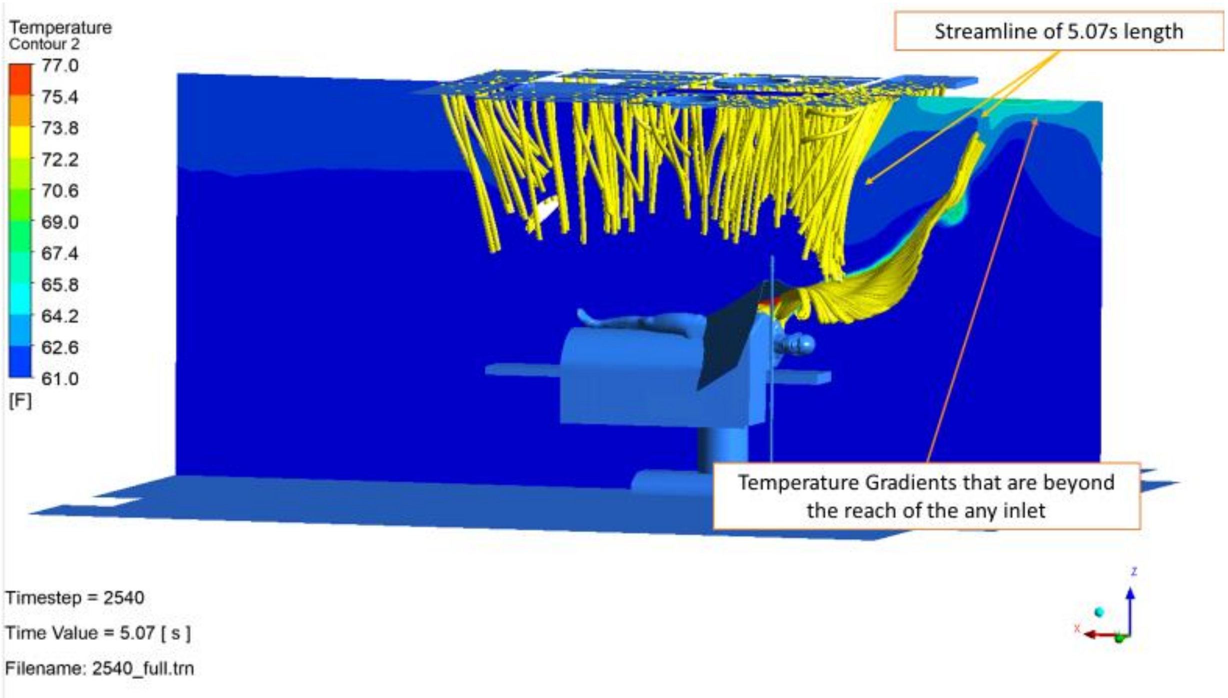

Figure 6 The temperature is contour plotted on a plane at y = -3.85986 m, with the scale trimmed to 61.0 (^{o}F) and 77 (^{o}F) for the 2540_full.trn results. Yellow streamlines are added to show approximately the distance the inlet flows traveled in 1.2 (s).

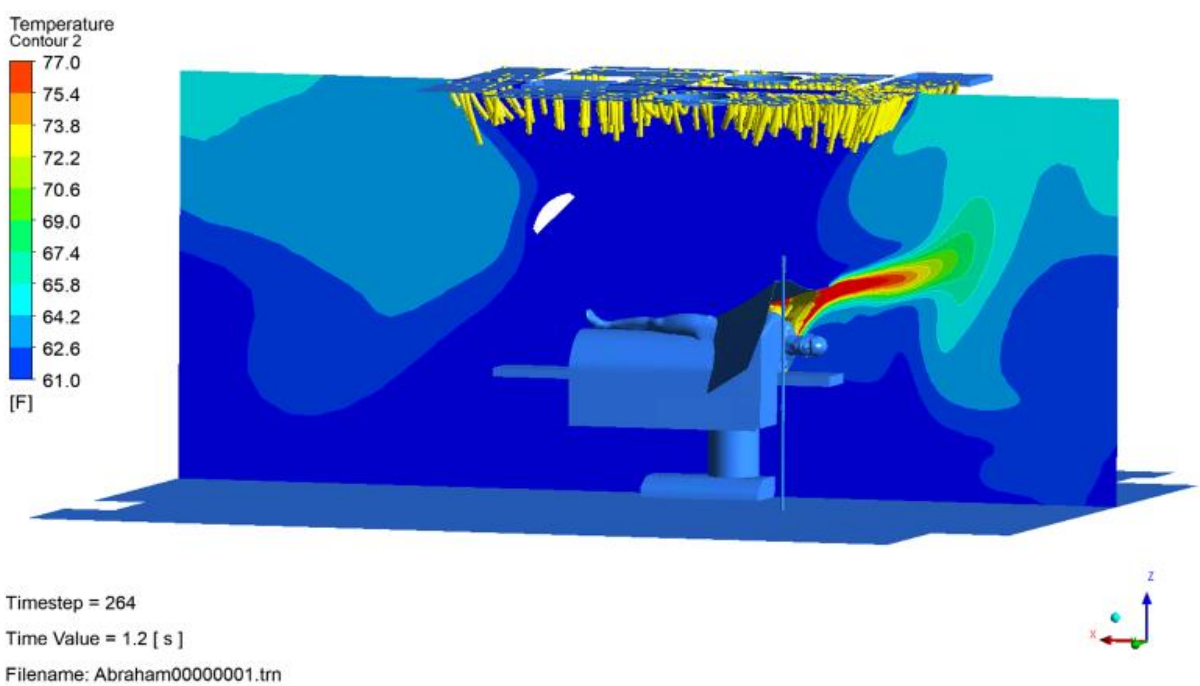

Figure 7 The temperature is contour plotted on a plane at y = -3.85986 (m), with the scale trimmed to 61.0 (^{o}F) and 77 (^{o}F) for the 2540_full.trn results. Yellow streamlines are added to show approximately the distance the inlet flows traveled in 1.2 (s).

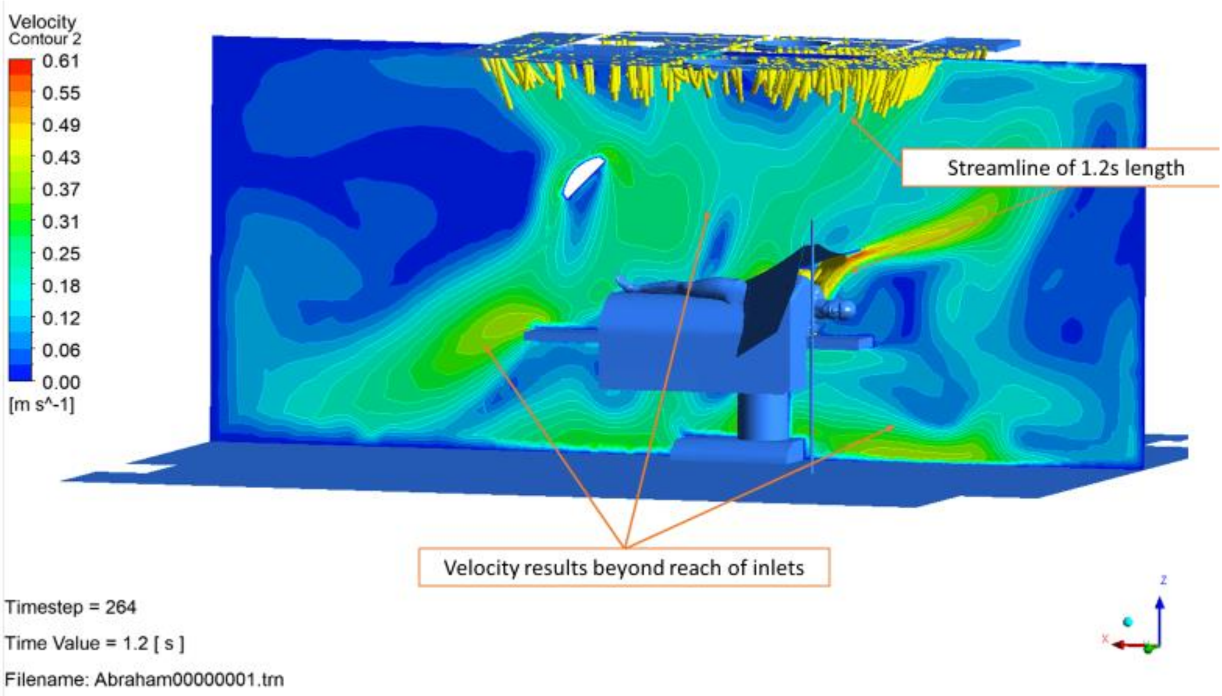

Figure 8 The velocity contour plotted on a plane at y = -3.85986 (m), for the Abraham00000001.trn results. Yellow streamlines are added to show approximately the distance the inlet flows traveled in 1.2 (s). Note the significant areas beyond the streamlines.

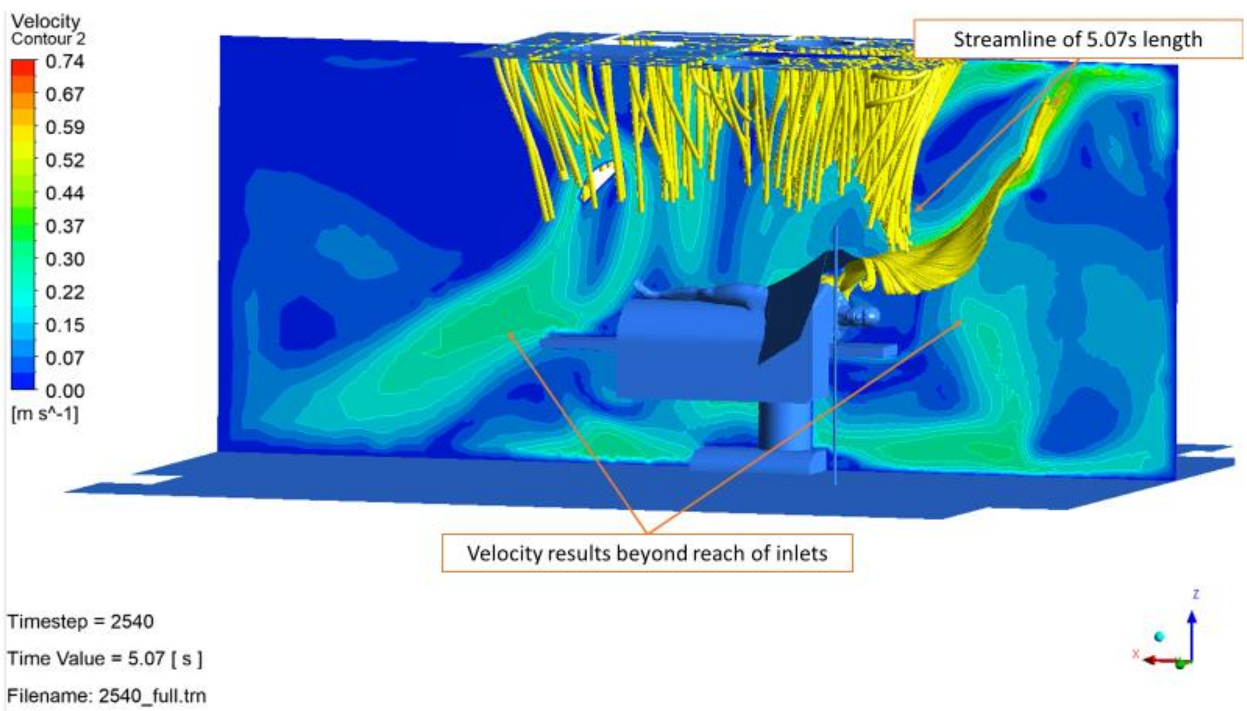

Figure 9 The velocity contour plotted on a plane at y = -3.85986 (m), for the 2540_full.trn results. Yellow streamlines are added to show approximately the distance the inlet flows traveled in 5.07 (s). Note the significant areas beyond the streamlines.

Results

The CFD solver will produce information at each of the elements/nodes at each timestep, these results are typically written to hard drives with some regular frequency. The intermediate result files are called trn files in CFX. Each trn result file contains the results at a specific time. The CFD post process is used to integrate the results, there are several different ways the results can be integrated, these include vector and contour plots and streamlines.

Changing results

The CFD results reported by Dr. Abraham only show the flow at the specific 1.2s (Abraham) and 5.07 (s) (2540_full) from unknown starting conditions, however if the transient models is run forward, the model results changes, as it would be expected given the short model times solved and the turbulent model choice. The model would have also been changing prior to the provided results at the specific timestep. Since the result change over time, it is not valid to use only a single specific timestep, since the results used would change dependent timestep was selected. It also means the steady state assumption cannot be used without error.

Figures 10 through 15 show examples of how the results are changing.

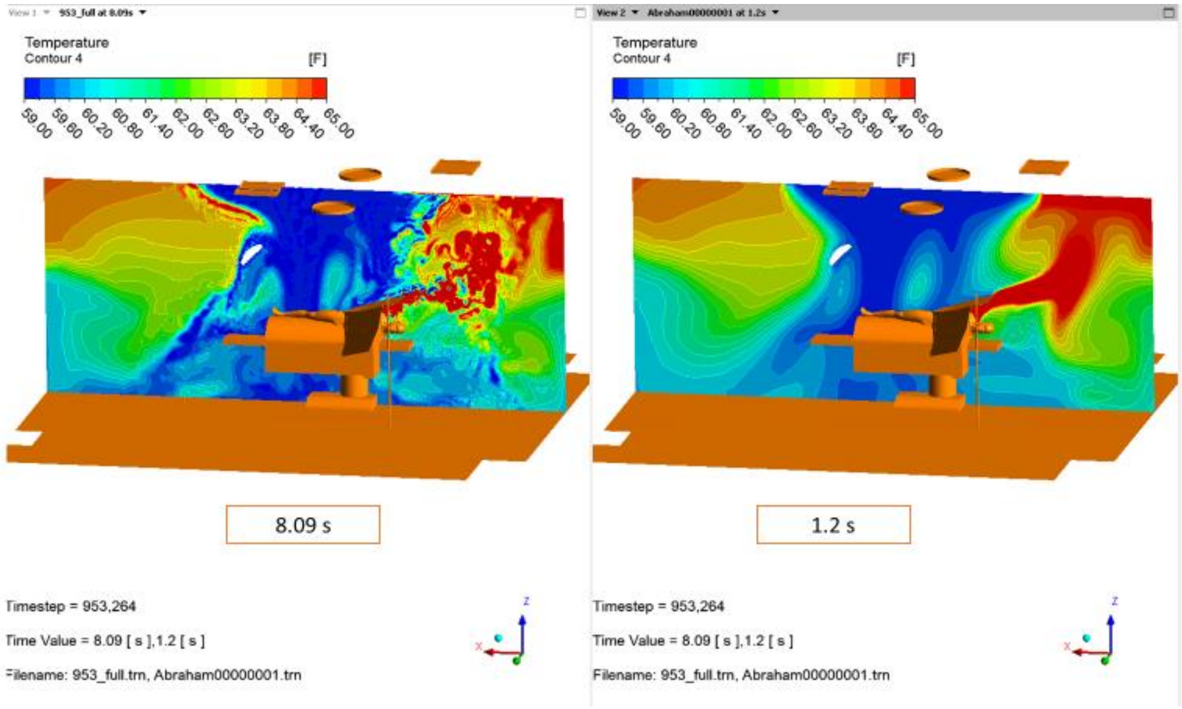

Figure 10 shows the difference in the temperature results once the Abraham00000001.trn model has been solved to 8.09 (s). Steady state requires that there is no change of any results with time. The temperature contours were limited to between 59.0 (°F) and 65 (°F) to help show the variation away from the Bair Hugger Inlet

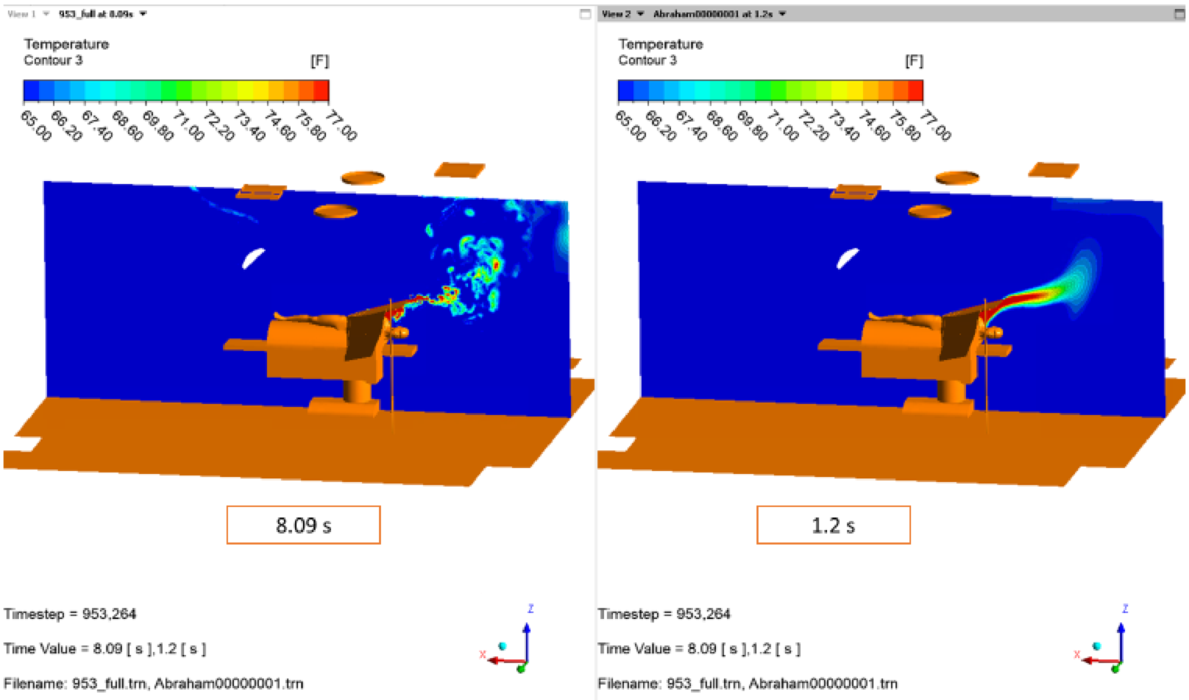

Figure 11 shows the difference in the temperature results once the Abraham00000001.trn model has been solved to 8.09 (s). Steady state requires that there is no change of any results with time, this is not the case. The temperature contours were limited to between 65.0 (°F) and 77 (°F) to help show the variation near the Bair Hugger Inlet

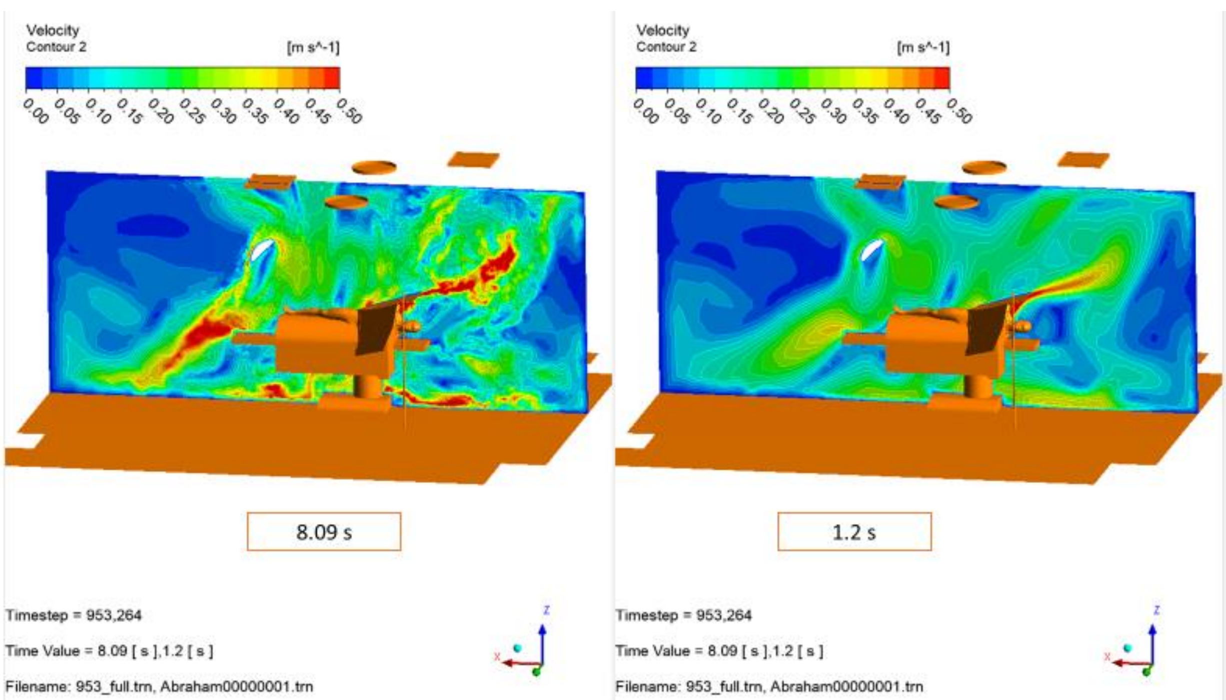

Figure 12 shows the difference in the velocity results once the Abraham00000001.trn model has been solved to 8.09 (s). Steady state requires that there is no change of any results with time

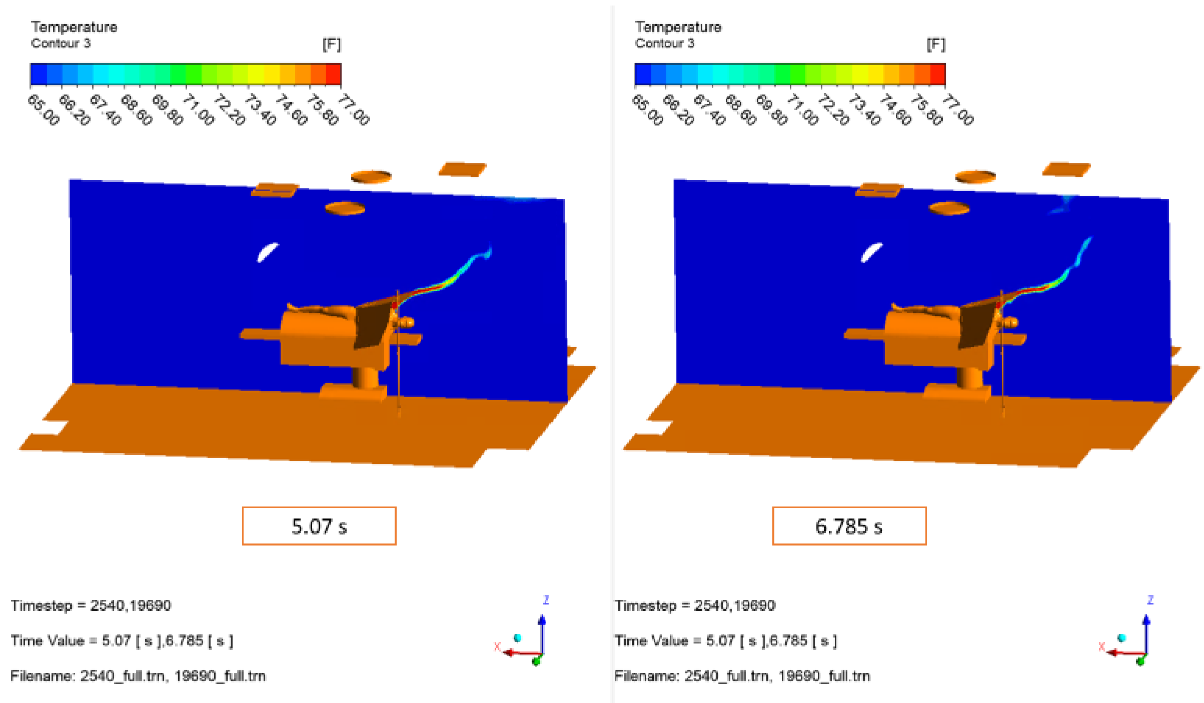

Figure 13 shows the difference in the velocity results once the 2540_full.trn model has been solved to 6.785 (s). Due to the scale, the differences are more subtle, a difference plot is shown in Figure 38 to highlight the differences.

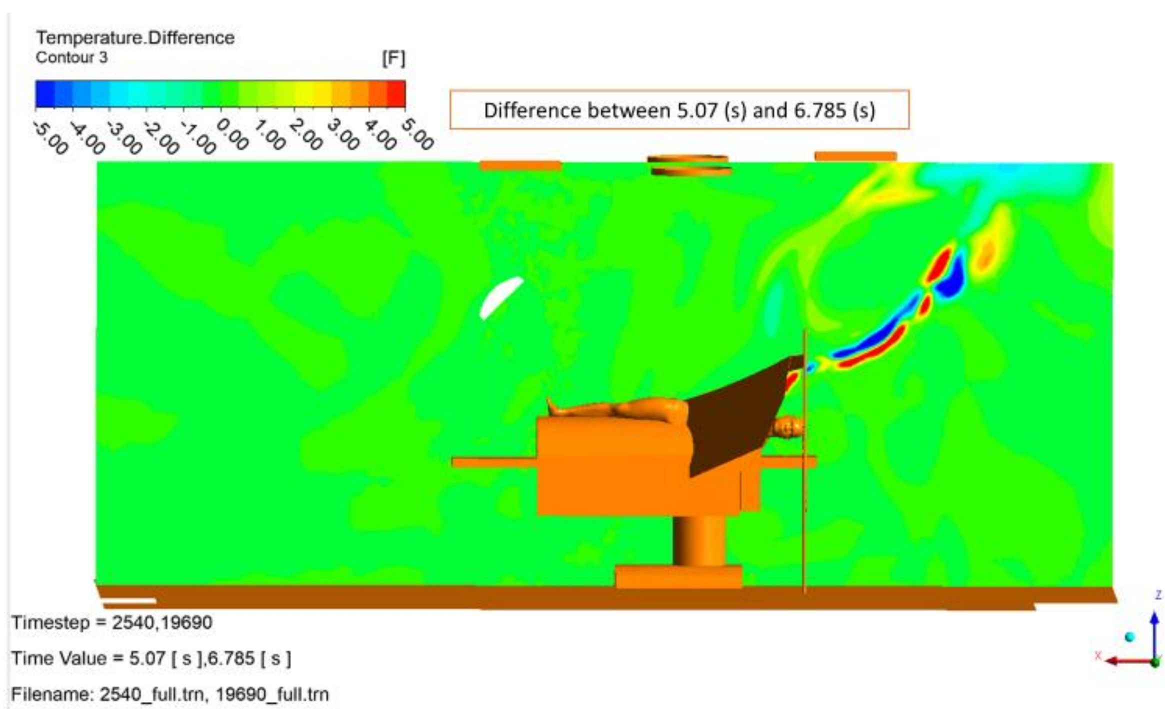

Figure 14 shows the difference in the velocity results once the 2540_full.trn model has been solved to 6.785 (s).

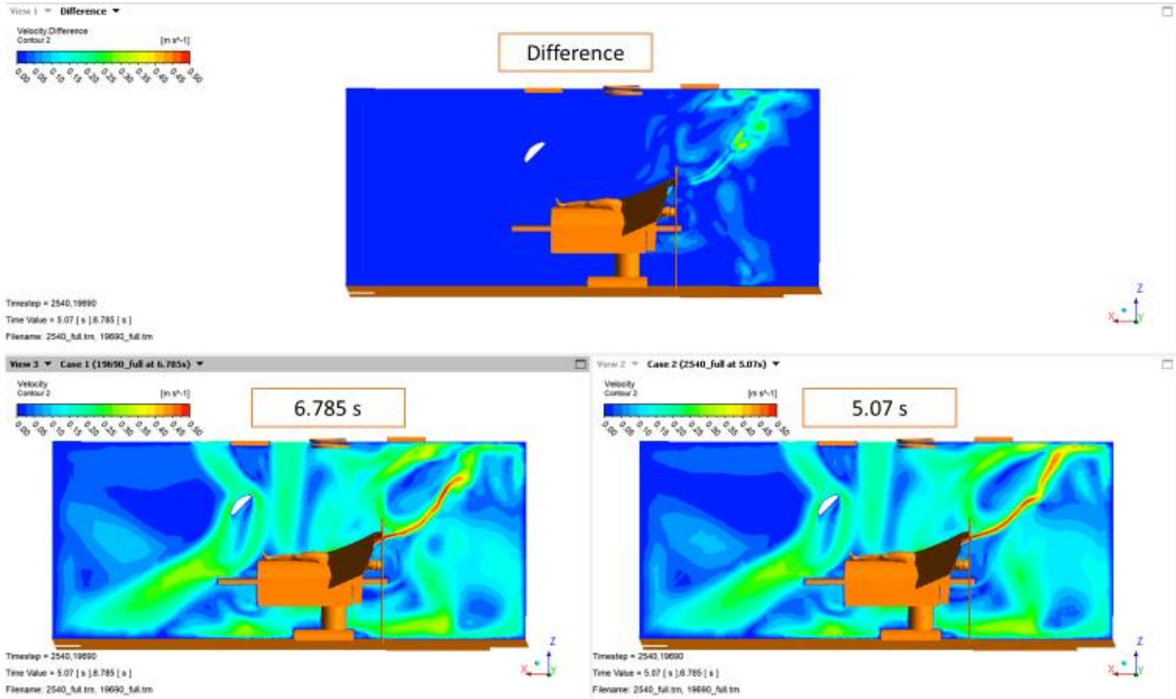

Figure 15 shows the difference in the velocity results once the 2540_full.trn model has been solved to 6.785 (s).

Turbulent Flow

When a fluid moves in a turbulent flow the fluid moves in an irregular, chaotic, unsteady manor. Eddies of different shapes and sizes are produced, these eddies will break down into smaller eddies which themselves can be transport by other larger eddies. Turbulence is by nature a transient phenomenon.

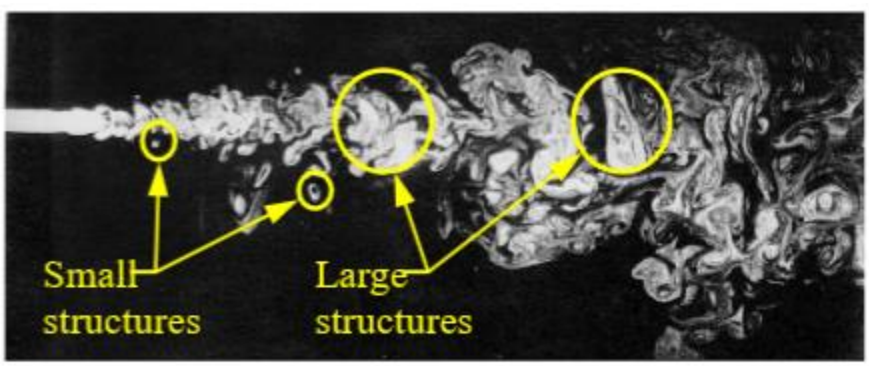

Figure 16 Picture of a turbulent jet. The turbulent structures will move downstream rotating and breakup in to smaller eddies.

WALE LES turbulence is a transient model

The WALE LES turbulence model Dr. Abraham has chosen to use can only be solve as a transient solution. For the model to work correctly the solution must resolve the changing details of the large turbulent structures like eddies as they change with time. The WALE LES model cannot be run steady state. "*alternative approaches of Large Eddy Simulation (LES) or Direct Numerical Simulation (DNS) can be adopted. With these methods, time dependent equations are solved for the turbulent motion*" [1]

Turbulence at inlet

Dr. Abraham, states in his rebuttal to Elghobashi that the inlet has grate *"As airflow passes through the ceiling grill, small eddies and turbulence are created"* and that will produce turbulence, however he does not include any turbulence at either of his inlets (Figures 17 and 18).

Table 7. Boundary Physics for Abraham00000001

Domain	Boundaries	
FluidRegion	**Boundary - Inlet**	
	Type	INLET
	Location	Inlet Lights
	Settings	
	Flow Direction	Normal to Boundary Condition
	Flow Regime	Subsonic
	Heat Transfer	Static Temperature
	Static Temperature	5.9000e+01 [F]
	Mass And Momentum	Mass Flow Rate
	Mass Flow Rate	1.3870e+00 [kg s^-1]
	Mass Flow Rate	As Specified

Figure 17 Inlet boundary definition for Abraham00000001.trn

Table 4. Boundary Physics for 2540_full

Domain	Boundaries	
FluidRegion	**Boundary - Inlet**	
	Type	INLET
	Location	Inlet Lights
	Settings	
	Flow Direction	Normal to Boundary Condition
	Flow Regime	Subsonic
	Heat Transfer	Static Temperature
	Static Temperature	5.9000e+01 [F]
	Mass And Momentum	Mass Flow Rate
	Mass Flow Rate	1.3870e+00 [kg s^-1]
	Mass Flow Rate Area	As Specified

Figure 18 Inlet boundary definition for 2540_full.trn

Streamlines

For streamline to accurately capture the motion of the flow the model velocity field must not change.

[1] 4.1.11.2 Introduction to LES, CFX-Solver Modeling Guide, Ansys Help.

Streamline require a steady state flow conditions to be accurate.

Dr. Abraham used a transient model to predict the velocity fields. The velocity solution that the streamline uses to calculate their paths changes with time making the steady state assumption incorrect.

Additionally, Dr. Abraham used a transient turbulence model to predict the velocity fields, the model cannot be run steady state as it need to change the velocity solution over time to explicitly model turbulence correctly. Steady state streamlines are inaccurate when used with a changing velocity field like one produced by the LES model.

Both errors together and independently cause the streamlines path to change depending on which timestep is choose. For the assumption to be valid the choice of timestep should not change the streamline path. Figures 19 through 27 show examples of how a streamline path will change depending on which transient result is used with the steady state streamlines. The predicted path also changes resulting in very unphysical prediction, like particle appearing and disappearing around the model a completely unphysical manor.

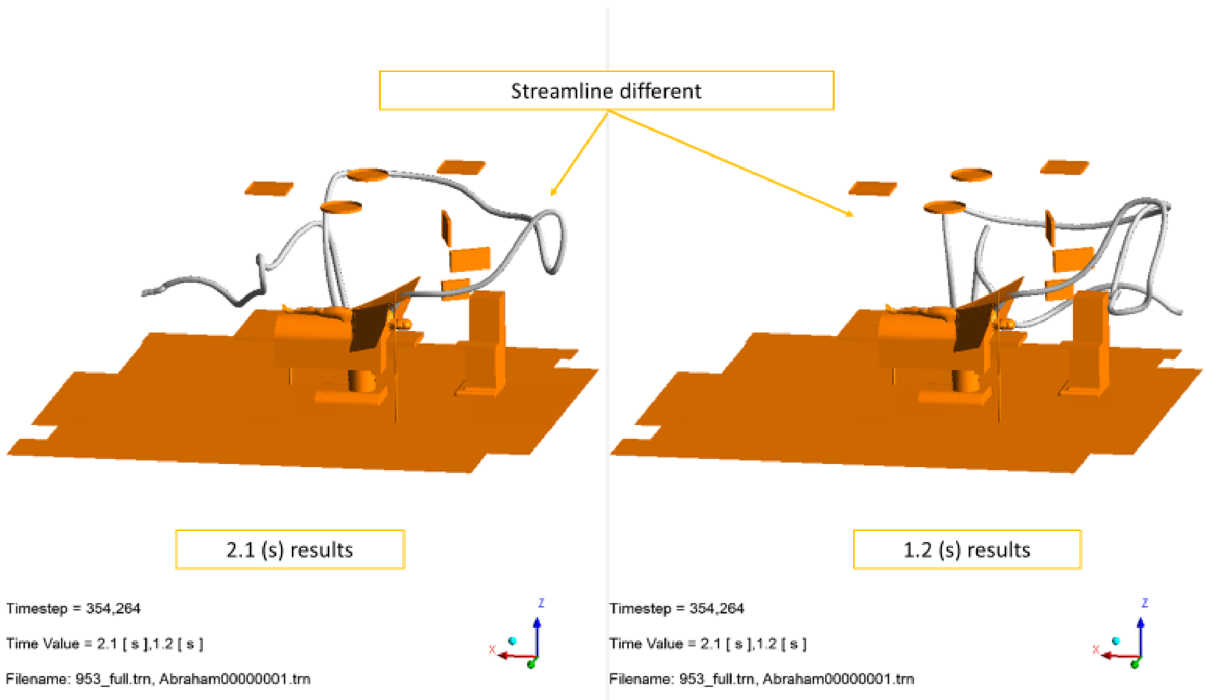

Figure 19 shows the predicted path of a streamline coming from the Bair Hugger Inlet for Abraham00000001.trn model for both 2.1 (s) on the left and the 1.2 (s) report on the right. The difference streamline paths is due the changes to the underlying velocity solution.

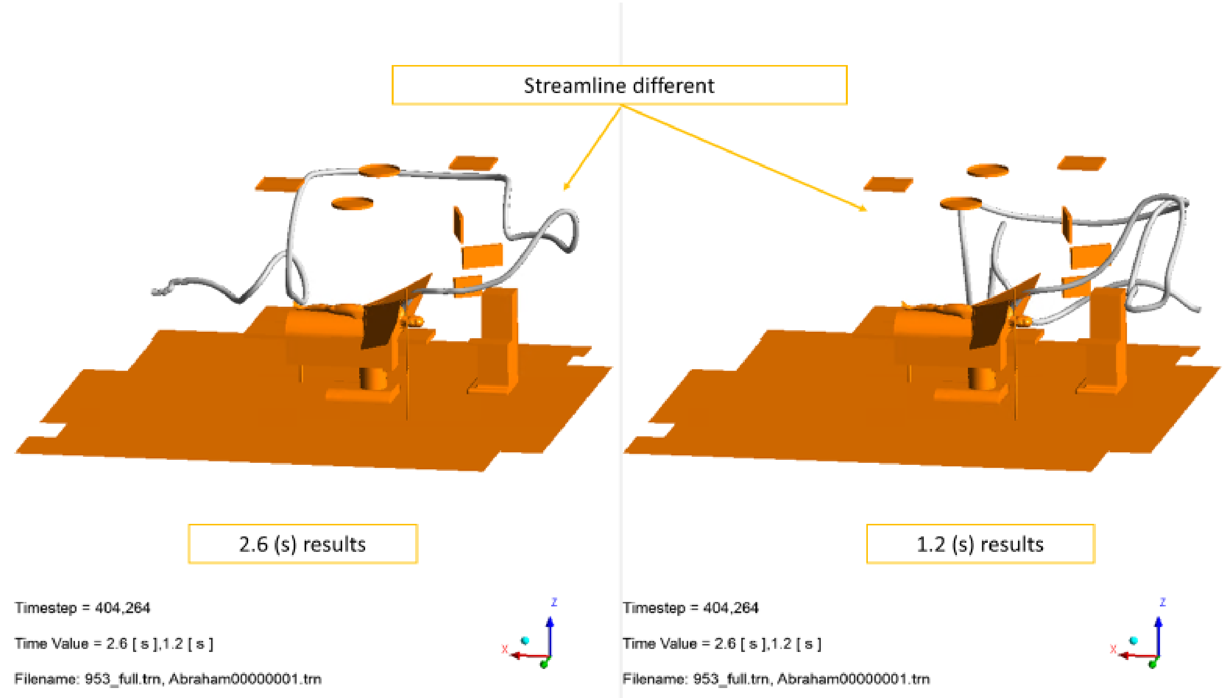

Figure 20 shows the predicted path of a streamline coming from the Bair Hugger Inlet for Abraham00000001.trn model for both 2.6 (s) on the left and the 1.2 (s) report on the right. The difference streamline paths is due the changes to the underlying velocity solution.

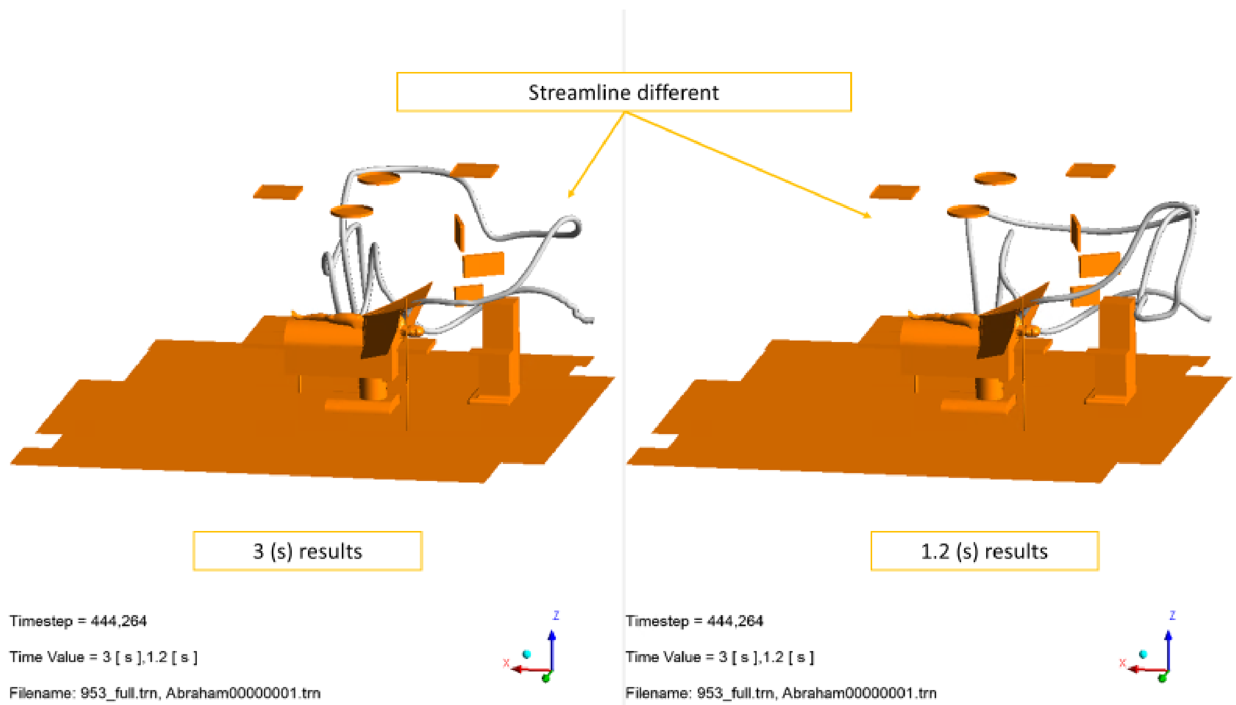

Figure 21 shows the predicted path of a streamline coming from the Bair Hugger Inlet for Abraham00000001.trn model for both 3 (s) on the left and the 1.2 (s) report on the right. The difference streamline paths is due the changes to the underlying velocity solution.

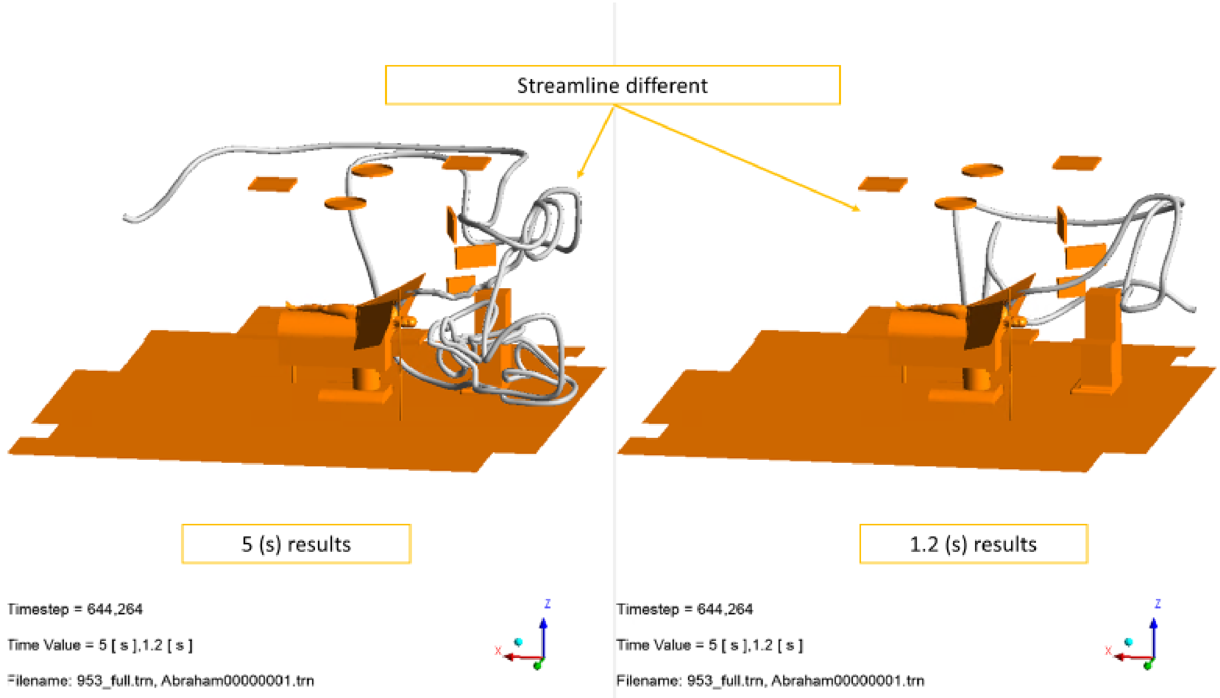

Figure 22 shows the predicted path of a streamline coming from the Bair Hugger Inlet for Abraham00000001.trn model for both 5 (s) on the left and the 1.2 (s) report on the right. The difference streamline paths is due the changes to the underlying velocity solution.

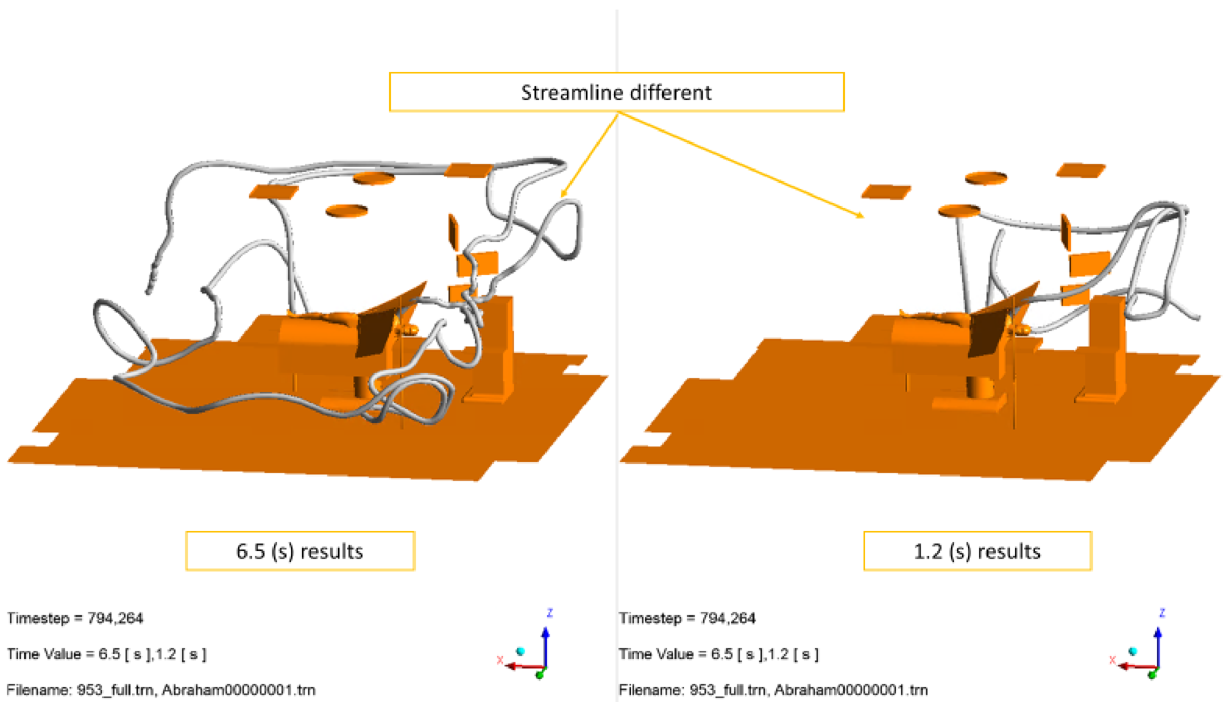

Figure 23 shows the predicted path of a streamline coming from the Bair Hugger Inlet for Abraham00000001.trn model for both 6.5 (s) on the left and the 1.2 (s) report on the right. The difference streamline paths is due the changes to the underlying velocity solution.

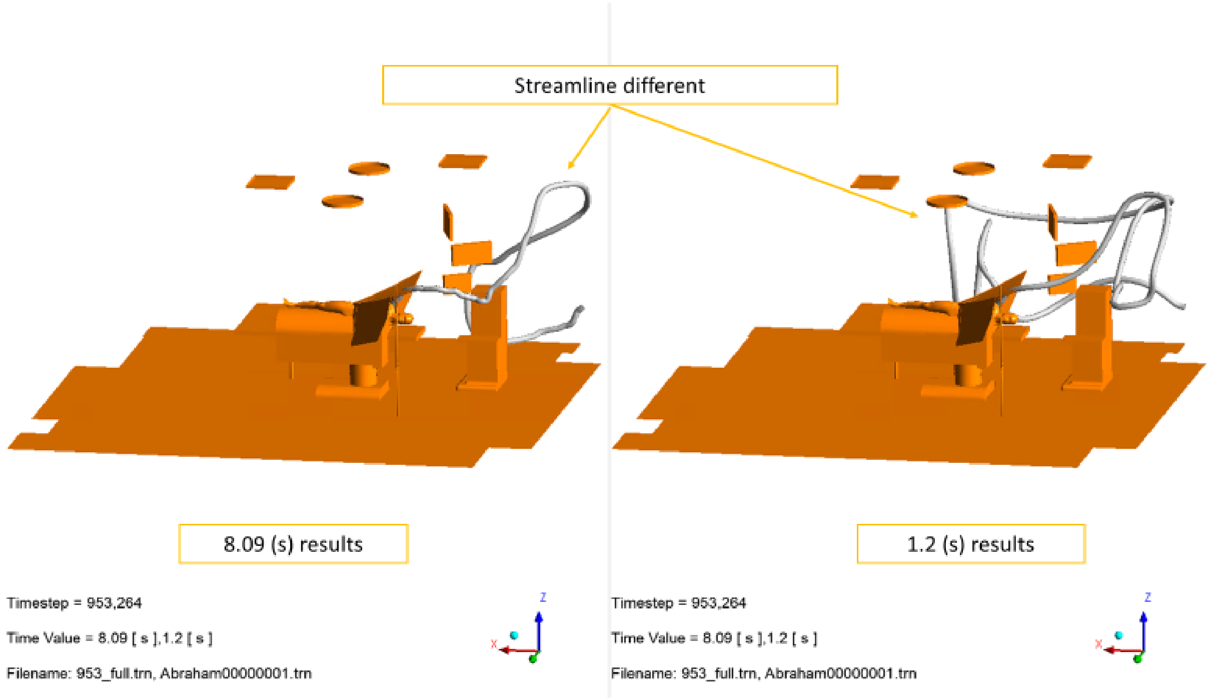

Figure 24 shows the predicted path of a streamline coming from the Bair Hugger Inlet for Abraham00000001.trn model for both 8.09 (s) on the left and the 1.2 (s) report on the right. The difference streamline paths is due the changes to the underlying velocity solution.

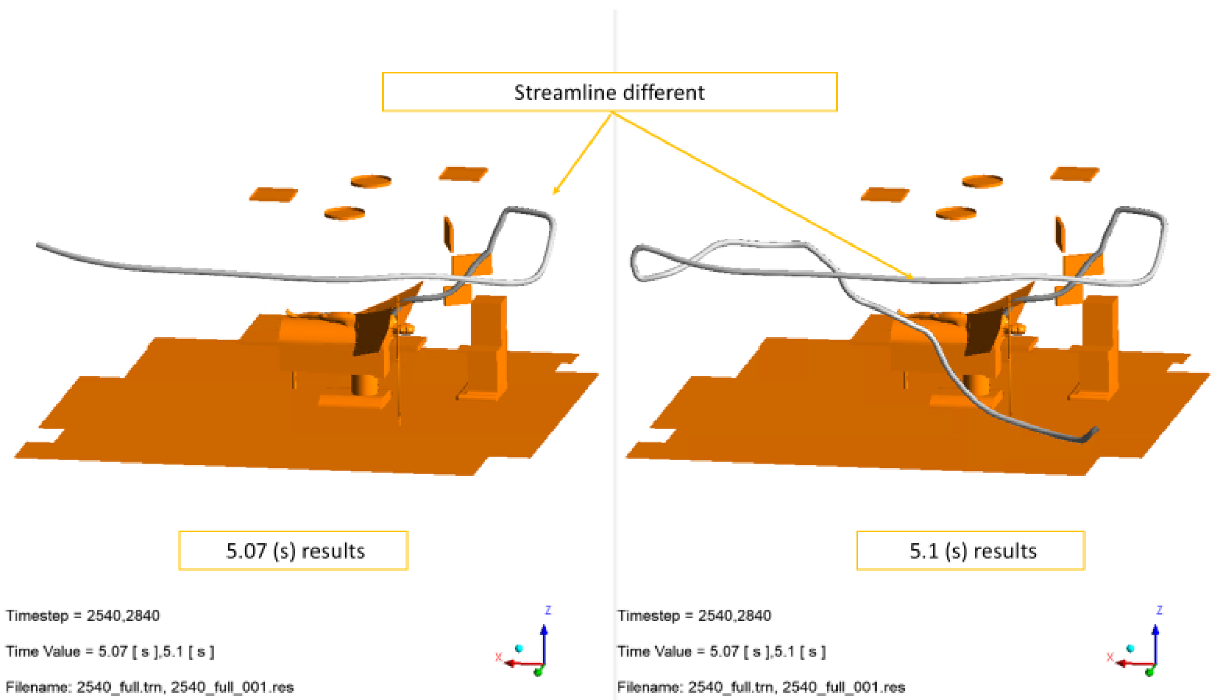

Figure 25 shows the predicted path of a streamline coming from the Bair Hugger Inlet for 2540_full.trn model for both 5.07 (s) on the left and the 5.1 (s) report on the right. The difference streamline paths is due the changes to the underlying velocity solution.

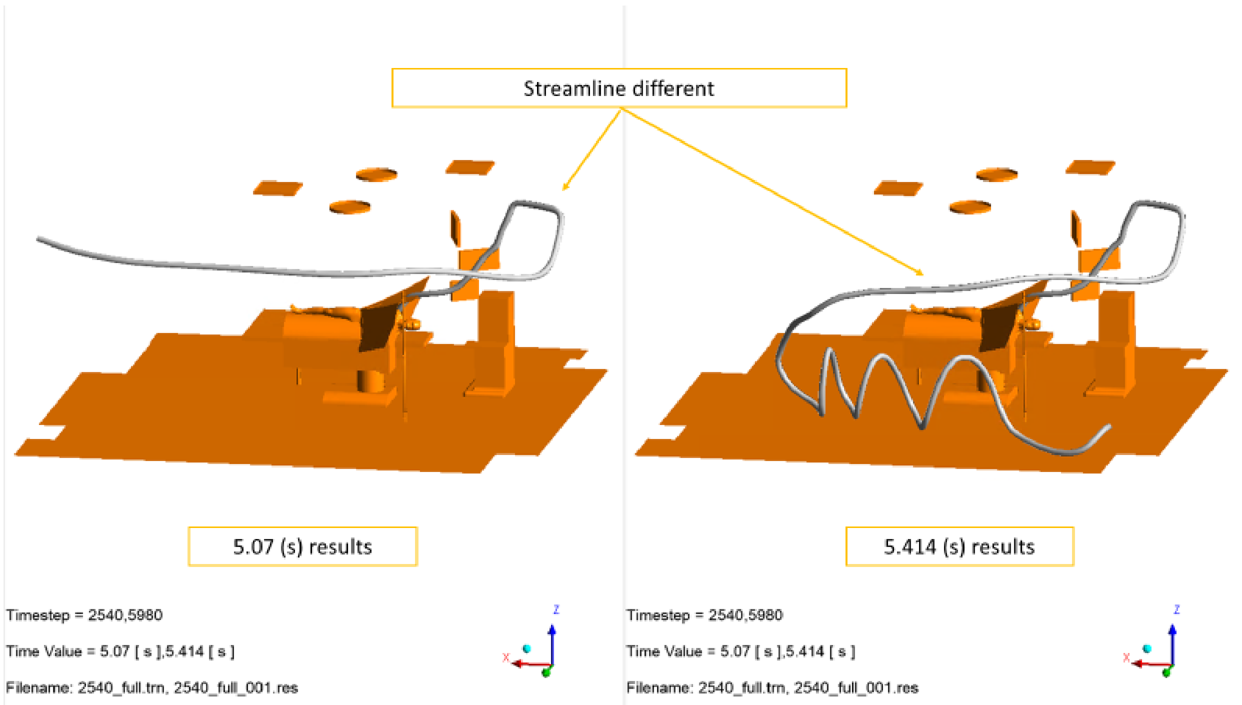

Figure 26 shows the predicted path of a streamline coming from the Bair Hugger Inlet for 2540_full.trn model for both 5.07 (s) on the left and the 5.414 (s) report on the right. The difference streamline paths is due the changes to the underlying velocity solution.

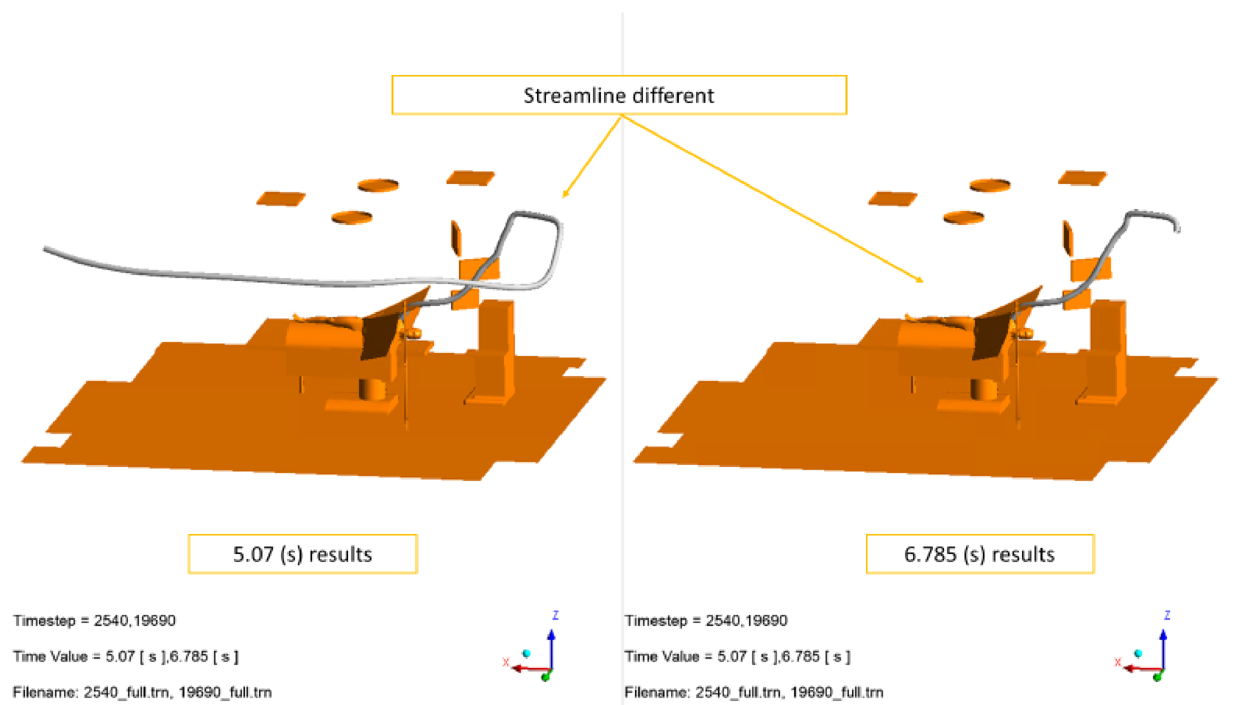

Figure 27 shows the predicted path of a streamline coming from the Bair Hugger Inlet for 2540_full.trn model for both 5.07 (s) on the left and the 6.785 (s) report on the right. The difference streamline paths is due the changes to the underlying velocity solution.

Streamlines do not capture settling (buoyancy) or slip

As a particle moves through a fluid, a number of different forces act on them, these forces include slip and will change the particles trajectory compared to what a streamline would predict. Both slip and buoyancy are known to effect particles, in fact, a lot of separation technology (cyclones and separators) are designed to use these forces in their designs. Streamlines do not include either forces.

Streamlines do not capture Turbulence Dispersion

The unsteady eddies in turbulent flow will cause particles to spread away from an average particle path line. This turbulent dispersion will result in particles released from the same point to take potentially very different paths depending on when they are released. Streamline do not capture the physical effect, to do so correctly would require modeling the particles as transient particles, which ANSYS CFX has the capability to do.

Mesh

In a CFD model the geometry (volume) that the air moves through is split into a discrete number of mesh cells. It is important that mesh contains enough nodes/elements, so the results are independent of the mesh used. The elements of the mesh also need to be within quality limitation or else the solver can have issues solving and/or give incorrect results.

Unacceptable mesh quality

Dr. Abraham has a number of his mesh elements that are not in the acceptable range of mesh quality as defined by ANSYS. Figure 28 through 31. Poor quality mesh elements are known to cause convergence issues and give incorrect answers (Figures 32 and 33).

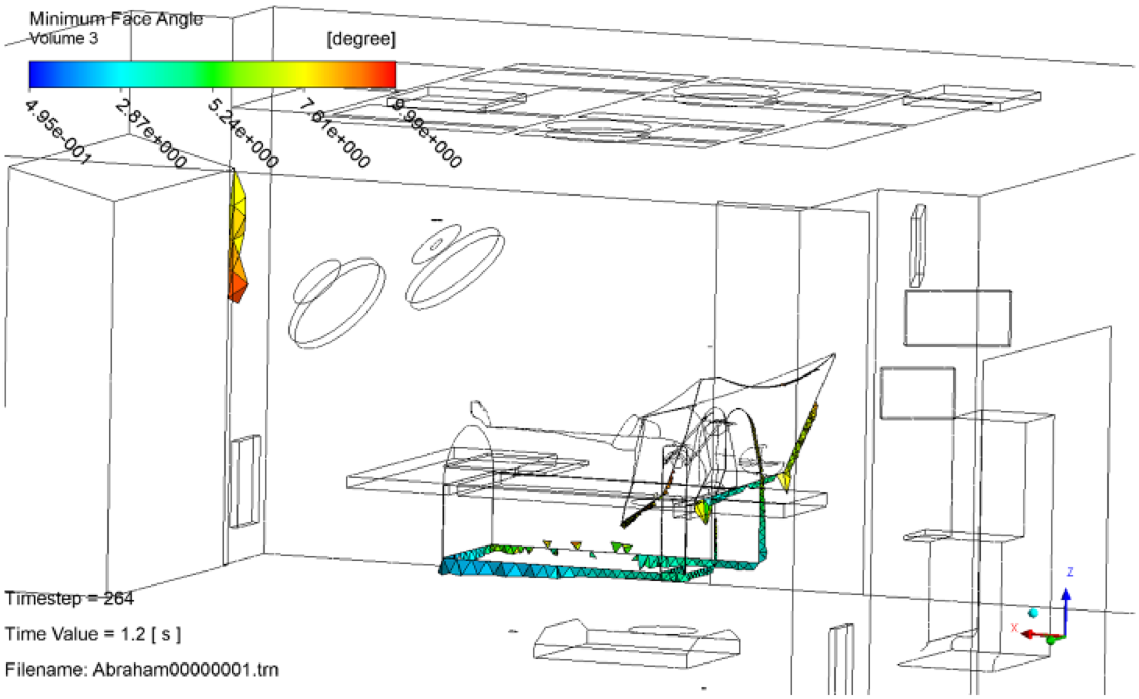

Figure 28 Poor Mesh quality Abraham00000001.trn Minimum Face Angle

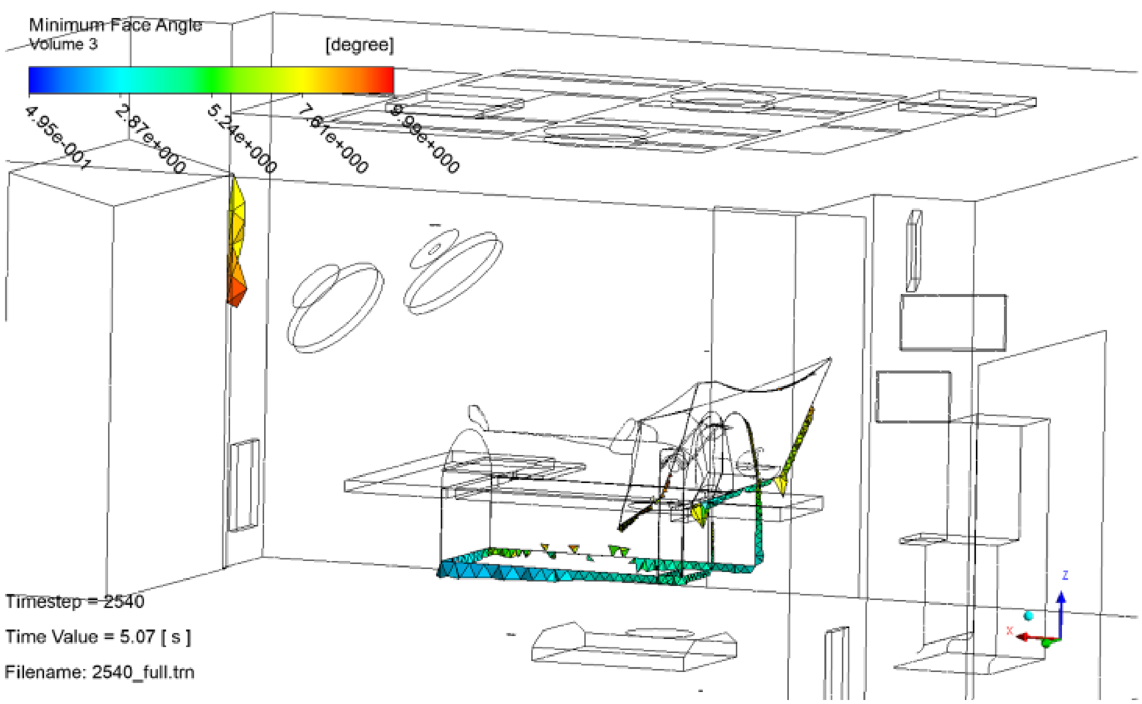

Figure 29 Poor Mesh quality 2540_full.trn Minimum Face Angle

Figure 30 Poor Mesh quality Abraham00000001.trn Element Volume Ratio

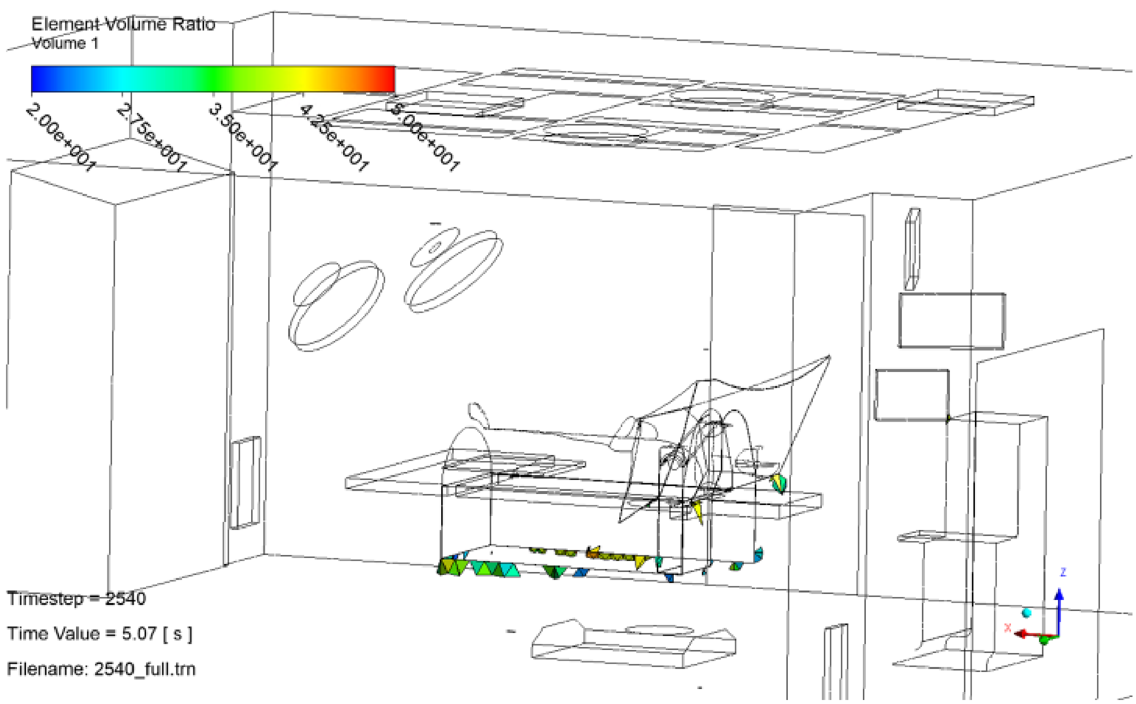

Figure 31 Poor Mesh quality 2540_full.trn Element Volume Ratio

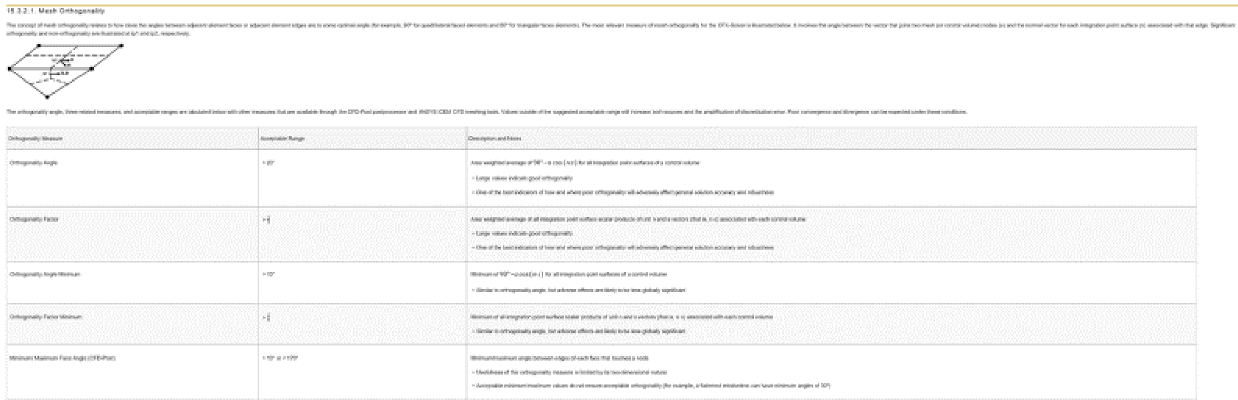

15.3.2.1. Mesh Orthogonality

Orthogonality Measure	Acceptable Range	Description and Notes
Orthogonality Angle	> 20°	[illegible]
Orthogonality Factor	> 1/3	[illegible]
Orthogonality Angle Minimum	> 10°	[illegible]
Orthogonality Factor Minimum	> 1/3	[illegible]
Minimum Maximum Face Angle (CFD-Post)	> 10° or < 170°	[illegible]

Figure 32 Mesh quality recommendations Mesh Aspect Ratio[2]

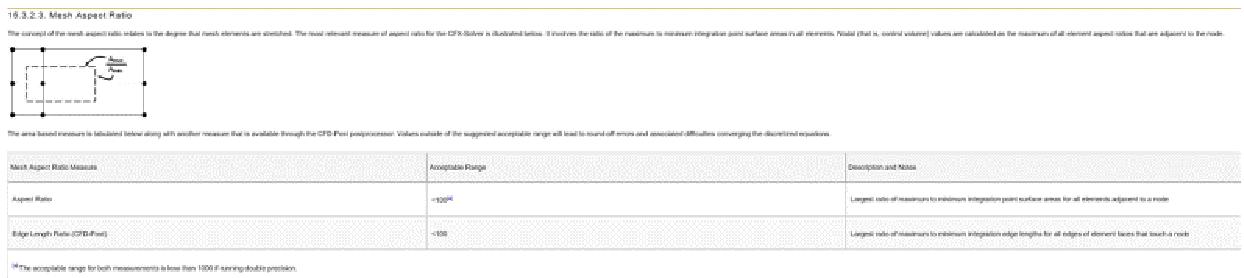

15.3.2.3. Mesh Aspect Ratio

Mesh Aspect Ratio Measure	Acceptable Range	Description and Notes
Aspect Ratio	<100[a]	Largest ratio of maximum to minimum integration point surface areas for all elements adjacent to a node
Edge Length Ratio (CFD-Post)	<100	Largest ratio of maximum to minimum integration edge lengths for all edges of element faces that touch a node

[a] The acceptable range for both measurements is less than 1000 if running double precision.

Figure 33 Mesh quality recommendations[3]

Mesh dependence of solution

Dr. Abraham does not have an adequately refined mesh. If Dr. Abraham was to run his model on a more refined mesh he would get a different result. It is standard industry practice to establish mesh independence of your model results.

Based on the best practice guidelines for LES modelling using ANSYS CFX by F.R. Menter[4] LES models require a fine enough mesh that can capture the large eddies. The lS_{crit} is an estimate of the number of nodes that shall be available to capture high resolution turbulent features for any LES simulation. It is calculated from,

$$lS_{crit} = \frac{l_t}{l_{mesh}} \quad (1)$$

[2] ANSYS Help
[3] ANSYS Help
[4] Best Practice: Scale-Resolving Simulations in ANSYS CFD, Version 2.00, F.R. Menter

where l_t is the turbulent length scale and l_{mesh} is representing the mesh length scale.

The mesh length scale calculated from,

$$l_{mesh} = \sqrt[3]{V} \qquad (2)$$

where V is the mesh sector volume for a node.

The turbulent length scale l_t is calculated from,

$$l_t = \frac{k^{3/2}}{\varepsilon} \qquad (3)$$

where k is the resolved kinetic turbulent energy which is from,

$$k = \frac{1}{2}(\overline{u'^2} + \overline{v'^2} + \overline{w'^2}) \qquad (4)$$

where $\overline{u'^2}$, $\overline{v'^2}$ and $\overline{w'^2}$ are the statistical Reynolds stresses, ε is the turbulent eddy dissipation which can be calculated using the following relationship

$$\varepsilon = \rho C_\mu \frac{k^2}{\mu_t} \qquad (5)$$

where C_μ is dimensionless constant of 0.09, μ_t is the eddy viscosity.

Figures 35 and 37 show the LES mesh criteria for the Abraham00000001.trn and 2540_full.trn has significant areas with less than 5 elements and even areas with less than 1, Figures 36 and 38. The mesh resolution is too coarse to capture the required turbulent features and with refinement would produce different results. It is recommended that a minimum of 5-10 elements ratio to the turbulent integral length scale to capture the required details for any LES type turbulence modelling (Figure 34). Based on the conclusion captured by F. R. Menter· Y. Egorov[5], "*In contrast, LES and DES models can return incorrect results and potentially numerical instabilities if the numerical grid is too coarse (insufficient for LES) or the time-step is too large (substantially larger than CFL ~1).*", thus LES models can return significant error and the wrong results if the numerical mesh is too coarse.

[5] The Scale-Adaptive Simulation Method for Unsteady Turbulent Flow Predictions. Part 1: Theory and Model Description F. R. Menter· Y. Egorov

4.2.3. Meshing Requirements

In order to generalize the concepts discussed for the mixing layer example (Figure 23), we introduce the terminology of a Separating Shear Layer (SSL). It refers to the shear layer that starts

33

at the point of separation from the body and moves into a free shear flow (we are not considering small separation bubbles embedded within the boundary layer). In Figure 23 this would be the mixing layer forming downstream of the plate. In other flows it can be a separating boundary layer from a corner. In the case of locally unstable flows, the Δ_{max} spacing should be sufficiently small to allow resolution of the initial flow instability of the SSL. The main quantity of relevance is the ratio of RANS to grid length scale:

$$R_L = \frac{\Delta_{max}}{L_t^{RANS}}; \quad L_t^{RANS} = \left(\frac{k^{3/2}}{\varepsilon}\right)^{RANS} = \left(\frac{k^{1/2}}{C_\mu \omega}\right)^{RANS}$$

It is important to emphasize that this quantity should be evaluated based on a precursor RANS solution. This implies that such a solution exists and is meaningful. If the precursor solution is not available, then one can estimate the ratio based on the thickness of SSL. For equilibrium mixing layers, the following ratio is approximately correct:

$$L_t^{RANS} = 0.7 \cdot \delta^{mixing}$$

where δ^{mixing} is the thickness of the mixing layer. The value of R_L should be:

$$R_L \leq 0.2 - 0.1$$

Figure 34 Best Practice: Scale-Resolving Simulations in ANSYS CFD, Version 2.00, by F.R. Menter, page 34

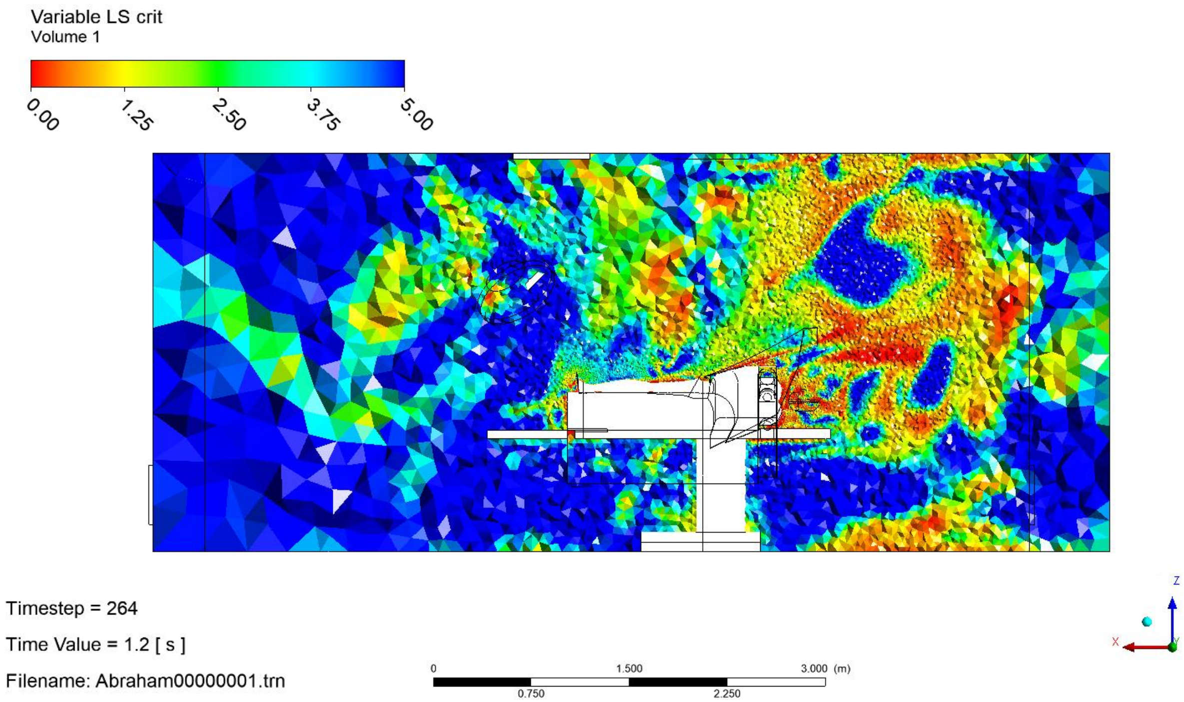

Figure 35 Mesh Criteria Abraham00000001.trn

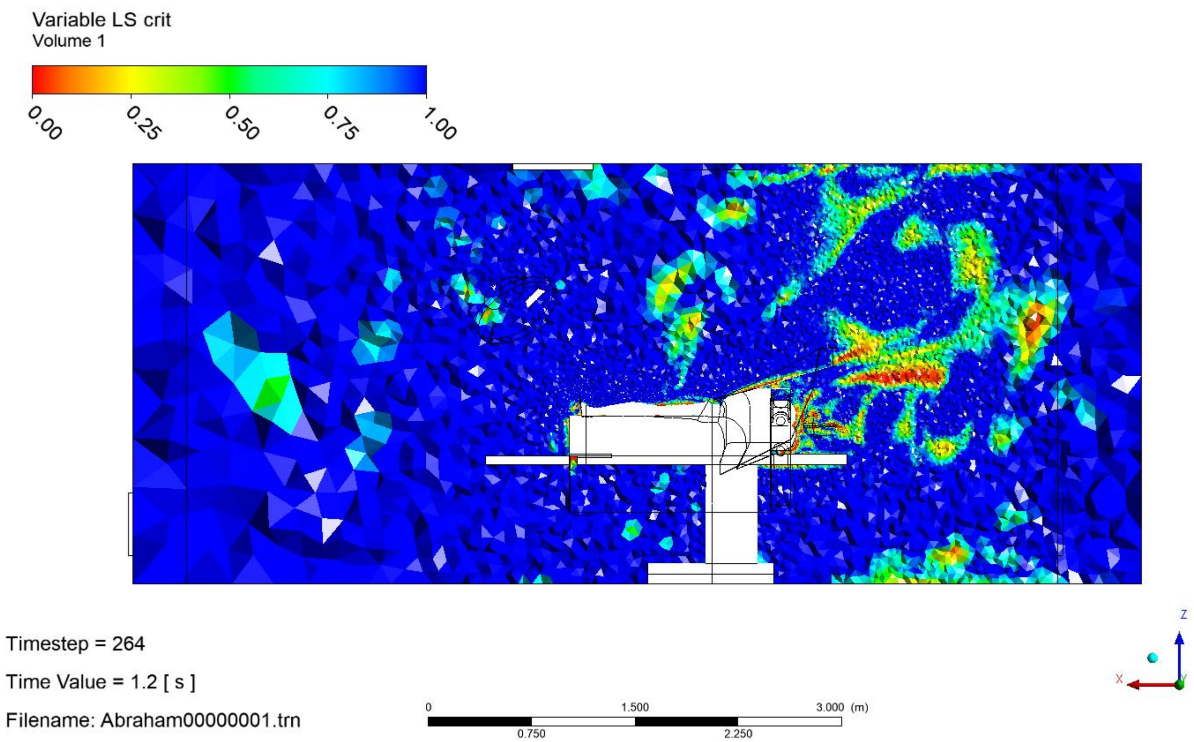

Figure 36 Mesh Criteria Abraham00000001.trn

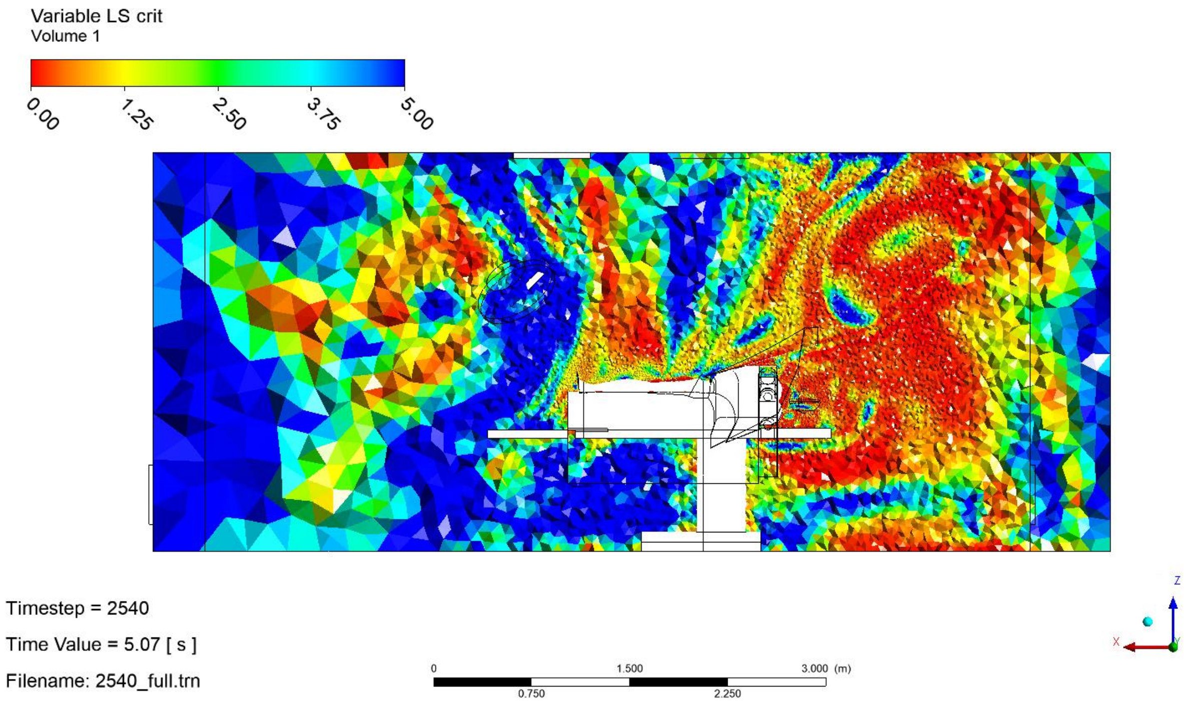

Figure 37 Mesh Criteria 2540_full.trn

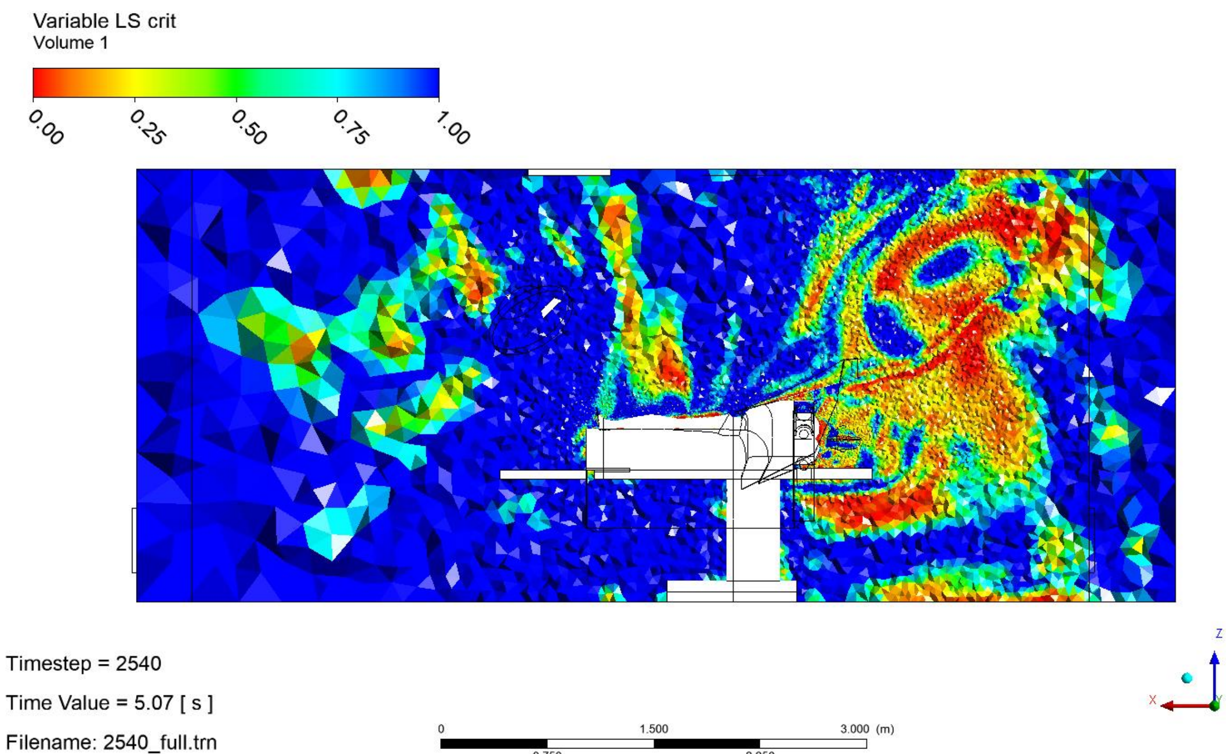

Figure 38 Mesh Criteria 2540_full.trn

Expressions	
Accumulated Time Step	*2540*
Current Time Step	*2540*
L0 crit	*ke^(1.5) /eddy*
LScrit	*L0 crit/Lmesh*
Lmesh	*Volume^(1/3)*
Reference Pressure	*1 [atm]*
Sequence Step	*2540*
Time	*5.07 [s]*
atstep	*Accumulated Time Step*
ctstep	*Current Time Step*
eddy	*(Density*0.09*ke^2)/Eddy Viscosity*
ke	*0.5*(Statistical Reynolds Stress uu+Statistical Reynolds Stress vv+Statistical Reynolds Stress ww)*
sstep	*Sequence Step*
t	*Time*

Figure 39 Calculation of LScrit

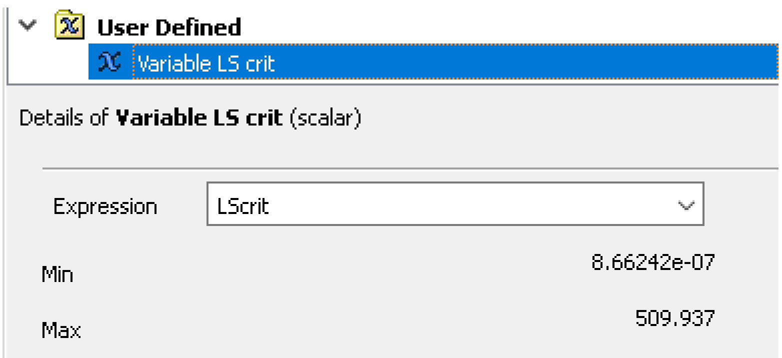

Figure 40 Definition of Variable LS crit

Solving CFD models

A CFD model is made up of the mathematic equations that description of the physics (models) we are trying to solve. Due to the complexity of the equations an iterative approach is used. This involves starting with an initial value and then the solver adjusts the values at the nodes until hopefully the equations are solved correctly. The iterative converge of the set of equations on the correct solution is required before the numerical errors in a limited and the model can be used.

Divergence Solution

Abraham00000001.trn model was run forward in time and the model diverged (Figure 41). Divergence means that the solver couldn't even keep trying to solve the model, let alone converged. As a standard industry practice diverged models are not trusted due to their obvious significant numerical errors.

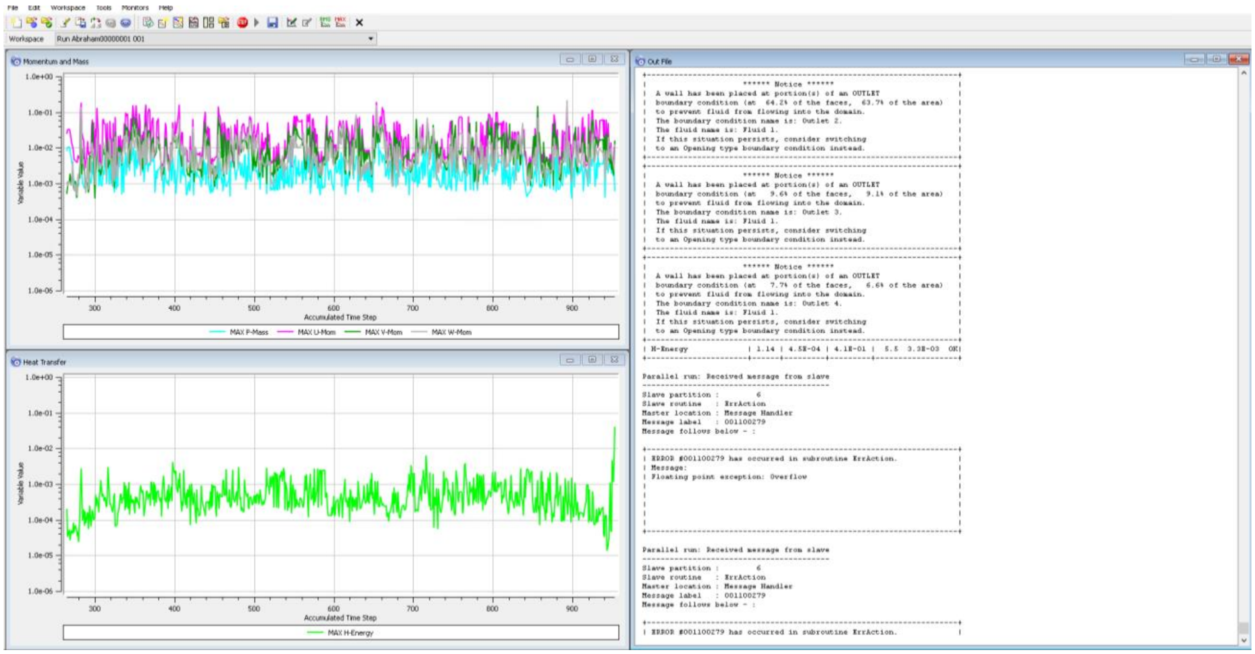

Figure 41 The solution output is shown when the Abraham000001.trn model is run forward. The solver gives a floating point error which indicates the divergence of the model.

1st order accurate

Dr. Abraham makes an error with the 2540_full.trn model by using the High Resolution advection scheme. This is inappropriate for LES turbulence models, the Central Differencing or Bounded Central Differencing scheme should be used. The High Resolution advection scheme is known to result in an inaccurate solution with LES modeling. Figure 42 shows the how the High Resolution Advection Scheme was used. Figure 43 shows the warning produced in the out file when the solver runs the 2540_full.trn file and Figure 44 shows the recommendation from the Ansys Best Practices for Scale-Resolving Simulations in ANSYS CFD Help. Mentor and Egorov state "*No proper LES behaviour can be achieved with an overly dissipative numerical treatment of the convective terms. In industrial LES, the usage of second order central discretisation (CD) schemes is an established technology*"[6]

[6] The Scale-Adaptive Simulation Method for Unsteady Turbulent Flow Predictions. Part 1: Theory and Model Description F. R. Menter· Y. Egorov

```
  SOLVER CONTROL:
    ADVECTION SCHEME:
      Option = High Resolution
    END
    CONVERGENCE CONTROL:
      Maximum Number of Coefficient Loops = 10
      Minimum Number of Coefficient Loops = 1
      Timescale Control = Coefficient Loops
    END
    CONVERGENCE CRITERIA:
      Residual Target = 0.00001
      Residual Type = RMS
    END
    EQUATION CLASS: momentum
      ADVECTION SCHEME:
        Option = High Resolution
      END
    END
    PRESSURE LEVEL INFORMATION:
      Option = Automatic
    END
    TRANSIENT SCHEME:
      Option = Second Order Backward Euler
      TIMESTEP INITIALISATION:
        Option = Automatic
      END
    END
  END
END
```

High Resolution advection scheme

Figure 42 High Resolution setting in 2540_full.trn

```
+--------------------------------------------------------------------+
| ERROR #001100279 has occurred in subroutine ErrAction.             |
| Message:                                                           |
| WARNING: Use of the central difference advection scheme is strong- |
| ly recommended for LES simulations. Another scheme has been used   |
| for one or more equation classes.                                  |
|                                                                    |
|                                                                    |
|                                                                    |
+--------------------------------------------------------------------+
```

Figure 43 Warning the solver provides with the use of High Resolution with LES model for 2540_full.trn

12.3.1. Spatial Discretization

12.3.1.1. Momentum

SRS models, as described in *Scale-Resolving Simulation (SRS) Models – Basic Formulations*, serve the main purpose of dissipating the energy out of the turbulence spectrum at the limit of the grid resolution. The eddy viscosity is defined to provide the correct dissipation at the larger LES scales. This assumes that the numerical scheme is non-dissipative and that all dissipation results from the LES model. For this reason, one is required to select a numerical scheme in the LES region with low dissipation, relative to the dissipation provided by a subgrid LES model. Another strategy is to avoid the introduction of the LES (subgrid) eddy viscosity and provide all damping through the numerical scheme. This approach is called MILES (Monotone Integrated Large Eddy Simulation) (Boris et al., 1992 [1]). In ANSYS CFD, the standard LES methodology is followed, whereby the dissipation is introduced by a LES eddy viscosity model and the numerical dissipation is kept at a low value.

In order to achieve low numerical dissipation, you cannot use the standard numerical schemes for convection that were developed for the RANS equations (Second Order Upwind Schemes, or SOU), which are dissipative by nature. In contrast, LES is carried out using Central Difference (CD) schemes. In industrial simulations, second order schemes are typically employed, however, in complex geometries with non-ideal grids, CD methods are frequently unstable and produce unphysical wiggles (see *Figure 12.60*), which can eventually destroy the solution. To overcome this problem, variations of CD schemes have been developed with more dissipative character, but still much less dissipative than Upwind Schemes. An example is the Bounded Central Difference (BCD) scheme of Jasak et al., 1999 [14].

Figure 44 Recommendation in Ansys Best Practices: Scale-Resolving Simulations in ANSYS CFD

Validation

Dr. Abraham attempts to validate his model based on temperature measurement away from the surgical site, he doesn't show that his model can accurately predict the temperature in the critical region nor that it can accurately predict particle motion, without this any validation claim is limited at best.

Dr. Abraham claims to validate his model, he gives *"the room-averaged temperature was 62^{o}F for an 8.1 million grid-cell calculation"*, however he gives no details of where, when and how his is measuring this value. Without this information it is not possible to evaluate the claim that the models agree with the experimental since the experimental is undefined. Also, the mesh used in his model is not 8.1 million elements as stated, it is unclear if the CFD measurement is from the provided results or not.

Likewise, Dr. Abraham gives a measurement of 60 (^{o}F) 3 inches from the floor. However again he gives no detail of where the measurement was taken. Figures 45 and 46 show the temperature contours 3 inches from the floor. Depending on when, where and how the measurements were taken it is not possible to confirm any agreement between the model result and experimental since significant areas outside of a 59.5 (^{o}F) to 60.5 (^{o}F) range could easily be not in agreement.

Again, the edge of the table agreement claim cannot be evaluated without when, where and how information about the experimental. Also, Figures 47 and 48 shows regions outside the reported range of measurement.

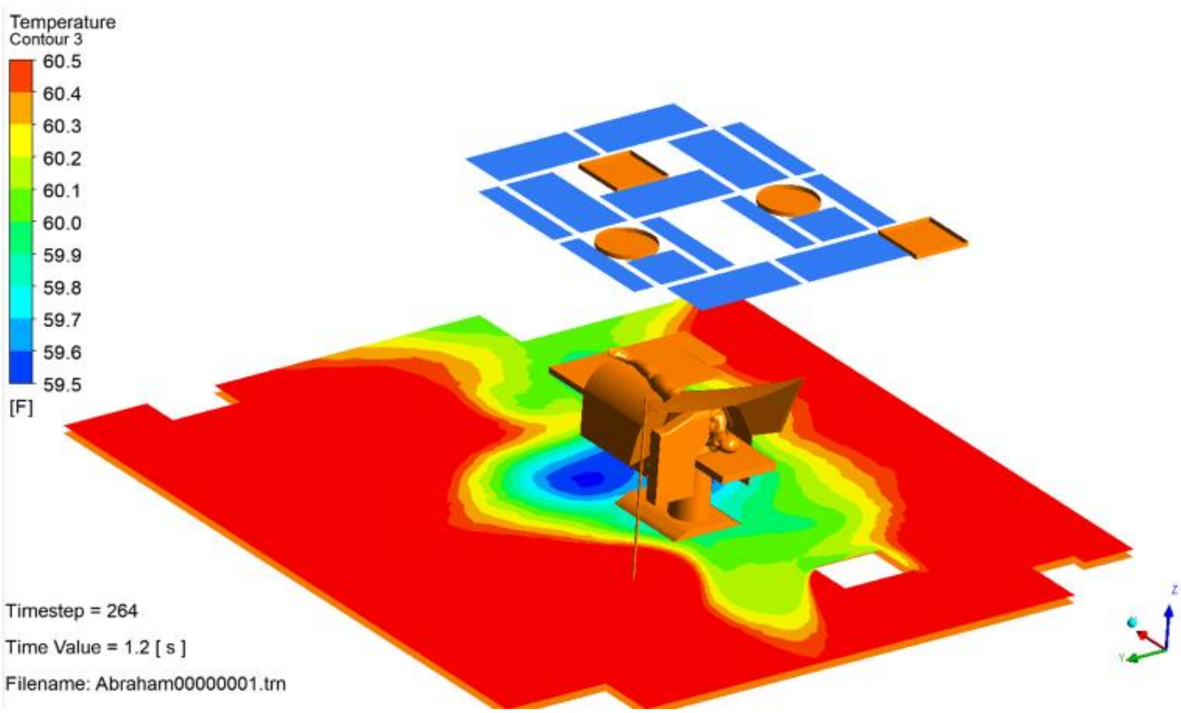

Figure 45 the temperature 3 inch from the floor is show for Abraham00000001.trn. The contours are clipped to between 59.5 (^{o}F) and 60.5 (^{o}F)

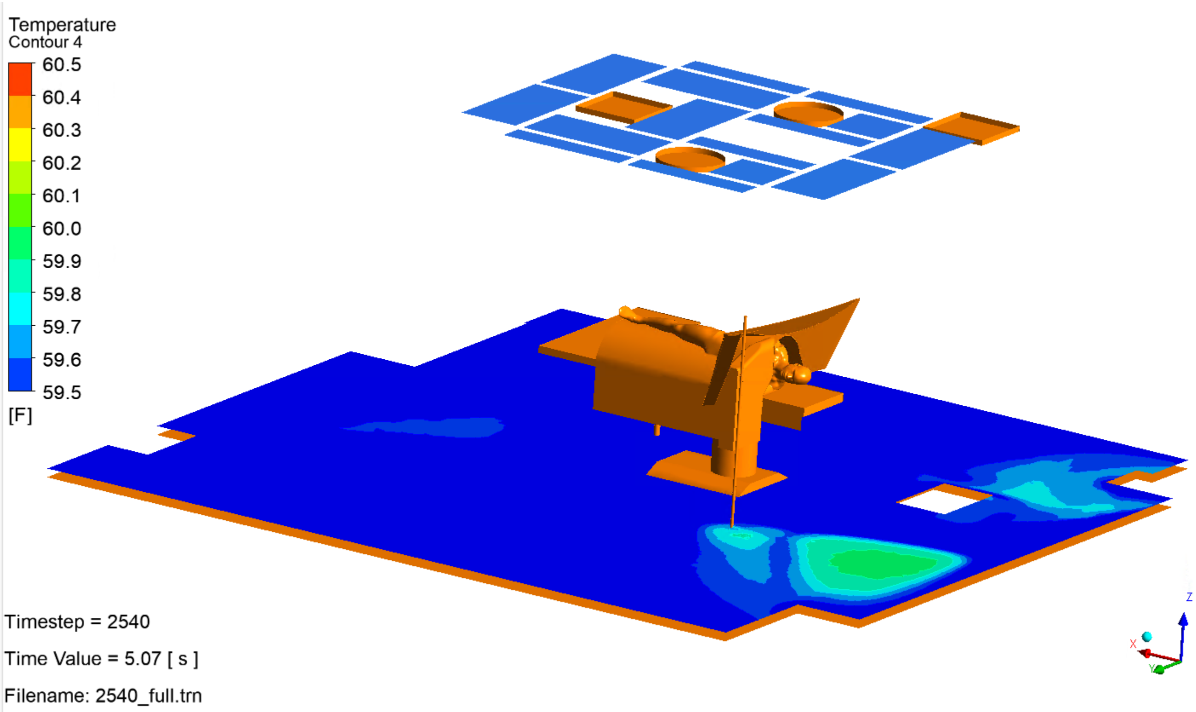

Figure 46 the temperature 3 inch from the floor is show for 2540_full.trn. The contours are clipped to between 59.5 (°F) and 60.5 (°F)

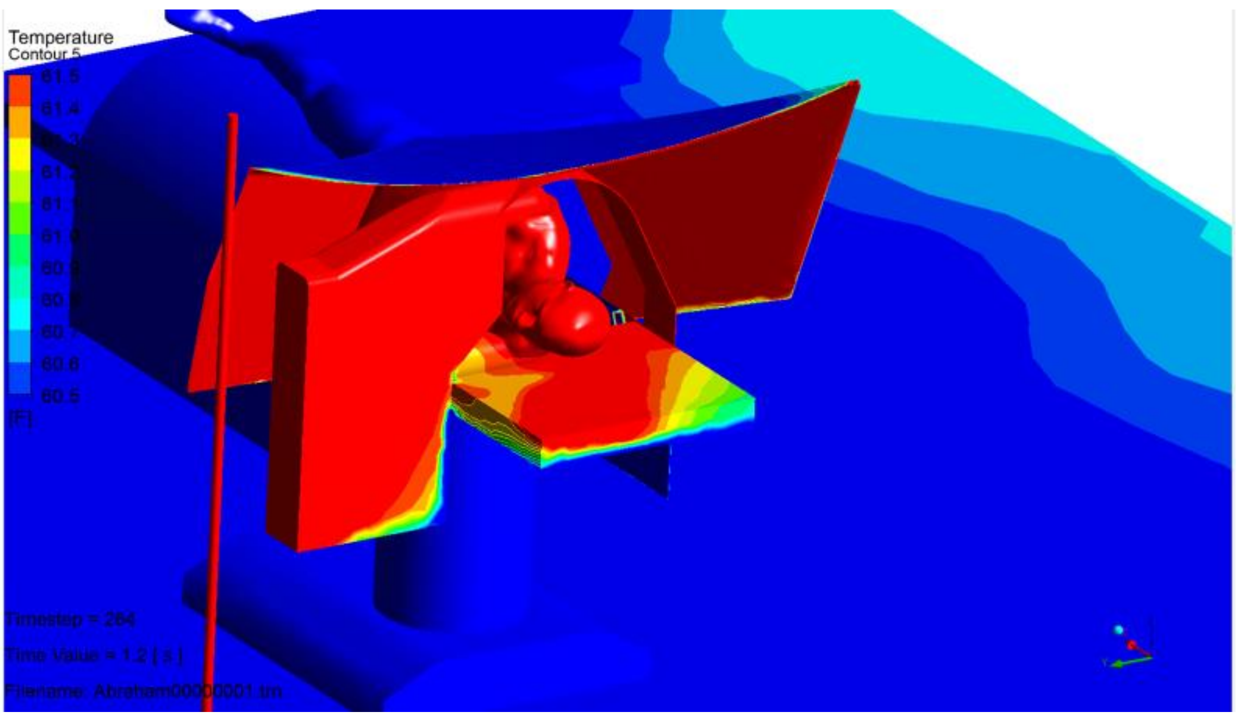

Figure 47 the on the table, drape and body are show for Abraham00000001.trn. The contours are clipped to between 60.5 (°F) and 61.5 (°F)

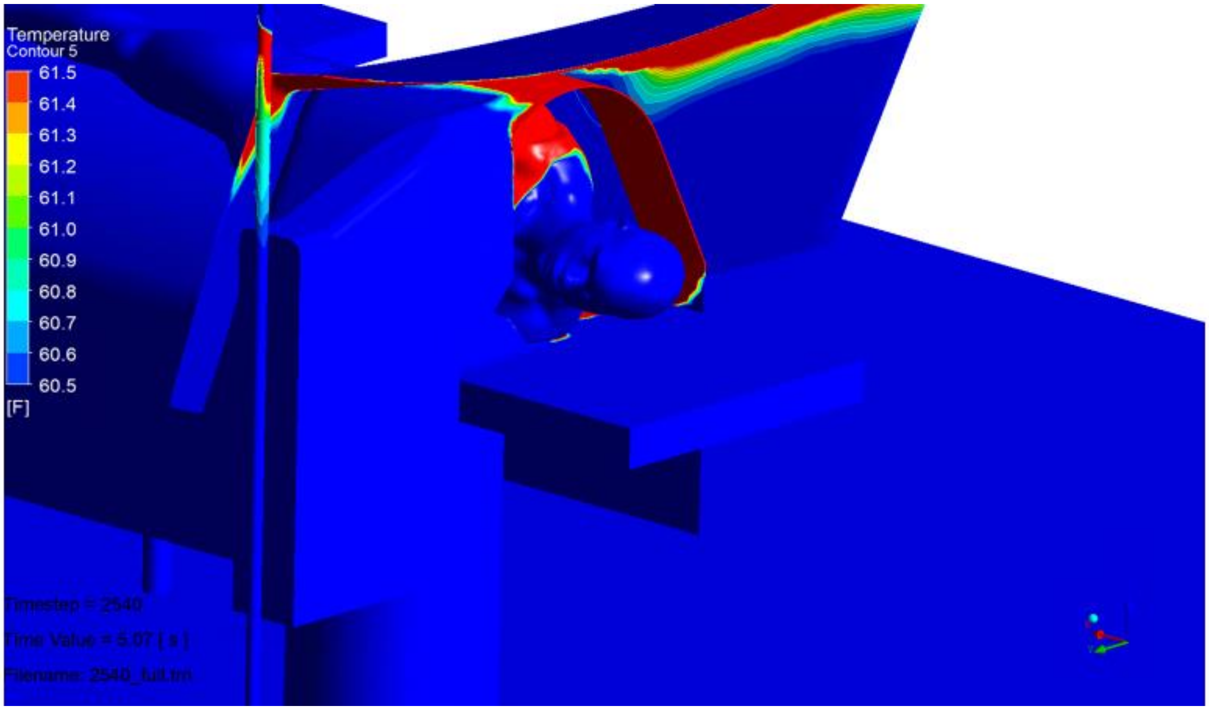

Figure 48 the on the table, drape and body are show for 2540_full.trn. The contours are clipped to between 60.5 (°F) and 61.5 (°F)

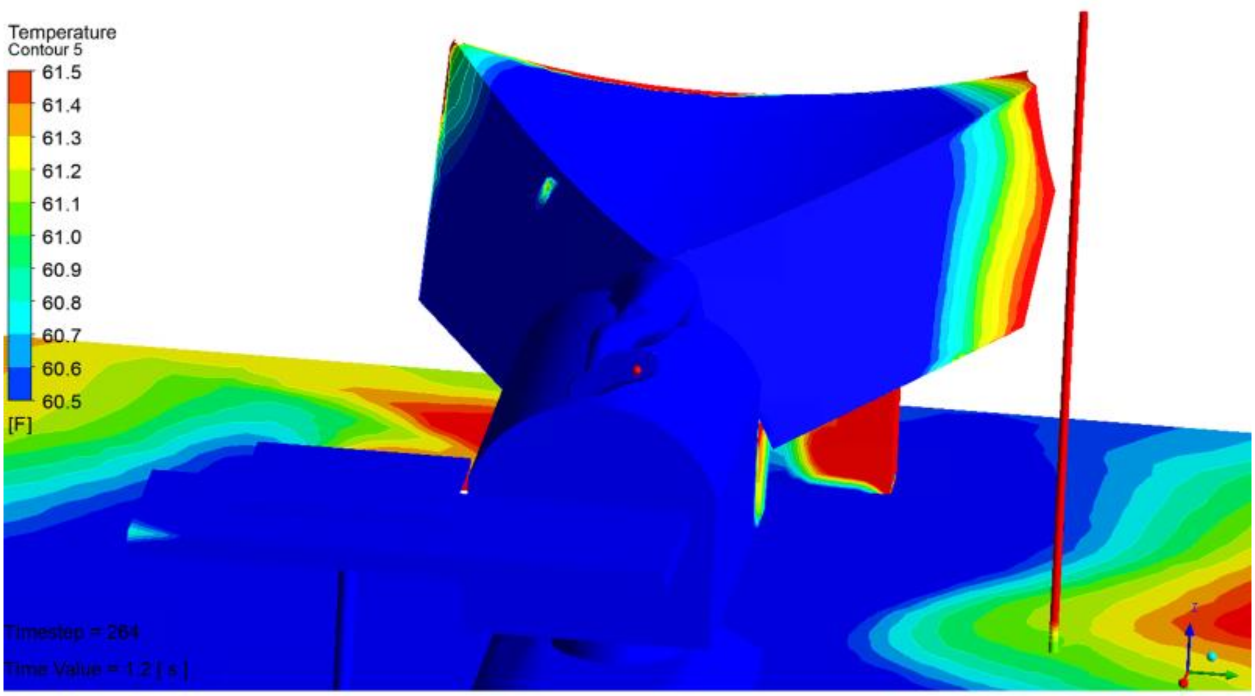

Figure 49 the on the table, drape and body are show for Abraham00000001.trn. The contours are clipped to between 60.5 (°F) and 61.5 (°F)

Figure 50 the on the table, drape and body are show for 2540_full.trn. The contours are clipped to between 60.5 (°F) and 61.5 (°F)

Lack of Confidence

There are other differences between the model and report, these differences are numerous and there is no discussion or modeling data to support the justification for the changes. This lack of information reduces the confidence that model will capture the true physical situation, given the lack of supporting information to allow reasonable review of his work.

Geometry

Having an accurate geometry in a CFD model is a critical to the correct definition of a CFD model. The results dependent on the shape and size of the geometry used any deviation from the actual geometry will introduce errors.

The geometry used in Dr. Abraham's models is different to the geometry in the report.

The geometry used in Dr. Abraham's models is different to the geometry in the report. The differences include the removal of a number of bodies, changing the dimensions of a body and even adding a body at the end of the surgery table. Figures 51 through 54 show the geometry as report in the report and the actual geometries used.

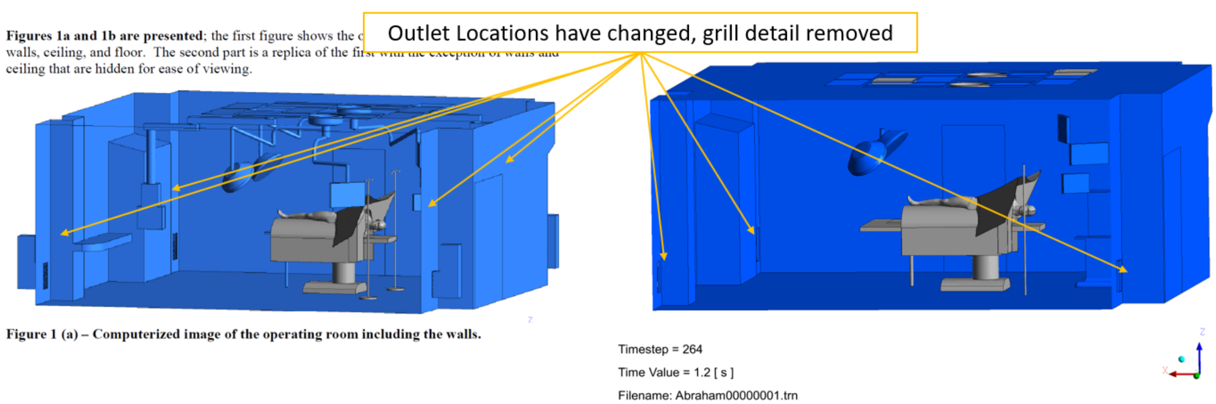

Figure 51 The reported geometry on the left is shown and the actual geometry used in the Abraham00000001.trn model is shown on the right.

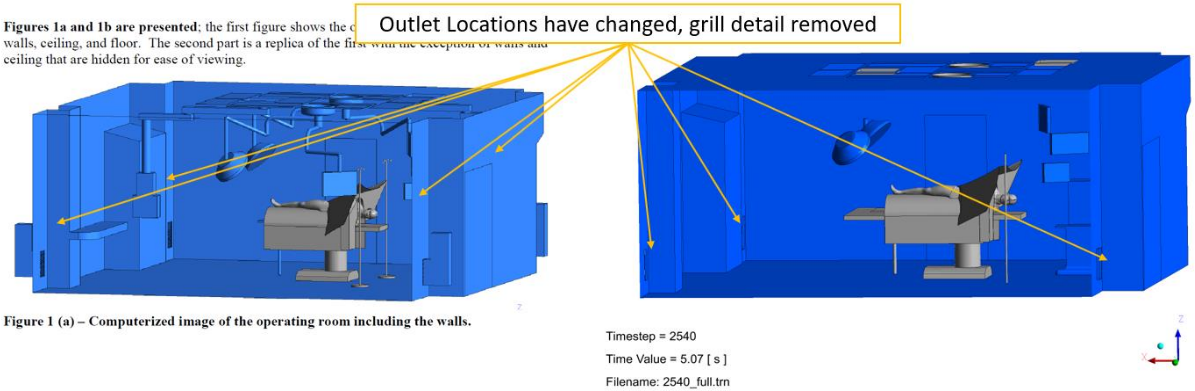

Figure 52 The reported geometry on the left is shown and the actual geometry used in the 2540_full.trn model is shown on the right.

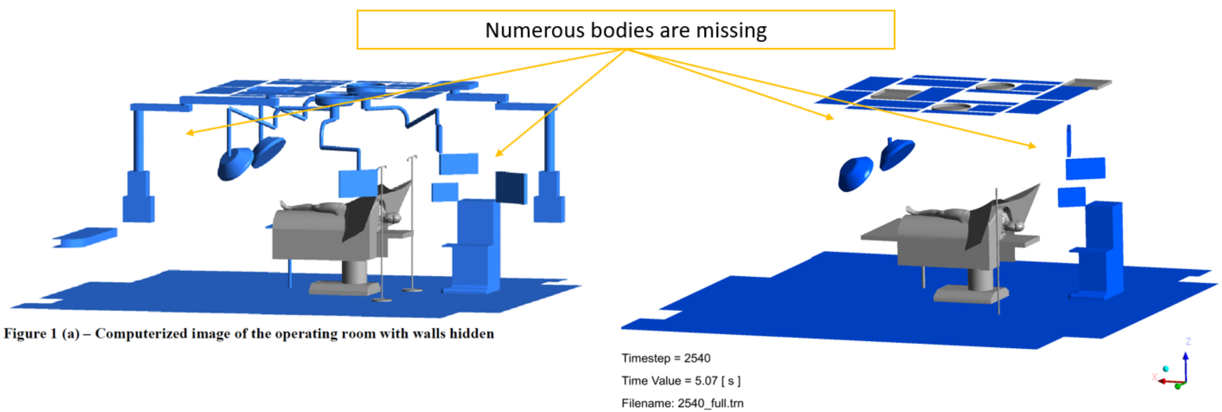

Figure 53 The reported geometry on the left is shown and the actual geometry used in the Abraham00000001.trn model is shown on the right.

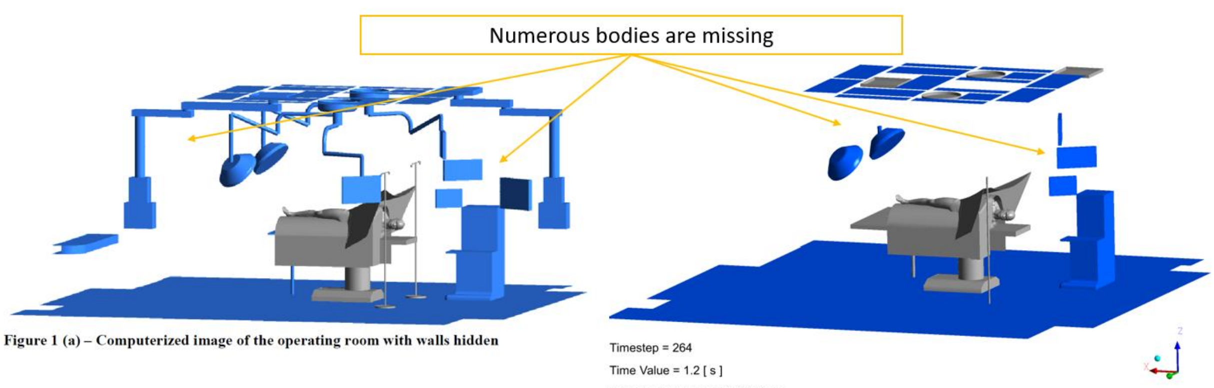

Figure 54 The reported geometry on the left is shown and the actual geometry used in the 2540_full.trn model is shown on the right

Geometry provided is different to the geometry used in the CFD models.

Dr. Abraham, provided a file called Abraham00000003 (2).agdb. The agdb file format is a standard Ansys DesignModeler CAD format. The file contains only one CAD modeling step where a Parasolid file called "D:\3M OR 2015\or-40b-cfd.x_t" is imported.

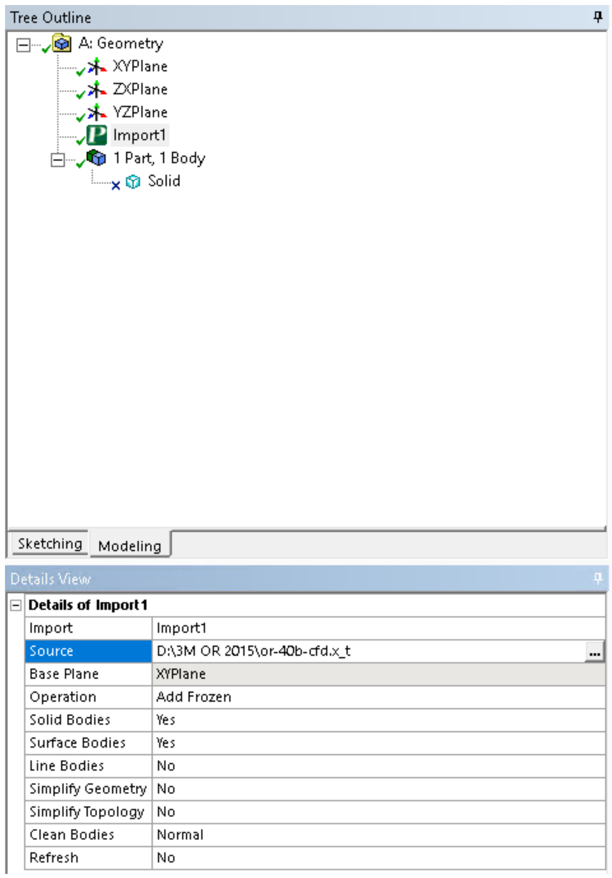

Figure 55 The CAD modeling feature tree is shown for steps are Abraham00000003 (2).agdb

Given the limited information in the report, it appears to be the CAD geometry that is reported in the report which is different to the geometry used in the models. Figures 56 and 57 show how Abraham00000003 (2).agdb is also different to the geometry used in the CFD models. The Abraham00000003 (2).agdb also has the same differences as the reported geometries in the Dr. Abraham's report.

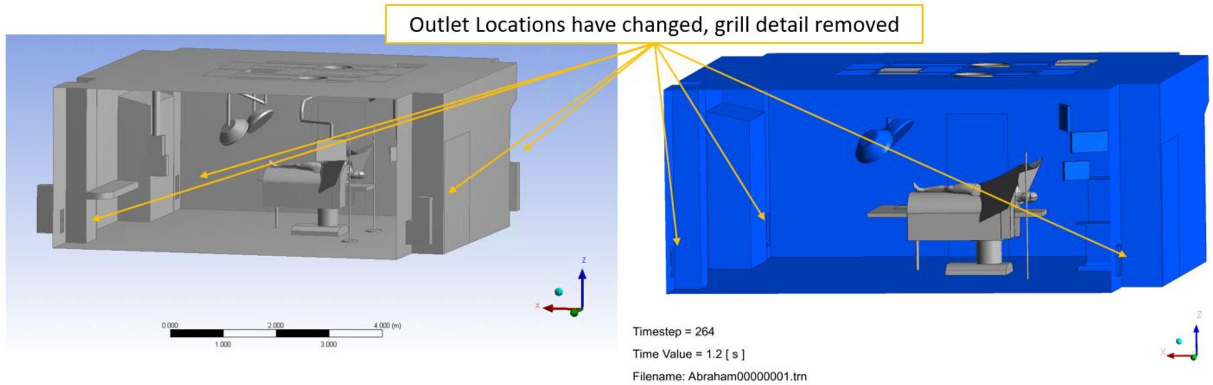

Figure 56 Abraham00000003 (2).agdb CAD geometry (left) is shown beside the model geometry used in Abraham00000001.trn (right)

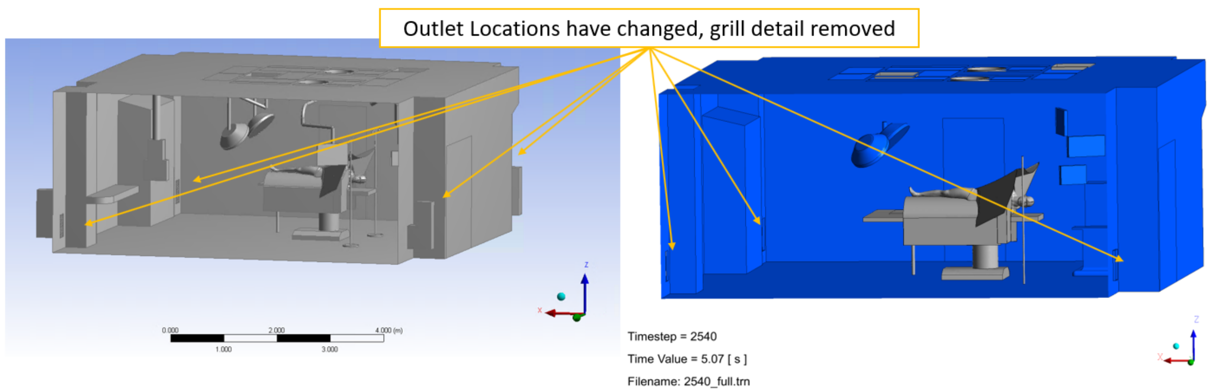

Figure 57 Abraham00000003 (2).agdb CAD geometry (left) is shown beside the model geometry used in Abraham00000001.trn (right)

Bodies were changed in the model.

Because the Abraham00000003 (2).agdb CAD is 3D unlike the 2D pictures, it is possible to further inspect the geometry. It is possible to show a number of additional differences between the CAD and the model geometries. These including the size of the equipment near the head was changed. The when you compare the length of a similar edge the body in the CAD is larger than the body used in the model. Figure 58 show the length an edge on the piece of equipment. Figures 59 and 60 show a line place at the same location and length as CAD edge. The line extends beyond the piece of equipment in the models. Thus, the size of the equipment is different.

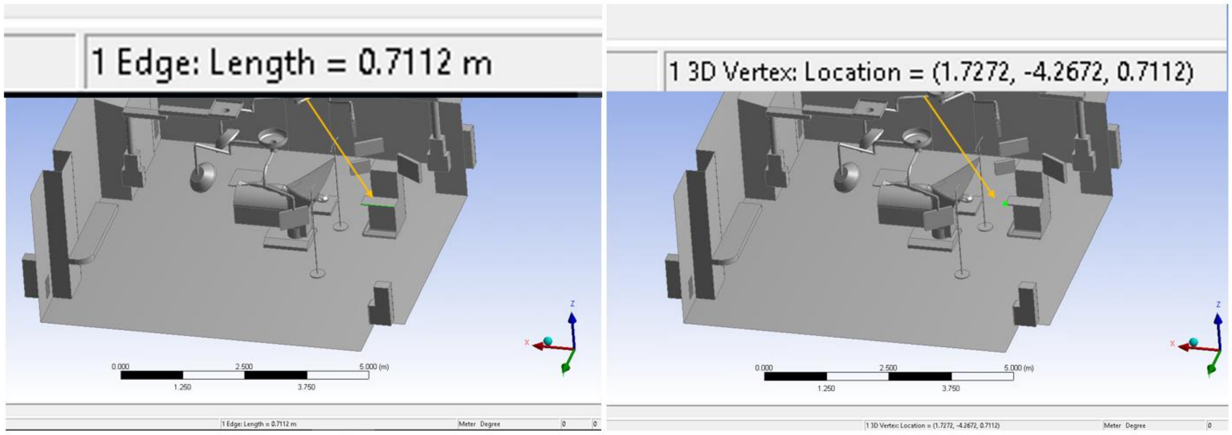

Figure 58 Measured length of edge (left) and vertex (right) location

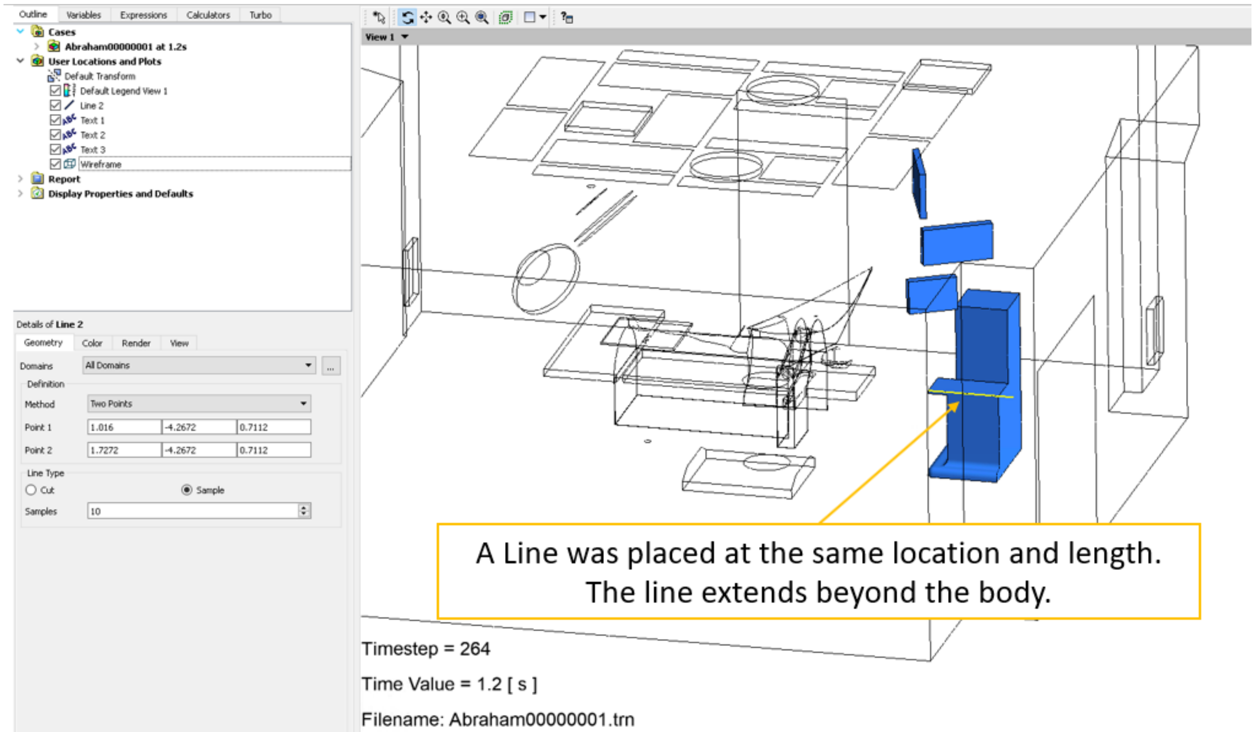

Figure 59 Line placed in same location with 0.7112m length on model the Abraham00000001.trn results.

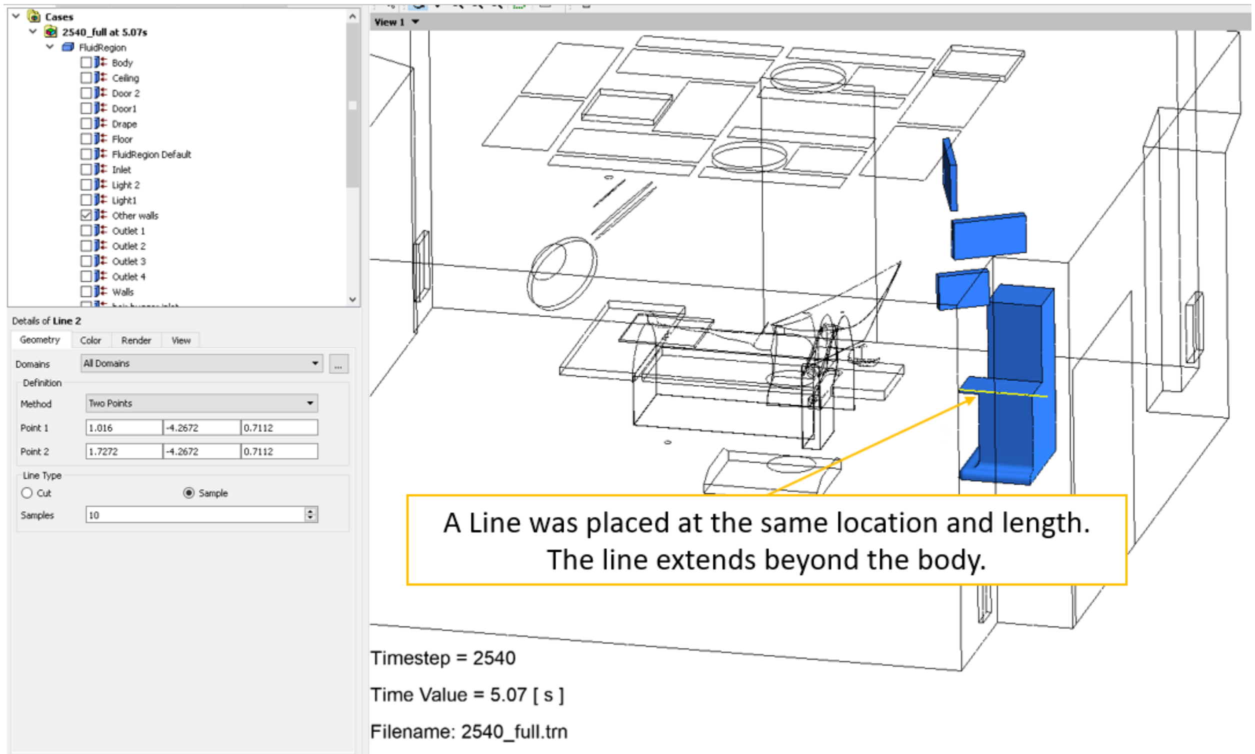

Figure 60 Line placed in same location with 0.7112m length on model 2540_full.trn results.

Bodies were added in the model.

Additionally, Dr. Abraham either changed the shape and size of the table at the feet or added a second connected table, either way results in blocking the floor at the end of the operating table. Figures 61 and 62 show the differences. No justification is given.

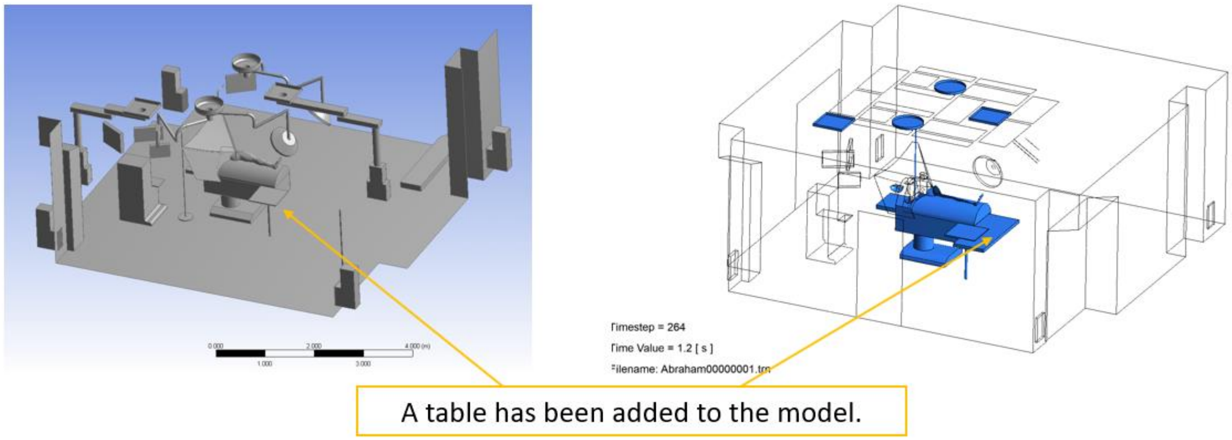

Figure 61 Location of added body not in original CAD but in Abraham00000001.trn CFD model

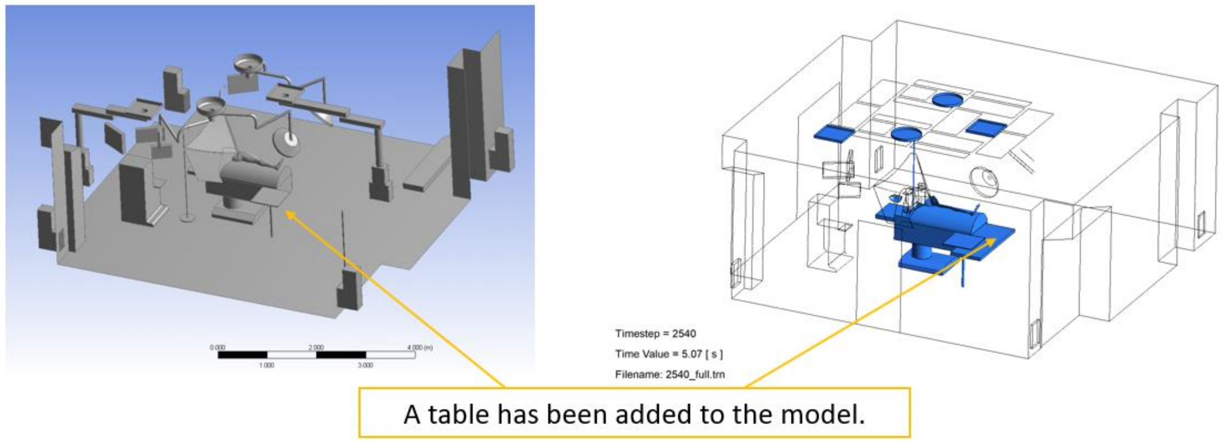

Figure 62 Location of added body not in original CAD but in 2540_full.trn CFD model

The mesh is in the model is incorrect compared to the report.

The mesh is shown below for the Abraham00000001.trn (Figure 64) and 2540.trn (Figure 65) is significantly different from the mesh in the report (Figure 63). The mesh is both different because the underlying geometry is different, and the sizing is different. The mesh used, and mesh reported in the report are significantly different.

The mesh in the report appears to be more refined, while the mesh used in the models is coarser than the mesh used shown in the report.

Report

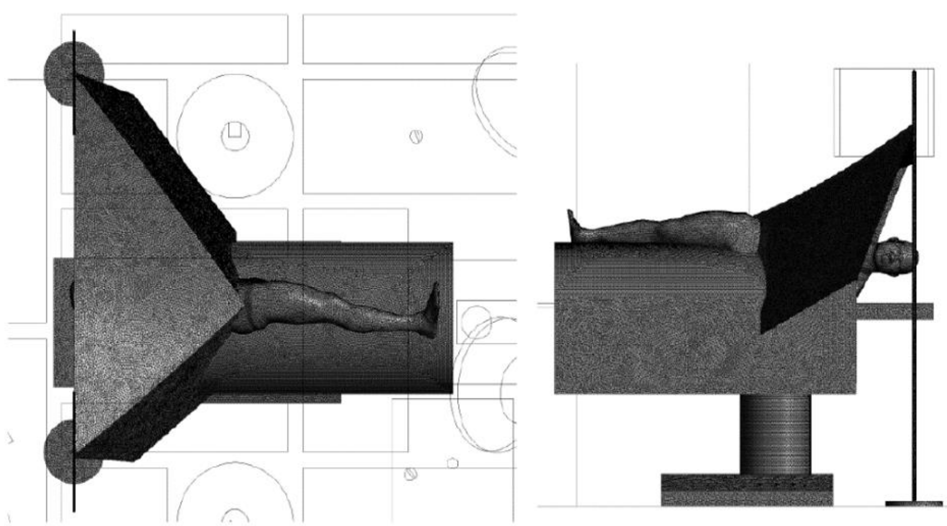

Figure 2 – Images of the cells projected onto the surgical surfaces

Figure 63 is the reported surface mesh used in report

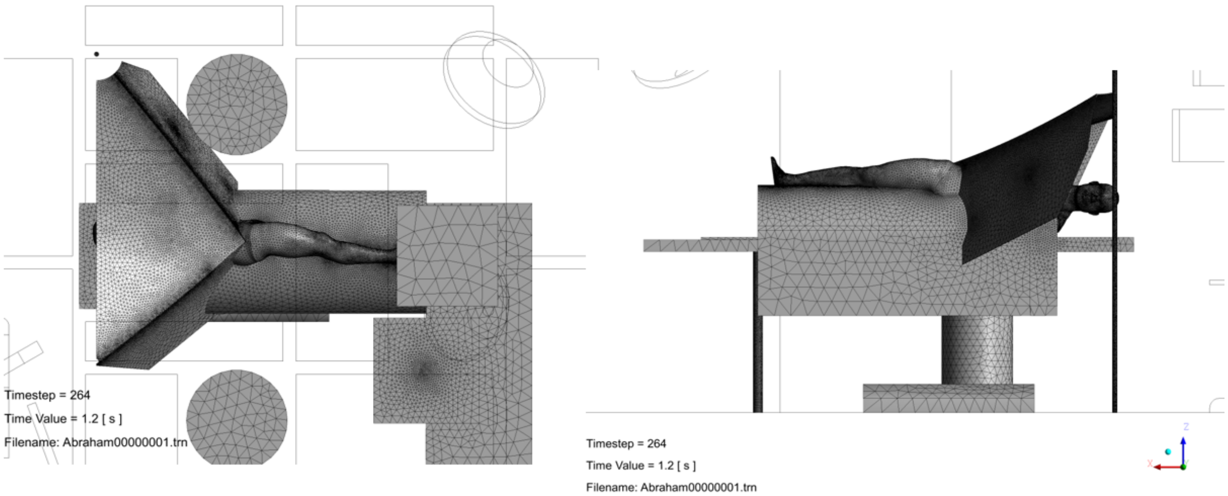

Figure 64 shows the surface mesh used in the Abraham00000001.trn results. The mesh resolution and the underlying bodies that are used to make the mesh are different.

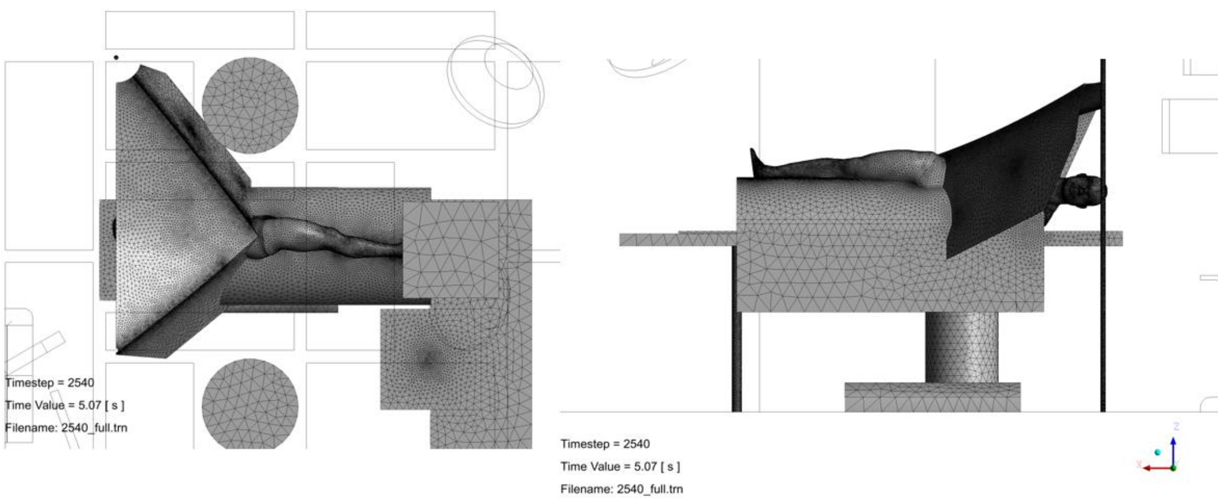

Figure 65 shows the surface mesh used in the 2540_full.trn results. The mesh resolution and the underlying bodies that are used to make the mesh are different.

Mesh count is also different to the report.

Dr. Abraham uses a different mesh size than the one report in his report. He claims *"up to 60,000,000 grid cells"* in this Step 2 of the analysis – calculation of cells paragraph. He also gives an "*for an 8.1 million grid-cell calculation*". Neither are correct the models contain 9.88 million elements and 1.72 million nodes, Figures 66 and 67 for Abraham00000001.trn and 2540_full.trn respectively.

Table 2. Mesh Information for Abraham00000001

Domain	Nodes	Elements
FluidRegion	1718978	9884667

Figure 66 Mesh count information for Abraham00000001.trn

Table 2. Mesh Information for 2540_full

Domain	Nodes	Elements
FluidRegion	1718978	9884667

Figure 67 Mesh count information for 2540_full.trn

Difference Equation of State

Dr. Abraham uses a difference equation of state with his two models. For the Abraham00000001.trn model he uses a constant density of 1.185 (kg m^{-3}), for the 2540_full.trn model he uses the ideal gas model. Figure 68 shows the density difference between the two models. Figure 69 shows the density at the inlet, which results in a 3.3% error (Figure 70). Figure 71 shows the velocity at the inlet, which results in a 3.3% error (Figure 72). Figure 73 shows the density at the Bair hugger inlet, which results in a 5.5% error (Figure 74).

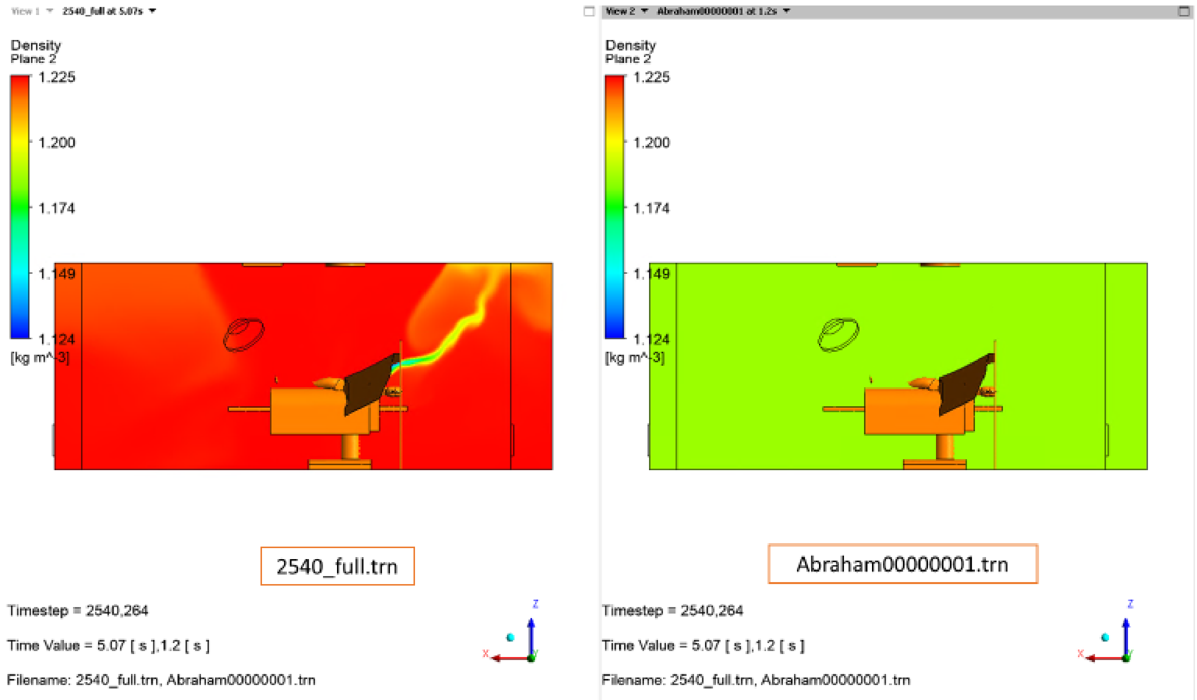

Figure 68 Density at Y=-3.67143 (m) for Abraham00000001.trn and 2540_full.trn

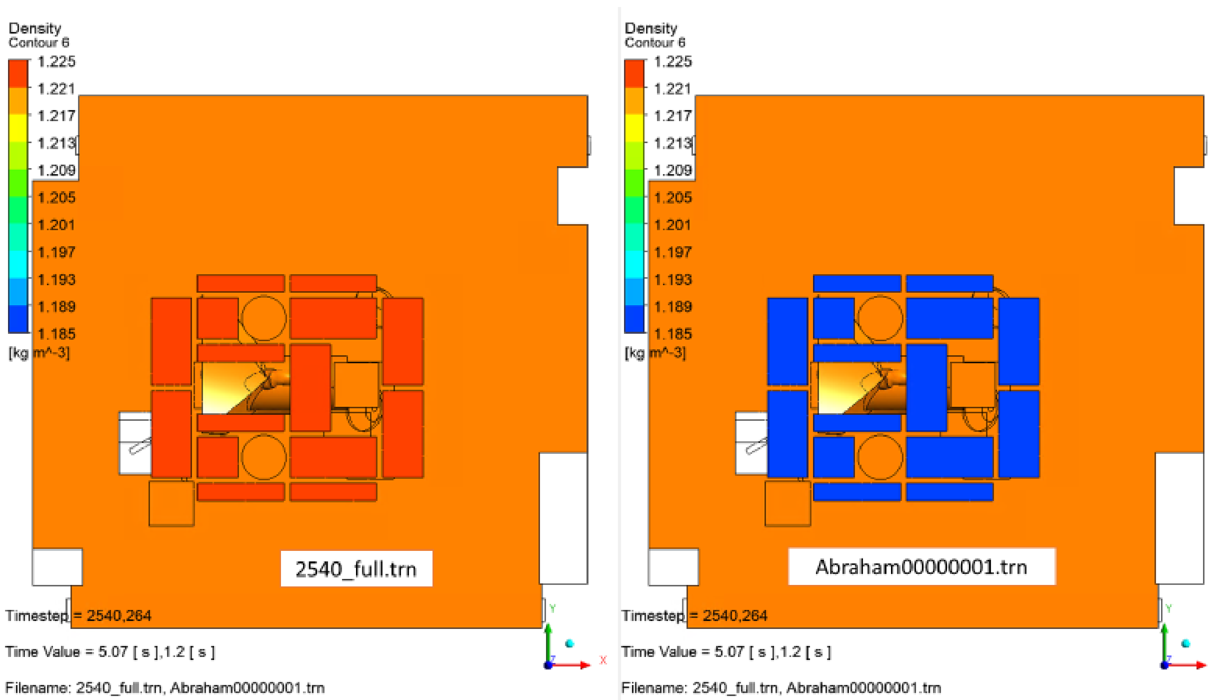

Figure 69 Density at Inlet for Abraham00000001.trn and 2540_full.trn

$$\frac{1.225\ \frac{kg}{m^3} - 1.185\ \frac{kg}{m^3}}{1.225\ \frac{kg}{m^3}} = 3.265\%$$

Figure 70 Calculation of density difference at Inlet between Abraham00000001.trn and 2540_full.trn

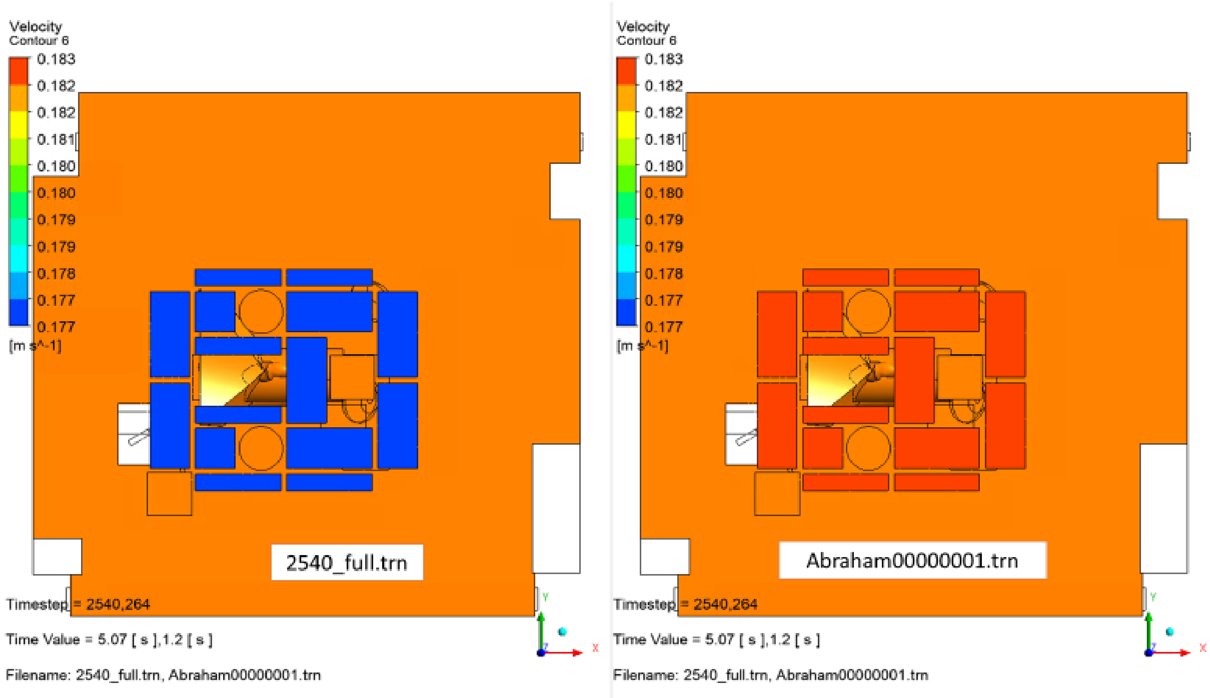

Figure 71 Velocity at Inlet for Abraham00000001.trn and 2540_full.trn

$$\frac{0.183\ \frac{m}{s} - 0.177\ \frac{m}{s}}{0.183\ \frac{m}{s}} = 3.279\%$$

Figure 72 Calculation of velocity difference at Inlet between Abraham00000001.trn and 2540_full.trn

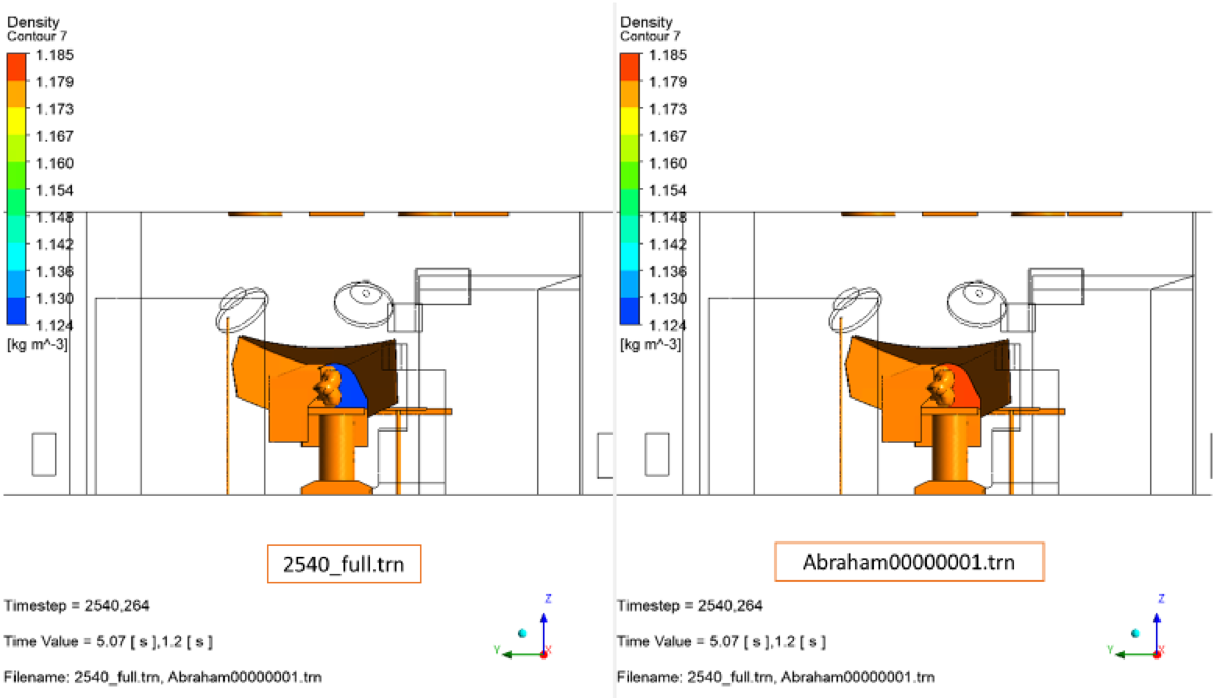

Figure 61 Density at Bair hugger inlet for Abraham00000001.trn and 2540_full.trn

$$\frac{1.12353\ \frac{kg}{m^3} - 1.185\ \frac{kg}{m^3}}{1.12353\ \frac{kg}{m^3}} = -5.471\%$$

Figure 61 Calculation of density difference at Bair hugger inlet between Abraham00000001.trn and 2540_full.trn

Summary

Dr. Abraham CFD modeling does not support his conclusions, there numerous errors in his CFD models. They included:

- Dr. Abraham errors by using a steady state streamline on a single transient result. Streamlines require a steady state solution to be accurate and the transient model Dr. Abraham used is not steady. It can clearly be shown the results will change depending on which result he choose to use.
- Dr. Abraham errors by not running his transient model long enough. He only runs his model for 1.2(s) and 5.07 (s) of simulation time. The model has not had long enough to predict the fluid motion in the operating room as he has defined it. The results can be shown to dependent the definition of his unknown initial condition
- Dr. Abraham uses results from a model that will diverge. This is outside standard industry practices and highly likely to give wrong results.
- Dr. Abraham uses a mesh that is under resolved and has unacceptable quality elements. If he refined his mesh he would get different results.
- Dr. Abraham used a High resolution scheme with his LES which is known to cause errors in the solution.
- Dr. Abraham used streamlines, he should have used particle tracking. Particle tracking is significantly more accurate and the industry standard approach to particle distribution problems.
- Dr. Abraham does not support any of his assumptions with any sensitivity analysis.
- Dr. Abraham's validated is not document enough to be confirmed by his results, also his choice of validation does not prove the accuracy of his methodology of a steady sate streamline on a single transient timestep to accurately particle motion.

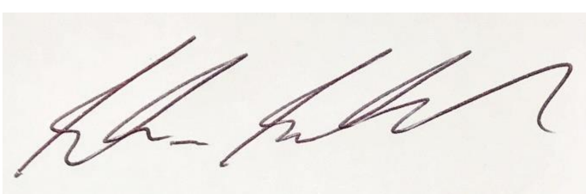

____

Nathan Bushnell, Ph.D.

Appendix I (Resume)

CFD Consulting Engineer

SimuTech Group - Seattle

EDUCATIONAL BACKGROUND

Doctor of Philosophy, Chemical and Process Engineering– University of Canterbury, Christchurch, New Zealand, 2008

Thesis: The Study of Liquid/Vapour Interaction inside a Falling Film Evaporator in the Dairy Industry.

Bachelor of Engineering with honors, Chemical and Process Engineering – University of Canterbury, Christchurch, New Zealand, 1999

Engineering Expertise

- Computational Fluid Dynamics
- Modeling of Multiphase Fluid Flows
- Modeling of Turbulence within complex industrial equipment
- Modeling of Complex Heat Transfer Radiation, Natural Convection and Phase Change

Industry Expertise

- Oil and Gas
- Process Industry
- Consumer Electronics
- Alternative Energy
- Homeland security and Government

PROFESSIONAL EXPERIENCE

CFD Consultant/ Lead Engineer, 2007 –present

SimuTech Group, Everett, WA

- Performed advanced CFD analyses using Ansys FLUENT and Ansys CFX packages.
- Prepared comprehensive technical proposals and secured more than 40 external consulting projects.
- Provide CFD specialized training for professional engineers.
- Provide Project specific training for commercial clients.
- Executed geometry de-featuring and advanced meshing technologies.
- Performed sophisticated post-processing of large CFD data using Ansys Fluent and Ansys CFD-Post packages.
- Provide Technical CFD support for SimuTech Group’s industrial customers.

- Provide and present information to SimuTech Group's customers on the state of the art capabilities for Ansys Fluent, CFX and Icepak as new software releases occur.

Sample of Completed Projects:

- Analysis of a novel inline pump for down-hole applications in the oil and gas industry *(CFX, Rotating Frame of Reference, Turbulence and Compressible Flow).*
- Analysis of the cooling and erosion potential for a spray cooled quench tower *(CFX, Steady State, Multiphase, Turbulence and Heat Transfer).*
- Mixing and Heating of non-Newtonian Nuclear sludge *(CFX, Multiphase, Phase Change, Fluid Structure Interactions).*
- Atomization of liquid stream into droplet prior to automated sorting *(Fluent, Transient, Multiphase and Laminar)*.
- Prediction of the collapse of a piston generated underwater cavitation cloud and the resulting acoustic pressure wave *(CFX, Transient, Multiphase, Compressible, Turbulence, FSI, Structural Deformation and Stress).*
- Simulations of Oil and Gas spills from Pipelines located at the bottom of the sea *(FLUENT and CFX, Multiphase, Compressible, Turbulent and Conjugate Heat Transfer).*
- Analysis of the fluid flow of a mobile water clarifier for portable clarification of Oil Sand well waste water *(CFX, Steady State, Single Phase, MFR and Turbulence).*
- Investigation of fluid failure mechanism and redesign of a positive displacement pump used in during fracking process *(CFX, Transient, Multiphase, Mesh Deformation and Turbulence).*
- Oil sands Steam Assisted Gravity Drainage bitumen recovery and production simulations *(CFX, Steady State, Laminar and Porous Media).*
- Analysis of the mixing time required for impeller stirred bio reactor tanks *(CFX and Fluent, Multiple Frame of Reference, Multiphase, Species Transfer and Turbulence).*
- Analysis of an inline mixer pump for down-hole applications in the oil and gas industry *(CFX Multiple Frame of Reference, Multiphase and Turbulence).*
- Multiple turbine projects, including under water and compressible flows *(CFX, FSI, Rotating Frame of Reference Turbulence and Multiphase).*
- Analysis of Ring Crystallizer fluid flow *(Ansys CFX, Steady State, Porous Medium and Turbulence).*
- Analysis of the shear induced cleaning of Solar Tubes under free surface motion *(Ansys CFX, Transient, Multiphase and Turbulence).*
- Analysis of flow through vibrating ball gate valve *(Ansys CFX, Transient, Fluid Structure Interaction, Mesh deformation, incompressible and Turbulence).*
- Analysis of biomedical valve *(Ansys CFX, Steady State, incompressible and Turbulence).*
- Analysis of flow and vibration of an Inline Burner *(Ansys CFX, Compressible, Conjugate Heat Transfer, Turbulence and Ansys Mechanical).*
- Modeling of a two-stage oxygen regulator *(Ansys CFX, Compressible, Conjugate Heat Transfer and Turbulence).*

Doctoral Student, 2004–2008

University of Canterbury

- Separation of Droplets inside of an integrated separator (Ansys CFX, Steady and Unsteady flow, Turbulence, Film Atomization and Multiphase).
- Wetting of Milk products on the distribution plate of a falling film evaporator (Ansys CFX, Steady and Unsteady flow, Multiphase and Laminar).

Professional Teaching Experience

CFD Consultant/ Lead Engineer, SimuTech Group

- Taught the Introduction to CFX (4-5day training course) seven times. 2007-present
- Developed and Taught the Ansys CFD short course (1/2 day workshop). 2011-present

Ansys Professional Certification

CFD Consultant/ Lead Engineer

- ANSYS Certified Professional, R19: Fluid Technical
- ANSYS Certified Professional, R18: Fluids – Technical
- ANSYS Certified Professional, R17: Fluids - Technical V1
- ANSYS Certified Professional: Fluids – Technical
- ANSYS Certified Professional: ANSYS Icepak – Technical
- ANSYS Certified Professional, R18: Preprocessing – Technical
- ANSYS Certified Professional, R18: AIM – Technical
- ANSYS Certified Professional: Structural – Technical
- ANSYS Certified Professional: ANSYS AIM – Technical
- ANSYS Certified Professional: ANSYS SpaceClaim - Technical
- 2007 Ansys Fluids Technologies certification for SimuTech Group, Fluent.
    - Certification model: Validation of turbulent flow over repeating hills
- 2011 Recertification SimuTech Group for Ansys CFX
    - Certification model: Turbulent multiphase flow through a positive displacement pump with fluid structure interactions

SPECIAL ACCOMPLISHMENTS AND AWARDS:

Conference Presentations and Journal Papers:

- “A new hybrid heat sink with impinging micro-jet arrays and microchannels fabricated using high volume additive manufacturing”, 2017 33rd Thermal Measurement, Modeling & Management Symposium (SEMI-THERM), Robinson, A.J. and Tan, W. and Kempers, R. and Colenbrander, J. and Bushnell, N. and Chen, R.,
- An ultra high performance heat sink using a novel hybrid impinging microjet — Microchannel structure, Robinson, A.J. and Tan, W. and Kempers, R. and Colenbrander, J. and Bushnell, N. and Chen, R., 2017 16th IEEE Intersociety Conference on Thermal and Thermomechanical Phenomena in Electronic Systems
-

“A single phase hybrid micro heat sink using impinging micro-jet arrays and microchannels”, Robinson, A.J. and Kempers, R. and Colenbrander, J. and Bushnell, N. and Chen, R., Applied Thermal Engineering, Volume 136, May 2018, p408-418

- Presented “Separation of droplets from vapour in the integrated separators of a falling film evaporator” Paper at the 7th World Congress of Chemical Engineering, Glasgow, 2005

National Scholarship Awards:

- Bright Futures Enterprise Ph.D. Scholarship, 2004-2006
- CHEMECA Scholarship, 2005

EXHIBIT I

UNITED STATES DISTRICT COURT

DISTRICT OF MINNESOTA

In Re: Bair Hugger Forced Air Warming Devices Products Liability Litigation	File No. 15-MD-2666 (JNE/DTS)
	August 16, 2018 Minneapolis, Minnesota Courtroom 12W 9:50 a.m.

BEFORE THE HONORABLE JOAN N. ERICKSEN
UNITED STATES DISTRICT COURT JUDGE

THE HONORABLE DAVID T. SCHULTZ
UNITED STATES MAGISTRATE JUDGE

(STATUS CONFERENCE)

APPEARANCES

FOR THE PLAINTIFFS:

MESHBESHER & SPENCE LTD.
Genevieve M. Zimmerman
1616 Park Avenue
Minneapolis, MN 55404

PRITZKER HAGEMAN
David Szerlag
45 South Seventh Street
Plaza Seven Building, Ste. 2950
Minneapolis, MN 55402

CIRESI CONLIN LLP
Michael A. Sacchet
225 South Sixth Street
Suite 4600
Minneapolis, MN 55402

KENNEDY HODGES LLP
David W. Hodges
711 West Alabama Street
Houston, TX 77006

to have an expert come in and list seven new alternative designs when no discovery has ever been done on those. It is also improper to try to go around the court's orders on surrebuttal expert reports and now submit this report from Nathan Bushnell. But the biggest point is these are generic opinions, they do not apply to Mrs. Axline, and the deadline has long since past. So we are concerned about that, and we wanted to raise the issue with the court so it would come as no surprise.

THE COURT: Do you have copies of the reports of Dr. David and Nathan Bushnell?

MS. PRUITT: Yes.

THE COURT: Ms. Zimmerman, any objection to the court receiving the copies of those at this point? We are not ready to hear argument, obviously. We don't have anything. But I know we are going to be required to read it, so we might as well get it now rather than later, because you may have heard that the district is highly overworked at the moment, so --

MS. ZIMMERMAN: We don't have an objection to the court receiving copies of the orders at this time.

THE COURT: Okay.

MS. ZIMMERMAN: We certainly think that to the extent that the defendants are intending to bring a motion to strike that we would request the opportunity to fully

brief those issues.

With respect to just kind of previewing issues, given that Ms. Pruitt did that, David's report did not include conductive warming reports on reasonable alternative design in the general causation stage primarily because the court had previously declined, refused to allow us to do discovery on VitaHEAT on the idea or finding that that was in fact not a reasonable alternative design. That decision was changed with respect to the Gareis case.

And so in an abundance of caution and given the law in Ohio, which has a broader standard for a reasonable alternative design, Dr. David has supplemented his general causation report to make clear that things like not warming, things like pre-warming, things like warming with cotton blankets are all appropriate alternatives available to surgeons.

THE COURT: All right. So we will take the reports either now, if you have them, or as soon as you can get us copies, and then we will be on the lookout for a motion and an explanation.

MS. ZIMMERMAN: And just so we are aware, is this going to be a motion to strike the expert reports or --

MS. PRUITT: We are considering what the proper motion is.

MS. ZIMMERMAN: All right. And with respect to

Nathan Bushnell's report, this is -- it's a rebuttal report to Dr. Abraham's general causation report. As the court is aware, the plaintiffs have moved to exclude Dr. Abraham under Daubert. We have renewed that motion in our motion for new trial. And we continue to believe that Dr. Abraham should not have been permitted to testify. Dr. Nathan Bushnell's report is simply to outline the errors and the inaccuracies in methodology in Dr. Abraham's report.

THE COURT: So you don't want Bushnell in *Axline*? You are offering Bushnell as part of the motion for a new trial?

MS. ZIMMERMAN: No, Your Honor. I am sorry if I misspoke. We do intend to bring Dr. Bushnell as part of plaintiffs' rebuttal case, should defendants intend to bring Dr. Abraham again.

THE COURT: Okay. All right. Thank you.

MR. BLACKWELL: Your Honor.

THE COURT: Hello, Mr. Blackwell.

MR. BLACKWELL: There is one other *Axline* issue I wanted to raise and ask a question about, if I may.

THE COURT: Go ahead.

MR. BLACKWELL: And, Your Honor, this may be more aptly addressed to Judge Schultz.

We had written a letter about an issue that arose in the deposition of the orthopedic surgeon Dr. Lombardi

that was a fairly significant issue. It is a discovery issue. And whether it's the preference of Your Honors, Judge Schultz, that we set it and have it heard with Judge Schultz or raise it now, we obviously defer, but we didn't want to sort of pass by the discussion of *Axline* discovery issues and not raise it.

THE COURT: Okay. And then there was a response also from the plaintiffs?

MR. BLACKWELL: Yes, from the plaintiffs.

THE COURT: Yeah. And I think we both read those.

MAGISTRATE JUDGE SCHULTZ: Yes.

THE COURT: Yeah, you will be in front of the magistrate judge.

MR. BLACKWELL: All right. Thank you, Your Honor.

THE COURT: Thank you.

MS. ZIMMERMAN: Your Honor, there were two additional things that I think we didn't add that are pending motions before the court. And because we, I think, neglected to include them on the joint status report, I did just want to remind the court there are pending motions with respect to defendants' motion on the bill of costs in Gareis and then there are also pending motions, joint motions, regarding sealing of certain documents that happened during trial. And because they weren't in the joint agenda, I just wanted to point those out.